

INFORMATION TO USERS

This manuscript has been reproduced from the microfilm master. UMI films the text directly from the original or copy submitted. Thus, some thesis and dissertation copies are in typewriter face, while others may be from any type of computer printer.

The quality of this reproduction is dependent upon the quality of the copy submitted. Broken or indistinct print, colored or poor quality illustrations and photographs, print bleedthrough, substandard margins, and improper alignment can adversely affect reproduction.

In the unlikely event that the author did not send UMI a complete manuscript and there are missing pages, these will be noted. Also, if unauthorized copyright material had to be removed, a note will indicate the deletion.

Oversize materials (e.g., maps, drawings, charts) are reproduced by sectioning the original, beginning at the upper left-hand corner and continuing from left to right in equal sections with small overlaps. Each original is also photographed in one exposure and is included in reduced form at the back of the book.

Photographs included in the original manuscript have been reproduced xerographically in this copy. Higher quality 6" x 9" black and white photographic prints are available for any photographs or illustrations appearing in this copy for an additional charge. Contact UMI directly to order.

UMI

**A Bell & Howell Information Company
300 North Zeeb Road, Ann Arbor MI 48106-1346 USA
313/761-4700 800/521-0600**

Dynamic Modeling and Global Optimal Operation of Multizone Variable Air Volume HVAC Systems

Guo Rong ZHENG

**A Thesis
in
The Centre for Building studies**

**Presented in Partial Fulfillment of the Requirements
for the Degree of Doctor of Philosophy at
Concordia University
Montreal, Quebec, Canada**

February 1997

©Guo Rong ZHENG, 1997



National Library
of Canada

Acquisitions and
Bibliographic Services

395 Wellington Street
Ottawa ON K1A 0N4
Canada

Bibliothèque nationale
du Canada

Acquisitions et
services bibliographiques

395, rue Wellington
Ottawa ON K1A 0N4
Canada

Your file Votre référence

Our file Notre référence

The author has granted a non-exclusive licence allowing the National Library of Canada to reproduce, loan, distribute or sell copies of this thesis in microform, paper or electronic formats.

The author retains ownership of the copyright in this thesis. Neither the thesis nor substantial extracts from it may be printed or otherwise reproduced without the author's permission.

L'auteur a accordé une licence non exclusive permettant à la Bibliothèque nationale du Canada de reproduire, prêter, distribuer ou vendre des copies de cette thèse sous la forme de microfiche/film, de reproduction sur papier ou sur format électronique.

L'auteur conserve la propriété du droit d'auteur qui protège cette thèse. Ni la thèse ni des extraits substantiels de celle-ci ne doivent être imprimés ou autrement reproduits sans son autorisation.

0-612-25927-7

Canada

CONCORDIA UNIVERSITY
SCHOOL OF GRADUATE STUDIES

This is certify that the thesis prepared

By: **Mr. Guo Rong ZHENG**

Entitled: **Dynamic Modeling and Global Optimal Operation of Multizone
Variable Air Volume HVAC Systems**

and submitted in partial fulfillment of the requirements for the degree of

DOCTOR OF PHILOSOPHY (Building Studies)

compiles with the regulations of the University and meets the accepted standards with
respect to originality and quality.

Signed by the final examining committee:

_____	Chair
_____	External Examiner
_____	External to Program
_____	Examiner
_____	Examiner
_____	Supervisor

Approved _____
Chair of Department or Graduate Programme Director

_____ 19 _____
Dean of Faculty

ABSTRACT

Dynamic Modeling and Global Optimal Operation of Multizone Variable Air Volume HVAC Systems

Guo Rong ZHENG, Ph.D.

Concordia University, 1997

Energy conservation and indoor environment concerns have motivated extensive research on various aspects of control of Heating, Ventilating and Air-Conditioning (HVAC) and building systems. The study on optimal operation as well as modeling of HVAC and building systems is one of the fastest growing fields that contribute to saving energy and improving indoor environment.

This thesis is devoted to the development of a comprehensive modeling and optimization methodology for global multiple-stage optimal operation of HVAC and building systems. Two different dynamic models of a multizone variable air volume (VAV) system have been developed using (i) bottom-up and (ii) top-down approaches. The models take account of the dynamic interactions between building shell, VAV system components and control systems. The models describe the dynamics of fan, air distribution system, zone(s), cooling coil and primary plant (chiller) as one multivariable nonlinear system in a way that is useful for control analysis. Using the bottom-up approach a large-scale VAV system model has been developed. This model considers the interactions between flow field and thermal field via distributed capacity and variable air density considerations. An alternate model which is computationally more efficient was developed using the top-down approach. Model reduction techniques were applied to develop a reduced-order state space model of the VAV system. Results show that

predictions from the reduced-order model are within 5% of those from the large scale model.

Optimal control schemes are developed for the efficient operation of VAV systems. In the control scheme proposed it is necessary to compute optimal setpoint profiles for local controllers. The optimal control profiles so computed can be used as tracking signals for local controllers for moving the system states from one setpoint to another. In order to determine optimal setpoint profiles an optimization methodology for formulating and solving the multiple stage optimal operation problems has been developed. The methodology is based on the maximum principle of Pontryagin and perturbation method in order to deal with the multiple time-scale of the HVAC processes and building operating schedules. A solution methodology and the corresponding computer models have been developed for solving the multiple stage optimal operation problems.

The applications of the VAV model and the multistage optimization methodology have been demonstrated by considering several practical examples. The examples include (i) a comparison of optimal strategies for constant and variable air volume systems with and without time-of-day price structure for electrical energy, (ii) a two-zone VAV heating system and (iii) a five-zone VAV cooling system. Results showing the 24-hour optimal setpoint profiles, energy cost savings and the output responses such as zone temperatures and humidity ratios are given for different building operation schedules. These applications show that the developed models and optimization methodology can be used to determine energy efficient operating strategies for VAV systems without violating the thermal comfort in buildings.

ACKNOWLEDGEMENTS

I would like to express my sincere gratitude to Dr. M. Zaheer-uddin for his constant guidance, help, sustained interest, and financial support throughout the course of this work.

My thanks are also to the members of staff in Centre for Building Studies for their help whenever I needed it. Special thanks go to Mr. S. Belanger and Mr. Dan Zhu for their support in computing facility and software.

My thanks also go to my colleagues, especially to Dr. Tingyao Chen, for their helpful discussion and suggestions.

I would like to dedicate this thesis to my wife, Danxi Que, and my lovely daughter, Yi Zheng for their patience, understanding and support during my whole studies.

TABLE OF CONTENTS

List of Figures

List of Tables

Nomenclature

Chapter 1.

Introduction.....	1
1.1. Variable air volume HVAC system	2
1.2. Importance of global optimal operation of VAV system.....	4
1.3. Scope and Objectives.....	7
1.4. Contributions and summary	8

Chapter 2.

Literature Review	10
2.1. Modeling.....	10
2.1.1. Component models.....	11
2.1.1.1. Coil models	12
2.1.1.2. Chiller models	15
2.1.1.3. Zone and building shell models	16
2.1.1.4. Duct and fan-motor models	17
2.1.2. Overall system models	18
2.2. Control studies	21

2.3. Summary and objectives	31
-----------------------------------	----

Chapter 3.

Dynamic Modeling of a Multizone VAV System: Large-

scale Dynamic Model of VAV System..... 34

3.1. Component models	37
3.1.1. Cooling and dehumidifying coil model	37
3.1.2. Chiller and storage tank model.....	50
3.1.3. Environmental zone(s) model	51
3.1.4. Model of variable air flow rates in the duct system.....	53
3.1.5. Fan-motor model.....	55
3.1.6. Correlations for pressure losses in the duct system.....	59
3.2. Integrated large-scale model of VAV system	61
3.3. Open-loop simulation results.....	63

Chapter 4.

Dynamic Modeling of a Multi-zone VAV System:

Reduced-order State Space Model..... 70

4.1. Development of reduced-order state space model of VAV system.....	70
4.1.1. A methodology and state space model of air flow subsystem.....	72
4.1.2. State space model of water flow subsystem.....	82
4.1.3. State space model of thermal subsystem.....	84
4.1.4. Reduced-order state space model of VAV system.....	97

4.2. Open-loop simulation results.....	99
4.3. Comparison of large-scale and reduced-order models.....	102
4.5. Applications of models	104

Chapter 5.

Methodology for Multiple Stage Optimal Operation

Problems	112
5.1. Formulation of single stage optimal control problems.....	114
5.2. Methodology for multiple stage optimal operation problems	119
5.2.1. Formulation of multiple stage optimal operation problems	120
5.2.2. The perturbation method for multiple time-scale systems	125
5.2.3. The multiple stage optimal operation problems with the perturbation method.....	129

Chapter 6.

Applications of the Optimization Methodology	135
6.1. Introduction.....	135
6.2 Comparison of operational efficiency of Constant- and Variable-Air-Volume HVAC systems	137
6.2.1. Dynamic model of a single zone space heating system.....	138
6.2.2. Formulation of optimal operation of a single zone space heating system.....	139
6.2.3. Simulation results	143

6.2.4. Discussion	156
6.3. Example 2: Optimal operation of a two-zone VAV heating system.....	157
6.3.1. Two zone VAVH system	158
6.3.2. Building operation schedule	159
6.3.3. Formulation of the problem	160
6.3.4. Simulation results	163
6.4. Example 3: Optimal operation of a five-zone VAV cooling system.....	167
6.4.1. Five-zone VAVC system	167
6.4.2. Building operation schedule	168
6.4.3. Formulation of the problem	168
6.4.4. Simulation results	174
 Chapter 7.	
 Conclusions and Recommendations for Future Research	185
References.....	189
 Appendix A	
 The Modeling of Building Shell.....	202

LIST OF FIGURES

1.1. Schematic diagram of Energy Management and Control for a VAV System	6
3.1. Schematic diagram of a multizone VAV system	36
3.2. Schematic diagrams of	
(a) the counter-cross flow coil arrangement	38
(b) the cooling & dehumidifying coil and control volume	39
(c) the chiller and storage tank.....	51
(d) the environmental zone	53
(e) the duct section	53
(f) the fan-motor system	56
(g) the converging section	60
(h) the diverging section.....	61
3.3. Nodal representation of the overall VAV system model.....	62
3.4. Fan and airflow system characteristics subject to step changes in inputs and external disturbances.....	64
(a) Fan speed	(b) Fan-motor power
(c) Mass flow rate of air to the zones	(d) Static pressure
3.5. Temperature and humidity ratio responses of air leaving the cooling and dehumidifying coil without and with bypass	66
without bypass: (a) Temperature	(b) Humidity ratio
with bypass: (c) Temperature	(d) Humidity ratio
3.6. Zone temperature and humidity ratio responses.....	68
(a) Temperature responses	(b) Humidity ratio responses
4.1 The interconnection of airflow, water flow, and thermal subsystems.....	71
4.2 Flow diagram for modeling air flow in VAV system (two-zone system as an example).....	73
4.3 Flow diagram for modeling water flow in VAV system	82
4.4. Comparison of the results from the proposed model and those given in Stoecker and Nesler et al.....	93
(a) Response of discharge air temperature following a step increase in mass flow rate of water	
(b) Response of return water temperature following a step increase in mass flow rate of water	

(c) Response of discharge air temperature following a step decrease in mass flow rate of water	
(d) Steady state performance of discharge air temperature	
4.5 Comparison of distributed and lumped sensible coil models	94
4.6 Comparison of distributed and lumped cooling and humidifying coil models	95
4.7 The schematic diagram of VAV system configuration	98
4.8 Fan and airflow system responses	100
(a) Fan speed and Fan-motor power (b) Mass flow rate of air to the zones	
4.9 Responses of temperature and humidity ratio of air leaving the coil	100
(a) Temperature (b) Humidity ratio	
4.10 Responses of temperatures and humidity ratios of air in the zones	101
(a) Temperature responses (b) Humidity ratio responses	
4.11 Comparison of large-scale and reduced-order models: Fan and airflow system responses	102
(a) Fan speed (b) Fan-motor power	
(b) Mass flow rates of air (d) Static Pressure	
4.12 Comparison of large-scale and reduced-order models: Zone temperatures and humidity ratios	103
(a) Temperature responses (b) Humidity ratio responses	
4.13 Zone temperature responses during night time.....	106
(a) Shut-down (b) Reduced capacity fan operation	
4.14 System responses during start-up	108
(a) Fan speed and Fan-motor power (b) Mass flow rate of air to the zones	
(c) Temperature of air leaving the coil (d) Zone temperatures	
4.15 System responses with PI control and duty cycling	110
(a) Zone temperature responses (b) Zone damper positions	
(c) Discharge air temperature (d) Chiller on-off schedule	
4.16 Zone temperature responses during a typical day operation	111
5.1 A Two-Tier Control Configuration	113
6.1 The schematic diagram of a single zone heating system	138

6.2 Time-of-day energy price structure	144
6.3 Optimal operation of a SZSH system (CV mode)	147-149
(a) Mass flow rate of supply air (b) Normalized heat pump energy input	
(c) Mass flow rate of water (d) Response of zone temperature	
(e) Response of supply water temperature	
(f) Response of discharge air temperature	
(g) Total power required	
(h) Operation cost in US\$	
6.4 Optimal operation of a SZSH system (VAV mode)	150-152
(a) Mass flow rate of supply air (b) Normalized heat pump energy input	
(c) Mass flow rate of water (d) Response of zone temperature	
(e) Response of supply water temperature	
(f) Response of discharge air temperature	
(g) Total power required	
(h) Operation cost in US\$	
6.5 Optimal operation of a SZSH system (GVAV mode)	153-155
(a) Mass flow rate of supply air (b) Normalized heat pump energy input	
(c) Mass flow rate of water (d) Response of zone temperature	
(e) Response of supply water temperature	
(f) Response of discharge air temperature	
(g) Total power required	
(h) Operation cost in US\$	
6.6 The schematic diagram of a two-zone VAV heating system	158
6.7 Global optimal operation of a two-zone VAV heating system	165-166
(a) Mass flow rate of air to zone 1 and 2	
(b) Normalized heat pump energy input	
(c) Static pressure of air flow	
(d) Temperatures of supply air and water	
(e) zone temperatures	
6.8 The floor plan of a five-zone building	168
6.9 The schematic diagram of a five zone cooling system	169
6.10 Global optimal operation of a five-zone VAV cooling system	177-184
(a) Damper position (zone 1)	
(b) Damper position (zone 2)	
(c) Damper position (zone 3)	
(d) Damper position (zone 4)	
(e) Damper position (zone 5)	

- (f) Mass flow rate of air entering to zone 1
- (g) Mass flow rate of air entering to zone 2
- (h) Mass flow rate of air entering to zone 3
- (i) Mass flow rate of air entering to zone 4
- (j) Mass flow rate of air entering to zone 5
- (k) Zone temperature responses
- (l) Zone humidity ratio responses
- (m) Normalized chiller energy input
- (n) Fan speed
- (o) Mass flow rate of water
- (p) Chilled water temperature
- (q) Static pressure
- (r) Discharge air temperature
- (s) Heat extraction rate from zones

LIST OF TABLES

Table 3.1. Parameters of the VAV system.....	69
Table 6.1. Summary of energy consumptions and operating costs.....	157

NOMENCLATURE

A	= cross sectional area (m^2)
A_d	= perimeter of the duct section (m)
A_o	= total area of coil per unit length (m)
A_t	= inside area of tube per unit length (m)
a_0, a_1, a_2	= fitting coefficients
a_{ch}	= heat loss factor of tank ($W/^\circ C$)
B_{eq}	= equivalent frictional factor ($kg\cdot m^2/s$)
C_f	= friction coefficient
C_{fin}	= specific heat of fins ($J/kg\ K$)
C_h	= dimensionless pressure head coefficient
C_{pa}	= specific heat of air at constant pressure ($J/kg\ K$)
C_{pd}	= specific heat of duct material ($J/kg\ K$)
C_t	= specific heat of tube ($J/kg\ K$)
C_{va}	= specific heat of air at constant volume ($J/kg\ K$)
C_w	= specific heat of water ($J/kg\ K$)
C_{ws}	= chilled water tank thermal capacity ($J/^\circ C$)
COP	= coefficient of performance
D	= diameter of impeller blades (m)
E	= energy (J/kg)
EP	= price of energy ($\$/kW\cdot h$)
e_a	= armature voltage (V)
h_{fg}	= heat of vaporization of water (J/kg)
h_t	= heat transfer coefficient between air and tube ($W/m^2\ K$)
$h_{e,d}$	= heat transfer coefficient between air and external surface of duct ($W/m^2\ K$)
$h_{i,d}$	= heat transfer coefficient between air and internal surface of duct ($W/m^2\ K$)
$h_{m,t}$	= mass transfer coefficient between air and tube ($kg/m^2\ s$)
$h_{me,d}$	= mass transfer coefficient between air and external surface of duct ($kg/m^2\ s$)
$h_{mi,d}$	= mass transfer coefficient between air and internal surface of duct ($kg/m^2\ s$)
I	= current (A)
i	= enthalpy (J/kg)
i_z	= specific enthalpy of moist air in zone (J/kg)
J_{eq}	= equivalent moment of inertia ($kg\cdot m^2$)
K_b	= back emf constant ($V\cdot s/rev$)
K_i	= torque constant ($N\cdot m\cdot rev/A$)
L_a	= armature inductance (H)
L	= length (m)
\dot{m}	= mass flow rate (kg/s)
m_a	= mass of air flow per unit length (kg/m)
m_d	= mass of duct material per unit length (kg/m)
m_{fin}	= mass of fin material per unit length (kg/m)
m_t	= mass of tube material per unit length (kg/m)
$m_{w,c}$	= mass of chilled water per unit length (kg/m)
m_w	= humidity load (kg/s)

N	= motor speed (rev/s)
n_m/n_f	= ratio of motor to fan speed
P	= pressure (Pa)
Q	= air flow rate (m^3/s)
q_s	= sensible heat load (W)
q_l	= latent heat load (W)
R_a	= armature resistance (Ω)
T_a	= temperature of air ($^{\circ}C$)
T_d	= temperature of duct ($^{\circ}C$)
$T_{t,o}$	= temperature of tube ($^{\circ}C$)
T_w	= temperature of water ($^{\circ}C$)
U_i	= normalized control inputs
U_c	= normalized energy input to the chiller
V_a	= velocity of air flow (m/s)
$V_{w,c}$	= velocity of chilled water (m/s)
V	= voltage (V)
v_z	= volume of zone (m^3)
W_a	= humidity ratio (kg_w/kg_a)

Greek letters

γ	= ratio of specific heats C_p/C_v
χ_a	= transverse tube spacing (m)
χ_b	= longitudinal tube spacing (m)
η_c	= efficiency of fins in latent heat transfer
$\eta_{c,ov}$	= overall efficiency of fins in latent heat transfer
η_f	= efficiency of fan
η_s	= efficiency of fins in sensible heat transfer
$\eta_{s,ov}$	= overall efficiency of fins in sensible heat transfer
λ	= latent heat of evaporation (J/kg)
μ	= absolute viscosity ($Pa \cdot s$)
ρ	= density of air (kg/m^3)

Subscripts

a	= referring to air
d	= referring to duct
e	= referring to external surface
f	= referring to fan
fin	= referring to fin
i	= referring to internal surface
max	= referring to maximum value
st	= referring to saturation
to	= referring to tube
w	= referring to water
z	= referring to zone
∞	= referring to environment

Chapter 1

Introduction

One of the major objectives of installing energy-management control (EMC) systems in buildings is to improve the energy efficiency of heating, ventilating and air-conditioning (HVAC) systems. This is achieved by incorporating several optimizing functions in EMC systems and performing real-time adjustments to the HVAC processes. Typical optimization functions in common use include: start-stop optimization, hot/cold deck temperature reset, discharge-air temperature reset, chilled water temperature reset, air-distribution optimization and the outdoor-air economizer cycle (Payne and McGowan, 1988). However, the consensus is that most EMC systems in practice have not performed to their potential with respect to optimizing functions. One of the reasons for poor performance is the fact that HVAC processes are optimized at the local loop level, which does not include systemwide process-to-process interactions.

Consider a typical variable air volume (VAV) HVAC system. The thermal processes taking place in a VAV system can be grouped as follows: sensible and latent energy flows in the zones and in the cooling coil; energy extracted from and added to the water; airflow rates in the duct system; mixing of outdoor and bypass air with the recirculated and discharge air, respectively; and conversion of electrical energy into static pressure at the fan and pump outlets. Because of the fact that several multiple processes are simultaneously undergoing changes and interacting with each other, a systems approach is necessary to accurately model these processes and their interactions. It is only

then feasible to find improved solutions to the problem of optimizing the thermal processes in VAV systems. To address the need of global optimal operation of VAV systems, a system level model and an optimization methodology are required.

This thesis deals with the development of a modeling methodology for the system-level models for VAV systems and presents an optimization technique for global optimal operation of VAV systems subject to realistic operating constraints. Emphasis is placed on (i) the application of fundamental principles to develop an analytical system-level models of VAV systems using both bottom-up and top-down approaches, (ii) the application of optimal control theory such as the maximum principle of Pontryagin and perturbation method to develop a methodology for determining the global dynamic optimal setpoint profiles for local controllers subject to realistic operating conditions which include the multiple operation schedules such as normal operation, off-normal operation and start-up.

1.1 Variable Air Volume HVAC systems

The all-air systems have been widely used in HVAC applications. In terms of their working and control method, the all-air HVAC systems can be broadly classified into two categories, namely, 1) constant volume (CV) systems and 2) variable air volume (VAV) systems (McQuiston and Parker 1988).

Control of the dry-bulb temperature and humidity ratio within a space requires a balance between the space load and the capacity of the supply air delivered to the space to offset the load. The designer can alter the supply air temperature while maintaining constant air volume. Single duct constant volume systems use this concept. One drawback of the CV systems is that the fan energy consumption remains the same irrespective of the

zone loads. Another drawback is that the single duct CV system can not supply conditioned air at different temperatures to meet the needs of individual zones. To overcome this problem, the supply air temperature is cooled to satisfy the zone with maximum load (cooling case) and then reheated to meet the needs of zones experiencing moderate to low loads. This reheating practice used in CV system contributes to energy waste.

On the other hand, a class of all-air systems that minimize the energy wastage and yet provides good control of dry bulb temperature within a space is known as variable air volume (VAV) system. In VAV systems the dry-bulb temperature within a space is controlled by varying the volume of supply air rather than the supply air temperature. Since the building HVAC loads generally vary considerably during occupied periods, specially in the perimeter zones, the HVAC system must be able to respond to these changes. The VAV systems are capable of supplying variable quantities of air to different zones to offset different loads. Since the quantity of supply air is proportional to the fan speed and fan power is proportional to cube of the fan speed, it is evident that at low loads only low quantities of air are required and hence considerable amount of fan energy could be saved. It is because of this energy saving potential, VAV systems have become quite popular in HVAC applications in the last 30 years.

However, whereas these systems are efficient, and expected to contribute to energy conservation, in some buildings numerous problems have been reported when VAV system did not function as intended. Since the VAV systems modulate the air flow rates as a function of load, poor control can give rise to a number of problems:

1. Because of the constant discharge air temperature maintained through out the day, too great a reduction in air flow will be necessary during the low-load period. This can lead to poor air distribution, inadequate ventilation, and high humidity within the space.
2. Variable air flow rates across the cooling coil can make control of discharge air temperature more difficult because of coupled heat and mass transfer processes taking place in the cooling coil.
3. In any VAV system the available static pressure will vary widely from one VAV terminal box to another. This means, the modulation of dampers in one zone will affect the airflow rates to other neighboring zones. To overcome this problem, some means of compensation must be used if adequate airflow and good zone temperature control are to be obtained.

Some researchers (Gupta 1987, Roberts 1987, Wessel 1987, Woods 1990) pointed out that these problems are mainly due to poor design and poor maintenance. For example, Woods (1990) investigated on common deficiencies in HVAC systems. In the HVAC systems investigated, 90% of the operational problems came from poor control strategies.

1.2 Importance of Global Optimal Operation of VAV systems

In most buildings the VAV systems provide air at constant temperature year round. This practice is not necessarily the most economical. In fact, it is because of this practice that numerous problems occur during part load operation of VAV systems. Therefore, it is recognized that the basic principle of a VAV system should be to control

both the volume and the temperature of air being introduced into a space for heating, ventilation, and air-conditioning. For example, it might be desirable to raise the supply air temperature during periods of part load to maintain adequate ventilation rates (in the cooling case). This strategy causes the fan to use more energy, but it also allows energy saving in other areas. For example, if the supply air temperature is raised, the chilled water temperature can also be raised with energy saving in chiller plant. If the outdoor temperature is low enough, it might be possible to eliminate or minimize the use of chilled water. Therefore, it is necessary to achieve the optimal performance of the system from the point of view of the whole system rather than the fan energy consumption alone.

To achieve this objective, a supervisory control system such as the energy management and control (EMC) system should have the capabilities to compute the desired time-of-day optimal setpoint profiles for the local controllers (Figure 1.1). The local controllers track the optimal setpoint profiles so that the HVAC system moves optimally from the current state to the new setpoint. These control schemes will improve the performance of VAV system in terms of providing good temperature and humidity control and as well as in reducing the energy costs significantly.

Several studies (Mehta 1987, Hartman 1988) have shown that the building, the HVAC system, and the control system are strongly coupled thermally. It is important to analyze the dynamic interactions between the building and all VAV components, and control system. However, because of the high nonlinearity and strong coupling between the various components until now, the dynamic interactions between the building and all VAV system components, and control system have not been examined. To address this need, a dynamic model of a VAV system which is suitable for control analysis is

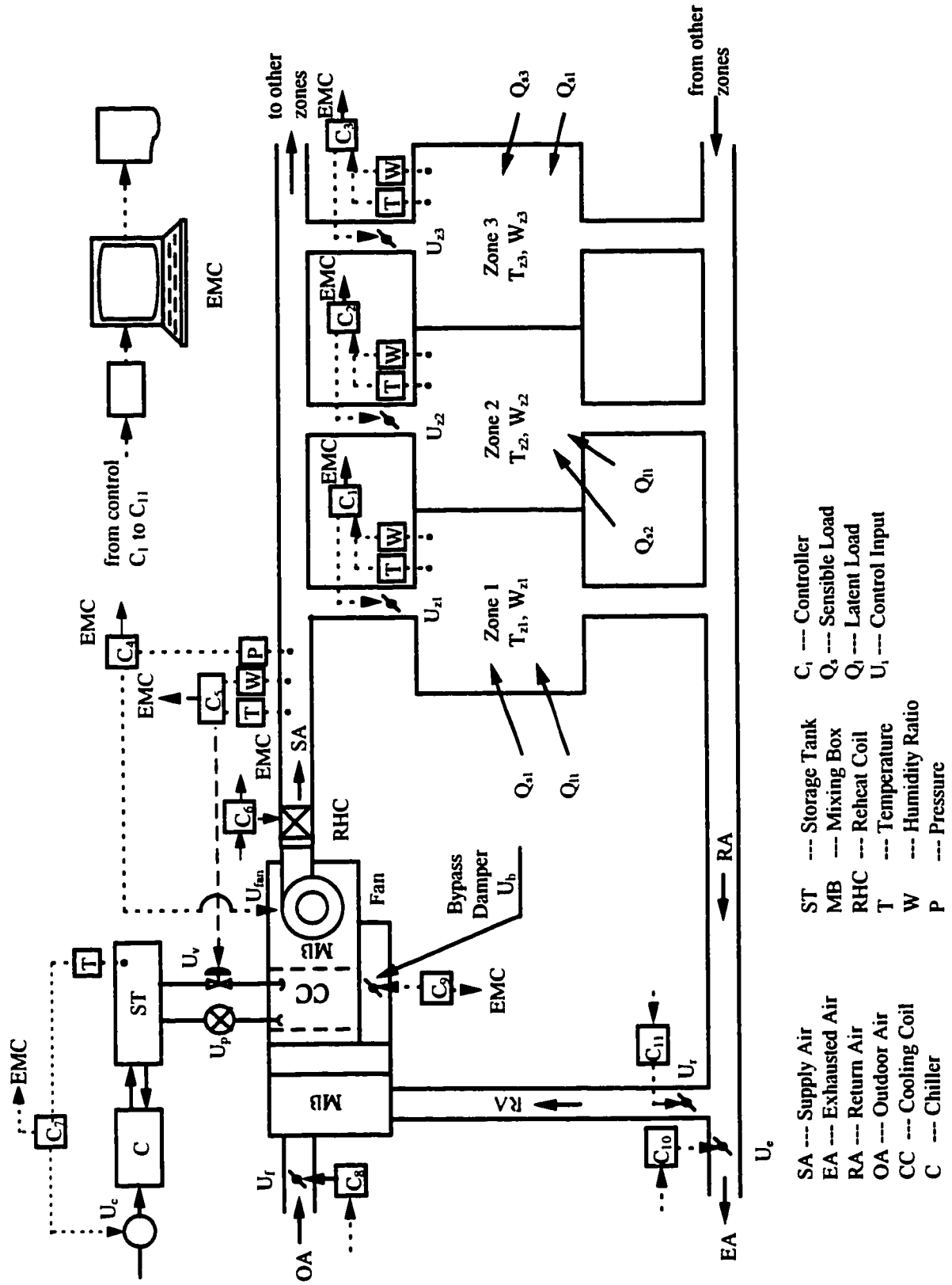


Figure 1.1 Schematic diagram of Energy Management and Control for a VAV system

required. Such a model will be useful not only for control analysis and design, but also for parametric analysis and to study the transient responses of the system under various operating modes. From the predicted responses the designer can check how a change in one particular parameter will affect the time required for the system to reach steady state. Furthermore, the model can be used to study the start-up and shut-down time responses of the VAV system. This will help the operator to determine the optimal start-up and shut-down time. The model can also be used for simulation of the control system to check the control system performance. Most importantly, the model can be used for the design of efficient control systems, specially for determining the global optimal control profiles of HVAC systems.

1.3 Scope and Objectives

The focus of this study is on modeling and optimal control of a multi-zone VAV system. The methodology to be described in the study can be applied to model other types of HVAC systems.

The main objectives of this study are the following:

- 1) To develop a dynamic analytical system-level model that can integrate the building loads and all the components of a multi-zone VAV system together, including (1) the environmental zones, (2) chiller and storage tank (3) cooling and dehumidifying coil, (4) fan and ductwork, such that the interactions between the building and VAV control system can be systematically analyzed.
- 2) To develop a methodology for multiple stage dynamic optimal operation problem to determine the optimal setpoint profiles (based on predicted loads)

for the VAV system which can be used to operate the VAV systems more efficiently. These setpoint profiles include the supply air temperature, the chilled or hot water temperature, and the static pressure.

- 3) To demonstrate the potential for energy savings and improved comfort of the proposed control strategies through several practical examples.

1.4 Contributions and Summary

The main contributions of this thesis are the following:

1. Based on the principles of mass, momentum and energy balances, a dynamic system-level model of a multi-zone VAV system is developed using two different approaches, bottom-up and top-down approaches. The developed model is useful for studying interactions between building loads, VAV system, and control system as a single large-scale multivariable system. The model can be used to simulate the performance of various energy management and control strategies.
2. A multiple stage optimization methodology is developed which combines the optimal control theory and perturbation method. The methodology is successfully applied to determine the global optimal setpoint profiles for multizone VAV systems.
3. Application of the model and optimization methodology are demonstrated by several practical building operation problems.

The remainder of the thesis is arranged into six chapters. In the next chapter, a literature review on modeling and control of HVAC systems is presented. This is followed by defining the objectives of this thesis.

In Chapter 3, the detailed dynamic models of HVAC system components and the detailed system-level model are developed using the bottom-up approach. The open-loop performance of VAV systems is given.

In Chapter 4, a reduced-order dynamic model of VAV system is developed using the top-down approach. The open-loop simulation results of reduced-order dynamic model are presented and compared with those from the detailed models. Some applications of the developed models such as simulation of several EMC (Energy Management and Control) functions are presented.

In Chapter 5, a methodology for multiple stage optimal operation problems is presented.

Three different examples showing the applications of the optimization methodology in terms of achieving energy efficiency and temperature control are illustrated in Chapter 6.

Conclusions, contributions of this thesis work and recommendations for future research are given in Chapter 7.

In the Appendix A, the modeling of building shell employed in this thesis is presented.

Chapter 2

Literature Review

The growing concerns about energy conservation and indoor environment have motivated extensive research on various aspects of control of HVAC and building systems. The study on optimal operation as well as modeling of HVAC and building systems is one of the fastest growing fields that contribute to saving energy and improving indoor environment.

In this chapter, the review is divided into two sections. Section 2.1 deals with the review of component and system-level HVAC models. In Section 2.2, the review of control studies will be given including traditional control, optimal control and building energy management. In Section 2.3, the objectives of this thesis are stated.

2.1 Modeling

In this section, attention is focused on modeling of HVAC components as well as building shell. The component models are reviewed including the models of heating coil, cooling and dehumidifying coil, chiller, environmental zone, duct and fan-motor and building shell.

2.1.1 Component Models

Many researchers have studied the dynamic models of HVAC components. We can classify the existing models in two categories: (i) Steady State Models, (ii) Transient Models. Each category contains both empirical models and theoretical models.

Empirical models use a simple "black box" concept that is partially supported by physical laws or that ignores physical laws (Yuill and Wray 1990). Statistical analyses with or without aided by a knowledge of general engineering principles are used to select input variables that are important in representing equipment that directly relates the input variables to the desired output variables. Regression analysis is used to fit the equations to discrete performance data obtained from the equipment manufacturer, from laboratory tests, or from more detailed models. The empirical models can be used to predict equipment performance within the range of available test data for the particular equipment operating in a specific environment. However they cannot be used to forecast performance outside this range of test data, or for other similar type of equipment operating in different environments. This trait extremely restrains the flexibility of applications for this approach. The simplicities of these models make them particularly suitable to be used in adaptive control modeling. The parameters required can be updated from the on-line measurement.

Theoretical models rely on fundamental physical laws. They use the general principles of thermodynamics, heat, mass and momentum transfer to predict pressures, temperatures, fluid flow rates to, from and within each component of the equipment. Information is required about the interactions between equipment components and the physical dimensions, properties, and processes that determine the behavior of the equipment. Little or no performance test data are used, since most of the information

required is obtained from physical descriptions of the equipment and its components. Sometimes, empirical correlations are used to fill in gaps in the theory. This approach permits more simulation flexibility than the semi-empirical approach. The models can be used to predict equipment performance within the range of applicability of the theories or correlations used in the models.

2.1.1.1. Coil Model

The heating or cooling coil is the most important interface between the primary plant (e.g., chiller, heat pump, boiler) and the secondary air distribution. Because of this importance many models for the heating or cooling coil have been developed.

Extensive research has been done on developing the heating coil and sensible cooling coil models (heat exchanger model). Most of the models are the type of steady state. Miller (1982) used the empirical relationships based on the steady state characteristics of cooling coils. Zhang and Warren (1988) used such steady state relationships to model the sensible gain of a cooling coil based on the air- and water-side effectiveness of the coil, as described in the ASHRAE 1986 Fundamentals (1986), for a counterflow heat exchanger. The time constant was computed on the assumption that the coil was a block of metal and was therefore equal to the product of the heat resistance and capacitance of the coil material. Braun et al. (1989a) developed a steady-state effectiveness model for cooling and dehumidifying coil by utilizing the assumption of a linearized air saturation enthalpy. Oskarsson et al. (1990a, 1990b) developed a steady-state evaporator model for operation with dry, wet and frosted finned surfaces. Hill and Jeter (1991) developed a linear subgrid cooling and dehumidification coil model. They

linearized the air process path and used a single-pass refrigerant in cross-flow to obtain the exit states of the refrigerant and air. Khan (1994) developed a steady-state model for cooling and dehumidifying coil by using the NTU approach and applied his model to analyze the part load performance of cooling coil.

Much literature is available for predicting the transient response characteristics of a sensible coil by use of governing equations. One way of characterizing the dynamic response of a coil that has been studied extensively is to use the governing differential equations (Myers et al. 1965, 1967). This approach is simplified by the assumption that one fluid has an infinite capacitance (Myers et al. 1970). Gartner and Harrison (1963) developed a model for a straight tube in cross-flow by considering variations in various temperatures along the axis of the tube. Partial differential equations in space and time were developed based on the energy balance principles to describe the dynamics of the coil. The method of Laplace transforms was used later to obtain transfer function relations for different coil parameters. Gartner and Harrison (1965) extended the above model to a finned tube crossflow heat exchanger. Gartner (1972) used a first-order simplification to find the effect of water modulation on the transient response of the coil. The transient response to step change was used as a way of finding the dynamic characteristics (Myers et al. 1965, 1967). Transfer function relations have been found by others (Gartner and Harrison 1963, McNamara and Harrison 1967, Gartner and Daane 1969, Tamm 1969) for different coil parameters. A number of simplifying models were also developed (Tobias 1973, Bhargava et al. 1975, Stoecker et al. 1978). Many studies have included experiments to verify the accuracy of the coil models (Gartner and Harrison 1965, Gartner and Daane 1969, Tamm and Green 1973). In order to obtain the transfer function, in the

studies mentioned above, they all assumed the heat transfer coefficients of primary and secondary fluids independent of the mass flow rates. Furthermore, they did not find the input-output relationship.

As we will see later, the cooling coil is rarely operated in sensible mode, even in the case of controlling the zone temperatures. The sensible cooling coil models have very limited range of applications. Therefore it is important to consider the dynamic characteristics of dehumidification in cooling coil process. However, the dynamic characteristics of cooling and dehumidifying coils have received much less attention than the dynamic characteristics of heating coils. This is due to the complexity of the combined effects of heat and mass transfer in cooling and dehumidifying process. McCullagh et al. (1969) and Elmahdy (1975) developed transient models of the chilled water cooling and dehumidifying coil. The developed equations (Elmahdy 1975) were obtained by treating the time and space as independent variables and humidity ratio, air, water and tube temperature as dependent variables. The model developed by Elmahdy (1975) is a good dynamic model that accounts for the fin efficiency, air and water-side heat transfer coefficients, and parameters that were not included in other models. However, he only studied steady-state performance of the cooling and dehumidifying coil. Clark et al. (1985) developed a model that is used in HVACSIM⁺ program. By first solving a steady-state problem based on the model developed by Elmahdy (1975), they developed a first order lumped-capacity model for the coil in which the time constant (determined from experiments) of the coil is introduced as a parameter.

McQuiston (1978) correlated the heat transfer coefficients of the coil during cooling and dehumidifying processes from experimental data and presented them in

empirical form as a function of air and water flow rate. In other studies, Tamm and Green (1973), Pearson and Leonard (1974), O'Neill (1988) and Maxwell et al. (1989) determined the cooling and dehumidifying coil gain and time constant through experiments. Underwood and Crawford (1991) developed an empirical nonlinear transient model of a hot-water-to-air coil.

2.1.1.2. Chiller Model

In the summer cooling case, chillers are needed to provide chilled water to the cooling coil to extract heat (cooling load) from the air streams across the cooling coils. Cooling towers are typically used to reject heat from the condenser of a chiller to the outside environment. The chilled water temperature can be controlled by modulating the chiller refrigerant flow and modulating the speed of the driver. Therefore, a typical chiller plant consists of one or more chillers with distribution piping, and evaporative cooling towers with condenser water pumps (Haines 1988, Spethmann 1985, Wong and Wang 1989, and Johnson 1985).

Many researchers have concentrated on the study of optimizing the chiller plant's energy consumption utilizing a central energy management and control system (Williams 1985) which includes direct digital control (Johnson 1985). Mitchell (1988) and Braun et al. (1987, 1989a, 1989b, 1989c) studied the performance and control characteristics of a large variable speed drive chiller system at discrete steady-state operating points. They concluded that the savings associated with the use of variable-speed control are significant at part-load conditions (40% savings).

Spethmann (1985), Kirshenbaum (1987), Waller (1988) and Wong and Wang(1989) stated that the chiller steady-state operating characteristics, such as pressure, temperature, fluid flow, heat transfer, and power input, are influenced by many factors, i.e., (i) the ratio of the operating refrigeration load to the design full-load, (ii) entering temperature of condenser water, (iii) constructional characteristics of the chiller, and (iv) control characteristics of the chiller at part-load operation.

Wong and Wang (1989) developed a simple model representing transient characteristics of the evaporator and condenser. Zaheer-uddin and Wang (1992) developed a transient model for a chiller and evaporative cooling system.

2.1.1.3. Zone and Building Shell Models

An important component model of HVAC system is the model describing the thermal behavior of the building. The zone models vary widely in complexity from simple to detailed. Simple models are first order models. A simple room model having a single-input, single-output transfer function was investigated by Zermuehlen and Harrison (1965) and Harrison et al. (1968). Major assumptions include perfect mixing and thermal storage only by the room air. Mehta (1980) and Mehta and Woods (1980) formulated a model for the dynamic response of a room assuming a uniform mixing of the room air. In their studies, the heat capacity of the furnishings was added to the room air heat capacity and the thermal capacity of the walls was neglected. However, the capacity was eventually taken into account by linearizing the experimental results around different operating points. A review covering various approaches regarding room models was given by Thompson and Chen (1979). They concluded that for closed loop control analysis the

simplified models based on full mixing of the room air would often be sufficient. More detailed discussion of four simplified dynamic room models was given by Borresen (1981). These models take into account the thermal interaction between room air and surrounding walls in different way.

Detailed models consider the thermal mass in the building that is useful for simulation of the loads (DOE-2 1981, BLAST 1979, Walton 1983). These detailed models differ in the way they model the effect of radiation and other thermal effects. A detailed model of a single zone was developed and validated by Zaheer-uddin (1986).

2.1.1.4. Duct and Fan-Motor Models

Several researchers have studied the thermal performance of the ductwork based on the constant mass flow rate. A thermal model of a duct was given by Harriott (1964) and Gartner and Harrison (1963). The model was simplified by Tobias (1973) to get the analytical solution to describe the thermal performance of the ductwork. Later, Grot and Harje (1981) presented a similar model but further assumed forced convection as the dominant heat transfer mechanism and neglected storage effects as well as axial wall conduction.

Similarly, the researchers were mainly interested in the temperature difference across the fan, and energy consumption at steady state fan speed. (HVACSIM⁺ 1986, Brothers and Warren 1986, DOE-2 1981, BLAST 1979, BESA 1987).

Pinnella (1986) developed a motor model describing the torque balance on the axis of the motor. He assumed the fan operated in steady state.

In all these models, air distribution in the ductwork of the multizone VAV system and the transient response of motor and corresponding air flow rates are not examined.

2.1.2 Overall System Models

In addition to the component models discussed above, effort is also being devoted to system models. A system model includes a complete set of HVAC components. Stoecker (1976) modeled a HVAC system with polynomial expressions whose coefficients were determined through experimental or on-site performance data. This formulation is quite valuable for estimating the steady state operation of an HVAC system. A dynamic model was developed by Thompson and Chen (1979) and Thompson (1981) that included transfer function expressions for various HVAC components. These linear component models were strung together to model a HVAC system. Though they developed a digital simulation scheme to identify energy sensitive parameters, they did not study the effects of system dynamics. Mehta (1984) described the concept of a rational model, which included the dynamic interaction between the HVAC system and the heating/cooling loads. This approach had been suggested by an earlier successful experimental validation (Mehta and Woods 1980) of HVAC models, obtained by linking proper modular blocks.

Apart from the studies mentioned above, several public domain programs have been developed which simulate the building and HVAC system operation. These simulation programs for modeling the dynamic behavior of building and HVAC systems are discussed by Kelly (1988). The programs, based on hourly simulation, such as DOE-2 (1981) and BLAST (1979), may be employed to simulate the quasi-dynamic-type operation of building systems for designing large buildings. Since they did not take control

dynamics into account, these programs are not suitable as tools to design control systems for HVAC.

The simulation program BLDSIM developed by Shavit (1977) can be used to calculate the building load, the energy requirement of different mechanical systems as a function of the type of controls employed, and total building energy consumption. Simulation is done with a typical time step of one minute to a few minutes, which enables one to study the effect of different HVAC systems and control alternatives on building energy consumption and thermal comfort in terms of temperature and humidity ratio.

The TRANSYS (Transient System Simulation) Program is one of these simulation programs released by the Solar Energy Laboratory at the University of Wisconsin-Madison (Klein et al., 1983). TRANSYS has a modular structure that allows the interconnection of system components in any desired manner, iterates by substitution to solve the system of equations defined by the component models and their interconnections, and facilitates the analysis and output of information resulting from the simulation. Originally employed primarily in the simulation of solar energy systems, it has undergone many revisions and expansions and is now a simulation program involving some HVAC components such as heating/cooling plants.

A different approach to building and HVAC system simulation is employed in the GEMS program developed around 1982 (Benton et al. 1982). It used state-space analysis techniques and casts linear and linearized models into a vector-matrix form. The building shell is modeled as a linear resistance-capacitance (RC) network that can be solved using sparse vector-matrix multiplication techniques to reduce simulation time and costs. Nonlinear models, such as furnace, air conditioner, or thermostat models are contained in

a library of nonlinear components. The system to be simulated is constructed by interconnecting the input/output vectors of the various subsystem modules. The use of multirate integration steps within a simulation enables modules with very fast dynamics and/or strong nonlinearities to be solved at a time step necessary for accuracy and stability.

The HVACSIM⁺ program was developed by National Bureau of Standards (Park et al. 1985, Clark et al. 1985), as a research tool for studying the dynamic interactions between the building shell, the HVAC system and control system. It uses advanced nonlinear equation solution techniques to solve systems of differential and algebraic equations, and utilizes a modular approach that was adapted from TRNSYS.

These programs were developed from the viewpoint of simulating different building (dynamic models) and system configurations (steady state, or quasi-dynamic models) and to study the impact of building & system operation on energy consumption. These programs did not involve the input/output relation. They are not intended for analysis and design of control systems.

Zaheer-uddin and Goh (1991) proposed a constant fan speed model of a single zone VAV system, which is useful to study thermal performance of the system.

The most important characteristic of a VAV system is the control of air flow rates. Therefore constant air flow models can not be used to study the transient response characteristics of VAV system.

2.2 Control Studies

Traditional control methodologies such as bang-bang and PID (Proportional-Integral-Derivative) control, that remain quite popular today, have been used in HVAC applications for decades. The popularity is mainly due to their relative simplicity. Many studies related to these controls can be found in the literature, most of them are for the purpose of simulating the control system, not for the design of control systems. For example, Shavit and Brandt (1982) simulated a discharge air temperature control system using an analog proportional plus integral controller for a heating coil. Nesler and Stoecker (1984) and Nesler (1986) studied a method of selecting the PI (Proportional-Integral) constants of the DDC (direct digital control) for discharge air temperature with parameter estimation. Pinnella et al. (1986) designed an integral-only control for fan static pressure control, in which a dynamic model of the motor and a steady state model of fan were employed. Roberts and Oak (1991) simulated the temperature control of a single zone environmental chamber operated in the heating mode by using P (Proportional) controllers for bypass damper, on-off controllers for electric heater to control single zone temperature. Ahmed (1991) studied a DDC-based variable-water-volume system using PID controllers. Wallenborg (1991) designed a general linear discrete time controller using pole placement based on input/output models for control of air temperature and air duct pressure. Zaheer-uddin and Goh (1991) developed a feedback PID type control algorithm for a single zone VAV system. Zhang and Nelson (1992) simulated PI control of temperature for a single zone based on the constant supply air temperature. Their study did not address the problem associated with the system interactions nor those associated with VAV air distribution system. Kamimura et. al. (1994) developed a computer-aided

tuning software for the tuning of PID controllers in a situation in which the transfer functions of the controlled plants are known perfectly. The tuning methods included the ultimate sensitivity method, step response method, frequency-response method and optimization method. All plant models were limited to linear systems and one-input/one-output systems. Krakow and Lin (1995) studied the selection of PI coefficients and sampling interval to avoid system instabilities of fan speed controllers to maintain constant discharge pressure.

Optimal control is utilized in HVAC systems primarily for energy conservation and thermal comfort improvement. An integral cost function should be established for searching the optimal control strategy. Typically, cost functions consist of two types of terms, namely, a term representing the energy use of components within the system and a penalty term used to enforce system constraints or to maintain system variables near setpoint values. The cost function is then minimized or maximized, depending on the choice of cost function, over the duration of the time interval of interest. Many studies related to optimal control of HVAC systems are available in the literature. Fan et al. (1970a, 1970b, 1970c, 1970d, 1970e) studied the application of modern control concepts to HVAC systems. They considered a single room model and discussed the feasibility of modern control applications. Nakanishi et al. (1973a, 1973b) considered the problem of simultaneous temperature and humidity controls for a single zone space. Nonlinear differential equations resulting from the material and mass balances were linearized around two setpoints corresponding to summer and winter operation. Nakanishi's work demonstrated that modern control formulations could eliminate some of the empiricism used in the classical control design of HVAC control systems. Kaya (1976, 1979, 1981)

and Kaya et al. (1982) engaged into the problem of the optimal control of a single zone space. Kaya (1976, 1979, 1981) developed an optimal control model featuring a linearized dynamic model for a thermal space and an associated cost function. The objective of the model was to derive the conditions within the space into a thermal comfort region and to force the conditions to remain within the thermal comfort region. Temperature, humidity, and air velocity were considered as thermal comfort factors. Kaya et al. (1982) employed a similar approach for an extended system model. The optimum steady state setpoints were first determined. A control action was taken by a PI controller according to optimal control setpoint that minimizes the deviations from the steady state points. The main objective of the study was to demonstrate the improvement in control and reduction in energy expenditure for controlling temperature, humidity, and velocity simultaneously rather than independently. The optimal control solution consisted of static and dynamic optimization. The findings indicated that the proposed control system, which accounts for control variable interactions, resulted in reduced energy use. Sud (1984) discussed a three-step hourly based optimization procedure for minimizing the energy usage, which included operational modes and control hierarchies. Cherches et al. (1985) used a bilinear mathematical model to design a DDC algorithm for controlling the dry bulb temperature of a single zone and considered a control strategy that combines PID, feedforward, and optimal control for regulating the temperature within a thermal space. The control strategy was based on maintaining the temperature within the thermal space near a setpoint value, and a linear cost function was employed. Townsend et al. (1986) utilized the maximum principle to determine optimal on-off control of a fan and heating coil in order to minimize

a cost function. The optimal on-off control was found to produce lower operating costs than the control strategy proposed by Cherches et al. (1985).

Nizet et al. (1984) developed an optimal control method for simplified dynamic model for one floor of a typical multi-story building. The objective of the study was to find the optimal air-conditioning policy to minimize energy use. The cost function consisted of energy costs for components and a thermal comfort penalty. The problem was solved using conjugate gradient method, and energy savings of 12% to 30% were reported for the optimal control policy in comparison to the normal regulation law for the system. The authors, however, noted that, for problems involving constraints, an alternative solution methodology was needed. Braun (1988), Braun et al. (1989b, 1989c) and Braun and Diderrich (1990) developed an algorithm for near-optimal control of central cooling plants for estimating the control parameters. Shoureshi and Rahmani (1989) developed an optimal control problem in which thermal comfort was to be maximized while energy and operating costs of a building system were minimized. A fuzzy optimal controller was utilized for control decisions in which “approximate reasoning” was required. Decisions involving thermal comfort were cited as typical functions of the fuzzy optimal controller. House et al. (1991) described an optimal control methodology for an electrical heating system with single zone environment. The solution approach involved discretizing the optimal control problem in time and determining optimal values of the control variables at discrete times. The optimal state variable response was computed from the discrete optimal control variable set. Their results show that the optimal control scheme using continuously varying control variables has some advantages over bang-bang control in terms of lower costs and fewer oscillations. Boyens and Mitchell (1991) developed a

methodology for steady-state optimization of a simple heating system consisting of a fan and a gas-fired furnace. Virk and Loveday (1991) presented a performance comparison of an DDC based predictive control with conventional on/off and PID control methods for the control of temperature in a single zone heating system. Zaheer-uddin (1992a) applied the linear quadratic optimal regulator theory to the problem of optimizing the operation of a heat pump heating system when the energy storage capability exists in two forms: as active storage in the form of a hot water storage tank and passive storage as a result of the heat storage in the enclosure elements of the environmental space. Zaheer-uddin (1992b) developed a decentralized control system for a HVAC system. Zaheer-uddin and Patel (1993) studied the sub-optimal control of a single-zone space heating problem. They linearized the developed bilinear model and solved the Riccati equation to find the optimal control law. Zaheer-uddin (1994) developed a decentralized preview control design method for a HVAC system based on optimization techniques using bilinear models by treating the disturbances as previewable terms. These studies have shown that significant reduction in energy costs can be achieved without loss of thermal comfort through the use of optimal control.

Some studies on *building energy management* (Belghith et al. 1985, Benard et al. 1987, Bloomfield and Fisk 1977, Dorato 1983, Winn and Winn 1985) have shown that both thermal comfort and energy saving could be greatly improved. Such an improvement can be achieved by controlling the HVAC system in such a way that all the dynamic aspects of the problem are considered: building thermal inertia, intermittent occupation, time-dependent energy rates, and natural energy gains. Benard et al. (1992a, 1992b) proposed a methodology of solving building energy management problems with the

technique of optimal control of electrical heating system. The approach consisted of describing the dynamic behavior of a heated building with a simple model and controlling the whole system by minimizing a criterion defined for a time horizon of a few days. Englander and Norford (1992a) pointed out the measurements revealed that reducing supply duct static pressure can significantly boost the savings achievable with variable speed-drive systems. Englander and Norford (1992b) described two methods of controlling the supply fan to minimize duct static pressure without sacrificing occupant thermal comfort or adequate ventilation for a DDC fan-powered terminal box, VAV supply fan, single zone system in which they treated the fan model as a steady state model. Both methods use feedback from the zone flow controllers but take quite different approaches. The first, a heuristic method, is a computerized implementation of a simple three-step procedure that might be followed by an ideal building operator whose only purpose is to minimize static pressure while keeping zone flow requirements satisfied. The other is a discrete-time implementation of classic PI control with a rather unconventional modification intended to continually "force" the controller output (and hence fan speed) to decrease. They (Englander and Norford 1992a, 1992b) considered saving fan energy only rather than saving the total energy.

Global optimal operation of HVAC and building systems has attracted more attention. Zheng and Zaheer-uddin (1996) developed a methodology to compute the optimal setpoint profiles for local controllers based on steady-state models of HVAC systems and dynamic building operation considering both temperature and humidity controls. They showed that the setpoint profiles for both temperature and humidity controls would be significantly different from those for temperature control only. Kintner-

Meyer and Emery (1995a, 1995b) investigated the optimal control of HVAC system components operation using cold storage and the thermal capacitance of the building. A 24 hour optimization that determines the least cost control protocol for chilled water loop system components was performed. In their study, performance index function to be minimized was defined:

$$Z = \sum_{k=1}^{24} (P_{chill,direct} + P_{chill,store} + P_{pump,cw} + P_{pump,store} + P_{fan,AH})_k E_k \Delta t + P_{max} \left(\frac{D}{30} \right)$$

where the terms $P_{chill,direct}$, $P_{chill,store}$, $P_{pump,cw}$, $P_{pump,store}$, $P_{fan,AH}$ indicate the power of chiller in direct mode, power of chiller in storage mode, power of pump for chilled water pumping and storing energy, power of fan for air handling system, and E is the price of energy. P_{max} is maximum value over a 24 hour period. The calculation of these terms is not given in their paper. House and Smith (1995) investigated the problem of optimal control of HVAC and building systems by using a systems approach. In their study, with the zone envelop modeled as a single lumped capacitance model, and no storage component in the HVAC system, an optimal operation problem was solved with 24 hour continuous operation of HVAC system. The performance index to be minimized was defined as:

$$J = \int_{t_0}^{t_f} \left\{ \sum_{j=1}^{N_z} [\alpha_{T_j,tc} (T_j - T_{j,set})^2 + \alpha_{f_j,dc} (f_j - f_{j,set})^2 + \alpha_{PMV_j,oc} (PMV_j - PMV_{j,set})^2] \right. \\ \left. + \alpha_{cc} F_{cc}^n + \alpha_{hc} F_{hc}^n + \sum_{j=1}^{N_z} \alpha_{rj} F_{rj}^n + \alpha_{fj} (f_{fj}^3)^n + \alpha_{rj} (f_{rj}^3)^n \right\} dt$$

where F_{cc} , F_{hc} , F_{rj} are the fuel used for cooling coil, heat coil and reheat coil, respectively. f_j is the volumetric airflow rate at the inlet to zone j , is PMV index value. $T_{j,set}$, $f_{j,set}$, and $PMV_{j,set}$ are the setpoint of T_j , f_j , PMV_j . One has to determine the setpoint of volumetric

airflow rate for each zone in order to use their method. Actually the setpoint profiles of volumetric airflow rate for each zone should be determined by optimal techniques. Note that in the above studies, the single stage optimal operation problem was considered, i.e., the HVAC system was running continuously to maintain zone air conditions all the day. Keeney and Braun (1996) developed a simplified method for determining optimal cooling control strategies for thermal storage in building mass. In their study, the only control variable is the storage energy rate Q . Using hourly time-steps, they reduced the daily optimization problem from 24 variables Q_i to 2 variables Q_1 and Q_2 , where Q_1 , Q_2 are the constant storage energy rates searched in certain amount of time at precooling period. In the occupied period, a set of rules in terms of occupant comfort was employed. Their method is only useful for their heuristic control strategies but not for global optimal control strategies.

Load prediction is a necessary step for the global optimal operation of HVAC and building systems. Some studies have been done in this area. For example, Kimbara et. al. (1995) applied ARIMA (autoregressive integrate moving average model) to predict the load profile which will be updated every hour on the basis of the newly obtained load data. Kawashima et. al. (1995) used a cooling and heating seasonal data set with known next-day weather to evaluate the accuracy of each prediction methods of ARIMA, EWMA (an exponential weighted moving average model), LR (linear regressive model) ANN (artificial neural network). The results indicate that an ANN model produces the most accurate thermal load predictions after proper training.

Adaptive Control has recently received increasing attention in HVAC applications mainly due to its distinctive capability to compensate for unknown system parameters,

nonlinear and dynamic variation of the system, long-term or seasonal changes in the operation of the process, and non-stationary disturbances acting on the process. Farris et al. (1977) developed adaptive control schemes that could automatically tune themselves to optimize the overall performance of a solar heated building. Schumann (1980) presented a simple air-conditioning system using a parameter-adaptive deadbeat controller and parameter-adaptive optimal state controller. There were also works devoted to the parameter estimation issue, which was considered as a major step toward the use of adaptive control. Forrester and Wepfer (1984) and Li and Wepfer (1985) applied off-line least squares estimation schemes to data taken from a large commercial office building and developed a load prediction algorithm. Li and Wepfer (1987) also developed an on-line recursive estimation method for a multi-input/multi-output single zone HVAC system. Chen and Lee (1990) described an adaptive robust control scheme to control the zone temperature and humidity ratio of a single-zone HVAC system. Brandt (1986) discussed adaptive control simulation and implementation methodology used in HVAC system application. Zaheer-uddin (1990) proposed a method of combining energy balance and least squares method to develop a simple, recursively updated model of a building. Energy balance principles were first used to obtain an estimate of the two most important parameters of a building: heat loss and heat storage. These parameters were then supplied as base values to the least squares model. Crawford et al. (1991) developed a segmented linear least-squares modeling procedure for deriving continuous single-input, single-output component models of HVAC equipment. Coley and Penman (1992) described a recursive least squares algorithm for identifying the parameter characterizing the thermal response of a building in terms of a second-order RC network.

Bekker et al. (1991) described a tuning method for first-order process with PI controllers using root locus and pole cancellation techniques that enables PI controllers used with first-order systems to be tuned to a critically damped response. Wallenborg (1991) described an algorithm for a self-tuning controller in which a discrete time process transfer function was calculated from the wave form of a periodic oscillation obtained with a relay feedback tuning experiment, and a general linear discrete time controller is designed using pole placement technique based on input-output models.

MacArthur and Woessner (1993) described a predictive control policy for a single-input and single-output system that uses a finite-time horizon with end-time constraints. The control law minimizes actuator movement while satisfying both process and control output constraints imposed at the end of the time horizon. A single user-definable parameter, directly related to the desired closed-loop settling time of the system, can be used to tune the controller. MacArthur and Foslien (1993) developed a multivariable predictive controller with nonlinear cost minimization capability. Basic servo-regulatory behavior was governed by a feedforward/feedback version of a receding horizon controller.

A prior knowledge of the plant should be utilized as much as possible to improve the performance of control systems and to simplify on-line control schemes. Nevertheless, this aspect of research has been largely ignored in past applications of adaptive control to building thermal systems.

Apart from the studies mentioned above, the new control techniques have been examined in HVAC applications. Kreider and Wang (1991) developed artificial neural networks for control of commercial buildings. They used ANN method for training ANNs

to automatically update energy consumption predictors for a commercial building. Huang and Nelson (1991) described a fuzzy controller for HVAC applications with a simple example. The controller is a fuzzy controller combined with the PID algorithm and based on rules obtained from operator's experiences. The concept of PID-law-combining fuzzy controller maintained the simplicity and applicability of PID algorithm and uses acquired knowledge to improve the performance of the control system. Albert et. al. (1995) applied ANN to serve both as a system identifier and as an controller for an air-handling unit. The results show that ANN has potential benefit in model identification as well as serving as local controllers.

2.3 Summary and Objectives

As noted in previous sections, many studies have been done on modeling of HVAC components and systems and also simulation and design of control systems for HVAC. However, in general the previous studies have one or more limitations when reviewed in the context of (i) transient modeling, (ii) control analysis and (iii) comprehensive control strategies, specially (iv) global optimal control strategies:

- 1) most models are of steady state type which are not suitable for control analysis, because they do not consider the dynamics of the equipment.
- 2) no work has been done for analyzing the interactions between the dynamics of the fan-motor and the static pressure in the ductwork. This kind of model and study is necessary for analysis of VAV system because the air flow rates continuously change in the VAV system.
- 3) no transient model is available for modeling of cooling and dehumidifying coil which takes into account the variable air flow rate.
- 4) integrated models to study the transient response characteristics of mutli-zone VAV systems are not available.

- 5) a systematic work to examine the dynamic interaction of the building, VAV system, and control system has not being done.
- 6) no study has been done on determining the global optimal setpoint profiles of VAV systems subject to predicted load profiles, which will be valuable in developing supervisory control strategies for efficient operation of VAV systems.

Therefore, the objectives of this thesis are to develop (i) a comprehensive system-wide model of a multizone VAV system and (ii) an optimization methodology for global multiple-stage optimal operation of VAV and building system. The model should take account of the dynamic interaction between building shell, VAV system components and control systems. To this end, a two-step approach to the development of the system-wide model will be considered. In the first approach a detailed large-scale model of the VAV system based on the principles of mass, momentum and energy balances will be developed. This model is intended to serve as a bench mark for analysis of VAV systems. In the second approach, the objective is to develop a reduced-order state space model of VAV system. A methodology for formulating the state space models for various VAV duct configuration will be developed. Both the large-scale and reduced-order models describe the dynamics of subsystems such as air distribution and fan system, environmental zone(s), building shell, cooling coil and primary plant (chiller) as one multivariable nonlinear interconnected system in a way that is useful for control analysis.

Next attention will be focussed on developing a multistage global optimal control methodology for the efficient operation of VAV system. The optimization methodology for global optimal operation of a VAV system takes account of dynamic interaction between the building shell, VAV system components and the time-scheduled actual operation schedules of HAVC systems, such as normal operation, off-normal operation, and start-up.

The applications of the developed models and multistage optimal control methodology are illustrated by formulating and solving typical examples of HVAC system operation practiced in buildings. These include

- (i). simulation of energy management control functions,
- (ii). comparison between optimal operation of CV and VAV systems without and with time-of-day energy price incentives
- (iii). optimal operation of multizone VAV system in heating and cooling modes.

Chapter 3

Dynamic Modeling of a Multi-zone VAV System: Large-scale Dynamic Model of VAV System

The design of efficient controllers for central HVAC systems largely depends on the availability of good dynamic models of the systems. Although system identification techniques (Franklin et al. 1990, Li and Wepfer 1987, Coley and Penman 1992) and neural network methods (Huang and Nelson 1991, Albert et al. 1995) can be used to identify and train the ANN from actual measurements and thus obtain reasonable models of the HVAC systems, it is also important to develop analytical models from fundamental principles. The models so developed would be useful for comparison, validation and more importantly for finding global optimal dynamic operating strategies, multivariable controller design using modern control theory (Patel and Munro 1982) and for simulation of energy management and control systems.

As reviewed in Chapter 2, many researchers have contributed to the development of HVAC component models, viz., (Clark et al. 1985; Hamilton et al. 1977; Borresen 1981; Braun et al. 1987; Zaheer-uddin and Goh 1991). Furthermore, several public domain programs such as BLAST (1979), DOE-2 (1981), HVACSIM⁺ (1985) and TRANSYS (Klein et al. 1983) have been developed which simulate the building and HVAC system operation. However, to develop global optimal operating strategies, dynamic models of the overall systems that lend themselves to state space formulation have to be developed. In this regard, here a multizone variable air volume (VAV) system

is considered. The objective of this chapter is to develop a large-scale dynamic model of a VAV system. The focus of the study will be to accurately model the dynamics of the fan and air distribution system, piping network, and the heat and mass transfer processes taking place in the coil, and the environmental zones.

Figure 3.1 shows a schematic diagram of a two-zone VAV system considered in this study. The major components of the system are: (i) two environmental zones; (ii) a fan and ductwork, (iii) a cooling and dehumidifying coil; (iv) a chiller and a storage tank arrangement; (v) a pump and pipework. The airflow rates to zones are controlled by the zone dampers U_{z1} and U_{z2} and/or by fan speed control U_{fan} . The outdoor airflow rates are changed by positioning the fresh (U_f), exhaust (U_e) and return air (U_r) dampers. The temperature and humidity of the supply air are controlled by several control actions, namely, by position control of face and bypass dampers (U_b), by varying the mass flow rate of chilled water flowing the cooling coil by modulating the pump speed (U_p) and/or the valve position (U_v), and/or by varying the temperature of the chilled water by modulating the capacity of the chiller via chiller input energy control U_c . Thus there are ten control inputs which can be changed simultaneously in response to variable cooling loads acting on the zones. The outputs of interest are the temperature and humidity ratios in the zones, discharge air conditions, temperature of chilled water, outdoor and supply airflow rates, static pressure in the duct system and the fan speed. The interactions between every component must be considered so that a change in any one input (e.g. fan speed) can be used to influence the system outputs such as zone temperature and relative humidity. With this as the motivation, we develop subsystem models that describe the functional relationships between appropriate inputs and outputs. Note that although the

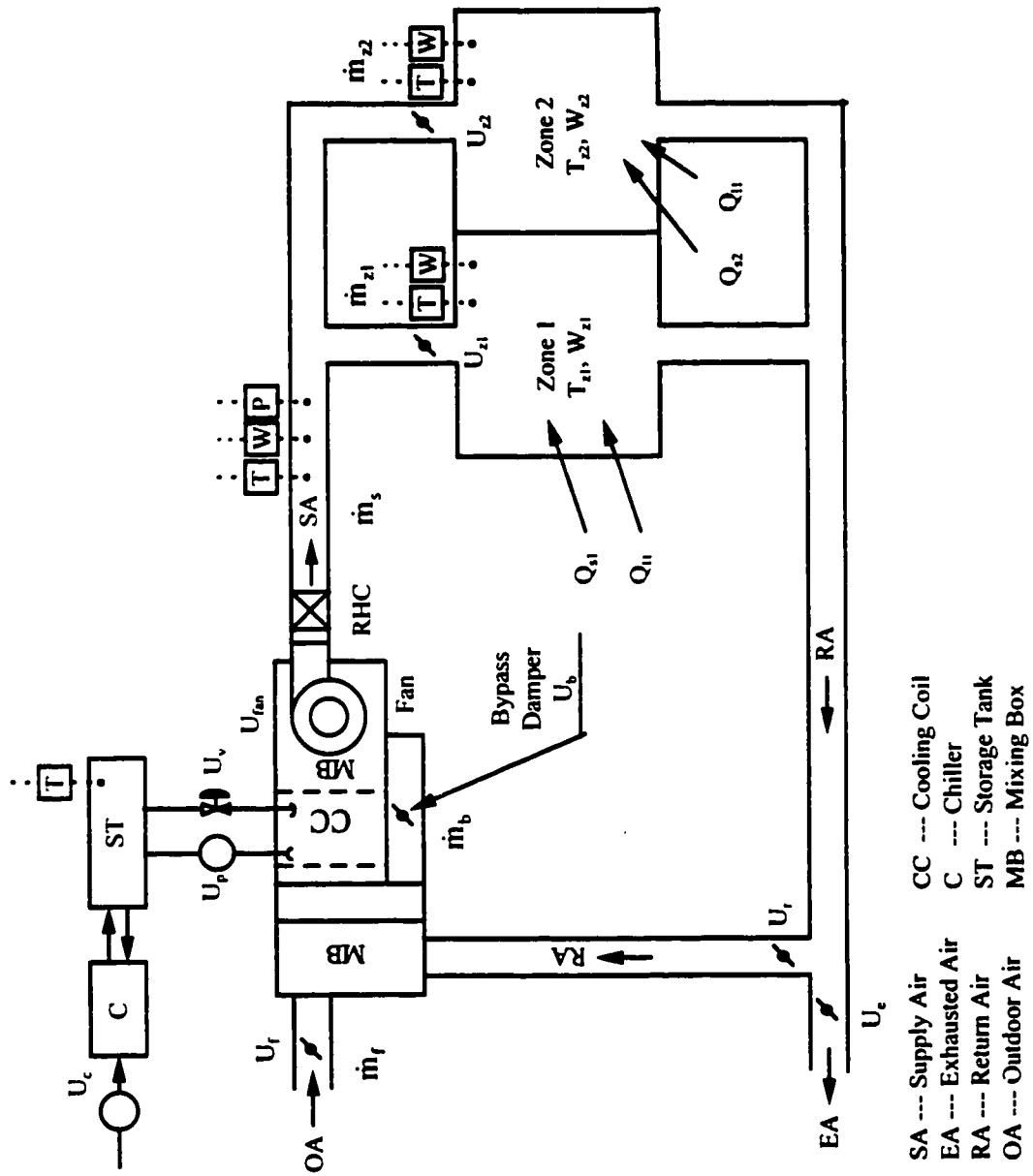


Figure 3.1 Schematic diagram of a multizone VAV system

model of the VAV system consists of two environmental zones, the model can be easily extended to buildings with large number of zones.

In Section 3.1, the development of the component models will be described in detail including the cooling and dehumidifying coil model, the chiller and storage tank model, the environment zone model, the air flow in the ducts and the fan system. In Section 3.2, the component models will be integrated to develop the overall model of the VAV system. The open-loop simulation results of the model will be presented in Section 3.3 to examine the dynamic interactions among the VAV processes.

3.1 Component Models

In this section the component models of VAV system (Figure 3.1) will be developed based on fundamental principles of mass, momentum and energy balances.

3.1.1. Cooling and Dehumidifying Coil Model

The cooling coil is the most important interface between the primary cooling plant (e.g., chiller) and the secondary air distribution system. Because of this importance several models for the cooling coils (Myers et al. 1967; Gartner 1972; McCullagh et al. 1969; Elmahdy 1975; Maxwell et al. 1989) have been developed. Here we use the modified version of the cooling and dehumidifying coil model (Elmahdy 1975, Zaheer-uddin and Goh 1991). The modifications made were in terms of incorporating the effects of variable airflow rates in the coil that occur in response to changes in fan speed.

The cooling and dehumidifying coil modeled is a typical counter-cross-flow type (Figure 3.2a) with continuous plate-fins on tubes. Since we are interested in the dynamic performance of the whole coil rather than the detailed heat transfer information, some basic assumptions are made to develop the model. These are:

- Uniform conditions of moist air and chilled water at each cross-section along the depth of the coil.
- All the heat is transferred from the air to both the primary and secondary surface areas, then through the tube wall, and finally to the chilled water.
- The temperature of air and chilled water are the mixed mean temperatures.

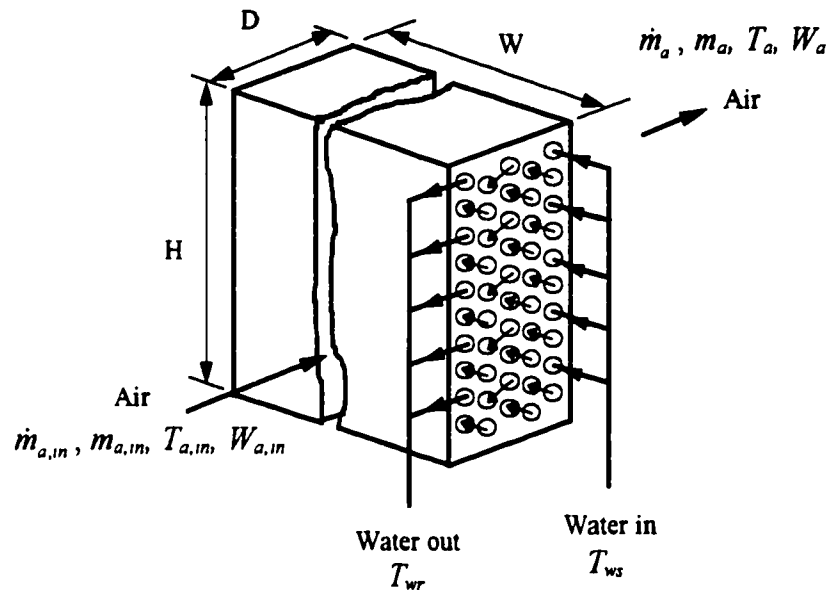


Figure 3.2 (a) Schematic diagram of the counter-cross flow coil arrangement

Let us take a control volume of dimension dy * duct height * duct width in the duct containing the coil shown in Fig. 3.2b. The energy balance on this control volume can be expressed as:

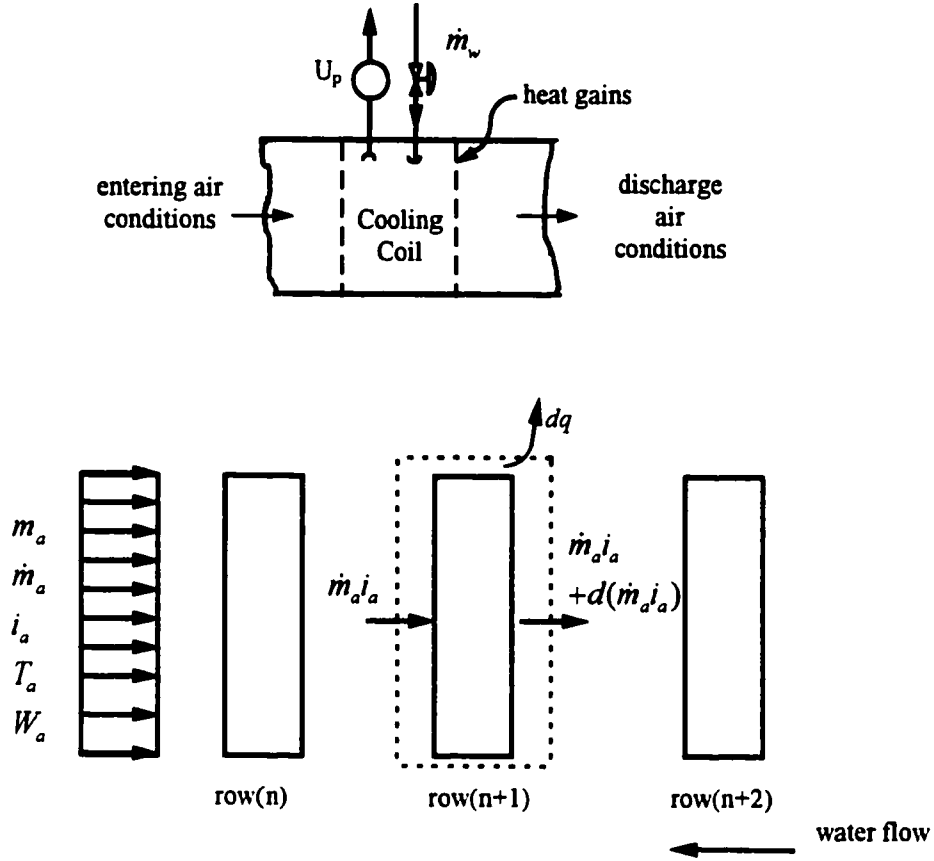


Figure 3.2 (b) Schematic diagram of the cooling & dehumidifying coil and control volume

$$\dot{m}_a i_a - [\dot{m}_a i_a + d(\dot{m}_a i_a)] = \frac{d(\dot{m}_a E)}{dt} dy + dq \quad (3.1)$$

Note that $\dot{m}_a = \rho A V$ and $m_a = \rho A$. In other words, changes in the density of air all along the duct (spatial dependence) and as function of time are considered in Equation (3.1). Equation (3.1) describes that the net flow of energy crossing the control surface during dt is equated to the rate of energy stored in the air and the rate of convective heat transfer between fin and tube surfaces and the air in the control volume.

The heat flux transferred, dq , the sum of the sensible and latent heat, can be expressed as

$$\begin{aligned}
dq = & h_{i,d}A_d(T_a - T_d)dy + h_{m,d}\lambda A_d(W_a - W_{d,st})dy \\
& + h_{i,p}A_p(T_a - T_t)dy + h_{m,t}A_p\lambda(W_a - W_{t,st})dy \\
& + \left[\int_{A_{fin}} h_t(T_a - T_{fin})dA_{fin} \right]dy + \left[\int_{A_{fin}} h_{m,t}\lambda(W_a - W_{fin,st})dA_{fin} \right]dy
\end{aligned} \tag{3.2}$$

where A_{fin} , A_p are the heat and mass transfer area of the fin and the tube per unit length in the direction of the air flow, respectively. T_d is the temperature of the duct material, $W_{d,st}$ and $W_{t,st}$ are the specific humidity ratios of saturated air at the duct and tube surface temperatures. A_d is the surface area of the duct per unit length in the direction of the air flow, i.e., the sectional perimeter of the duct.

In Equation (3.2), the rate of total convective heat transfer is equated to the sum of the rate of sensible and latent heat transfer between the air and the duct surface, between the air and the tube surface, and between the air and the fin surface.

Introduce the following parameters to define the fin efficiency in the sensible and latent heat transfer modes,

$$\eta_s = \frac{\int_{A_{fin}} h_t(T_{fin} - T_a)dA_{fin}}{h_t(T_t - T_a)A_{fin}} \tag{3.3}$$

and

$$\eta_c = \frac{\int_{A_{fin}} h_{m,t}(W_{fin,st} - W_a)dA_{fin}}{h_{m,t}(W_{t,st} - W_a)A_{fin}} \tag{3.4}$$

The sum of the heat transfer area of the fins (secondary area) and that of the bare tube (primary area) is the total area, that is

$$A_o = A_p + A_{fin} \tag{3.5}$$

Substituting Eqs. (3.3), (3.4), (3.5) into Eq. (3.2), and rearranging, we have

$$\begin{aligned}
dq = & h_t(T_a - T_t)A_o[1 - \frac{A_{fin}}{A_o}(1 - \eta_s)]dy + h_{i,d}(T_a - T_d)A_d dy \\
& + h_{m,t}(W_a - W_{t,st})\lambda A_o[1 - \frac{A_{fin}}{A_o}(1 - \eta_c)]dy + h_{m,d}\lambda(W_a - W_{d,st})A_d dy
\end{aligned} \tag{3.6}$$

By defining the following coefficients

$$\eta_{s,ov} = 1 - \frac{A_{fin}}{A_o}(1 - \eta_s) \tag{3.7}$$

and

$$\eta_{c,ov} = 1 - \frac{A_{fin}}{A_o}(1 - \eta_c) \tag{3.8}$$

and using Eqs. (3.7), (3.8), Eq. (3.6) becomes

$$\begin{aligned}
dq = & h_t \eta_{s,ov} A_o (T_a - T_t) dy + h_{m,t} \lambda \eta_{c,ov} A_o (W_a - W_{t,st}) dy \\
& + h_{i,d} A_d (W_a - W_{d,st}) dy + h_{m,d} \lambda A_d (W_a - W_{d,st}) dy
\end{aligned} \tag{3.9}$$

the enthalpy of moist air can be written as (ASHRAE 1993):

$$i_a = c_p T_a + W_a i_g = c_p T_a + W_a (h_{fg} + c_{p,va} T_a) \tag{3.10}$$

where i_g is the enthalpy of saturated water vapour, $c_{p,va}$ is the specific heat of the water vapour (1850 J/kg k), h_{fg} is the heat of vaporization of water (2,501,000 J/kg). It is found that the term, $c_{p,va} T_a$, is much less than the term, h_{fg} , over the air temperature range encountered in HVAC applications. Consequently the term $c_{p,va} T_a$ is neglected, and i_g is assumed to be constant. The enthalpy change can be written as

$$d(\dot{m}_a i_a) = \dot{m}_a [c_p \frac{\partial T_a}{\partial y} + i_g \frac{\partial W_a}{\partial y}] dy + [c_p T_a + i_g W_a] d\dot{m}_a \tag{3.11}$$

the internal energy of the air can be expressed as

$$E = u_a = c_v T_a + u_g W_a \tag{3.12}$$

where c_v is the specific heat of moist air at constant volume, and u_g is the internal energy of the saturated water vapour.

The change of the internal energy of the air can be expressed as

$$\begin{aligned} \frac{d(m_a E)}{dt} &= m_a \frac{du_a}{dt} + u_a \frac{dm_a}{dt} = m_a (c_v \frac{\partial T_a}{\partial t} + u_g \frac{\partial W_a}{\partial t}) \\ &\quad + (c_v T_a + u_g W_a) \frac{\partial m_a}{\partial t} \end{aligned} \quad (3.13)$$

Now substituting Eqs. (3.9), (3.11) and (3.13) into Eq. (3.1), we have

$$\begin{aligned} c_p \frac{\partial(\dot{m}_a T_a)}{\partial y} + i_g \frac{\partial(\dot{m}_a W_a)}{\partial y} + c_v \frac{\partial(m_a T_a)}{\partial t} + u_g \frac{\partial(m_a W_a)}{\partial t} &= -h_{i,d}(T_a - T_d)A_d \\ &\quad - \lambda h_{m,d} A_d (W_a - W_{d,st}) - h_t \eta_{s,ov} A_o (T_a - T_t) - h_{m,t} \lambda \eta_{c,ov} A_o (W_a - W_{t,st}) \end{aligned} \quad (3.14)$$

From the mass balance of moisture in the air flow, we have

$$\begin{aligned} \frac{\partial(m_a W_a)}{\partial t} + \frac{\partial(\dot{m}_a W_a)}{\partial y} &= -h_{m,d}(W_a - W_{d,st})A_d - h_{m,t}(W_a - W_{t,st})A_p \\ &\quad - \int_{A_{fin}} h_{m,t}(W_a - W_{fin,st})dA_{fin} \end{aligned} \quad (3.15)$$

By using Eq. (3.4) and Eq. (3.8), Eq. (3.15) becomes

$$\frac{\partial(m_a W_a)}{\partial t} + \frac{\partial(\dot{m}_a W_a)}{\partial y} = -h_{m,t} \eta_{c,ov} A_o (W_a - W_{t,st}) - h_{m,d} A_d (W_a - W_{d,st}) \quad (3.16)$$

Equation (3.16) is the statement of the vapor balance. The rates of changes in water vapor (non-steady and convective components) are equated to the moisture transfer between the air and the fin-coil and inside surfaces of the duct.

By using Eq.(3.16), Eq. (3.14) becomes

$$\begin{aligned} c_p \frac{\partial(\dot{m}_a T_a)}{\partial y} + c_v \frac{\partial(m_a T_a)}{\partial t} + (u_g - i_g) \frac{\partial(m_a W_a)}{\partial t} &= -(\lambda - i_g) h_{m,t} \eta_{c,ov} A_o (W_a - W_{t,st}) \\ &\quad - h_t \eta_{s,ov} A_o (T_a - T_t) - (\lambda - i_g) h_{m,d} A_d (W_a - W_{d,st}) - h_{i,d}(T_a - T_d) \end{aligned} \quad (3.17)$$

The difference between λ and i_g when evaluated at the same temperature is the enthalpy of the saturated water:

$$i_g - \lambda = c_w T_a$$

and we also have

$$i_g - u_g = (c_p - c_v) T_a$$

for the perfect air. Therefore Eq. (3.17) can be rearranged as

$$\begin{aligned} \gamma \frac{\partial(\dot{m}_a T_a)}{\partial t} + \frac{\partial(\dot{m}_a T_a)}{\partial t} + (1 - \gamma) T_a \frac{\partial(\dot{m}_a W_a)}{\partial t} &= \frac{c_w}{c_v} T_a h_{m,t} A_o \eta_{c,ov} (W_a - W_{t,st}) \\ + \frac{c_w}{c_v} T_a h_{m,d} A_d (W_a - W_{d,st}) - \frac{h_t A_o \eta_{c,ov}}{c_v} (T_a - T_t) - \frac{h_{t,d} A_d}{c_v} (T_a - T_d) \end{aligned} \quad (3.18)$$

where $\gamma = \frac{c_p}{c_v}$.

Equation (3.18) is the statement of the energy balance of air. The rate of change of energy (due to temperature and humidity of air) is equated to rate of energy transfer between air and fin-tube surfaces and the duct surfaces.

A part of the total heat transferred through the water film of the fins and bare tubes surface is stored in the material of the fins and bare tubes, and the rest is transferred to the chilled water which flows in the tube. This can be expressed as

$$\begin{aligned} m_{fin} c_{fin} \frac{1}{A_{fin}} \frac{\partial}{\partial t} \left(\int_{A_{fin}} T_{fin} dA_{fin} \right) + m_t c_t \frac{\partial T_t}{\partial t} \\ = h_t A_o \eta_{c,ov} (T_a - T_t) + \eta_{c,ov} h_{m,t} \lambda A_o (W_a - W_{t,st}) - h_{t,t} A_{t,t} (T_t - T_w) \end{aligned} \quad (3.19)$$

where m_{fin} , m_t , c_{fin} , c_t represent the mass and specific heat of the fins and tubes per unit length in the direction of the air flow. $h_{t,t}$ is the convective heat transfer coefficient between the tube

wall and the water. $A_{i,t}$ is the water-side heat transfer area per unit length in direction of the air flow.

In fact it has been assumed that the thickness of the tube wall is very small so that the temperature drop through the tube wall can be neglected.

From Eq. (3.3), we have

$$\frac{\partial}{\partial t} (\int_{A_{fin}} T_{fin} dA_{fin}) = \frac{\partial}{\partial t} [T_a - \eta_s (T_a - T_t)] A_{fin} \quad (3.20)$$

substituting Eq. (3.20) into Eq. (3.19), and rearranging, Eq. (3.19) becomes

$$\begin{aligned} \frac{\partial T_a}{\partial t} + \frac{\eta_g + \frac{m_t c_t}{m_{fin} c_{fin}}}{1 - \eta_g} \frac{\partial T_t}{\partial t} &= \frac{\eta_{s,ov} h_t A_o}{m_{fin} c_{fin} (1 - \eta_g)} (T_a - T_t) \\ &+ \frac{\eta_{c,ov} \lambda h_{m,t} A_o}{m_{fin} c_{fin} (1 - \eta_g)} (W_a - W_{t,st}) - \frac{h_{i,t} A_{i,t}}{m_{fin} c_{fin} (1 - \eta_g)} (T_t - T_w) \end{aligned} \quad (3.21)$$

Equation (3.21) is the statement of the energy balance on tube material. The rate of energy stored in the tube metal is equated to the rate of sensible and latent heat transfer taking place between air and the tube surfaces and between the tube and the chilled water flowing inside the tubes.

We also have (McCullagh, et al. 1969)

$$W_{t,st} = 0.00199 + 0.000558 T_t + 0.000243 (T_t - 11.67)^2 \quad (\text{in S.I. units})$$

Based on the energy balance on the chilled water,

$$-d(\dot{m}_w i_w) = \frac{d(m_w E_w)}{dt} dx + dq \quad (3.22)$$

i.e.

$$-d(\dot{m}_w i_w) + h_{i,t} A_{i,t} (T_t - T_w) dx = \frac{\partial(m_w u_w)}{\partial t} dx \quad (3.23)$$

where i_w , u_w are the enthalpy and the internal energy, dx is the length of the control volume in the direction of the air flow, m_w is the mass of the chilled water per unit length.

Because the specific heat of the water can be assumed constant, we have

$$\frac{\partial i_w}{\partial x} = c_w \frac{\partial T_w}{\partial t} \quad (3.24)$$

and

$$i_w = u_w \quad (3.25)$$

Since $dx = -dy$, by using Eq. (3.24), (3.25), Eq. (3.23) becomes

$$\frac{\partial(m_w T_w)}{\partial t} - \frac{\partial(\dot{m}_w T_w)}{\partial y} = -\frac{h_{i,t} A_{i,t}}{c_w} (T_i - T_w) \quad (3.26)$$

In Equation (3.26) the rate of changes in energy stored in the chilled water (due to unsteady and convective components) are equated to the net rate of heat transfer between tube surfaces and the chilled water.

Now assume that the thickness of the duct wall is very small so that the temperature drop in the duct wall can be neglected. In the control volume, based on the energy balance of the duct material, we have

$$-d(\dot{m}_d i_d) = \frac{d(m_d E_d)}{dt} dx + dq \quad (3.27)$$

The net transferred heat flux can be expressed as

$$\begin{aligned} dq = & h_{i,d} A_d (T_a - T_d) dy + h_{mi,d} \lambda A_d (W_a - W_{d,st}) dy \\ & + h_{e,d} A_d (T_{\infty,d} - T_d) dy + h_{me,d} \lambda A_d (W_{\infty,d} - W_{d,st}) dy \end{aligned} \quad (3.28)$$

where $h_{e,d}$, $h_{me,d}$ are the convective heat and mass transfer coefficients between the external surface and the ambient medium.

and the stored energy is

$$\frac{d(m_d E_d)}{dt} = m_d \frac{dE_d}{dt} = m_d c_d \frac{dT_d}{dt} \quad (3.29)$$

because $\dot{m}_d = 0$, the change in enthalpy

$$d(\dot{m}_d i_d) = 0 \quad (3.30)$$

Substituting Eqs. (3.28), (3.29), (3.30) into Eq. (3.27), we have

$$\begin{aligned} m_d c_d \frac{dT_d}{dt} = & h_{i,d} A_d (T_a - T_d) + h_{mi,d} \lambda A_d (W_a - W_{d,st}) \\ & + h_{e,d} A_d (T_{\infty,d} - T_d) + h_{me,d} \lambda A_d (W_{\infty,d} - W_{d,st}) \end{aligned} \quad (3.31)$$

The heat loss or gain through the duct surfaces are computed by determining the duct surface temperature T_d (Equation 3.31). The rate of energy stored in the duct material is equated to sensible and latent heat gain or losses between the air inside the duct and the plenum air.

Now based on the mass balance of the air flow in the control volume we have,

$$\dot{m}_a - (\dot{m}_a + d\dot{m}_a) = \frac{\partial \dot{m}_a}{\partial t} dy \quad (3.32)$$

that is

$$\frac{\partial \dot{m}_a}{\partial t} + \frac{\partial \dot{m}_a}{\partial y} = 0 \quad (3.33)$$

The mass balance equation (3.33) expresses the fact that per unit volume basis there is a balance between masses of air entering and leaving, and the change in density. Note that the mass flow rate of air in the coil is influenced by the position of the bypass damper. This functional relationship is dependent on the damper characteristics which are described in the damper model proposed in this chapter.

Based on the momentum balance of the air flow, we have

$$-\frac{\partial(PA)}{\partial y} dy - d\left(\frac{\dot{m}_a^2}{m_a}\right) - F_{\tau,d} A_d dy - F_{\tau,fin} A_o dy = \frac{\partial \dot{m}_a}{\partial t} dy \quad (3.34)$$

using the equations

$$F_{\tau,d} = C_{\tau,d} \frac{\dot{m}_a^2}{2m_a A} \quad \text{and} \quad F_{\tau,fin} = C_{\tau,fin} \frac{\dot{m}_a^2}{2m_a A} \quad (3.35)$$

Eq. (3.34) becomes

$$\frac{\partial \dot{m}_a}{\partial t} + \frac{\partial(\dot{m}_a^2 / m_a)}{\partial y} = -\frac{\partial(PA)}{\partial y} - \frac{C_{\tau,d}}{2m_a A} A_d \dot{m}_a^2 - \frac{C_{\tau,fin}}{2m_a A} A_o \dot{m}_a^2 \quad (3.36)$$

Equation (3.36) describes the force balance on the control volume where the product of mass and acceleration (both non-steady flow and convective components) is equal to external forces acting on the control volume. These external forces are due to static pressure and frictional forces (first, second and third terms on right hand side of Equation 3.36).

We also have the state equation of the air (perfect air is assumed),

$$P = \rho R(T_a + 273.15) \quad (3.37)$$

Equations (3.16, 3.18, 3.21, 3.26, 3.31, 3.33, 3.36, 3.37) together constitute a coil model. In summary, the coil model is described by the following equations,

The mass balance on the dry air

$$\frac{\partial \dot{m}_a}{\partial t} + \frac{\partial \dot{m}_a}{\partial y} = 0 \quad (3.38)$$

The momentum equation

$$\frac{\partial \dot{m}_a}{\partial t} + \frac{\partial(\dot{m}_a^2 / m_a)}{\partial y} = -\frac{\partial(PA)}{\partial y} - \frac{C_{\tau,d}}{2m_a A} A_d \dot{m}_a^2 - \frac{C_{\tau,fin}}{2m_a A} A_o \dot{m}_a^2 \quad (3.39)$$

The thermodynamic state equation

$$P = \rho R(T_a + 273.15) \quad (3.40)$$

The energy equation

$$\begin{aligned} \frac{\partial(m_a T_a)}{\partial t} + \gamma \frac{\partial(\dot{m}_a T_a)}{\partial y} + (1 - \gamma) T_a \frac{\partial(m_a W_a)}{\partial t} &= \frac{c_w}{c_v} T_a h_{m,t} A_o \eta_{c,ov} (W_a - W_{t,st}) f_{w,t} \\ &+ \frac{c_w}{c_v} T_a h_{m,d} A_d (W_a - W_{d,st}) f_{w,id} - \frac{h_{i,o} \eta_{s,ov}}{c_v} (T_a - T_i) - \frac{h_{i,d} A_d}{c_v} (T_a - T_d) \end{aligned} \quad (3.41)$$

The vapour balance equation

$$\frac{\partial(m_a W_a)}{\partial t} + \frac{\partial(\dot{m}_a W_a)}{\partial y} = -h_{m,t} \eta_{c,ov} A_o (W_a - W_{t,st}) f_{w,t} - h_{m,d} A_d (W_a - W_{d,st}) f_{w,id} \quad (3.42)$$

Equation for the tube temperature

$$\begin{aligned} \frac{\partial T_a}{\partial t} + \frac{\eta_s + \frac{m_t c_t}{m_{fin} c_{fin}}}{1 - \eta_s} \frac{\partial T_i}{\partial t} &= \frac{\eta_{s,ov} h_i A_o}{m_{fin} c_{fin} (1 - \eta_s)} (T_a - T_i) \\ &+ \frac{\eta_{c,ov} \lambda h_{m,t} A_o}{m_{fin} c_{fin} (1 - \eta_s)} (W_a - W_{t,st}) f_{w,t} - \frac{h_{i,t} A_{i,t}}{m_{fin} c_{fin} (1 - \eta_s)} (T_i - T_w) \end{aligned} \quad (3.43)$$

Energy balance on the chilled water in the tubes

$$\frac{\partial(m_w T_w)}{\partial t} - \frac{\partial(\dot{m}_w T_w)}{\partial y} = - \frac{h_{i,t} A_{i,t}}{c_w} (T_i - T_w) \quad (3.44)$$

Heat transfer from the duct surfaces

$$\begin{aligned} m_d c_d \frac{dT_d}{dt} &= h_{i,d} A_d (T_a - T_d) + h_{m,d} \lambda A_d (W_a - W_{d,st}) f_{w,id} \\ &+ h_{e,d} A_d (T_{\infty,d} - T_d) + h_{me,d} \lambda A_d (W_{\infty,d} - W_{d,st}) f_{w,ed} \end{aligned} \quad (3.45)$$

Note that in the coil model, i.e., Equations (3.38) - (3.45), three parameters $f_{w,t}$, $f_{w,id}$, $f_{w,ed}$ have been added to account for the condensation of moisture occurring at tube-fin surfaces, at internal surfaces of the duct and at external surfaces of the duct. For example, during continuous operation of the coil, there may develop a moving interface in the coil separating dry and wet regions. If the dew point of air is greater than tube

temperature and the humidity ratio of air is greater than the humidity ratio of saturated air at any point in the direction y , then condensation of moisture will occur at tube-fin surface, i.e., at this point $f_{w,t}=1$ (wet case), otherwise $f_{w,t}=0$ (dry case).

Note that $C_{\tau,fin}$ in Equation (3.39) is a function of Reynolds number and the coil configuration (McQuiston and Parker 1988). Note also that the heat transfer coefficient h_t , mass transfer coefficients $h_{m,t}$, the coil sensible efficiency factors η_s , $\eta_{s,ov}$, and the latent efficiency factors η_c , $\eta_{c,ov}$, are functions of the coil geometry and flow field. They were computed using the following relationships (McQuiston and Parker 1988):

$$h_t = \dot{m}_a f_1 \left[\frac{1 - f_2 \dot{m}_a^{-1.2}}{1 - f_3 \dot{m}_a^{-1.2}} (0.0014 + f_4 \dot{m}_a^{-0.4}) \right] \quad (3.46)$$

for dry case

$$h_t = \dot{m}_a f_1 \left[\frac{1 - f_2 \dot{m}_a^{-1.2}}{1 - f_3 \dot{m}_a^{-1.2}} (0.0014 + f_4 \dot{m}_a^{-0.4}) \right] (0.84 + 4.0 \times 10^{-5} \text{Re}_s^{1.25}) \quad (3.47)$$

for wet case

where

$$f_1 = \frac{C_p}{A} \text{Pr}^{-\frac{1}{2}}$$

$$f_2 = 1280 N_r \left(\frac{\chi_b}{\mu A} \right)^{-1.2}$$

$$f_3 = 5120 \left(\frac{\chi_b}{\mu A} \right)^{-1.2}$$

$$f_4 = 0.2618 \left(\frac{D_{out}}{\mu A} \right)^{-0.4} R^{-0.15}$$

$$\text{Re}_s = \frac{\dot{m}_a S}{A \mu}$$

$$h_{it} = 0.023 \left(\frac{D_{in}}{A_w \mu_w} \right)^{0.8} \text{Pr}_w^{0.3} \frac{K_w}{D_{in}} \dot{m}_w^{0.8}$$

$$R = \frac{4 \chi_b \chi_a \chi}{\pi D_h D_{out}}$$

$$D_h = \frac{4 L_c A}{A_o}$$

Since exact evaluation of the specific humidity fin efficiency was not practical due to the unavailability of data, we assume that the specific humidity fin efficiency is equal to the sensible fin efficiency.

The model is capable of simulating different coil configurations by specifying parameters, viz., number of rows, number of tubes, fin geometry, frontal area, depth of coil etc. Given the inlet water temperature and the condition of the entering air, the leaving conditions of the air from the coil are determined.

3.1.2. Chiller and Storage Tank Model

Figure 3.2c shows a schematic diagram of a compression refrigeration cycle driven chiller and storage tank arrangement. The chilled water at T_{ws} is supplied to the cooling coil that returns at a temperature of T_{wr} to the storage tank. By identifying the energy flows to and from the storage tank we can express the energy balance by the following equation (Zaheeruddin and Goh 1990), viz.,

$$\frac{dT_{ws}}{dt} = \frac{1}{\rho_w c_w V_{tank}} \{ -\dot{m}_w c_w (T_{ws} - T_{wr}) - U_c E_{c,max} COP + \alpha_h (T_{\infty,t} - T_{ws}) \} \quad (3.48)$$

where V_{tank} is the volume of the storage tank. The coefficient of performance of the chiller COP can be calculated from

$$COP = (COP_{max} - 1) \left(1 - \frac{T_{\infty,t} - T_{w,s}}{\Delta T_{max}} \right) \quad (3.49)$$

where $T_{\infty,t}$ is the sink temperature and ΔT_{max} is the maximum temperature differential the chiller is designed to work with.

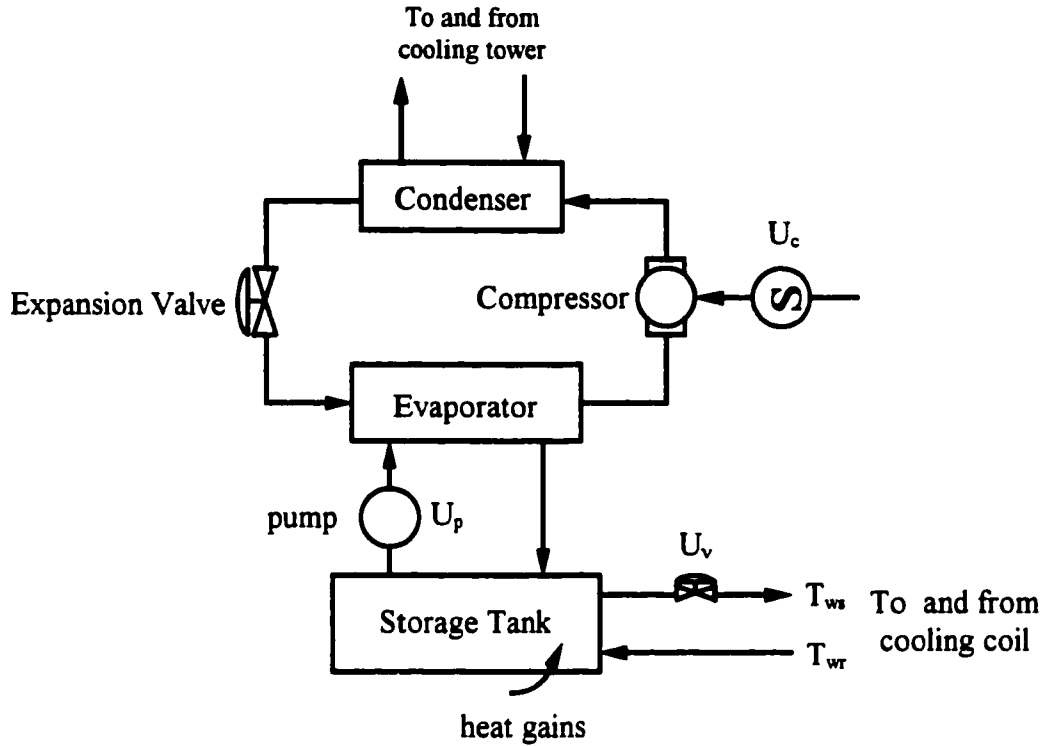


Figure 3.2(c) Schematic diagram of the chiller and storage tank

In Equation (3.48) the rate of cool energy stored in the storage tank is equated to energy extracted by the chiller, and the energy added to the tank via return water from the coil and through heat gains from the surrounding space.

3.1.3. Environmental Zone(s) Model

Figure 3.2d shows a schematic diagram of the zone model. We characterize the zone model by three state variables; density ρ , enthalpy h_z , and humidity ratio W_z of air in the zone, viz.,

$$\Phi_{zj}(t) = [\rho_z, h_z, W_z]^T$$

where the subscript j refers to the particular zone of interest. The governing equations of the zone model were derived by applying the principles of mass and energy balance. These are:

The mass balance on the dry air

$$\frac{d\rho_{\eta}}{dt} = \frac{1}{v_{\eta}} \{\dot{m}_{\eta} - \dot{m}_{\eta}\} \quad (3.50)$$

The mass balance on the water vapor

$$\frac{dW_{z,j}}{dt} = \frac{1}{\rho_{z,j} v_{z,j}} \{\dot{m}_{s,j} W_{s,j} - \dot{m}_{r,j} W_{r,j} + \dot{m}_{w,j}(t)\} \quad (3.51)$$

Enthalpy balance

$$\frac{dh_{z,j}}{dt} = \frac{1}{\rho_{z,j} v_{z,j}} \{\dot{m}_{s,j} h_{s,j} - \dot{m}_{r,j} h_{r,j} + q_{s,j}(t) + q_{l,j}(t)\} \quad (3.52)$$

$$h_{\eta} = c_p T_{\eta} + W_{\eta} (h_{fg} + c_{p,va} T_{\eta})$$

Thermodynamic state equation

$$P = \rho R (T_a + 273.15) \quad (3.53)$$

Equation (3.50) expresses the fact that the time rate of change in the mass flow rate of air in the zones is equal to the difference between the supply and return air flow rates to and from the zone(s). Likewise, Equation (3.51) states that the rate of change of moisture in the zone is equal to the difference between moisture added to and removed from the zone. The rate of change of h_z in Equation (3.52) is equated to the rate of changes in supply and return air enthalpies (h_s , h_r), the instantaneous gains from sensible and latent heat sources. Note that the sensible heat loads, $q_{s,j}(t)$ in Equation (3.52) acting on the zones were computed by using the existing models for the prediction of zone loads

(Appendix A). The zone load model simulates the dynamic effects of the enclosure elements using the distributed capacity approach.

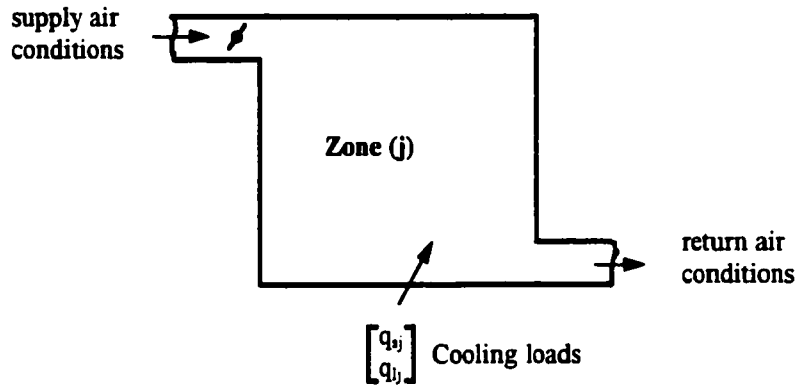


Figure 3.2(d) Schematic diagram of the environmental zone

3.1.4. Model of Variable Air flow rates in the duct system

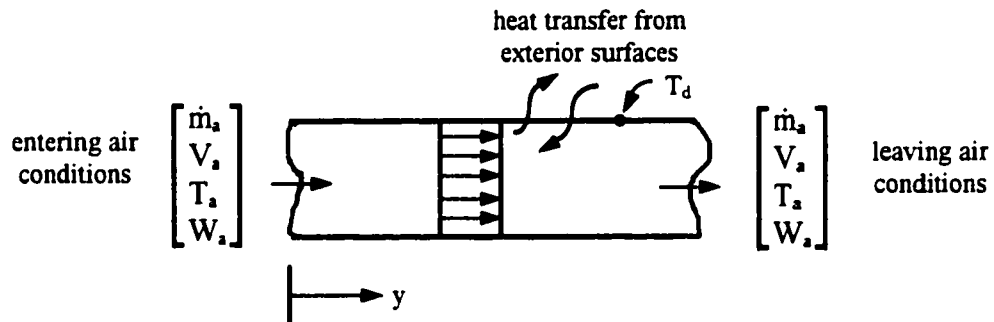


Figure 3.2(e) Schematic diagram of the duct section

We model the air flow in the duct system (Figure 3.2e) as a variable density, one-dimensional fluid flow problem. Associated with the fluid flow are the energy and moisture transport equations. Given the entering air conditions in a straight section of the duct, the leaving air conditions can be computed by using the mass, momentum and energy balance equations. The state variables of interest in describing the model are

$$\Phi_d(y, t) = [m_a, \dot{m}_a, T_a, W_a, T_d]^T$$

The governing equations of the duct model were developed by using the principle of mass, momentum and energy balance similar to those stated in the coil model. These are

The continuity equation

$$\frac{\partial m_a}{\partial t} + \frac{\partial \dot{m}_a}{\partial y} = 0 \quad (3.54)$$

The momentum balance equation

$$\frac{\partial \dot{m}_a}{\partial t} + \frac{\partial (\dot{m}_a^2 / m_a)}{\partial y} = -\frac{\partial (PA)}{\partial y} - \frac{C_{\tau, d}}{2m_a A} A_d \dot{m}_a^2 \quad (3.55)$$

The equation of state

$$P = \rho R(T_a + 273.15) \quad (3.56)$$

The energy equation

$$\begin{aligned} \frac{\partial (m_a T_a)}{\partial t} + \gamma \frac{\partial (\dot{m}_a T_a)}{\partial y} + (1 - \gamma) T_a \frac{\partial (m_a W_a)}{\partial t} &= \frac{c_w}{c_v} T_a h_{m, d} A_d (W_a - W_{d, st}) f_{w, id} \\ - \frac{h_{i, d} A_d}{c_v} (T_a - T_d) & \end{aligned} \quad (3.57)$$

The moisture balance equation

$$\frac{\partial}{\partial t} [m_a W_a] + \frac{\partial}{\partial t} [\dot{m}_a W_a] = -h_{m, d} A_d (W_a - W_{d, st}) f_{w, id} \quad (3.58)$$

The duct temperature equation

$$\begin{aligned} \frac{\partial T_d}{\partial t} &= \frac{h_{i, d} A_d}{m_d C_{pd}} (T_a - T_d) + \frac{h_{m, d} \lambda A_d}{m_d C_{pd}} (W_a - W_{d, st}) f_{w, id} + \frac{h_{e, d} A_d}{m_d C_{pd}} (T_{\infty, d} - T_d) \\ &+ \frac{h_{m, d} \lambda A_d}{m_d C_{pd}} (W_{\infty, d} - W_{d, st}) f_{w, ed} \end{aligned} \quad (3.59)$$

The mass balance equation (3.54) expresses the fact that per unit volume basis there is a balance between masses of air entering and leaving, and the change in density.

Note that the velocity of air in the ductwork is influenced by the position of the dampers and the fan speed. This functional relationship is dependent on the damper and fan characteristics that are described in the damper and fan models proposed in this chapter.

Equation (3.55) describes the force balance on the control volume where the product of mass and acceleration (both non-steady flow and convective components) are equal to external forces acting on the control volume. These external forces are due to static pressure and frictional forces (first and second terms on right hand side of Equation 3.55). Also to note is the fact that C_f in Equation (3.55) is a function of Reynolds number. The static pressure is related to thermodynamic state equation (3.56).

In Equation (3.57) the rate of change of energy (due to temperature and humidity) is equated to rate of energy transfer between air and the duct surfaces. The heat transfer coefficient h is a function of the flow field.

Equation (3.58) is the statement of the vapor balance. The rates of changes in water vapor (non-steady and convective components) are equated to the moisture transfer between the air and the saturated air around the inside surfaces of the duct.

The heat loss or gain through the duct surfaces are computed by determining the duct surface temperature T_d (Equation 3.59). The rate of energy stored in the duct material is equated to sensible and latent heat gain or losses between the air inside the duct and the plenum air.

3.1.5. Fan-Motor Model

Figure 3.2f shows a schematic diagram of motor-fan arrangement. The applied voltage (U_{fan}) to the D.C. motor can be varied. The resulting torque developed is

transformed into motor speed that is transmitted to the fan via the belt or gear train arrangement shown in the figure.

The torque developed in the motor can be expressed as,

$$T_m = J_m \frac{dw_m}{dt} + B_m w_m + T_{L,m} \quad (3.60)$$

where T_m is the torque developed in the motor, $T_{L,m}$ is the load torque, B_m is the equivalent frictional factor of the motor, J_m is the equivalent moment of inertia in the motor, and w_m is angular velocity of the motor.

The equation for power balance in the motor can be obtained by multiplying Eq. (3.60) by w_m ,

$$T_m w_m = J_m \frac{dw_m}{dt} w_m + B_m w_m^2 + T_{L,m} w_m \quad (3.61)$$

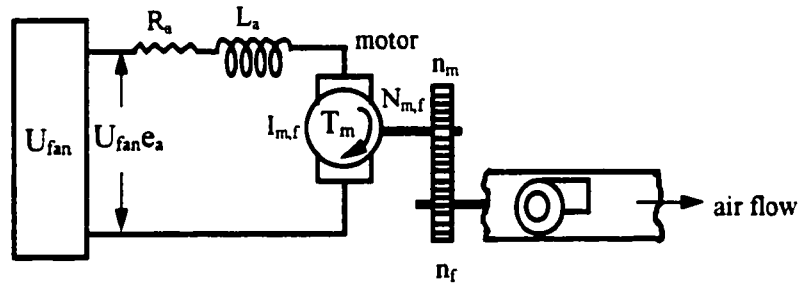


Figure 3.2(f) Schematic diagram of the fan-motor system

where the first term in the right side represents the power which accelerates the motor, the second term represents the friction loss in the motor, the third term represents the load power.

Similarly, the torque balance on the fan can be expressed as,

$$T_f = J_f \frac{dw_f}{dt} + B_f w_f + T_{L,f} \quad (3.62)$$

and the power balance on the fan can be written

$$T_f w_f = J_f \frac{dw_f}{dt} w_f + B_f w_f^2 + T_{L,f} w_f \quad (3.63)$$

where the first term in the right side represents the power which accelerates the fan, the second term represents the friction loss in the fan, the third term represents the required load power. Equation (3.63) can be rewritten as

$$T_f w_f = J_f \frac{dw_f}{dt} w_f + B_f w_f^2 + \frac{Q\Delta P_{fan}}{\eta_f} \quad (3.64)$$

Since the power supplied by the motor is equal to the power required by the fan, i.e.,

$$T_{L,m} w_m = T_f w_f \quad (3.65)$$

substituting Eq. (3.64) into Eq.(3.60) and by using Eq. (3.65), Eq. (3.60) becomes

$$J_m \frac{dw_m}{dt} = T_m - J_f \frac{dw_f}{dt} \frac{w_f}{w_m} - B_m w_m - B_f \frac{w_f^2}{w_m} - \frac{Q\Delta P_{fan}}{\eta_f w_m} \quad (3.66)$$

Applying the relationship between the angular velocity of the fan and that of the motor

$$w_m = \frac{n_f}{n_m} w_f \quad \text{and} \quad N_m = 2\pi w_m \quad (3.67)$$

and assuming that the torque of the motor, T_m , is proportional to the current I_m , Eq. (3.66)

becomes

$$J_{eq} \frac{dN_m}{dt} = \frac{k_t I_m}{2\pi} - B_{eq} N_m - \frac{Q\Delta P_{fan}}{(2\pi)^2 \eta_f N_m} \quad (3.68)$$

where $J_{eq} = J_m + J_f \left(\frac{n_m}{n_f}\right)^2$, $B_{eq} = B_m + B_f \left(\frac{n_m}{n_f}\right)^2$ and k_t is proportional constant, i.e.,

torque constant. n_m/n_f is the drive ratio.

Applying Kirchhoff's law for the circuit, we have

$$U_{fan} e_a = L_a \frac{dI_m}{dt} + R_a I_m + e_b \quad (3.69)$$

where e_b is the back emf voltage, which tends to oppose the current flow. Assuming that the e_b is a proportional to the speed of the motor speed, we have

$$L_a \frac{dI_m}{dt} = U_{fan} e_a - R_a I_m - 2\pi k_b N_m \quad (3.70)$$

where k_b is a proportional constant, i.e., back emf constant.

Note that although functionally the torque constant, k_t , and the back emf constant, k_b , are two separate parameters, for a given motor, their values are closely related. In S.I. units, the values of k_b and k_t are identical if k_b is represented in V/rad/sec, and k_t in N-m/A (Kuo 1991).

In summary, the fan and motor model describes the relationship between the fan speed, motor input power and the fan pressure. The state variables of interest for the fan-motor model are

$$\Phi_f = [N, I]^T$$

and the corresponding model equations are

$$\frac{dN_{m,f}}{dt} = \frac{k_t I_{m,f}}{2\pi J_{eq,f}} - \frac{B_{eq,f}}{J_{eq,f}} N_{m,f} - \frac{\dot{m}_a \Delta P_{fan}}{(2\pi)^2 \rho N_{m,f} \eta_f J_{eq,f}} \quad (3.71)$$

$$\frac{dI_{m,f}}{dt} = \frac{e_{a,f}}{L_{a,f}} U_{fan} - \frac{R_{a,f}}{L_{a,f}} I_{m,f} - \frac{2\pi k_{b,f}}{L_{a,f}} N_{m,f} \quad (3.72)$$

$$\Delta P_{fan} = C_h \rho D^2 N_{m,f}^2 \left(\frac{n_m}{n_f} \right)^2 \quad (3.73)$$

Equation (3.71) expresses the fact that the armature current produces the torque that is applied to overcome the inertia and frictional forces. Equation (3.72) states that the rate of change of armature voltage is equal to the voltage applied to the motor, the voltage drop across the armature and the induced voltage. Equation (3.73) gives the correlation between fan pressure and the motor speed together with other parameters shown.

3.1.6. Correlations for Pressure Losses in the Duct System

Frictional losses occurring in the duct system, fittings and across the dampers and elsewhere in the duct system were accounted for by using the correlations available in the literature. These are

Pressure loss across the dampers

$$\Delta P_d = \{a_0 \exp(a_1 U_f) + a_2\} \frac{\rho V_a^2}{2} \quad (3.74)$$

The coefficients a_0 , a_1 and a_2 were obtained by fitting curves to the data given in Croome and Roberts (1981).

Pressure loss due to sudden expansion and contraction

Sudden expansion and contraction of areas occur at several places in the duct system, for example at inlet to outdoor duct, at outlet of exhaust duct, and at supply and return outlets to zones. The pressure losses occurring at these sections were modeled as follows (McQuiston and Parker 1988).

$$\Delta P = \frac{\xi}{2} \rho V_a^2 \quad (3.75)$$

where ξ is the friction factor.

Pressure loss in converging and diverging sections

The pressure losses occurring in the mixing (outdoor air and recirculated air) section, and in the exhaust and return air section, were modeled using the correlations given in Fenstel and Reynor-Hoosen (1990). These are

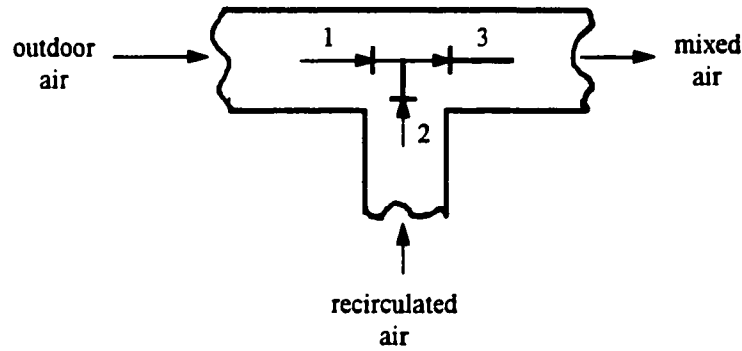


Figure 3.2(g) Schematic diagram of the converging section

Converging section (Figure 3.2g)

$$P_1 = P_3 + \frac{(1 + \xi_{31})}{2} \rho_3 V_3^2 - \frac{1}{2} \rho_1 V_1^2 \quad (3.76)$$

$$P_2 = P_3 + \frac{(1 + \xi_{32})}{2} \rho_3 V_3^2 - \frac{1}{2} \rho_2 V_2^2 \quad (3.77)$$

Diverging section (Figure 3.2h)

$$P_1 = P_3 + \frac{(1 - \xi_{31})}{2} \rho_3 V_3^2 - \frac{1}{2} \rho_1 V_1^2 \quad (3.78)$$

$$P_2 = P_3 + \frac{(1 - \xi_{32})}{2} \rho_3 V_3^2 - \frac{1}{2} \rho_2 V_2^2 \quad (3.79)$$

where ξ_{ij} is the friction coefficient.

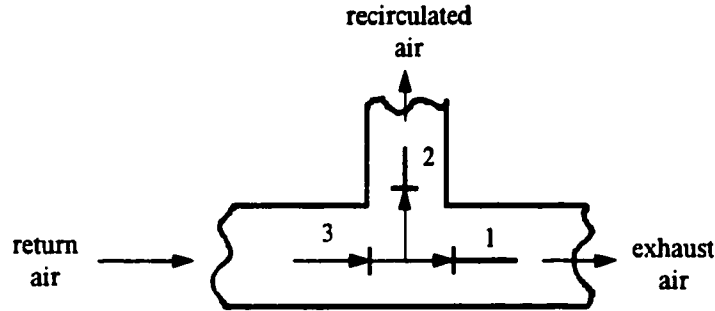


Figure 3.2(h) Schematic diagrams of the diverging section

3.2 Integrated large-scale model of VAV system

The development of the overall model of VAV system is accomplished using the bottom-up approach. In other words first component models are developed and then interconnected to develop an overall model satisfying the chosen VAV configuration. The VAV system configuration (Figure 3.3) is divided into several nodes strategically chosen to interconnect various components. The number of nodes depend not only on the number of components and their sequence in the VAV system but also on the desired accuracy of numerical solution. At each node, appropriate equations of the components are discretized in space and time.

The two-zone VAV system shown in Figure 3.3 was described by 54 nodes and at each node the equations of state were discretized in space and in time using an implicit backward difference scheme (Gerald and Wheatley 1984). In all a set of 328 equations were solved at each time step after linearization. The nonlinear terms such as products of ϕ_1, ϕ_2, ϕ_3 , were linearized as follows

$$(\phi_1 \phi_2 \phi_3)^n = (\phi_2 \phi_3) \phi_1^n + (\phi_1 \phi_3) \phi_2^n + (\phi_1 \phi_2) \phi_3^n - 2(\phi_1 \phi_2 \phi_3)^{n-1} \quad (3.80)$$

where n represents the current time step.

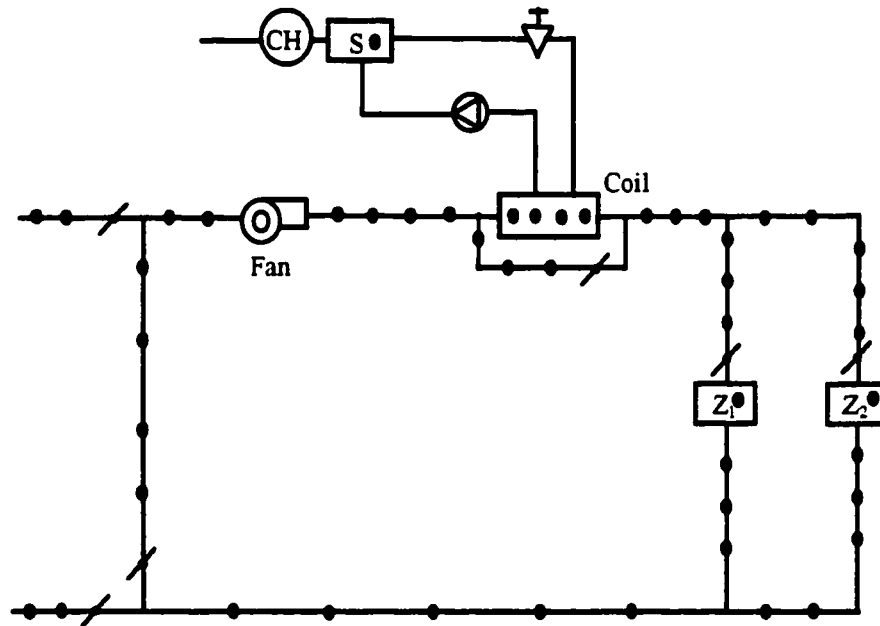


Figure 3.3 Nodal representation of the overall VAV system model

In summary we note that in the development of the above overall VAV system model, the classical approach to model development practiced in computational heat transfer and fluid flow is applied. The advantages of the method stem from its fundamental nature of model development, better representation of system dynamics and node-by-node

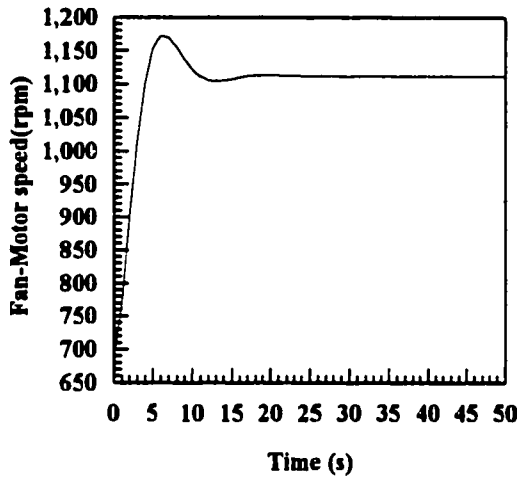
system wide tracking of system states as a function of time. The limitations of this approach are that it is computationally extensive and is not flexible enough to accommodate changes in system configuration which would require redefinition of system nodes and additional equations at each of the new nodes.

In the following chapter, we address some of these limitations by the way of developing a reduced-order state space model of VAV system.

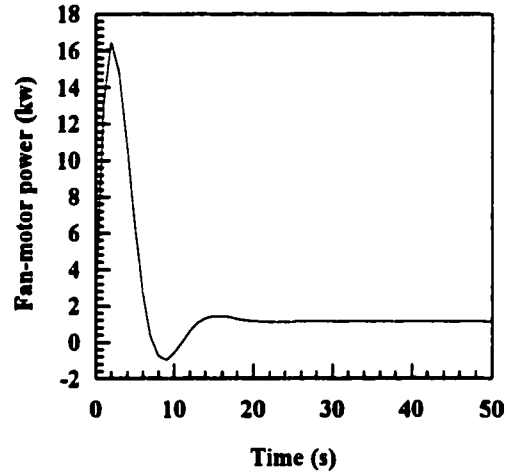
3.3 Open-loop Simulation Results

Equations (3.38-3.45, 3.48, 3.50-3.53, 3.54-3.59, 3.71-3.72, 3.74-3.79) together constitute a multivariable nonlinear model of the VAV system. It is instructive to study the open-loop responses of the system subject to constant inputs (i.e. without feedback) and constant external disturbances. In this section the characteristics of the system obtained from open-loop simulation results are examined.

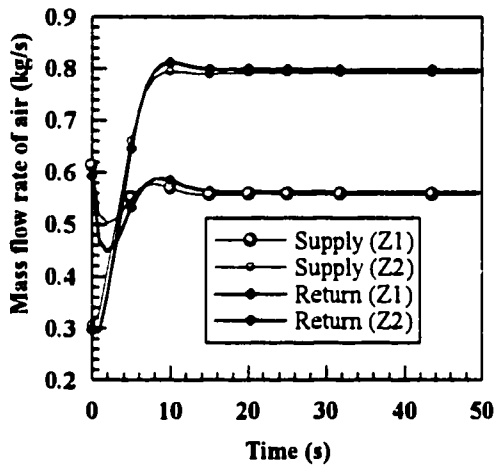
The simulated VAV system consisted of two zones with about 92 m² each in floor area. The cooling loads acting on the zones were: 4.2 kW sensible and 1.4 kW latent for zone 1; and 6.4 kW sensible and 2.1 kW latent for zone 2. The environmental zones were assumed to be about 100 meters away from the central system and therefore a total of 300 m of duct length was used. An 8-row 16 tube, plate-fin-tube cooling and dehumidifying coil was simulated. Also a fan with a 2-HP motor that can develop a rated pressure of 500 Pa at 1200 rpm was used. Apart from these specifications, the magnitudes of the major parameters of the subsystem models used in this study are given in Table 3.1. The interest here is to study the dynamic response characteristics of the overall VAV system. In the following, we present results obtained from several open-loop simulation runs.



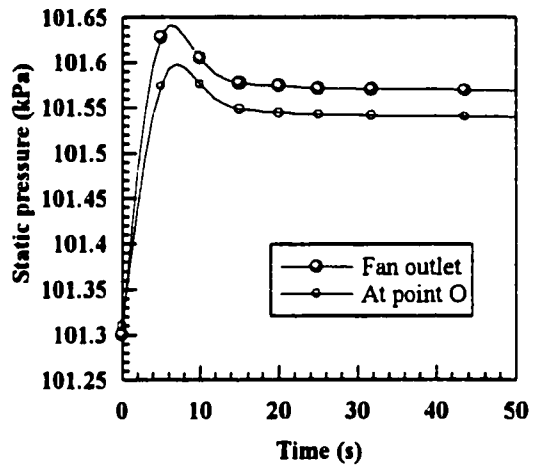
(a) Fan speed



(b) Fan-motor power



(c) Mass flow rate of air to the zones



(d) Static pressure

Figure 3.4 Fan and airflow system characteristics subject to step changes in inputs and external disturbances

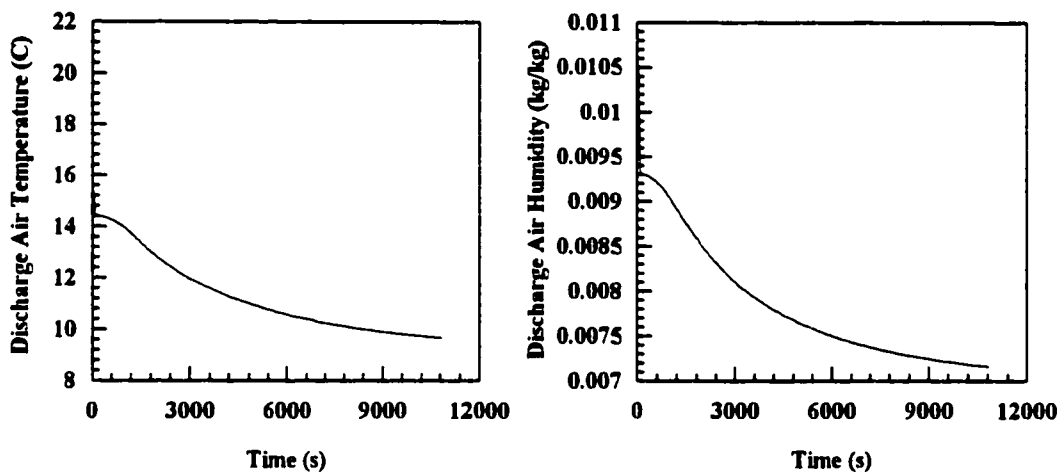
Figures 3.4a-d show the fan speed and power and the airflow characteristics of the VAV system. These results were obtained under the following conditions. $q_{s1}= 4.2$ kW, $q_{s2}= 6.4$ kW, $q_{l1}= 1.4$ kW, $q_{l2}= 2.1$ kW, $U_{z1}= U_{z2}=1.0$ (i.e. zone dampers were kept full open. The outdoor damper position was open 15% i.e. $U_f=0.15$, and the exhaust, return, bypass damper settings were $U_e=0.15$, $U_r=0.50$, $U_b=0$, respectively. With chiller and fan

full on $U_c=U_{fan}=1.0$ and the mass flow rate of chilled water full on $U_w=1.0$, the system responses were obtained. Figure 3.4a shows that fan speed rises rapidly to 1175 rpm and reaches the steady state value of 1110 rpm in 30 seconds. How the motor power varied during the same time is shown in Figure 3.4b. After the initial transients (Kovacs 1984), the power settles to a steady state value of about 1 kW. We can expect that because of the fast transient response characteristics of the fan, the static pressure and consequently the air flow rates in the duct system will also change rapidly. This is depicted in Figures 3.4c-d. Figure 3.4c shows the supply and return airflow rates to and from the zones. It may be noted that there is a small difference in supply and return airflow rates to zone 1 and 2 during the first 15s and this difference reduces to zero under steady state. The outdoor air damper position $U_f=0.15$ translated into 0.171 kg/s of fresh air into the system. This amounted to about 12.3% of the total airflow rate in the system. Also shown in Figure 3.4d are the variations in the static pressure at the fan outlet and at a point O, 3/4 of the distance from the coil. Taken together Figures 3.4a-d show that the fan system and airflow rates have very fast responses and their steady state times are of the order of 30s.

The transient response characteristics of the cooling and dehumidifying coil were examined by studying the temperature and humidity ratio of the air leaving the coil. We assume the same set of conditions as those used in Figures 3.4a-d. Figures 3.5a-b show the dry bulb temperature and humidity ratio of the air leaving the coil. Note that these responses are not only influenced by the coil dynamics but also by the dynamics of the overall system. Nevertheless, we are interested here in examining the time response characteristics of air leaving the coil. As shown in Figures 3.5a-b the temperature and humidity ratio decrease exponentially and reach steady state in about 12000s. Note that

the results in Figures 3.5a-b are for the case with no bypass (i.e. the bypass dampers were assumed to be fully closed).

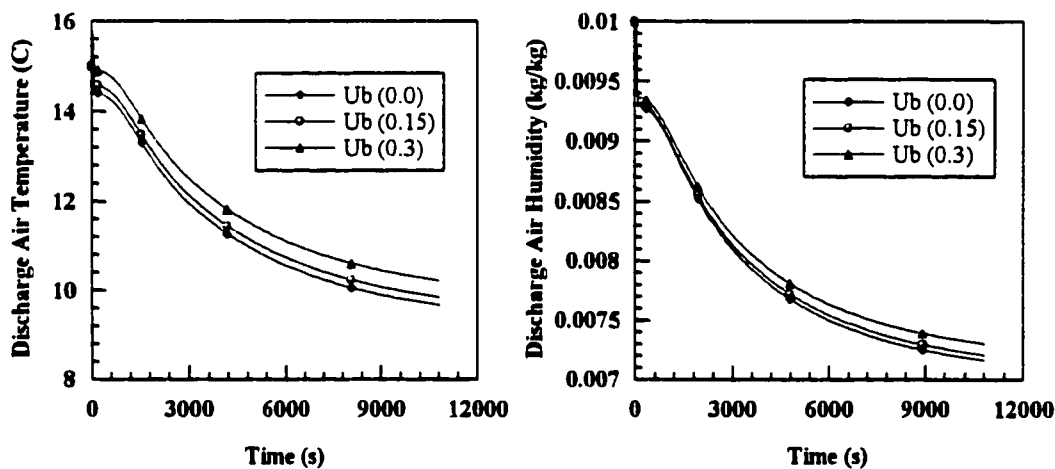
The effect of increasing the opening fraction of the bypass damper on the



(a) Temperature

(b) Humidity ratio

Without bypass



(c) Temperature

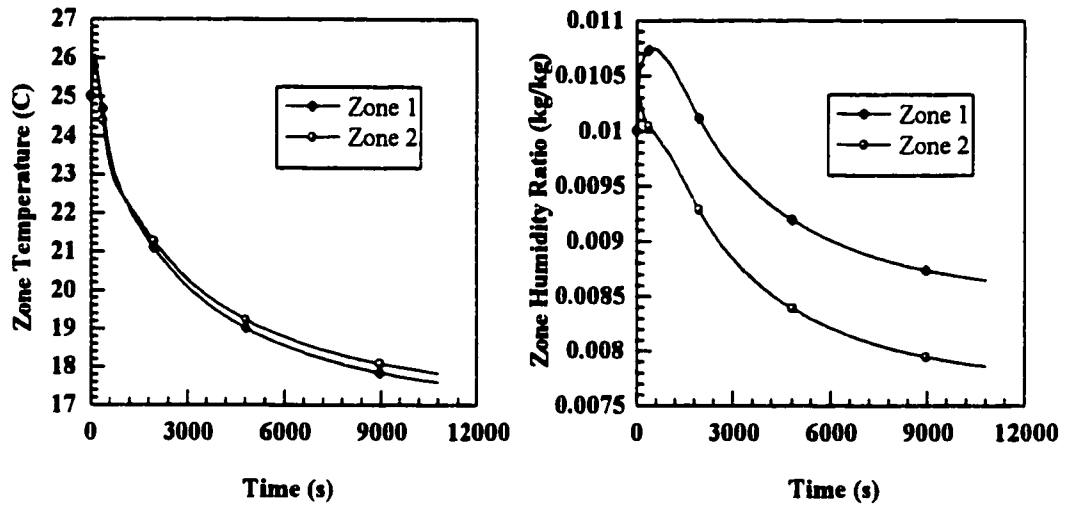
(d) Humidity ratio

With bypass

Figure 3.5 Temperature and humidity ratio responses of air leaving the cooling & dehumidifying coil without and with bypass

temperature and humidity ratio of air leaving the coil is depicted in Figures 3.5c-d. Note that although the steady state time remains the same (compared to the case with no bypass) the magnitudes of temperature and humidity ratio are higher as more hot and humid air is directly mixed with the cool air. Compared to the dynamics of the fan and the air system, the dynamic responses of the coil system are very slow. The slow responses of the coil system are due to the large capacity of the storage tank.

Figures 3.6a-b show the temperature and humidity ratio responses of air in zones 1 and 2. These responses were obtained under the same set of conditions as those used in Figure 3.4. It is apparent from Figures 3.6a-b that approximately 3.5 hours are needed for T_z and W_z to reach near steady state. It should be noted that the steady state time is a function of thermal capacity of subsystems, viz., thermal capacity of the storage tank, zone air, cooling coil etc., also the magnitude of the loads acting on the zone and the initial states of the system. It is evident from the results presented in Figures 3.4, 3.5, 3.6 that the overall VAV system can be thought of as consisting of a fast subsystem (the fan and air system characteristics), and a slow subsystem (thermal characteristics of the zones, chiller and coil etc.). The simulation results also reveal the fact that the model equations and the system parameters used yield results that are consistent with the expected trends from a VAV system. Note that the slow responses of the cooling coil are due to the large capacity of the storage tank. Actually, as will be shown later (Figs. 4.4-4.6), the responses of the cooling coil are very fast.



(a) Temperature responses

(b) Humidity ratio responses

Figure 3.6 Zone temperature and humidity responses

Table 3.1 Parameters of the VAV system

variable	magnitude(units)	variable	magnitude (units)
<u>Zone Model</u>		<u>Chiller Model</u>	
V_{z1}	280.0 m ³	V_{tank}	3.0 m ³
V_{z2}	280.0 m ³	$U_{c,max}$	20.0 kW
q_{sz1}	4.2 kW	a_{ch}	39.6 W/°C
q_{sz2}	6.4 kW	$T_{a,t}$	28.3°C
q_{lz1}	1.4 kW	<u>Duct Model</u>	
q_{lz2}	2.1 kW	A	0.25 m ²
\dot{m}_{wz1}	0.84 g/s	A_d	0.20 m
\dot{m}_{wz2}	0.56 g/s	m_d	6.4 kg/m
<u>Coil Model</u>		C_{pd}	418.7 J/kg K
A_f	76.8 m ²	<u>Fan Model</u>	
A_o	80.4 m ²	B_{eqf}	0.01 kg-m ² /s
A_{it}	10.4 m ²	e_{af}	220.0 V
c_{fin}	883.0 J/kg K	J_{eqf}	10.0 kg-m ²
c_t	384.0 J/kg K	k_{bf}	1.9 V-s/rev
m_{fin}	51.5 kg/m	K_i	1.9 N-m-rev/A
m_t	61.8 kg/m	L_{af}	1.0H
		R_{af}	0.5 Ω

Chapter 4

Dynamic Modeling of a Multi-zone VAV System: Reduced-order State Space Model

In Chapter 3 a dynamic model of a VAV system (large-scale model) was developed. The large-scale model developed is useful for detailed simulation of the VAV system. However, it is too large and requires extensive computations from the control analysis point of view. In this section, we will develop a reduced order model that is computationally more efficient, and more suitable for the purpose of control analysis.

In Section 4.1, reduced-order subsystem models as well as an overall system model will be developed. The open-loop simulation results of the reduced-order model will be presented and compared with those from the large-scale model in Section 4.2 and 4.3. In Section 4.4, an application of the model in simulating energy management functions will be given.

4.1 Development of reduced-order state space model of VAV system

In order to develop a reduced-order state space model of VAV system, it will be instructive to use a top-down approach. That is, the chosen VAV system configuration (Fig. 3.1) will be divided into important subsystems based on the knowledge derived from the simulation of large-scale system as well as physics of the problem.

The overall VAV system can be thought of as an interconnection of three subsystems: (i) airflow subsystem, (ii) water flow subsystem, and (iii) thermal subsystem

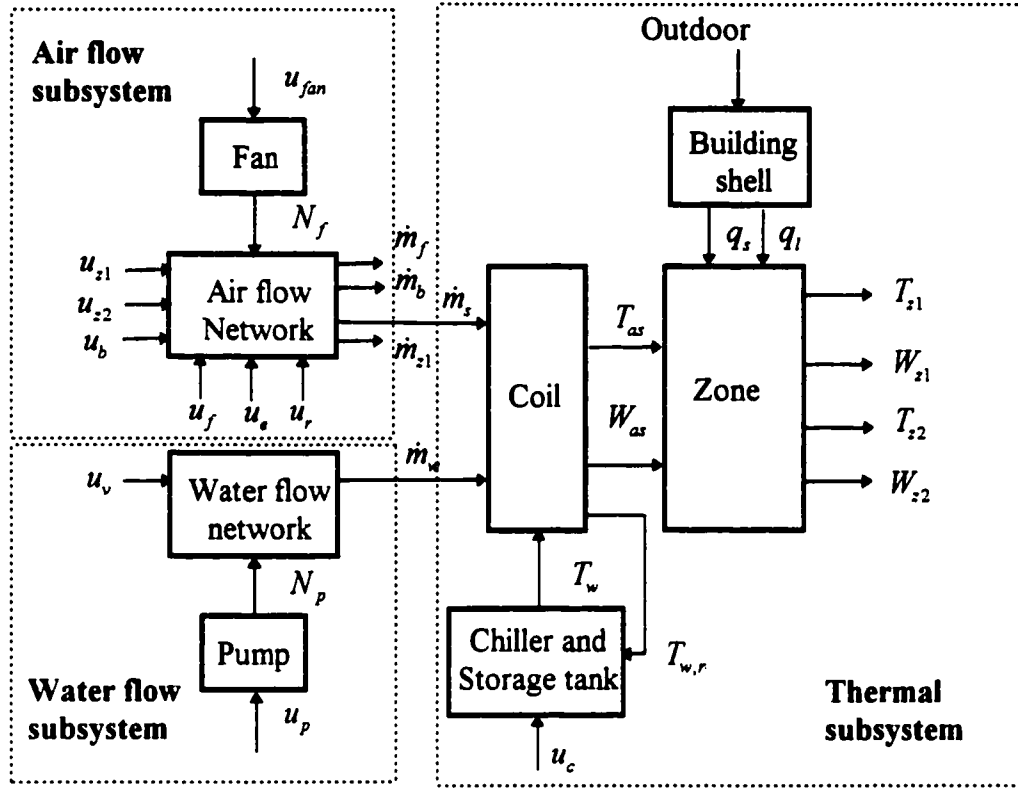


Figure 4.1 The interconnection of airflow, water flow, and thermal subsystems

as shown in Figure 4.1. The respective inputs and outputs of each subsystem are shown in the figure. In the following the state space models of these subsystems will be developed.

The overall model will be the augmented model consisting of all subsystems. That is

let

$$\dot{\mathbf{x}}_a = \mathbf{f}_a(\mathbf{x}_a, \mathbf{u}_a, \mathbf{d}_a, t)$$

$$\dot{\mathbf{x}}_w = \mathbf{f}_w(\mathbf{x}_w, \mathbf{u}_w, \mathbf{d}_w, t)$$

$$\dot{\mathbf{x}}_T = \mathbf{f}_T(\mathbf{x}_T, \mathbf{u}_T, \mathbf{d}_T, t)$$

where \mathbf{x}_a , \mathbf{x}_w and \mathbf{x}_T are the states of air flow, water flow, and thermal subsystems respectively, then the overall augmented model of VAV system in the vector form can be obtained as

$$\dot{\mathbf{x}} = \mathbf{f}(\mathbf{x}_a, \mathbf{x}_w, \mathbf{x}_T, \mathbf{u}_a, \mathbf{u}_w, \mathbf{u}_T, \mathbf{d}_a, \mathbf{d}_w, \mathbf{d}_T, t)$$

The objective of this section is to develop such a state space model and at the same time reduce the order of the system model.

4.1.1. A methodology and state space model of air flow subsystem

The state space model of the air flow subsystem is developed by applying the following principles to network of ducts: (i) the continuity equation must hold for each closed-circuit of the network and at each junction in the network the air flow into the junction must be equal to air flow out of the junction, (ii) the momentum equation must be satisfied for each duct in the network, and (iii) the cyclic integral of pressure drops around each circuit must be zero.

The application of continuity principle (i) to the VAV network shown in Figure 4.2 reveals that of the several possible closed circuit configurations, only four of them are independent. Thus four independent mass flow rates corresponding to the four circuits will suffice to describe the dynamics of air flow system. These mass flow rates are identified in Figure 4.2. These are outdoor air flow rate \dot{m}_f ; supply air \dot{m}_s , bypass air \dot{m}_b , and the air flow rate entering the zone 1 \dot{m}_{z1} . The corresponding closed circuits are (a) 1-2-3-34-33-32-29-30-31-∞-1; (b) 8-9-12-11-10-8; (c) 16-17-18-19-20-21-26-25-24-23-22-15-16; (d) 4-5-6-7-8-9-13-14-16-17-18-19-20-21-27-28-32-33-34-4.

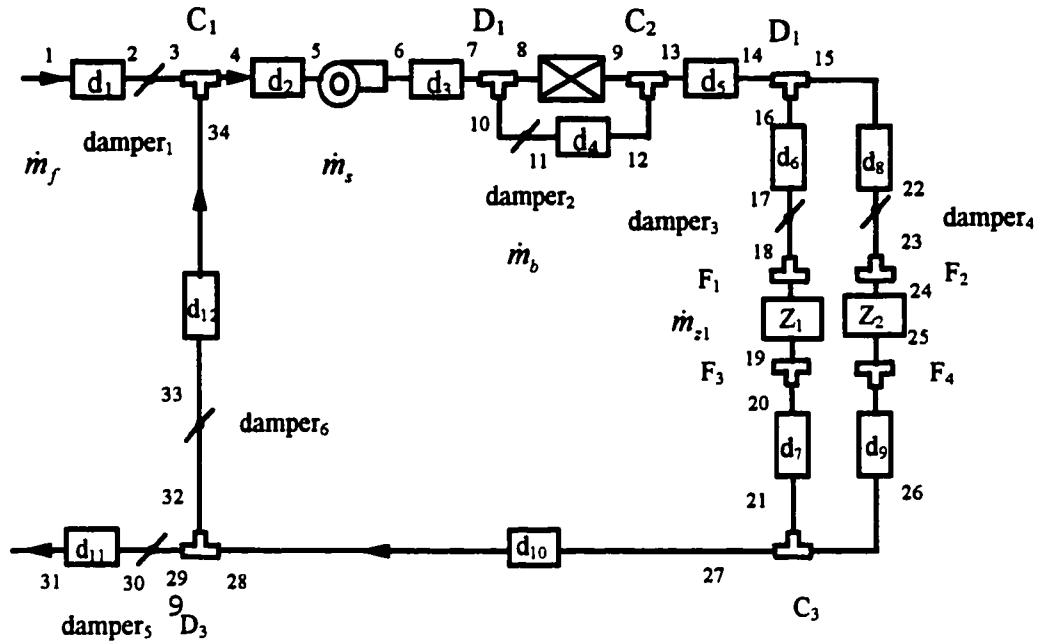


**Figure 4.2 Flow diagram for modeling air flow in VAV system
(two-zone system as an example)**

The application of second principle to the VAV network (Figure 4.2) requires that the momentum equation be satisfied for each duct section in the loop. At this point we apply the following model reduction technique. It may be noted, from model equations presented in Chapter 3, that in the large-scale model the air flow system is coupled with thermal system. In other words, as temperature changes the density of air consequently the mass flow rate also changes. However these changes are not significant in HVAC processes. Thus we can assume airflow in the duct as a constant density one dimensional fluid flow problem. As far as the overall VAV system is concerned the constant density assumption means the airflow system influences the thermal system but the thermal system does not effect the airflow system. And thus the airflow system is decoupled from the

thermal system. This assumption reduces the order of the model significantly. The momentum balance equation for airflow in a duct can be written as:

$$\frac{\partial}{\partial t}(\rho A V_a) = -A \frac{\partial P}{\partial y} - \frac{C_f A_d}{2} \rho V_a^2 \quad (4.1)$$

Equation (4.1) describes force balance on the control volume where the acceleration term is equal to the external forces acting on the control volume. These external forces are due to static pressure and frictional forces (first and second terms on right hand side of Equation 4.1). Also to note is the fact that C_f in Equation (4.1) is a function of Reynolds number, and the duct or the coil configuration (McQuiston and Parker 1988). In Equation (4.1), the air mass flow rate and frictional factor are constant along the duct length. This allows us to integrate the equation from 0 to L , which yields

$$\frac{L}{A} \frac{d\dot{m}_a}{dt} = P_{in} - P_{out} - \frac{C_f A_d L}{2\rho A^3} \dot{m}_a^2 \quad (4.2)$$

Equation (4.2) describes that the momentum change in the duct is due to the net pressure force and frictional forces. Eq. (4.2) can be rewritten:

$$\frac{L}{A} \frac{d\dot{m}_a}{dt} = P_{in} - P_{out} - f \quad (4.2a)$$

where $f = \frac{C_f A_d L}{2\rho A^3} \dot{m}_a^2$ is the frictional force.

Applying Eq. (4.2a) to each duct in Fig. 4.2 we have the following set of momentum equations:

for duct 1

$$\frac{L_1}{A_1} \frac{d\dot{m}_f}{dt} = P_1 - P_2 - f_1 \quad (4.3a)$$

for duct 2

$$\frac{L_2}{A_2} \frac{d\dot{m}_s}{dt} = P_4 - P_5 - f_2 \quad (4.3b)$$

for duct 3

$$\frac{L_3}{A_3} \frac{d\dot{m}_s}{dt} = P_6 - P_7 - f_3 \quad (4.3c)$$

for coil

$$\frac{L_c}{A_c} \frac{d(\dot{m}_s - \dot{m}_b)}{dt} = P_8 - P_9 - f_c \quad (4.3d)$$

for duct 4

$$\frac{L_4}{A_4} \frac{d\dot{m}_b}{dt} = P_{11} - P_{12} - f_4 \quad (4.3e)$$

for duct 5

$$\frac{L_5}{A_5} \frac{d\dot{m}_s}{dt} = P_{13} - P_{14} - f_5 \quad (4.3f)$$

for duct 6

$$\frac{L_6}{A_6} \frac{d\dot{m}_{z1}}{dt} = P_{16} - P_{17} - f_6 \quad (4.3g)$$

for duct 7

$$\frac{L_7}{A_7} \frac{d\dot{m}_{z1}}{dt} = P_{20} - P_{21} - f_7 \quad (4.3h)$$

for duct 8

$$\frac{L_8}{A_8} \frac{d(\dot{m}_s - \dot{m}_{z1})}{dt} = P_{15} - P_{16} - f_8 \quad (4.3i)$$

for duct 9

$$\frac{L_9}{A_9} \frac{d(\dot{m}_s - \dot{m}_{s1})}{dt} = P_{25} - P_{26} - f_9 \quad (4.3j)$$

for duct 10

$$\frac{L_{10}}{A_{10}} \frac{d\dot{m}_s}{dt} = P_{27} - P_{28} - f_{10} \quad (4.3k)$$

for duct 11

$$\frac{L_{11}}{A_{11}} \frac{d\dot{m}_f}{dt} = P_{30} - P_{31} - f_{11} \quad (4.3l)$$

for duct 12

$$\frac{L_{12}}{A_{12}} \frac{d(\dot{m}_s - \dot{m}_f)}{dt} = P_{33} - P_{34} - f_{12} \quad (4.3m)$$

Now applying the third principle (cyclic integral of pressure drops around each circuit must be zero), the above equations are added/subtracted according to the flow direction. Thus for the loop 1-2-3-34-33-32-29-30-31-∞-1 (duct sections 1, 12 and 11), the equation can be obtained from Eq. (4.3a) - Eq.(4.3m) + Eq.(4.3l):

$$\begin{aligned} & \left(\frac{L_1}{A_1} + \frac{L_{11}}{A_{11}} + \frac{L_{12}}{A_{12}} \right) \frac{d\dot{m}_f}{dt} - \frac{L_{12}}{A_{12}} \frac{d\dot{m}_s}{dt} = (P_1 - P_2) \\ & -(P_{33} - P_{34}) + (P_{30} - P_{31}) - f_1 + f_{12} - f_{11} \end{aligned} \quad (4.4)$$

we have

$$P_{34} - P_2 = \Delta C_1^T - \Delta C_1 - \Delta P_{d1}, \quad P_{31} - P_1 = \Delta P_{out} + \Delta P_{in}$$

$$P_{30} - P_{33} = \Delta P_{d6} + \Delta D_3 - \Delta D_3^T$$

where $\Delta C_i, \Delta C_i^T$ are the pressure losses at the converge section i corresponding to main stream, $\Delta D_i, \Delta D_i^T$ are the pressure losses at the diverge section i corresponding to main

stream. The expressions for $\Delta C_i, \Delta C_i^T$ and $\Delta D_i, \Delta D_i^T$ will be given in equations for pressure loss in converging and diverging section. ΔP_{di} is the pressure loss at the i th damper.

Eq. (4-4) can be written as:

$$\begin{aligned} & \left(\frac{L_1}{A_1} + \frac{L_{11}}{A_{11}} + \frac{L_{12}}{A_{12}} \right) \frac{d\dot{m}_f}{dt} - \frac{L_{12}}{A_{12}} \frac{d\dot{m}_s}{dt} = -f_1 - \Delta P_{d1} \\ & + \Delta C_1^T - \Delta C_1 + f_{12} + \Delta P_{d6} + \Delta D_3 - \Delta D_3^T - f_{11} - \Delta P_{out} - \Delta P_{in} \end{aligned} \quad (4.5)$$

For the loop 4-5-6-7-8-9-13-14-16-17-18-19-20-21-27-28-32-33-34-4 (duct sections 2, 3, 4, 5, 6, 7, 10, 12), the equation can be obtained from Eq. (4.3b) + Eq. (4.3c) + Eq. (4.3e) + Eq. (4.3f) + Eq. (4.3g) + Eq. (4.3h) + Eq. (4.3k) + Eq. (4.3m):

$$\begin{aligned} & \left(\frac{L_2}{A_2} + \frac{L_3}{A_3} + \frac{L_5}{A_5} + \frac{L_{10}}{A_{10}} + \frac{L_{12}}{A_{12}} \right) \frac{d\dot{m}_s}{dt} + \left(\frac{L_6}{A_6} + \frac{L_7}{A_7} \right) \frac{d\dot{m}_{z1}}{dt} + \frac{L_4}{A_4} \frac{d\dot{m}_b}{dt} - \frac{L_{12}}{A_{12}} \frac{d\dot{m}_f}{dt} \\ & = (P_4 - P_5) + (P_6 - P_7) + (P_{11} - P_{12}) + (P_{13} - P_{14}) + (P_{16} - P_{17}) + (P_{20} - P_{21}) \\ & + (P_{27} - P_{28}) + (P_{33} - P_{34}) - f_2 - f_3 - f_4 - f_5 - f_6 - f_7 - f_{10} - f_{12} \end{aligned} \quad (4.6)$$

we have

$$\begin{aligned} P_6 - P_5 &= \Delta P_{fan} & P_7 - P_{11} &= \Delta d_2 + \Delta D_1^T & P_{12} - P_{13} &= \Delta C_2^T \\ P_{14} - P_{16} &= \Delta D_2^T & P_{17} - P_{20} &= \Delta d_3 + \Delta P_{z1,in} + \Delta P_{z1,out} \\ P_{21} - P_{27} &= \Delta C_3^T & P_{28} - P_{33} &= \Delta D_3^T & P_{34} - P_4 &= \Delta C_1^T \end{aligned}$$

where ΔP_{fan} is the pressure gain due to fan and the equation for computing ΔP_{fan} will be given in the fan-motor model.

Eq. (4.6) can be written as:

$$\begin{aligned} & \left(\frac{L_2}{A_2} + \frac{L_3}{A_3} + \frac{L_5}{A_5} + \frac{L_{10}}{A_{10}} + \frac{L_{12}}{A_{12}} \right) \frac{d\dot{m}_s}{dt} + \left(\frac{L_6}{A_6} + \frac{L_7}{A_7} \right) \frac{d\dot{m}_{z1}}{dt} + \frac{L_4}{A_4} \frac{d\dot{m}_b}{dt} - \frac{L_{12}}{A_{12}} \frac{d\dot{m}_f}{dt} \\ & = \Delta P_{fan} - \Delta d_2 - \Delta D_1^T - \Delta C_2^T - \Delta D_2^T - \Delta d_3 - \Delta P_{z1,in} - \Delta P_{z1,out} - \Delta C_3^T \\ & - \Delta D_3^T - \Delta C_1^T - f_2 - f_3 - f_4 - f_5 - f_6 - f_7 - f_{10} - f_{12} \end{aligned} \quad (4.7)$$

For the loop 8-9-12-11-10-8 (duct section 4 and coil) , the equation can be obtained from Eq. (4.3e) - Eq.(4.3d),

$$\left(\frac{L_c}{A_c} + \frac{L_4}{A_4}\right) \frac{d\dot{m}_b}{dt} - \frac{L_4}{A_4} \frac{d\dot{m}_s}{dt} = (P_{11} - P_{12}) - (P_8 - P_9) - f_4 - f_c \quad (4.8)$$

we have

$$P_{11} - P_8 = \Delta D_1^T - \Delta D_1 - \Delta P_{d2} \quad P_{12} - P_9 = \Delta C_2^T - \Delta C_2$$

Eq. (4.8) can be written as:

$$\left(\frac{L_c}{A_c} + \frac{L_4}{A_4}\right) \frac{d\dot{m}_b}{dt} - \frac{L_4}{A_4} \frac{d\dot{m}_s}{dt} = \Delta D_1^T - \Delta D_1 - \Delta P_{d2} - \Delta C_2^T + \Delta C_2 - f_4 - f_c \quad (4.9)$$

For the loop 16-17-18-19-20-21-26-25-24-23-22-15-16 (duct sections 6, 7, 9, 8), the equation can be obtained from Eq. (4.3g) + Eq. (4.3h) - Eq. (4.3i) - Eq. (4.3j) :

$$\begin{aligned} &\left(\frac{L_6}{A_6} + \frac{L_7}{A_7} + \frac{L_8}{A_8} + \frac{L_9}{A_9}\right) \frac{d\dot{m}_{z1}}{dt} - \left(\frac{L_8}{A_8} + \frac{L_9}{A_9}\right) \frac{d\dot{m}_s}{dt} = (P_{16} - P_{17}) \\ &+ (P_{20} - P_{21}) - (P_{15} - P_{22}) - (P_{25} - P_{26}) + f_6 + f_7 - f_8 - f_9 \end{aligned} \quad (4.10)$$

we have

$$\begin{aligned} P_{16} - P_{15} &= \Delta D_2 - \Delta D_2^T & P_{17} - P_{20} &= \Delta d_3 + \Delta P_{z1,in} + \Delta P_{z1,out} \\ P_{26} - P_{21} &= \Delta C_3 - \Delta C_3^T & P_{22} - P_{25} &= \Delta d_4 + \Delta P_{z2,in} + \Delta P_{z2,out} \end{aligned}$$

Eq. (4.10) can be written as:

$$\begin{aligned} &\left(\frac{L_6}{A_6} + \frac{L_7}{A_7} + \frac{L_8}{A_8} + \frac{L_9}{A_9}\right) \frac{d\dot{m}_{z1}}{dt} - \left(\frac{L_8}{A_8} + \frac{L_9}{A_9}\right) \frac{d\dot{m}_s}{dt} = \Delta D_2 - \Delta D_2^T + \Delta C_3 - \Delta C_3^T \\ &- \Delta d_3 - \Delta P_{z1,in} - \Delta P_{z1,out} + \Delta d_4 + \Delta P_{z2,in} + \Delta P_{z2,out} + f_6 + f_7 - f_8 - f_9 \end{aligned} \quad (4.11)$$

We have developed four equations (4.5, 4.7, 4.9, 4.11) for four independent loops.

The four equations can be rewritten in matrix form as

$$\mathbf{L} \begin{Bmatrix} \frac{d\dot{m}_f}{dt} \\ \frac{d\dot{m}_s}{dt} \\ \frac{d\dot{m}_b}{dt} \\ \frac{d\dot{m}_{z1}}{dt} \end{Bmatrix} = \begin{Bmatrix} f_1'(\dot{m}_f, \dot{m}_s, \dot{m}_b, \dot{m}_{z1}, N_{m,f}(U_{fan}), U_i) \\ f_2'(\dot{m}_f, \dot{m}_s, \dot{m}_b, \dot{m}_{z1}, N_{m,f}(U_{fan}), U_i) \\ f_3'(\dot{m}_f, \dot{m}_s, \dot{m}_b, \dot{m}_{z1}, N_{m,f}(U_{fan}), U_i) \\ f_4'(\dot{m}_f, \dot{m}_s, \dot{m}_b, \dot{m}_{z1}, N_{m,f}(U_{fan}), U_i) \end{Bmatrix} \quad (4.12)$$

where \mathbf{L} is a matrix, the elements of which contain the duct length and cross-section area.

$$\mathbf{L} = \begin{bmatrix} (\frac{L_1}{A_1} + \frac{L_{11}}{A_{11}} + \frac{L_{12}}{A_{12}}) & -\frac{L_{12}}{A_{12}} & 0 & 0 \\ -\frac{L_{12}}{A_{12}} & (\frac{L_2}{A_2} + \frac{L_3}{A_3} + \frac{L_5}{A_5} + \frac{L_{10}}{A_{10}} + \frac{L_{12}}{A_{12}}) & \frac{L_4}{A_4} & (\frac{L_6}{A_6} + \frac{L_7}{A_7}) \\ 0 & -\frac{L_4}{A_4} & (\frac{L_c}{A_c} + \frac{L_4}{A_4}) & 0 \\ 0 & -(\frac{L_8}{A_8} + \frac{L_9}{A_9}) & 0 & (\frac{L_6}{A_6} + \frac{L_7}{A_7} + \frac{L_8}{A_8} + \frac{L_9}{A_9}) \end{bmatrix}$$

and f_1' , f_2' , f_3' , f_4' are the expressions at right side of Eq. (4.5), (4.7), (4.8), (4.11), respectively. All terms in the expressions are function of air flow rates, fan-motor speed $N_{m,f}$ (influenced by fan voltage input U_{fan}), and damper positions U_i .

In the matrix \mathbf{L} , all the elements include only duct physical parameters. Once the duct system is designed, all these parameters are known. Therefore, we can invert the matrix \mathbf{L} to get state equations for air flow subsystem:

$$\begin{Bmatrix} \frac{d\dot{m}_f}{dt} \\ \frac{d\dot{m}_s}{dt} \\ \frac{d\dot{m}_b}{dt} \\ \frac{d\dot{m}_{z1}}{dt} \end{Bmatrix} = \mathbf{L}^{-1} \begin{Bmatrix} f_1'(\dot{m}_f, \dot{m}_s, \dot{m}_b, \dot{m}_{z1}, N_{m,f}(U_{fan}), U_i) \\ f_2'(\dot{m}_f, \dot{m}_s, \dot{m}_b, \dot{m}_{z1}, N_{m,f}(U_{fan}), U_i) \\ f_3'(\dot{m}_f, \dot{m}_s, \dot{m}_b, \dot{m}_{z1}, N_{m,f}(U_{fan}), U_i) \\ f_4'(\dot{m}_f, \dot{m}_s, \dot{m}_b, \dot{m}_{z1}, N_{m,f}(U_{fan}), U_i) \end{Bmatrix} = \begin{Bmatrix} f_1(\dot{m}_f, \dot{m}_s, \dot{m}_b, \dot{m}_{z1}, N_{m,f}(U_{fan}), U_i) \\ f_2(\dot{m}_f, \dot{m}_s, \dot{m}_b, \dot{m}_{z1}, N_{m,f}(U_{fan}), U_i) \\ f_3(\dot{m}_f, \dot{m}_s, \dot{m}_b, \dot{m}_{z1}, N_{m,f}(U_{fan}), U_i) \\ f_4(\dot{m}_f, \dot{m}_s, \dot{m}_b, \dot{m}_{z1}, N_{m,f}(U_{fan}), U_i) \end{Bmatrix} \quad (4.13)$$

In general, for the air flow subsystem which has m independent mass flow rates, n fans and k dampers, the model has the form

$$\left\{ \begin{array}{c} \frac{dm_1}{dt} \\ \vdots \\ \vdots \\ \frac{dm_m}{dt} \end{array} \right\} = \left\{ \begin{array}{c} f_1(m_1, \dots, m_m, N_{1,f}, \dots, N_{n,f}, U_1, \dots, U_k) \\ \vdots \\ \vdots \\ f_m(m_1, \dots, m_m, N_{1,f}, \dots, N_{n,f}, U_1, \dots, U_k) \end{array} \right\}$$

where m_i is the i -th independent air flow rate, $N_{j,f}$ is the speed of the j -th fan, U_l is the l -th damper position.


Fan-Motor Model

The fan and motor model describes the relationship between the fan speed, motor input power and the fan pressure. The model equations remain same as those described by Equations (3.71 - 3.73).

Correlations for Pressure Losses in the Duct System

Frictional losses occurring in the duct system, fittings and across the dampers and elsewhere in the duct system were accounted for by using the correlations available in the literature, which are described by Equations (3.76 - 3.79). Those equations can be rewritten as follows:

Pressure loss in converging and diverging sections

Diverging section ()


$$P_1 = P_3 + \Delta C \quad (3.76a)$$

$$P_2 = P_3 + \Delta C^T \quad (3.77a)$$

where

$$\Delta C = \frac{(1 + \xi_{31})}{2} \rho_3 V_3^2 - \frac{1}{2} \rho_1 V_1^2$$

$$\Delta C^T = \frac{(1 + \xi_{32})}{2} \rho_3 V_3^2 - \frac{1}{2} \rho_2 V_2^2$$

Diverging section (3  1)

$$P_1 = P_3 + \Delta D \quad (3.78a)$$

$$P_2 = P_3 + \Delta D^T \quad (3.79a)$$

where

$$\Delta C = \frac{(1 - \xi_{31})}{2} \rho_3 V_3^2 - \frac{1}{2} \rho_1 V_1^2$$

$$\Delta C^T = \frac{(1 - \xi_{32})}{2} \rho_3 V_3^2 - \frac{1}{2} \rho_2 V_2^2$$

To summarize the state space model of airflow subsystem shown in Fig. 4.2 has six state equations and has the following structure:

$$\left\{ \begin{array}{l} \frac{d\dot{m}_f}{dt} \\ \frac{d\dot{m}_s}{dt} \\ \frac{d\dot{m}_b}{dt} \\ \frac{d\dot{m}_{z1}}{dt} \\ \frac{dN_{m,f}}{dt} \\ \frac{dI_{m,f}}{dt} \end{array} \right\} = \left\{ \begin{array}{l} f_1(\dot{m}_f, \dot{m}_s, \dot{m}_b, \dot{m}_{z1}, N_{m,f}, U_i) \\ f_2(\dot{m}_f, \dot{m}_s, \dot{m}_b, \dot{m}_{z1}, N_{m,f}, U_i) \\ f_3(\dot{m}_f, \dot{m}_s, \dot{m}_b, \dot{m}_{z1}, N_{m,f}, U_i) \\ f_4(\dot{m}_f, \dot{m}_s, \dot{m}_b, \dot{m}_{z1}, N_{m,f}, U_i) \\ f_5(\dot{m}_s, N_{m,f}, I_{m,f}) \\ f_6(N_{m,f}, I_{m,f}, U_{fan}) \end{array} \right\} \quad (4.14)$$

4.1.2. State space model of water flow subsystem

We now consider the second subsystem of Figure 4.1 namely, the water flow subsystem. The physical configuration of the water flow network is shown in Figure 4.3. As shown in Figure 4.3 chilled water from storage is circulated via a pump and piping to the cooling and dehumidifying coil. The piping network has a single loop (with one valve and a pump) which can be modeled by the network principles described in Section 4.1.1. Thus the state space equation of water flow subsystem is

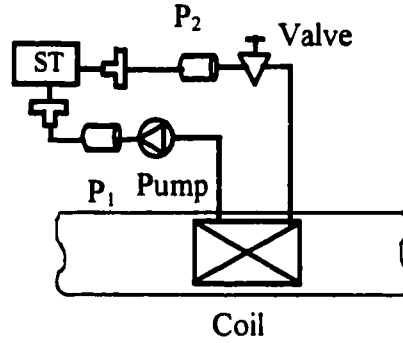


Figure 4.3 Flow diagram for modeling water flow in VAV system

$$\frac{dm_w}{dt} = \Delta P_p - \Delta P_v - f_{p1} - \Delta P_{\text{tank},in} - \Delta P_{\text{tank},out} - f_{p2} \quad (4.15)$$

where ΔP_p is the pressure increase driven by pump. ΔP_v is the pressure drop across the valve. $\Delta P_{\text{tank},in}$ and $\Delta P_{\text{tank},out}$ are the pressure drops corresponding to expansion and extraction respectively. $f_{p1} = \frac{C_f A_d L_{p1}}{2\rho_w A_1^3} \dot{m}_w^2$ and $f_{p2} = \frac{C_f A_d L_{p2}}{2\rho_w A_2^3} \dot{m}_w^2$ are the pressure drops due to friction losses in the pipe 1 and 2 respectively.

Pump-Motor Model ()

The pump-motor model is similar to the fan-motor model. The model equations are


$$\frac{dN_p}{dt} = \frac{k_i I_p}{2\pi J_{eq,p}} - \frac{B_{eq,p}}{J_{eq,p}} N_p - \frac{\dot{m}_w \Delta P_p}{(2\pi)^2 \rho_w N_p \eta_p J_{eq,p}} \quad (4.16)$$

$$\frac{dI_p}{dt} = \frac{e_{a,p}}{L_{a,p}} U_p - \frac{R_{a,p}}{L_{a,p}} I_p - \frac{2\pi k_{b,p}}{L_{a,p}} N_p \quad (4.17)$$

$$\Delta P_p = C_h \rho_w D^2 N_p^2 \left(\frac{n_m}{n_p} \right)^2 \quad (4.18)$$



Correlations for Pressure Losses in the Piping System

Frictional losses occurring in the piping system, fittings and across the valves and elsewhere in the piping system were accounted for by using the correlations available in the literature. These are

Pressure loss across the valves ()

$$\Delta P_v = \{a_1 U_v^{a_2}\} \frac{\dot{m}_w^2}{2\rho_w A^2} \quad (4.19)$$

The coefficients a_1 and a_2 were obtained by fitting curves to the data given by Lyons (1982).

Pressure loss due to sudden expansion () and contraction ()

The pressure losses occurring at sudden expansion and contraction of areas were modeled as follows (McQuiston and Parker 1988).

$$\Delta P = \xi \frac{\dot{m}_w^2}{2\rho_w A^2} \quad (4.20)$$

where the friction factor ξ is different for each case.

To summarize a third-order water flow subsystem model can be expressed by the following state equations:

$$\begin{Bmatrix} \frac{d\dot{m}_w}{dt} \\ \frac{dN_{m,p}}{dt} \\ \frac{dI_{m,p}}{dt} \end{Bmatrix} = \begin{Bmatrix} f_1(\dot{m}_w, N_{m,p}, U_v) \\ f_2(\dot{m}_w, N_{m,f}, I_{m,f}) \\ f_3(N_{m,f}, I_{m,f}, U_{fan}) \end{Bmatrix} \quad (4.21)$$

4.1.3. State space model of thermal subsystem

The thermal system as shown in Fig. 4.1 receives input from the airflow and water flow subsystems. The main components of thermal subsystem are: a cooling and dehumidifying coil, a chiller and storage tank arrangement, and environmental zones including the building shell.

Coil Model

In this section, modifications will be made to the coil model developed in Chapter 3 to develop a reduced-order distributed cooling and dehumidifying coil model. Then lumped coil models will be developed which include both the sensible coil model and the cooling and dehumidifying coil model.

1. Distributed Cooling and Dehumidifying Coil Model

The cooling and dehumidifying coil modeled is the same as that in Chapter 3, i.e., a typical counter-cross-flow type with continuous plate-fins on tubes (Figure 3.2a). The simplifications in the coil model were achieved mainly due to the assumption of constant density of air and neglecting the sensible and latent heat transfer from the duct surface enclosing the coil. Under above assumptions, Eqs. (3.38-3.45) can be simplified. These are:

The energy equation

$$\begin{aligned} \frac{\partial T_a}{\partial t} + \frac{\dot{m}_a}{m_a} \frac{\partial T_a}{\partial y} + (1 - \gamma) T_a \frac{\partial W_a}{\partial t} = \frac{c_w}{c_v} \frac{T_a h_{m,t} A_o \eta_{c,ov}}{m_a} (W_a - W_{t,st}) f_{w,t} \\ - \frac{h_t A_o \eta_{s,ov}}{c_v m_a} (T_a - T_t) \end{aligned} \quad (3.41a)$$

The vapor balance equation

$$\frac{\partial W_a}{\partial t} + \frac{\dot{m}_a}{m_a} \frac{\partial W_a}{\partial y} = - \frac{h_{m,t} \eta_{c,ov} A_o}{m_a} (W_a - W_{t,st}) f_{w,t} \quad (3.42a)$$

Equation for the tube temperature

$$\begin{aligned} \frac{\partial T_a}{\partial t} + \frac{\eta_s + \frac{m_t c_t}{m_{fin} c_{fin}}}{1 - \eta_s} \frac{\partial T_t}{\partial t} = \frac{\eta_{s,ov} h_t A_o}{m_{fin} c_{fin} (1 - \eta_s)} (T_a - T_t) \\ + \frac{\eta_{c,ov} \lambda h_{m,t} A_o}{m_{fin} c_{fin} (1 - \eta_s)} (W_a - W_{t,st}) f_{w,t} - \frac{h_{t,t} A_{t,t}}{m_{fin} c_{fin} (1 - \eta_s)} (T_t - T_w) \end{aligned} \quad (3.43a)$$

Energy balance on the chilled water in the tubes

$$\frac{\partial T_w}{\partial t} - \frac{\dot{m}_w}{m_w} \frac{\partial T_w}{\partial y} = - \frac{h_{t,t} A_{t,t}}{c_w m_w} (T_t - T_w) \quad (3.44a)$$

Note that both Eq. (3.38) (the mass balance of dry air) and (3.39) (the momentum equation) have been decoupled from the coil model.

Eqs. (3.42a) and (3.44a) can be rewritten as:

$$\frac{\partial W_a}{\partial t} = -\frac{\dot{m}_a}{m_a} \frac{\partial W_a}{\partial y} - \frac{h_{m,t} \eta_{c,ov} A_o}{m_a} (W_a - W_{t,st}) f_{w,t} \quad (4.22)$$

$$\frac{\partial T_w}{\partial t} = \frac{\dot{m}_w}{m_w} \frac{\partial T_w}{\partial y} + \frac{h_{it} A_{it}}{m_w c_w} (T_i - T_w) \quad (4.23)$$

Substituting Eq. (4-22) into Eq. (3.41a), Eq. (3.41a) can be expressed as:

$$\begin{aligned} \frac{\partial T_a}{\partial t} = & -\frac{h_t \eta_{s,ov} A_o}{\rho c_v A} (T_a - T_i) - \frac{\gamma \dot{m}_a}{\rho A} \frac{\partial T_a}{\partial y} - \frac{(\gamma - 1) \dot{m}_a T_a}{\rho A} \frac{\partial W_a}{\partial y} \\ & + \frac{h_{m,t} \eta_{c,ov} A_o T_a}{\rho A} \left(\frac{c_w}{c_v} + 1 - \gamma \right) (W_a - W_{t,st}) f_{w,t} \end{aligned} \quad (4.24)$$

Substituting Eq. (4.24) into Eq. (3.43a), Eq. (3.43a) can be rewritten as

$$\begin{aligned} \frac{\partial T_i}{\partial t} = & \frac{1 - \eta_s}{\eta_s + \frac{m_i c_i}{m_{fin} c_{fin}}} \left\{ \frac{\gamma \dot{m}_a}{\rho A} \frac{\partial T_a}{\partial y} + \frac{(\gamma - 1) \dot{m}_a T_a}{\rho A} \frac{\partial W_a}{\partial y} \right. \\ & + \left[\left(\gamma - 1 - \frac{c_w}{c_v} \right) \frac{T_a}{\rho A} + \frac{\lambda}{m_{fin} c_{fin} (1 - \eta_s)} \right] h_{m,t} \eta_{c,ov} A_o (W_a - W_{t,st}) f_{w,t} \\ & \left. + \left(\frac{\eta_{s,ov} h_c A_o}{\rho c_v A} + \frac{\eta_{s,ov} h_c A_o}{m_{fin} c_{fin} (1 - \eta_s)} \right) (T_a - T_i) - \frac{h_{it} A_{it}}{m_{fin} c_{fin} (1 - \eta_s)} (T_i - T_w) \right\} \end{aligned} \quad (4.25)$$

In summary, the distributed cooling and dehumidifying coil model can be described

by the following state equations:

Air Temperature

$$\begin{aligned} \frac{\partial T_a}{\partial t} = & -\frac{h_t \eta_{s,ov} A_o}{\rho c_v A} (T_a - T_i) - \frac{\gamma \dot{m}_a}{\rho A} \frac{\partial T_a}{\partial y} - \frac{(\gamma - 1) \dot{m}_a T_a}{\rho A} \frac{\partial W_a}{\partial y} \\ & + \frac{h_{m,t} \eta_{c,ov} A_o T_a}{\rho A} \left(\frac{c_w}{c_v} + 1 - \gamma \right) (W_a - W_{t,st}) f_{w,t} \end{aligned} \quad (4.26)$$

Air Humidity Ratio

$$\frac{\partial W_a}{\partial t} = -\frac{\dot{m}_a}{\rho A} \frac{\partial W_a}{\partial y} - \frac{h_{m,t} \eta_{c,ov} A_o T_a}{\rho A} (W_a - W_{t,st}) f_{w,t} \quad (4.27)$$

Water Temperature

$$\frac{\partial T_w}{\partial t} = \frac{\dot{m}_w}{m_w} \frac{\partial T_w}{\partial x} + \frac{h_{it} A_{it}}{m_w c_w} (T_i - T_w) \quad (4.28)$$

Tube Temperature

$$\begin{aligned} \frac{\partial T_i}{\partial t} = & \frac{1 - \eta_s}{\eta_s + \frac{m_i c_i}{m_{fin} c_{fin}}} \left\{ \frac{\gamma \dot{m}_a}{\rho A} \frac{\partial T_a}{\partial y} + \frac{(\gamma - 1) \dot{m}_a T_a}{\rho A} \frac{\partial W_a}{\partial y} \right. \\ & + \left[(\gamma - 1 - \frac{c_w}{c_v}) \frac{T_a}{\rho A} + \frac{\lambda}{m_{fin} c_{fin} (1 - \eta_s)} \right] h_{m,t} \eta_{c,ov} A_o (W_a - W_{t,st}) f_{w,t} \\ & \left. + \left(\frac{\eta_{s,ov} h_c A_o}{\rho c_v A} + \frac{\eta_{s,ov} h_c A_o}{m_{fin} c_{fin} (1 - \eta_s)} \right) (T_a - T_i) - \frac{h_{it} A_{it}}{m_{fin} c_{fin} (1 - \eta_s)} (T_i - T_w) \right\} \end{aligned} \quad (4.29)$$

The symbols in the model are same as those in the large-scale model. In the model, there are distributed terms involved, such as $\frac{\partial T_a}{\partial y}$, $\frac{\partial W_a}{\partial y}$, and $\frac{\partial T_w}{\partial y}$. We can divide the coil into several nodes along its depth and discretize the distributed terms at these nodes. For a coil with four nodes, the order of the distributed coil model will be sixteen.

2. Lumped Sensible Coil Model

Some times the coil is operated in sensible mode such as in the heating case. Under these conditions, we can take the whole coil as one control volume (i.e., one node), and develop the following model equations. Note that the spatial dependence is averaged over the entire depth of the coil. The sensible coil model equations are:

Air Temperature

$$\frac{dT_a}{dt} = - \frac{h_i \eta_{s,ov} A_o}{\rho c_v A} (\bar{T}_a - \bar{T}_i) - \frac{\gamma \dot{m}_a}{\rho A L_c} (T_a - T_{a,in}) \quad (4.30)$$

Water Temperature

$$\frac{dT_w}{dt} = \frac{\dot{m}_w}{m_w L_c} (T_{w,s} - T_w) + \frac{h_{it} A_{it}}{m_w c_w} (\bar{T}_t - \bar{T}_w) \quad (4.31)$$

Tube Temperature

$$\begin{aligned} \frac{d\bar{T}_t}{dt} = & \frac{1 - \eta_s}{\eta_s + \frac{m_t c_t}{m_{fin} c_{fin}}} \left\{ \frac{\gamma \dot{m}_a}{\rho A L_c} (T_a - T_{a,in}) - \frac{h_{it} A_{it}}{m_{fin} c_{fin} (1 - \eta_s)} (\bar{T}_t - \bar{T}_w) \right. \\ & \left. + \left(\frac{\eta_{s,ov} h_c A_o}{\rho c_v A} + \frac{\eta_{s,ov} h_c A_o}{m_{fin} c_{fin} (1 - \eta_s)} \right) (\bar{T}_a - \bar{T}_t) \right\} \end{aligned} \quad (4.32)$$

where T_a is the temperature of air leaving the coil, $T_{a,in}$ is the temperature of air entering the coil, T_w is the temperature of return water, $T_{w,s}$ is the temperature of supply water. \bar{T}_a , \bar{T}_w , \bar{T}_t are the mean bulk temperature of air, water, tube within the coil, respectively. Note that heat transfer between tube and water is proportional to the driving potential $(\bar{T}_w - \bar{T}_t)$, heat transfer between air and the tube is proportional to the term $(\bar{T}_a - \bar{T}_t)$.

Some studies simply used the arithmetic average of inlet temperature and outlet temperature to represent the mean bulk temperature. For example, Stoecker et al. (1978), in their study, assumed the driving forces between air and tube, between tube and water can be represented by $[\frac{1}{2}(T_a + T_{a,in}) - \bar{T}_t]$ and $[\bar{T}_t - \frac{1}{2}(T_w + T_{w,s})]$. This is acceptable when the coil depth is very small because exponential distributions in a very small range are close to linear distributions of temperatures of air and water. However, for large coil depth, the arithmetic average assumption will lead to noticeable error as will be shown later.

In our study, we found that for the counter-cross-flow coil configuration, the mean bulk temperature of air \bar{T}_a can be assumed as $\bar{T}_a = \frac{\dot{m}_a c_{pa} T_{a,in} + \dot{m}_w c_w T_a}{\dot{m}_a c_{pa} + \dot{m}_w c_w}$, the mean bulk temperature of water \bar{T}_w as $\bar{T}_w = \frac{\dot{m}_a c_{pa} T_w + \dot{m}_w c_w T_{w,s}}{\dot{m}_a c_{pa} + \dot{m}_w c_w}$. In other words, instead of taking arithmetic average, we take the weighted average. If the temperature is on the air-side inlet, the weighting factor is $\dot{m}_a c_{pa}$, i.e., the heat capacity of air flow. When the temperature is on the water-side inlet, the weighting factor is $\dot{m}_w c_w$, i.e., the heat capacity of water flow. It may be noted that only three state equations are needed to model a sensible heat coil.

3. Lumped Model of Cooling and Dehumidifying Coil

In a manner similar to the heating coil, a lumped capacity cooling and dehumidifying coil model was developed. The coil model can be described by the following state equations.

Air Temperature

$$\begin{aligned} \frac{dT_a}{dt} = & -\frac{h_t \eta_{s,ov} A_o}{\rho c_v A} (\bar{T}_a - \bar{T}_t) - \frac{\gamma \dot{m}_a}{\rho A} (T_a - T_{ann}) - \frac{(\gamma - 1) \dot{m}_a \bar{T}_a}{\rho A} (W_a - W_{ann}) \\ & + \frac{h_{m,t} \eta_{c,ov} A_o \bar{T}_a}{\rho A} \left(\frac{c_w}{c_v} + 1 - \gamma \right) (\bar{W}_a - \bar{W}_{t,st}) f_{w,t} \end{aligned} \quad (4.33)$$

Air Humidity Ratio

$$\frac{dW_a}{dt} = \frac{\dot{m}_a}{\rho A} (W_a - W_{ann}) - \frac{h_{m,t} \eta_{c,ov} A_o \bar{T}_a}{\rho A} (\bar{W}_a - \bar{W}_{t,st}) f_{w,t} \quad (4.34)$$

Water Temperature

$$\frac{dT_w}{dt} = \frac{\dot{m}_w}{m_w} (T_w - T_{ws}) + \frac{h_{it} A_{it}}{m_w c_w} (\bar{T}_t - \bar{T}_w) \quad (4.35)$$

Tube Temperature

$$\begin{aligned} \frac{d\bar{T}_t}{dt} = & \frac{1 - \eta_s}{\eta_s + \frac{m_t c_t}{m_{fin} c_{fin}}} \left\{ \frac{\gamma \dot{m}_a}{\rho A} (T_a - T_{ain}) + \frac{(\gamma - 1) \dot{m}_a \bar{T}_a}{\rho A} (W_a - W_{ain}) \right. \\ & + \left[(\gamma - 1 - \frac{c_w}{c_v}) \frac{\bar{T}_a}{\rho A} + \frac{\lambda}{m_{fin} c_{fin} (1 - \eta_s)} \right] h_{m,t} \eta_{c,ov} A_o (\bar{W}_a - \bar{W}_{t,st}) f_{w,t} \\ & \left. + \left(\frac{\eta_{s,ov} h_c A_o}{\rho c_v A} + \frac{\eta_{s,ov} h_c A_o}{m_{fin} c_{fin} (1 - \eta_s)} \right) (\bar{T}_a - \bar{T}_t) - \frac{h_{it} A_{it}}{m_{fin} c_{fin} (1 - \eta_s)} (\bar{T}_t - \bar{T}_w) \right\} \end{aligned} \quad (4.36)$$

where T_a , W_a are the temperature of air leaving the coil, $T_{a,in}$, $W_{a,in}$ are the temperature and humidity ratio of air entering the coil, T_w is the temperature of return water, $T_{w,s}$ is the temperature of supply water. \bar{T}_a , \bar{T}_w , \bar{T}_t is the mean bulk temperature of air, water, tube within the coil, respectively. \bar{W}_a is the mean bulk humidity ratio of air. $\bar{W}_{t,st}$ is the mean bulk specific humidity of saturated air at the mean bulk temperature of tube. Note that heat transfer between tube and water is proportional to the driving potential $(\bar{T}_w - \bar{T}_t)$, sensible and latent heat transfer between air and the tube are proportional to the terms $(\bar{T}_a - \bar{T}_t)$ and $(\bar{W}_a - \bar{W}_{t,st})$, respectively. The mean bulk temperature of air \bar{T}_a can be expressed as

$$\bar{T}_a = \frac{\dot{m}_a c_{pa} T_{a,in} + \dot{m}_w c_w T_a}{\dot{m}_a c_{pa} + \dot{m}_w c_w}, \quad \text{the mean bulk humidity ratio of air as}$$

$$\bar{W}_a = \frac{\dot{m}_a c_{pa} W_{a,in} + \dot{m}_w c_w W_a}{\dot{m}_a c_{pa} + \dot{m}_w c_w}, \quad \text{the mean bulk temperature of water as}$$

$$\bar{T}_w = \frac{\dot{m}_a c_{pa} T_w + \dot{m}_w c_w T_{w,s}}{\dot{m}_a c_{pa} + \dot{m}_w c_w}.$$

NOTE TO USERS

Page(s) not included in the original manuscript are unavailable from the author or university. The manuscript was microfilmed as received.

MANY

UMI

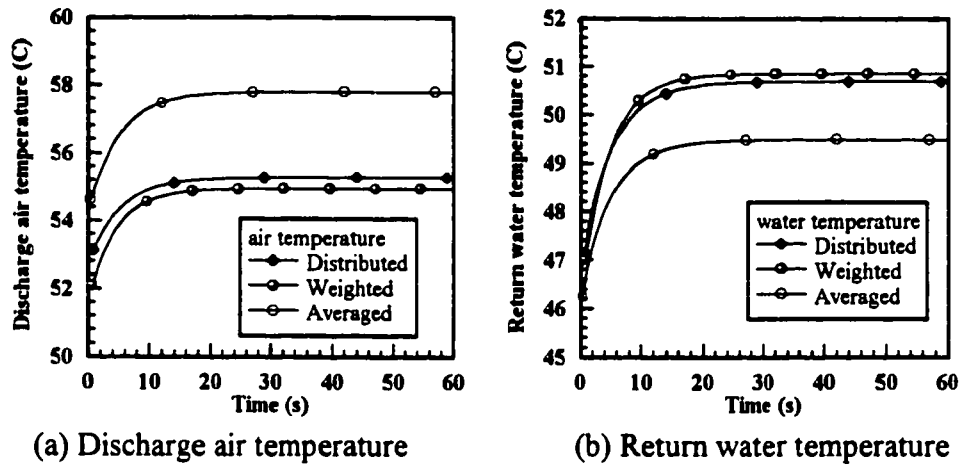


Figure 4.5 Comparison of distributed and lumped sensible coil models

humidity ratio of the air leaving the coil and return water temperature due to a step change in mass flow rate of air. We can see that the water temperatures obtained from three models are almost same. That means the total energy transferred in these models is equal. However, the air temperature from the arithmetic average model is much lower than that of the distributed model while the humidity ratio of the air in the arithmetic average model is much higher than that of the distributed model. Meanwhile, the responses of the weighted average model are close to those of the distributed model. We note that the weighted average coil model (fourth order) captures the dynamic of the distributed coil (sixteenth order) with a significant reduction in the order of the model.

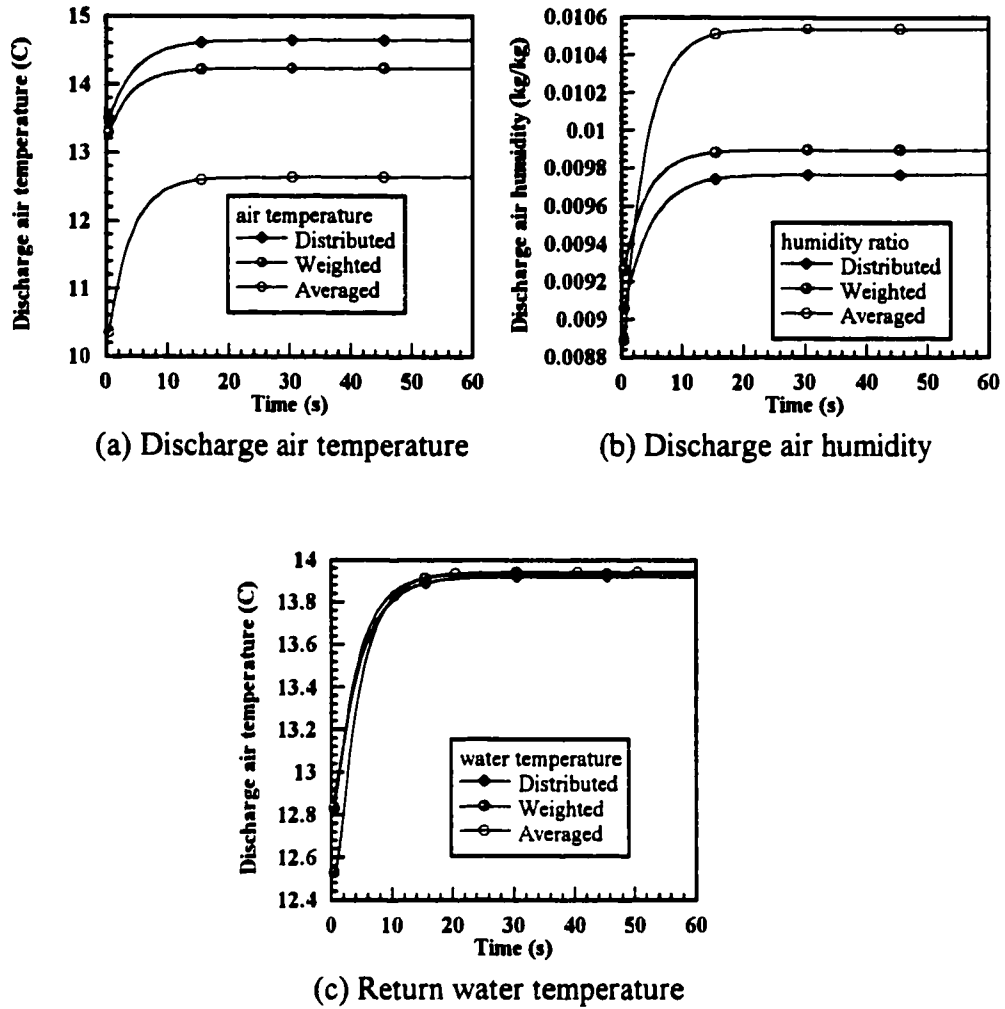


Figure 4.6 Comparison of distributed and lumped cooling and humidifying coil models

Chiller and Storage Tank Model

The chiller and storage tank model describes the energy balance between the chiller energy input, the storage energy in the tank, the heat gain via return water from the coil and from the surrounding space. The corresponding model equation remains the same as those described in Equations (3.48).

Environmental Zone(s) Model

A schematic diagram of the zone model is shown in Figure 3.2e. By assuming constant density of air, we can characterize the zone model by two state variables; enthalpy h_z , and humidity ratio W_z of air in the zone. The governing equations of the zone model were derived by applying the principles of mass and energy balance. These are:

The mass balance on the water vapor

$$\frac{dW_{z,j}}{dt} = \frac{\dot{m}_z}{\rho v_z} W_z - \frac{\dot{m}_z}{\rho v_z} W_z + \frac{\dot{m}_{wz}(t)}{\rho v_z} \quad (4.37)$$

Enthalpy balance

$$\frac{dh_{z,j}}{dt} = \frac{\dot{m}_z}{\rho v_z} h_z - \frac{\dot{m}_z}{\rho v_z} h_z + \frac{q_z(t)}{\rho v_z} + \frac{q_{lj}(t)}{\rho v_z} \quad (4.38)$$

$$h_{z,j} = c_{pa} T_{z,j} + W_{z,j} (h_{fg} + c_{p,va} T_{z,j})$$

The difference in the above and the one developed for the large-scale model is that the density of air ρ is a variable in the large-scale model. In other words, the equations in large-scale model consist of variable density term and thus increase the order of the model. The sensible load $q_{sj}(t)$ and $q_{lj}(t)$ in Equation (4.38) are coupled to the dynamics of building shell. The model of building shell is described in the Appendix A.

Heat Loss from the duct

For simplicity, we consider that heat losses or gains from the duct surfaces can be described by a lumped-capacity model, i.e.

$$\frac{dT_{out}}{dt} = -\frac{\dot{m}_a}{\rho AL} (T_{out} - T_{in}) + \frac{hA_d}{\rho A c_{p,a}} (T_e - T_{out}) \quad (4.39)$$

Equation (4.39) describes that the rate of energy stored in the air is equated to the rate of connective heat transfer between inlet and outlet of the air flow and the rate of heat transfer from the exterior surface of the duct to the plenum air space. Note that the condensation occurring on the duct surface is neglected in the above reduce-order model.

To summarize the thermal subsystem model consists of a coil model (\mathbf{x}_{cc}), chiller and storage tank model (\mathbf{x}_c), zone model (\mathbf{x}_z), and heat loss from the duct surface (\mathbf{x}_d). The state space model of the thermal subsystem can be expressed as

$$\begin{Bmatrix} \dot{\mathbf{x}}_{cc} \\ \dot{\mathbf{x}}_c \\ \dot{\mathbf{x}}_z \\ \dot{\mathbf{x}}_d \end{Bmatrix} = \begin{Bmatrix} \mathbf{f}_{cc}(\mathbf{x}_{cc}, \mathbf{u}_{cc}, \mathbf{d}_{cc}) \\ \mathbf{f}_c(\mathbf{x}_c, \mathbf{u}_c, \mathbf{d}_c) \\ \mathbf{f}_z(\mathbf{x}_z, \mathbf{u}_z, \mathbf{d}_z) \\ \mathbf{f}_d(\mathbf{x}_d, \mathbf{u}_d, \mathbf{d}_d) \end{Bmatrix} \quad (4.40)$$

Note that the order of the thermal subsystem model depends on the coil model used. With the distributed cooling and dehumidifying coil model, the order of the thermal subsystem model is 22. With lumped cooling and dehumidifying coil model, the order reduces to 10 and with sensible heat coil the order of the thermal subsystem model becomes 7 which is a significant reduction without great loss in accuracy.

4.1.4. Reduced-order state space model of VAV system

The three subsystem models developed in Section 4.1.1 to 4.1.3 taken together describe an interconnected model of VAV system, the physical configuration of which is depicted in Figure 4.7. The overall reduced-order model in vector notation can be written as

$$\dot{\mathbf{x}} = \mathbf{f}(\mathbf{x}, \mathbf{u}, \mathbf{d}, t) \quad (4.41)$$

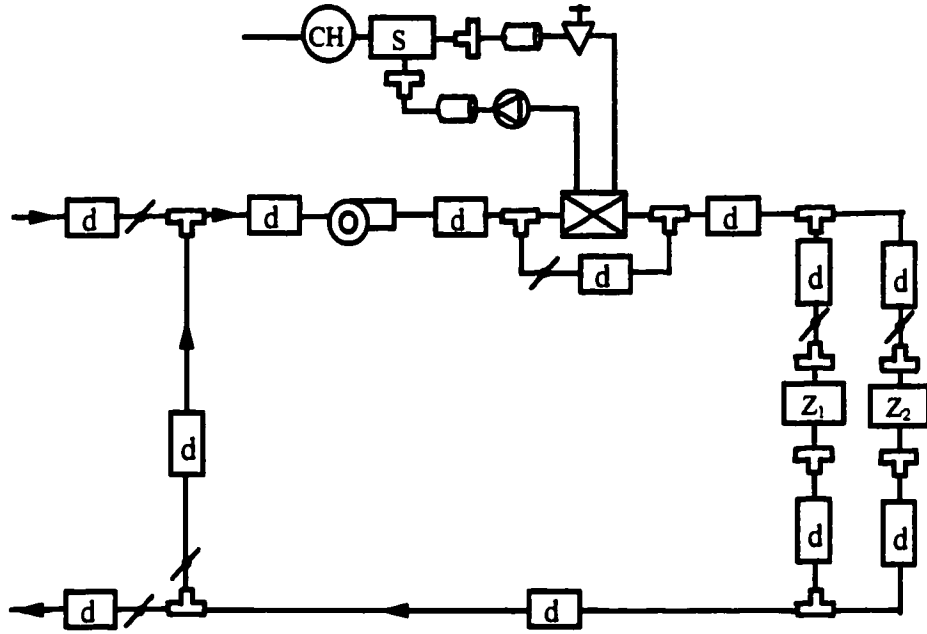


Figure 4.7 The schematic diagram of VAV system configuration

where $\mathbf{x} = (\mathbf{x}_a, \mathbf{x}_w, \mathbf{x}_T)^T$ in Equation (4.41) is a vector of the state variables, $\mathbf{u} = (\mathbf{u}_a, \mathbf{u}_w, \mathbf{u}_T)^T$ is a vector of the control inputs, $\mathbf{d} = (\mathbf{d}_a, \mathbf{d}_w, \mathbf{d}_T)^T$ is a vector of the disturbances.

This model has three different versions. The corresponding orders of these models are as follows:

with distributed cooling and dehumidifying coil, $N=31$

with lumped cooling and dehumidifying coil, $N=19$

with lumped heating coil, $N=16$.

Compared with 328 equations in the large-scale model, the reduced-order model represent a significant reduction in computational effort. The following is a summary of main capabilities of this model:

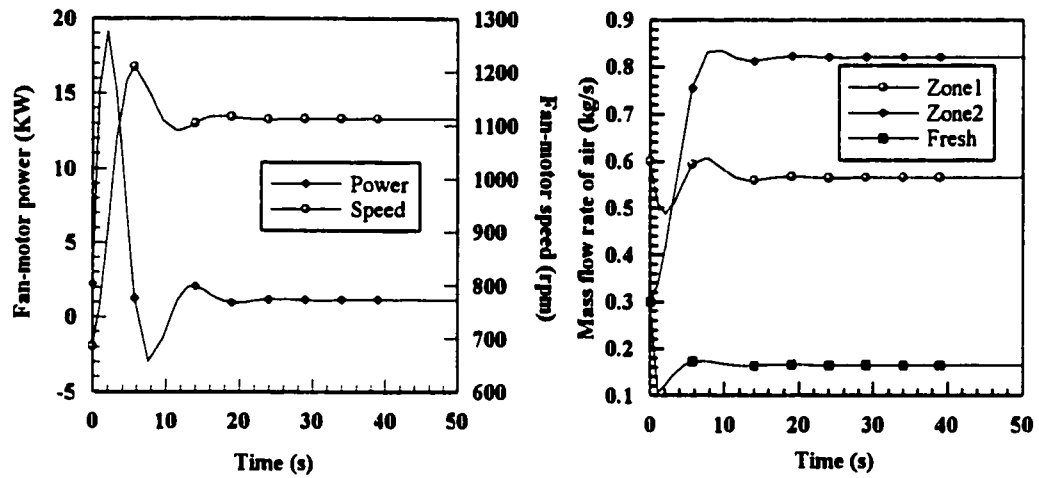
- (1). Variable speed fan motors and the corresponding variable flow of air can be simulated.
- (2). Heat and mass transfer processes taking place in the coil, duct and elsewhere in the system are modeled.
- (3). Nonlinear damper characteristics (pressure drop vs damper position) are considered.
- (4). Air-side and water-air heat transfer coefficients are computed as a function of temperature and flow field characteristics. The efficiency of the coil is variable thus accounting for the part-load performance of the system.
- (5). Both sensible and latent loads acting on the zones and due to outdoor air intake are considered.
- (6). The static pressure in the duct is computed which is useful for balancing the system under variable load conditions.

The model equations were discretized in space using finite difference schemes (Gerald and Wheatley 1984) when the distributed coil model was employed. The resulting equations were integrated by using Gear method (Gear 1971).

4.2 Open-loop Simulation Results

Using the same parameters as those given in Chapter 3 and in Table 3.1, we present results obtained from an open-loop simulation run.

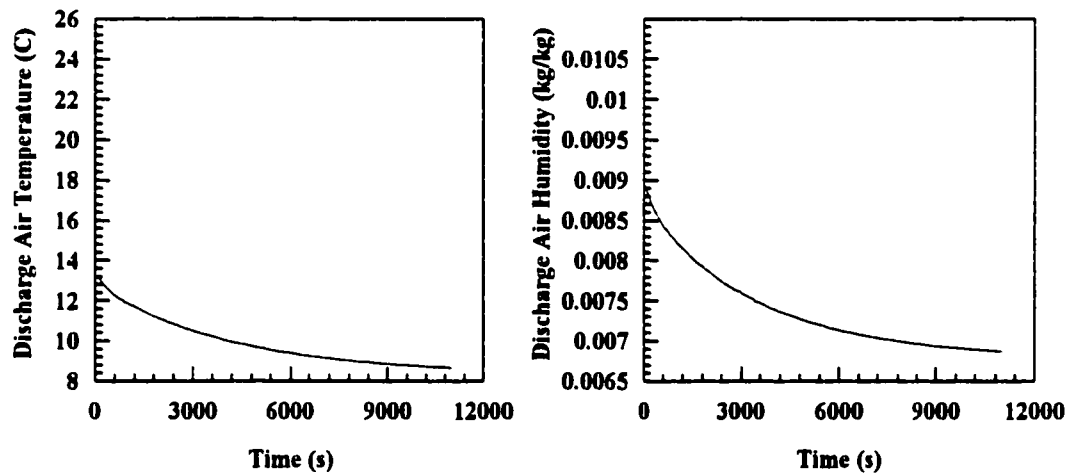
Figures 4.8a-b show the fan speed and power and the airflow characteristics of the VAV system. Figure 4.8a shows that fan speed response is fast and reaches the steady state value of 1110 rpm. Similarly, the motor power also shows fast response characteristics (Figure 4.8a). Figure 4.8b shows the airflow rates to the zones and also the outdoor airflow rate admitted into the system.



(a) Fan speed and fan-motor power

(b) Mass flow rate of air to the zones

Figure 4.8 Fan and airflow subsystem responses



(a) Temperature

(b) Humidity ratio

Figure 4.9 Responses of temperature and humidity ratio of air leaving the coil

The transient response characteristics of the cooling and dehumidifying coil are studied by examining the temperature and humidity ratio of the air leaving the coil (Figures 4.9a-b). As shown in Figures 4.9a-b the temperature and humidity ratio decrease exponentially with time.

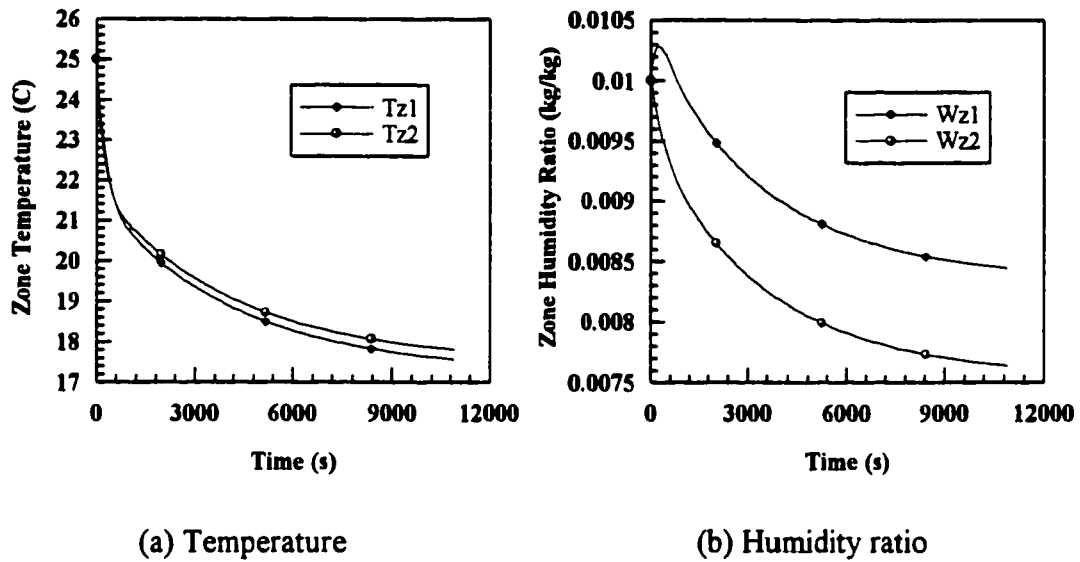
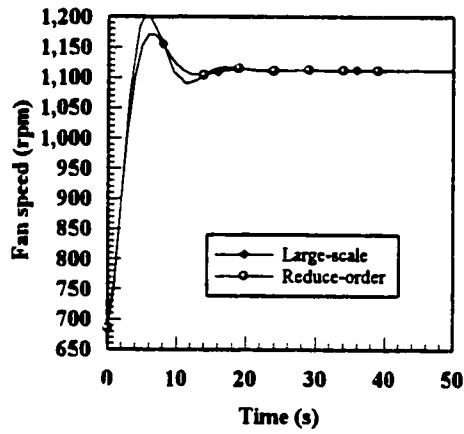


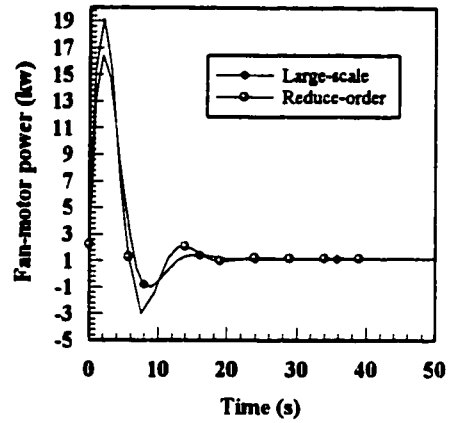
Figure 4.10 Responses of temperatures and humidity ratios of air in the zones

The slow response of the discharge air conditions shown in Figure 4.9 is due to the slow response of the chilled water temperature which is tied to the large thermal capacity associated with the storage tank.

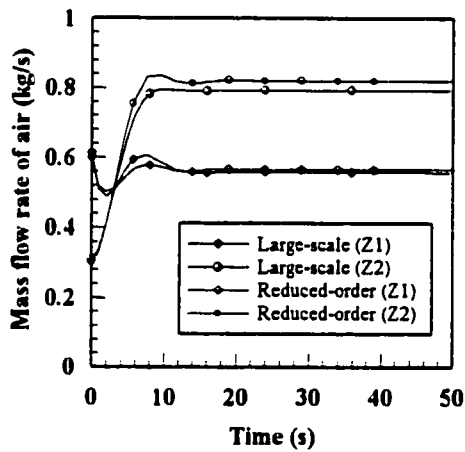
The responses of the temperatures and the humidity ratios of air in zones 1 and 2 are shown in Figure 4.10. It is apparent from Figures 4.10a-b that approximately 3 hours are needed for T_z and W_z to reach near steady state. It is evident from the results presented in Figures 4.8, 4.9, 4.10 that the reduced-order VAV system also shows the two-time scale property in that it consists of a fast subsystem (the airflow subsystem, and water flow subsystem), and a slow subsystem (thermal subsystem consisting of coil, the zones, chiller etc.).



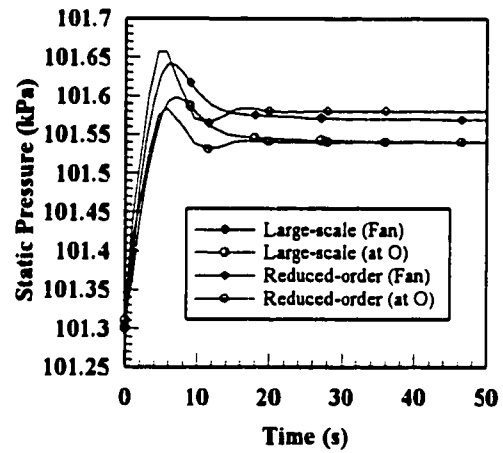
(a) Fan speed



(b) Fan-motor power



(c) Mass flow rates of air



(d) Static pressure

**Figure 4.11 Comparison of large-scale and reduced-order models:
Fan and airflow system responses**

4.3 Comparison of Large-scale and Reduced-order Models

In Chapter 3 and section 4.1, we have developed the large-scale and reduced-order models for a multi-zone VAV system. In this section, we will compare the open-loop results obtained from these two models.

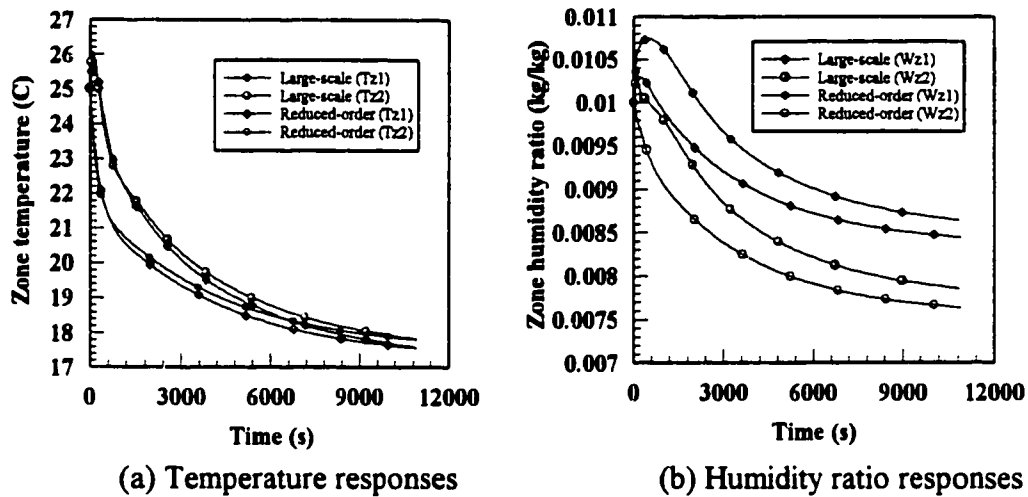


**Figure 4.12 Comparison of large-scale and reduced-order models:
Zone temperatures and humidity ratios**

Figures 4.11a-d show the comparison of the air flow subsystem characteristics obtained from the large-scale and the reduced-order models. The responses of the fan speed and motor power are depicted in Figures 4.11a-b. Figure 4.11c shows the responses of mass flow rates of fresh air and air entering zone 1 and zone 2. The responses of the static pressures at the fan outlet and at a point O, 3/4 of the distance from the coil are shown in Figure 4.11d. The thermal characteristics of zone are depicted in Figures 4.12a-b. From these figures, we can see that there are some slight differences between the predicted results from the large-scale and reduced-order models. Part of the reason for these differences is due to the differences in initial conditions. The large-scale model requires more initial conditions. As shown in the figures, the predictions from the reduced-order model compare favorably (within 5%) with those from the large-scale model.

Although, we can use the reduced-order model to analyze and design control systems for the VAV system, the advantage of the large-scale model is that it serves as a bench mark for comparing the accuracy of the reduced-order models.

4.5. Applications of Model

The VAV system model developed can be used for several applications. For example, the model can be used to study the part load performance of the VAV system (Zaheer-uddin and Zheng 1993), to simulate the control profiles for energy management control systems, and to determine the optimal setpoints for the local controllers. In this section, we will present some results to show the application of the model in simulating several EMC functions.

Energy Management Simulation

Time scheduled operation of HVAC systems is one of the important functions of Energy Management Control Systems (EMCS). In time scheduled mode, HVAC systems are operated in start-stop sequence or duty cycled depending on the time and type of day viz., off normal schedule operation during unoccupied periods (evenings, nights and weekends/holidays). These functions are easier to implement using EMCS and represent greatest potential for energy conservation (Payne and McGowan 1988).

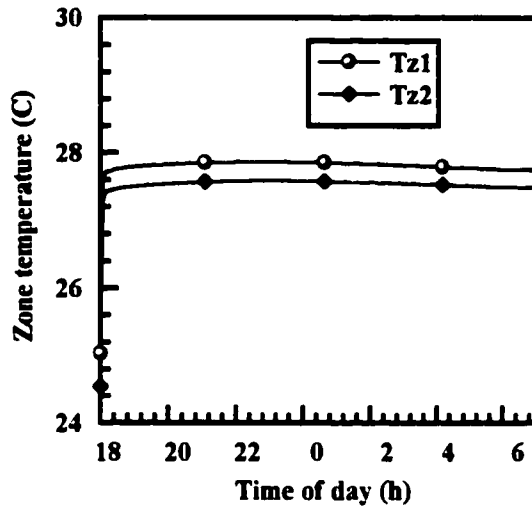
The following four functions of EMCS are of great economic significance: (i) Night time shut down (ii) fixed capacity timed operation (night time open-loop operation) (iii) morning start-up and (iv) duty cycling during normal building operation. Night time shut down although saves energy, it may also cause higher night time building temperature and consequently higher energy consumption during morning start-up. However, if the air system can be operated at reduced capacity to utilize outdoor air to obtain free cooling, then further reduction in morning start-up energy requirements can be achieved. In order to utilize these EMCS functions effectively, it will be necessary to study the transient response of the HVAC

system and the zones under going shut-down, start-up and reduced capacity (open-loop) operation. Based on such tests, optimum operating strategies can be found.

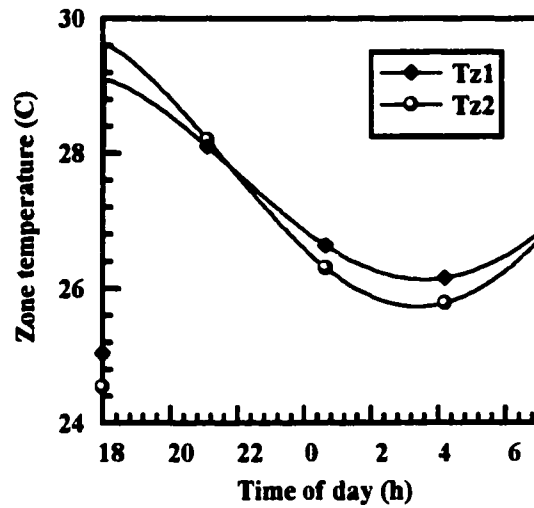
While the above three strategies (shut-down, start-up and reduced capacity operation) are of the open-loop type in which zone temperature control is temporarily disabled, the duty cycling of HVAC systems is implemented during normal closed-loop operation. In other words, zone temperature regulation is taking place while the cooling system is duty cycled to reduce the demand for auxiliary energy. For example, HVAC systems are shut-down for a predetermined short period of time during normal operation. The rationale is to limit auxiliary energy and/or reduce electrical demand from exceeding some predetermined maximum level. This strategy, some times referred to as demand control, is applied to water chillers as well (Payne and McGowan 1988).

Although duty cycling of fans and pumps in HVAC systems does not reduce cooling loads, nevertheless it has potential to limit the energy demand. On the other hand, duty cycling of systems causes temperature drifts which are associated with the transient response characteristics of the HVAC systems. The developed model can be used to study the above cited EMCS functions.

To study the above cited EMCS functions, we have simulated several cases by using the developed model. The simulated VAV system consisted of two zones with 92 m² each in floor area. A 8-row 16 tube, plate-fin-tube cooling and dehumidifying coil was simulated. Also a fan with a 2-HP motor which can develop a rated pressure of 500 Pa at 1200 rpm was used. Apart from these specifications, the magnitudes of the major parameters of the subsystem models used in this study are given in Table 3.1.



(a) Shut-down



(b) Reduced capacity fan operation

Figure 4.13 Zone Temperature Responses During Night Time

Night time shut-down:

For this test, a design day with an outdoor temperature of 35°C and a daily range of 12°C was considered. The VAV system (both chiller and fan) was shut-down at 18:00h. With the outdoor air dampers fully closed the obtained system responses were plotted (Fig. 4.13a). The loads acting on the zone were transmission gains, infiltration and internal heat gains. How the zone temperatures varied between 18:00h to 07:00h are depicted in Fig 4.13a. It is apparent that the zone temperatures decrease only marginally to $T_{z1}=27.75^{\circ}\text{C}$, $T_{z2}=27.21^{\circ}\text{C}$ at 7 A.M. in the morning. This is expected in buildings with large thermal capacity. Depending on the thermal capacity of the zones and cooling loads, the temperature responses will vary.

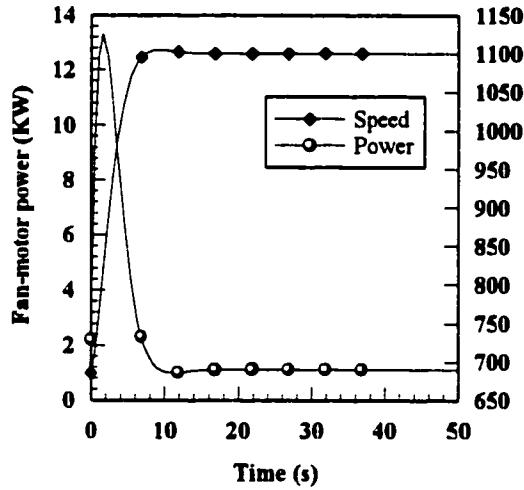
Reduced capacity night time operation

Rather than turning off the VAV system during night time that could result in higher zone temperatures, it is feasible to use outdoor air as a means of achieving partial free cooling of the zones. Normally this function is implemented by running the fan at low speed with outdoor dampers and zone dampers in full open position. We have simulated this scenario by using the same set of data as that was used in Fig. 4.13a. The results of this simulation are shown in Fig. 4.13b. Note that compared to the full-off case, the zone temperatures with reduced capacity fan operation are lower (compare T_{z1} , T_{z2} at 07:00h in Figs. 4.13a and 4.13b). In other words, less energy will be needed in the reduced capacity operation to bring the zone temperature from night time value to daytime comfort setpoint temperatures.

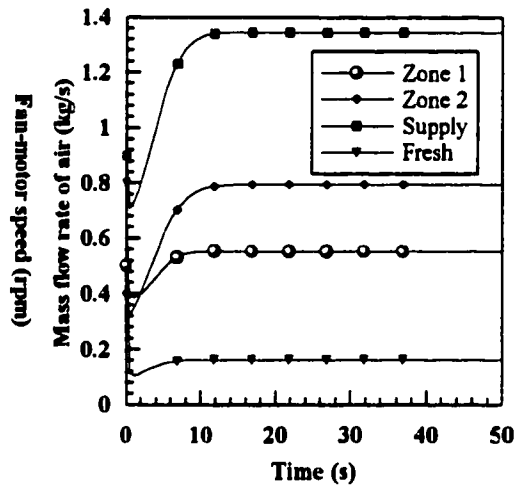
It is apparent that the dynamic model developed in this study can be suitably tuned to reflect the actual building-system parameters and then can be used to simulate different operating scenarios. With this knowledge of zone temperature responses, the VAV system could be started ahead of time to bring the zone temperatures back to comfort setpoints. Such results will be of great value in assessing several different night time operating strategies which when implemented on real systems will translate into significant energy savings.

Start-up response:

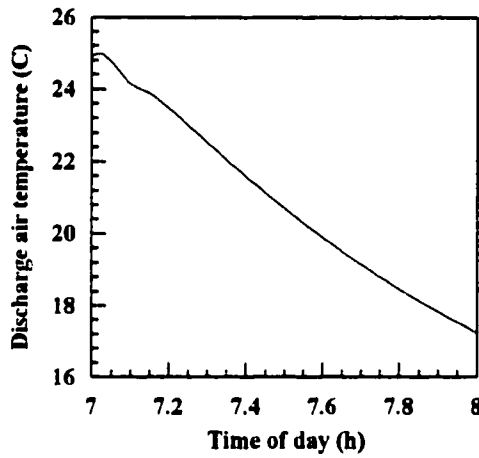
From the night time shut down tests or the simulation of reduced capacity operation, it is possible to predict the zone temperature conditions before morning start-up. We consider the following conditions (from the reduced capacity night time



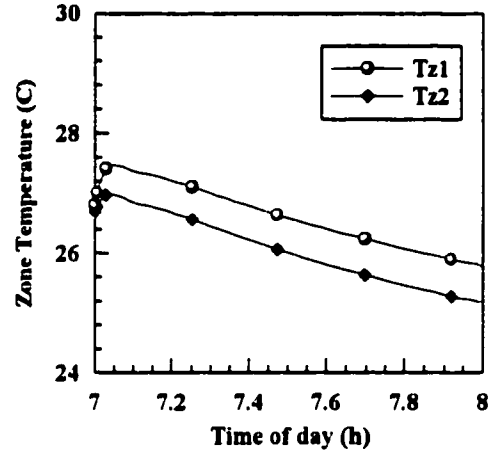
(a) Fan speed and fan-motor power



(b) Mass flow rate of air



(c) Temperature of air leaving the coil



(d) Zone temperatures

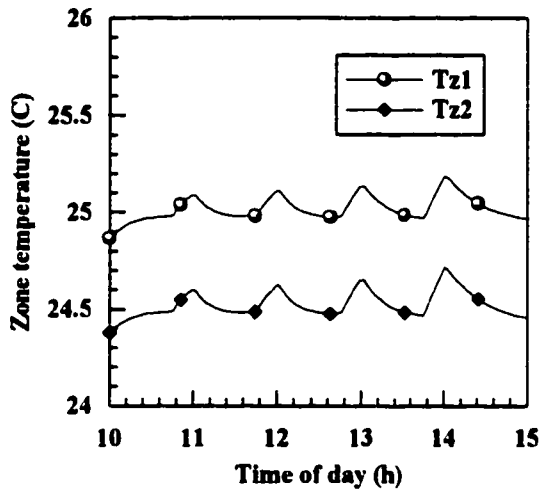
Figure 4.14 System Responses during Start-up

operation), $T_{z1}=26.79^{\circ}\text{C}$, $T_{z2}=26.69^{\circ}\text{C}$, as those that were existing just before the start up time. Given this set of initial conditions the VAV system (with minimum outdoor air) was switched on. The obtained time responses of the system were plotted as shown in Figs. 4.14a-d. The mass flow rate of air to zone 1 and 2 were respectively 0.5 kg/s and 0.8 kg/s as shown in Figure 4.14b.

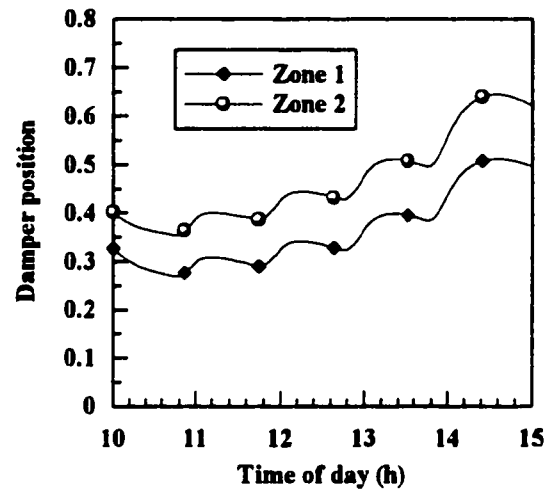
The zone temperature responses during the start-up time (between 07:00 to 08:00 h) are depicted in Fig. 4.14d. It may be noted that at 08:00 h T_{z1} and T_{z2} reach within $\pm 0.75^\circ\text{C}$ of their respective setpoints. At this time (i.e. at 08:00) the feedback control system takes over and regulates the zone temperatures. Since different sets of initial conditions give different responses, such response times as a function of initial conditions will be of value in choosing optimal start-up times.

Duty Cycling

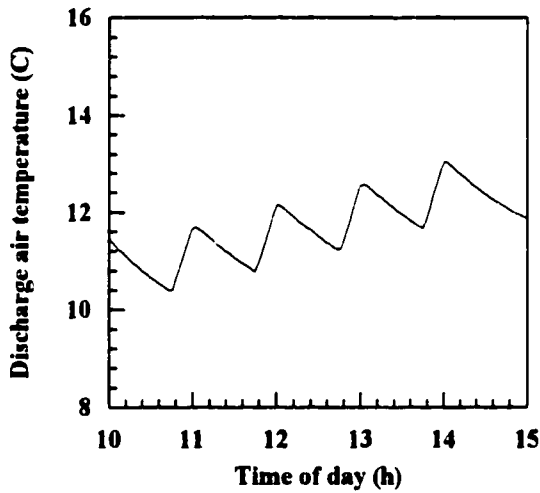
As opposed to the open-loop strategies discussed in previous sections, duty cycling is a closed-loop operation. In other words, zone temperatures are regulated close to their chosen setpoints while the cooling system is duty cycled. To simulate this scenario, we considered a day with maximum outdoor temperature of 35°C and a daily range of 12°C . The zone dampers were controlled with two suitably tuned PI-controllers. Both fan- and pump-motors were operated at constant speed and only the chiller was duty cycled. The cycle times were chosen arbitrarily as $\tau_{on} = 45$ minutes and $\tau_{off} = 15$ minutes. The results of this simulation during occupied hours are depicted in Figs. 4.15a-d. It is apparent from Fig. 4.15c that although the supply air temperature follows the cyclic pattern, the zone temperatures are maintained close to their setpoints ($T_{z1,set} = 25^\circ\text{C}$, $T_{z2,set} = 24.5^\circ\text{C}$). The advantage of duty cycling is obvious in the sense that electrical demand during chiller off cycle (see Fig. 4.15d) is reduced without compromising comfort.



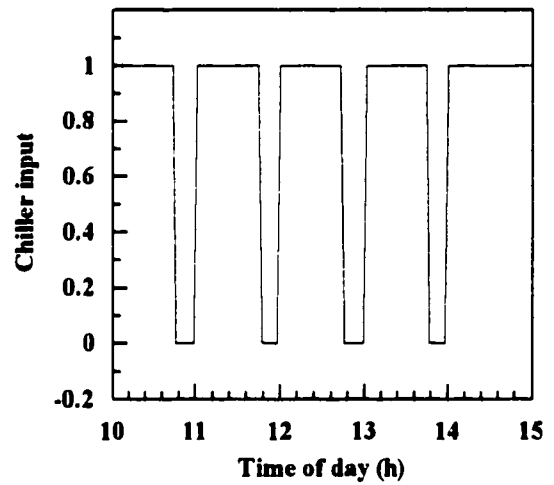
(a) Zone temperature responses



(b) Zone damper positions



(c) Discharge air temperature



(d) Chiller on-off Schedule

Figure 4.15 System Responses With PI Control and Duty Cycling

Typical Daily Operation

Figure 4.16 shows the zone temperature responses predicted by the model on a typical day. In this simulation the chiller was shut down at 18:00h and the fan speed was reduced by one half (reduced capacity operation). As shown in Fig. 4.16, the zone air

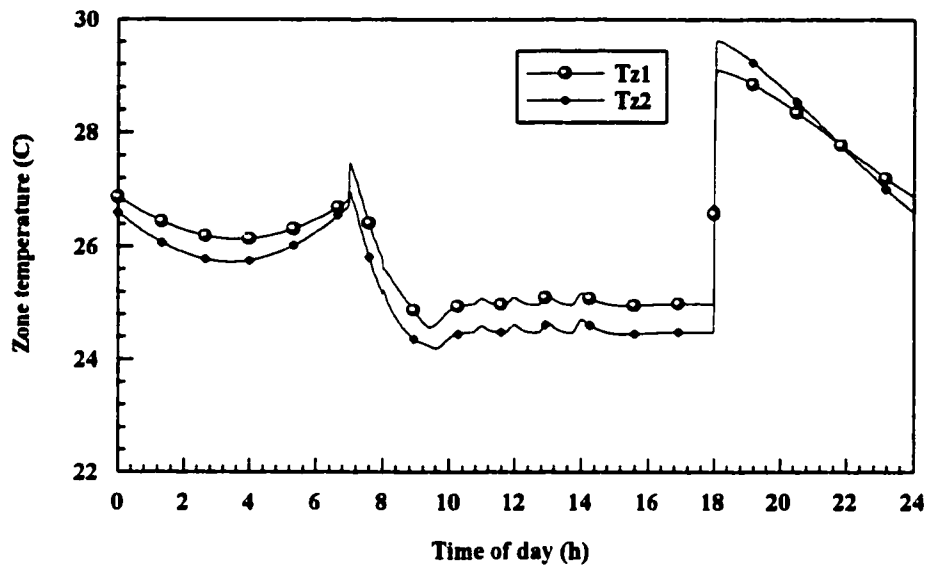


Figure 4.16 Zone Temperature Responses During a Typical Day Operation

temperatures rise rapidly due to shut down of the chiller. Some cooling with outdoor air is obtained during night time and the temperatures reach between 26-27°C at 7:00 AM. At this time the chiller and fan were switched on to full capacity (start-up operation). As shown in Fig. 4.16 the zone temperatures reach to within $\pm 0.75^{\circ}\text{C}$ of their set points at 08:00 AM. At this time the zone dampers were put into modulating mode using two PI-controllers. From 10:00 until 14:00h the chiller was duty cycled. In spite of chiller duty cycling the zone temperatures are maintained to within $\pm 0.25^{\circ}\text{C}$ of their respective setpoints throughout the occupied period. To summarize, the VAV system was operated in open-loop mode during 18:00h - 07:00h and in closed-loop PI control mode during the normal hours from 08:00h - 18:00h. The zone temperatures during closed loop control are very close to the setpoints even though the cooling load is variable and the chiller is duty cycled. Thus several such simulated operating strategies can be assessed using the developed model.

Chapter 5

Methodology for multiple stage optimal operation problems

One of the major objectives of installing energy management control systems (EMCS) in buildings is to improve the energy efficiency of HVAC systems. However, the general consensus is that most EMC systems in practice have not performed to their potential with respect to optimizing functions. One of the reasons for poor performance is the fact that HVAC processes are optimized at local loop level that do not include system wide process-to-process interactions. Because of the fact that several multiple processes are simultaneously undergoing changes and interacting with each other, a system approach is necessary to model these processes and their interactions correctly. It is only then possible to find improved solutions to the problem of globally optimizing the thermal processes in VAV systems.

To achieve global optimal operation of HVAC systems, it is necessary to obtain optimal trajectories of HVAC process setpoints by considering all process interactions. Such optimal trajectories can then be down-loaded to local controllers for on-line tracking and regulation of the process outputs. The mechanism by which the proposed optimal trajectories can be implemented is illustrated in Fig. 5.1. Based on past history of load patterns and mathematical models of building loads and HVAC systems, the EMCS computes the optimal control trajectories for all the system outputs. Each local controller is then supplied with the appropriate optimal trajectory that acts as a reference signal to be tracked by the local controller. Since the predicted and actual loads are likely to be

different, the local controller is given the task of regulating the process outputs against any mismatches in the predicted and actual loads. This latter objective is achieved by suitably tuning the PI (proportional-integral) controllers.

While optimization at local level may be easier from the point of view of implementation, it is not likely to be energy efficient since system level interactions and optimization are not taken into consideration. On the other hand, optimization at the

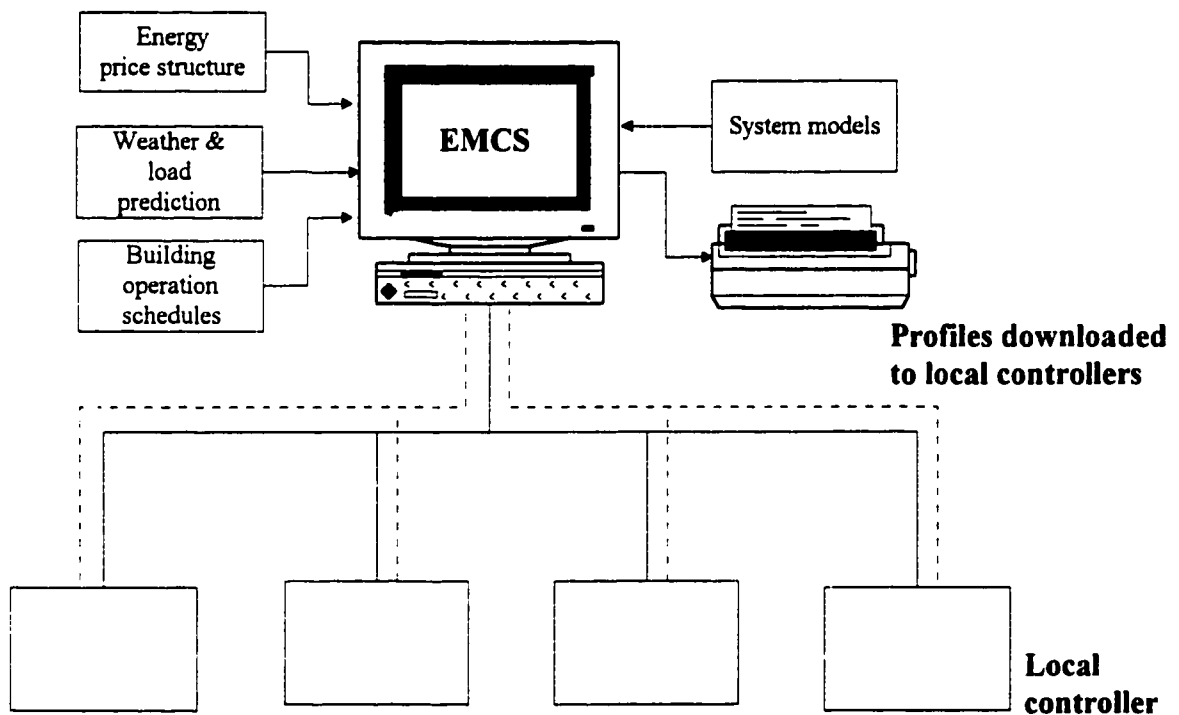


Figure 5.1 A Two-Tier Control Configuration

system-level is difficult as a result not much work has been done in this area. To address the need of global optimal operation of HVAC, a system level model and an optimization methodology for computing an optimal set of all control inputs and outputs subject to

realistic cooling loads acting on the VAV system are required. These optimal control inputs and the corresponding state/output trajectories (such as discharge air temperature, chilled water temperature, static pressure in the ducts, etc.) are then supplied as variable setpoints to the local PI controllers.

In Chapter 3 and Chapter 4, the system-level models (the full-order and the reduced-order models) for multizone VAV systems were developed. In this chapter, we are interested in developing a methodology to determine the optimal control strategies for the HVAC system. To this end, first, the formulation of nonlinear constrained optimal control problems as a means to determining optimal setpoints will be reviewed in Section 5.1. In Section 5.2, the methodology for the multiple stage optimal operation problems will be developed based on the maximum principle of Pontryagin and perturbation methods followed by the numerical algorithm for solving the multiple stage optimal operation problems.

5.1 Formulation of single stage optimal control problems

In some buildings indoor environment conditions must be maintained constant throughout the day irrespective of any changes in loads acting on the zones. The control problem of this nature is referred as single-stage control problem. The control objective will be to compute an optimal operating sequence of inputs which will take the system from its initial temperature to the desired final setpoint temperature. Also, if the load acting on the zone changes, it is of interest to determine an optimal control input sequence to maintain a constant setpoint temperature. In the following, an optimal control technique that is useful for single stage problems is reviewed.

The control problem of Bolza

The dynamic models of VAV system developed in Chapter 4 can be written in compact form following the state vector form. Thus the dynamic model of VAV system can be expressed as

$$\begin{aligned}\dot{\mathbf{x}}(t) &= \mathbf{f}(\mathbf{x}(t), \mathbf{u}(t), t) \\ \mathbf{x}(t_0) &= \mathbf{x}_0, \quad t_0, \mathbf{x}_0 \text{ are given}\end{aligned}\tag{5.1}$$

where \mathbf{x} , the state vector, (such as zone temperatures, discharge air temperature, etc.) and \mathbf{f} are n -vectors. The m -dimensional vector $\mathbf{u}(t)$ that is called the control function or the control input (e.g., damper positions, voltage input to fan, energy input to chiller, etc.) for the system may have to satisfy the capacity constraints of the form:

$$\alpha_j \leq u_j \leq \beta_j, \quad \beta_j > \alpha_j, \quad j = 1, 2, \dots, m.\tag{5.2}$$

Then the optimal objective must be given in concept and expressed mathematically into an objective function (or cost function). Usually, objective function is expressed as:

$$J = \Theta(\mathbf{x}(t_f), t_f) + \int_{t_0}^{t_f} \Phi(\mathbf{x}(t), \mathbf{u}(t), t) dt\tag{5.3}$$

The objective function J includes two terms: first term in Eq. (5.3) indicates some requirement of the final state performance, second term defines some requirements of the transient performance of the system, e.g., the transient error, the energy consumption , etc.

The problem of optimal control is to choose the control $\mathbf{u}(t)$ so as to transfer the initial state \mathbf{x}_0 in accordance with $\dot{\mathbf{x}} = \mathbf{f}(\mathbf{x}, \mathbf{u}, t)$ to the final state $\mathbf{x}(t_f)$ in such a way as to minimize the objective function. This problem, in the literature, is called a control problem of Bolza.

Maximum principle of Pontryagin

Let us consider the free end point optimal control problem. Under appropriate conditions of continuity and differentiability of the functions involved, i.e. $\mathbf{x} \in \mathbb{R}^n$, $\mathbf{u} \in \Omega \in \mathbb{R}^m$, t_0, t_f fixed, the following theorem can be proved (Hestenes 1966):

Let \mathbf{u}^* be an optimal control and let \mathbf{x}^* be the corresponding optimal trajectory. Then there exist multipliers $\lambda_0 \geq 0$, $\lambda_1(t)$, ... $\lambda_n(t)$, not vanishing simultaneously, such that the following conditions are fulfilled:

(a) The vector $\lambda(t) = (\lambda_1(t) \dots \lambda_n(t))^T$ is continuous on $[t_0, t_f]$ and the functions $\mathbf{x}^*(t)$ and $\lambda(t)$ satisfy the canonical (or Hamiltonian) system of differential equations,

$$\dot{\mathbf{x}} = \frac{\partial H}{\partial \lambda}, \quad \dot{\lambda} = - \frac{\partial H}{\partial \mathbf{x}} \quad (5.4)$$

where H, the Hamiltonian function, is given by

$$H(\mathbf{x}, \lambda_0, \lambda, \mathbf{u}, t) = \lambda_0 \Phi + \lambda^T \mathbf{f} \quad (5.5)$$

(b) $\mathbf{u}^*(t)$ minimizes $H(\mathbf{x}^*, \lambda_0, \lambda, \mathbf{u}, t)$ over the admissible set U of \mathbf{u} for $t \in [t_0, t_f]$, i.e.,

$$H(\mathbf{x}^*, \lambda_0, \lambda, \mathbf{u}^*, t) \leq H(\mathbf{x}^*, \lambda_0, \lambda, \mathbf{u}, t) \quad (5.6)$$

for all $\mathbf{u} \in U$

(c) At the terminal point $(t_f, \mathbf{x}^*(t_f))$ the transversality conditions hold:

$$\lambda(t_f) = \lambda_0 \frac{\partial \Phi}{\partial \mathbf{x}^*} \quad (5.7)$$

Note that for the constraints on \mathbf{u} as given by (5.2), the equation (5.6) implies that along the optimal trajectory

$$\frac{\partial H}{\partial u_j} = \begin{cases} \geq 0 & \text{if } u_j^* = \alpha_j \\ = 0 & \text{if } \alpha_j < u_j < \beta_j \\ \leq 0 & \text{if } u_j^* = \beta_j \end{cases} \quad j=1, \dots, m \quad (5.8)$$

Many numerical methods have been developed for the solution of the control problem of Bolza based on the maximum principle of Pontryagin (e.g. Athans 1966, Balakrishnan and Neustadt 1964, Kopp and Moyer 1966) such as the gradient method, the successive sweep method, the second-variation method, the shooting methods and the generalized Newton-Raphson method (Mufti 1970). Here, an introduction to the gradient method will be given.

The gradient method

For the sake of simplicity and clarity, we should first consider the problem where there are no constraints of the form (5.2). From the Theorem stated above, the necessary conditions which the optimal control, the optimal trajectory and the associated multipliers satisfy are

$$\dot{\mathbf{x}} = \frac{\partial H}{\partial \lambda} = \mathbf{f}(\mathbf{x}, \mathbf{u}, t), \quad \mathbf{x}(t_0) = \mathbf{x}_0 \quad (5.9)$$

$$\dot{\lambda} = -\frac{\partial H}{\partial \mathbf{x}} = -\lambda_0 \frac{\partial \Phi}{\partial \mathbf{x}} - \left(\frac{\partial \mathbf{f}}{\partial \mathbf{x}}\right)^T \lambda \quad (5.10)$$

$$H(\mathbf{x}^*, \lambda_0, \lambda, \mathbf{u}^*, t) \leq H(\mathbf{x}^*, \lambda_0, \lambda, \mathbf{u}, t) \quad \text{for all } \mathbf{u} \quad (5.11)$$

$$\lambda(t_f) = \lambda_0 \frac{\partial \Theta}{\partial \mathbf{x}} \quad (5.12)$$

where the vector $(\lambda_0, \lambda(t))$ never vanishes. It is easy to see that $\lambda_0 \neq 0$ and to choose $\lambda_0 = 1$.

In the gradient method an initial control profile is chosen and the state equations with the chosen initial conditions are solved to determine the nominal trajectory. In general, this nominal trajectory is not the optimal trajectory. A correction $\delta \mathbf{u}(t)$ to the nominal control is found by taking the derivative of the Hamiltonian function H , viz.,

$$\delta \mathbf{u} = -k \left(\frac{\partial H}{\partial \mathbf{u}} \right) \quad k > 0 \quad (5.13)$$

such that the cost functional $J(\mathbf{u} + \delta \mathbf{u}) < J(\mathbf{u})$.

The computer algorithm for determining optimal control trajectories of single state control problems might proceed as follows (Mufti 1970):

(I). Pick an initial control profile $\hat{\mathbf{u}}(t)$ and solve the state equation (5.9) with given initial conditions. Store $\hat{\mathbf{x}}(t)$, $t_0 \leq t \leq t_f$,

(II). Determine $\lambda(t_f)$ by Eq. (5-12) and integrate Eq. (5.11) backwards from t_f to t_0 .

During the backward integration calculate $\left(\frac{\partial H}{\partial \mathbf{u}} \right)$,

(III). Solve Eq. (5.9) forward with $\mathbf{u} = \hat{\mathbf{u}} - k \left(\frac{\partial H}{\partial \mathbf{u}} \right)$ for several values of k and determine the corresponding values of J ,

(IV). Find the best value of k (the value that yields the least value of J) and use this value to determine the next estimate for \mathbf{u} ,

(V). Return to step (I) and repeat. The process ends when the change in the performance tends to zero.

For the gradient method which has the control constraint of the form (5.2), we follow the same procedure as mentioned above except for the computation of δu , (Berkovitz 1961) that is

$$\delta u_j = -k\left(\frac{\partial H}{\partial u_j}\right) \quad k > 0 \quad (5.14)$$

when $\hat{\mathbf{u}}(t)$ satisfies $\alpha_j < \hat{\mathbf{u}}(t) < \beta_j$;

$$\delta u_j = \begin{cases} -k\left(\frac{\partial H}{\partial u_j}\right) & k > 0 & \text{if } \frac{\partial H}{\partial u_j} \leq 0 \\ 0 & & \text{if } \frac{\partial H}{\partial u_j} > 0 \end{cases} \quad (5.15)$$

when $\hat{\mathbf{u}}(t)$ satisfies $\hat{\mathbf{u}}(t) = \alpha_j$;

$$\delta u_j = \begin{cases} -k\left(\frac{\partial H}{\partial u_j}\right) & k > 0 & \text{if } \frac{\partial H}{\partial u_j} \geq 0 \\ 0 & & \text{if } \frac{\partial H}{\partial u_j} < 0 \end{cases} \quad (5.16)$$

when $\hat{\mathbf{u}}(t)$ satisfies $\hat{\mathbf{u}}(t) = \beta_j$.

In simple words, the above relations mean that at each iteration, the corrected controls $\mathbf{u} = \hat{\mathbf{u}} - k\left(\frac{\partial H}{\partial \mathbf{u}}\right)$ should be clipped off if they violate the control constraints.

5.2 Methodology for multiple stage optimal operation problems

Most HVAC systems are operated in time scheduled mode. In the time scheduled mode, HVAC systems are operated in start-up, normal operation during occupied period, off-normal operation during unoccupied period (evenings, nights and weekends/holidays). Such control problems are referred as multiple stage problems. Let us take the cooling application as an example. In the occupied period, all the subsystems will be operated to achieve thermal comfort. During the unoccupied period, the HVAC system is operated in off normal mode in which zone temperatures are allowed to fluctuate and maybe some

subsystems (e.g. chiller, coil) will be shut-down to save energy. During the start-up period, the HVAC systems may run at full capacity to bring the zone temperatures within the range of setpoints just before the occupancy. We can see that during different periods, the system models have different structures and the desired objectives are different. Here the optimal operation problem is one in which the objective function is minimized over several periods with the system models of different structures. Since the theorem and algorithm stated in the previous section is only suitable for the single stage problem, i.e., uniform system model, uniform objective over the entire stage, it is, therefore, necessary to develop a methodology to deal with multiple stage optimal operation problems.

5.2.1 Formulation of multiple stage optimal operation problems

Multiple stage optimal operation problems

For the sake of simplicity and clarity, let us take a three stage optimal operation problem as an example, although the methodology developed here can be applied for the problems with as many stages as required.

Consider an HVAC system whose dynamic model can be described by vector differential equations on time interval $[t_0, t_f]$. And let the HVAC system be operated in three stages so that we have

$$\dot{\mathbf{x}} = \frac{d\mathbf{x}}{dt} = \begin{cases} \mathbf{f}^1(\mathbf{x}, \mathbf{u}^1, t) & \text{on } [t_0, t_1] \\ \mathbf{f}^2(\mathbf{x}, \mathbf{u}^2, t) & \text{on } [t_1, t_2] \\ \mathbf{f}^3(\mathbf{x}, \mathbf{u}^3, t) & \text{on } [t_2, t_f] \end{cases} \quad (5.17)$$

where $\mathbf{x}(t)$ the state vector and $\mathbf{u}^1(t)$, $\mathbf{u}^2(t)$, $\mathbf{u}^3(t)$ are the control vectors corresponding to three stages. Start time t_0 , end time t_f , first and second switching times t_1 , t_2 are fixed

which are assumed to be known. Note that at different stages, the form of state equations can be different, and the number of control variables can be different. The initial condition is given by

$$\mathbf{x}(t_0) = \mathbf{x}_0 \quad (5.18)$$

The three-stage performance index can be defined as

$$J(\mathbf{u}^1, \mathbf{u}^2, \mathbf{u}^3) = \Theta(\mathbf{x}(t_f), t_f) + \int_{t_0}^{t_1} \Phi^1(\mathbf{x}, \mathbf{u}^1, t) dt + \int_{t_1}^{t_2} \Phi^2(\mathbf{x}, \mathbf{u}^2, t) dt + \int_{t_2}^{t_f} \Phi^3(\mathbf{x}, \mathbf{u}^3, t) dt \quad (5.19)$$

where \mathbf{x} is a solution of (5.17) and (5.18) and Φ^i , $i=1,2,3$ are at least continuously differentiable in \mathbf{x} , \mathbf{u}^1 , \mathbf{u}^2 , \mathbf{u}^3 and t . Note that some special considerations can be included in the performance indexes in Eq. (5.19) to account for time-of-day energy price structures.

Since, in HAVC processes, temperatures and flow rates are to be held between acceptable limits, the problem has constraints on the state and control variables. These can be expressed for each stage.

in the first stage t_0 to t_1

$$\mathbf{h}^1(\mathbf{u}^1, t) \geq 0 \quad \mathbf{g}^1(\mathbf{x}, t) \geq 0 \quad (5.20)$$

$$u_{i,\min}^1 \leq u_i^1 \leq u_{i,\max}^1 \quad (5.21)$$

in the second stage t_1 to t_2

$$\mathbf{h}^2(\mathbf{u}^2, t) \geq 0 \quad \mathbf{g}^2(\mathbf{x}, t) \geq 0 \quad (5.22)$$

$$u_{i,\min}^2 \leq u_i^2 \leq u_{i,\max}^2 \quad (5.23)$$

in the third stage t_2 to t_f

$$\mathbf{h}^3(\mathbf{u}^3, t) \geq 0 \quad \mathbf{g}^3(\mathbf{x}, t) \geq 0 \quad (5.24)$$

$$u_{i,\min}^3 \leq u_i^3 \leq u_{i,\max}^3 \quad (5.25)$$

the terminal condition at time t_f

$$\mathbf{N}[\mathbf{x}(t_f), t_f] \geq 0 \quad (5.26)$$

The constraints (5.20), (5.22), (5.24), (5.26) have their physical meanings. For example, in the first stage, the constraints (5.20) could represent the requirement of thermal comfort such as the temperature, humidity ratio, fresh air requirement. The terminal condition (5.26) could refer to the requirement of temperatures at t_f .

The multiple stage optimal operation problem is to find $\mathbf{u}^1, \mathbf{u}^2, \mathbf{u}^3$ that minimize the objective function (5.19) subject to the state equation (5.17), the initial condition (5.18), the capacity constraints (5.21), (5.23), (5.25) and the other constraint (5.20), (5.22), (5.24), (5.26).

The necessary conditions of multiple stage optimization

Applying the penalty function and Lagrange methods, we can convert the constraint problem into an unconstrained problem

$$\begin{aligned} J(\mathbf{u}^1, \mathbf{u}^2, \mathbf{u}^3) = & \int_{t_0}^{t_1} \{ \Phi^1(\mathbf{x}, \mathbf{u}^1, t) + \lambda^{1T} [\mathbf{f}^1(\mathbf{x}, \mathbf{u}^1, t) - \dot{\mathbf{x}}] + \omega^{1T} \mathbf{h}^1(\mathbf{u}^1, t) + \eta^{1T} \mathbf{g}^1(\mathbf{x}, t) \} dt \\ & + \int_{t_1}^{t_2} \{ \Phi^2(\mathbf{x}, \mathbf{u}^2, t) + \lambda^{2T} [\mathbf{f}^2(\mathbf{x}, \mathbf{u}^2, t) - \dot{\mathbf{x}}] + \omega^{2T} \mathbf{h}^2(\mathbf{u}^2, t) + \eta^{2T} \mathbf{g}^2(\mathbf{x}, t) \} dt \\ & + \int_{t_2}^{t_f} \{ \Phi^3(\mathbf{x}, \mathbf{u}^3, t) + \lambda^{3T} [\mathbf{f}^3(\mathbf{x}, \mathbf{u}^3, t) - \dot{\mathbf{x}}] + \omega^{3T} \mathbf{h}^3(\mathbf{u}^3, t) + \eta^{3T} \mathbf{g}^3(\mathbf{x}, t) \} dt \\ & + \mathbf{v}^T \mathbf{N}[\mathbf{x}(t_f), t_f] + \Theta[\mathbf{x}(t_f), t_f] \end{aligned} \quad (5.27)$$

defining the Hamiltonian functions as follows

$$\begin{aligned}
H^1 &= \Phi^1 + \lambda^{1\top} \mathbf{f}^1 + \omega^{1\top} \mathbf{h}^1 + \eta^{1\top} \mathbf{g}^1 \\
H^2 &= \Phi^2 + \lambda^{2\top} \mathbf{f}^2 + \omega^{2\top} \mathbf{h}^2 + \eta^{2\top} \mathbf{g}^2 \\
H^3 &= \Phi^3 + \lambda^{3\top} \mathbf{f}^3 + \omega^{3\top} \mathbf{h}^3 + \eta^{3\top} \mathbf{g}^3
\end{aligned} \tag{5.28}$$

Eq. (5.27) becomes

$$\begin{aligned}
J(\mathbf{u}^1, \mathbf{u}^2, \mathbf{u}^3) &= \Theta[\mathbf{x}(t_f), t_f] + \int_{t_0}^{t_1} (H^1 - \lambda^{1\top} \dot{\mathbf{x}}) dt + \int_{t_1}^{t_2} (H^2 - \lambda^{2\top} \dot{\mathbf{x}}) dt \\
&\quad + \int_{t_2}^{t_f} (H^3 - \lambda^{3\top} \dot{\mathbf{x}}) dt + \mathbf{v}^\top \mathbf{N}[\mathbf{x}(t_f), t_f]
\end{aligned} \tag{5.29}$$

The variation of the cost function is

$$\begin{aligned}
\delta J &= \int_{t_0}^{t_1} (\delta \mathbf{x})^\top \left(\frac{\partial H^1}{\partial \mathbf{x}} - \dot{\lambda}^1 \right) dt + \int_{t_1}^{t_2} (\delta \mathbf{x})^\top \left(\frac{\partial H^2}{\partial \mathbf{x}} - \dot{\lambda}^2 \right) dt + \int_{t_2}^{t_f} (\delta \mathbf{x})^\top \left(\frac{\partial H^3}{\partial \mathbf{x}} - \dot{\lambda}^3 \right) dt \\
&\quad + \int_{t_0}^{t_1} (\delta \mathbf{u}^1)^\top \frac{\partial H^1}{\partial \mathbf{u}^1} dt + \int_{t_1}^{t_2} (\delta \mathbf{u}^2)^\top \frac{\partial H^2}{\partial \mathbf{u}^2} dt + \int_{t_2}^{t_f} (\delta \mathbf{u}^3)^\top \frac{\partial H^3}{\partial \mathbf{u}^3} dt \\
&\quad + (\delta \mathbf{x})^\top (-\lambda^1) \Big|_{t_0} + (\delta \mathbf{x})^\top (\lambda^2) \Big|_{t_1} + (\delta \mathbf{x})^\top (-\lambda^2) \Big|_{t_2} + (\delta \mathbf{x})^\top (\lambda^3) \Big|_{t_2} \\
&\quad + (\delta \mathbf{x})^\top (-\lambda^3) \Big|_{t_f} + (\delta \mathbf{x})^\top \frac{\partial \mathbf{N}^\top}{\partial \mathbf{x}} \cdot \mathbf{v} \Big|_{t_f} + \frac{\partial \Theta}{\partial \mathbf{x}} \Big|_{t_f}
\end{aligned} \tag{5.30}$$

Letting the variation of cost function to be zero, the optimal conditions can be written as

$$\left(\frac{\partial H^1}{\partial \mathbf{x}} - \dot{\lambda}^1 \right) = 0 \tag{5.31}$$

$$\left(\frac{\partial H^2}{\partial \mathbf{x}} - \dot{\lambda}^2 \right) = 0 \tag{5.32}$$

$$\left(\frac{\partial H^3}{\partial \mathbf{x}} - \dot{\lambda}^3 \right) = 0 \tag{5.33}$$

$$\frac{\partial H^1}{\partial \mathbf{u}^1} = 0, \quad \frac{\partial H^2}{\partial \mathbf{u}^2} = 0, \quad \frac{\partial H^3}{\partial \mathbf{u}^3} = 0 \tag{5.34}$$

$$\lambda^1 \Big|_{t_0} = \lambda^2 \Big|_{t_1} \quad \lambda^2 \Big|_{t_2} = \lambda^3 \Big|_{t_2} \tag{5.35}$$

$$\left[-\lambda^3 + \frac{\partial \mathbf{N}^T}{\partial \mathbf{x}} \cdot \mathbf{v} + \frac{\partial \Theta}{\partial \mathbf{x}} \right] \bigg|_{t_f} = 0 \quad (5.36)$$

The computer algorithm for multiple stage optimal operation problems

The basic steps required in obtaining the optimal control solution remains the same as those described for the single stage problems. However, the computational methodology should now keep track of the states, co-states and control inputs for each stage. For completeness, the solution steps are summarized as follows:

- (I). Pick an initial control profile $\hat{\mathbf{u}}^1(t), \hat{\mathbf{u}}^2(t), \hat{\mathbf{u}}^3(t)$ and solve the state equation (5.17) with given initial conditions. Store $\hat{\mathbf{x}}(t)$, $t_0 \leq t \leq t_f$,
- (II). Determine $\lambda^3(t_f)$ by Eq. (5.36) and integrate Eq. (5.33), (5.32), (5.31) backwards from t_f to t_0 with the continuous conditions of Eq. (5.35). During the backward integration calculate $(\frac{\partial H^1}{\partial \mathbf{u}^1})$, $(\frac{\partial H^2}{\partial \mathbf{u}^2})$, $(\frac{\partial H^3}{\partial \mathbf{u}^3})$,
- (III). Solve Eq. (5.17) forward with $\mathbf{u}^1 = \hat{\mathbf{u}}^1 - k^1(\frac{\partial H^1}{\partial \mathbf{u}^1})$, $\mathbf{u}^2 = \hat{\mathbf{u}}^2 - k^2(\frac{\partial H^2}{\partial \mathbf{u}^2})$,
 $\mathbf{u}^3 = \hat{\mathbf{u}}^3 - k^3(\frac{\partial H^3}{\partial \mathbf{u}^3})$ for several values of a pair (k^1, k^2, k^3) and determine the corresponding values of J , Note that the continuity of the state vector \mathbf{x} must be satisfied at the switching times t_1, t_2 ,
- (IV). Find the best value of pair (k^1, k^2, k^3) (the value that yields the least value of J) and use this value to determine the next estimate for $\mathbf{u}^1, \mathbf{u}^2, \mathbf{u}^3$. Note that the corrected controls $\mathbf{u}^1, \mathbf{u}^2, \mathbf{u}^3$ should be clipped off if they violate the control constraints (5.21), (5.23), (5.25),

(V). Return to step (I) and repeat. The process ends when the change in the performance tends to zero.

Since HVAC system models are large scale models, finding optimal control trajectories of systems with multiple stages requires considerable computational effort. Furthermore, if the overall model consists of multiple time scales as in the case with VAV systems, numerical difficulties arise in finding accurate and reliable control solutions. To address this issue it is proposed to use perturbation methods.

As noted in Chapter 4, the VAV system is a multiple time-scale system that can be divided into a slow subsystem and a fast subsystem. The slow subsystem is the subsystem that has large capacity, therefore has long time delay in the dynamic response, e.g., storage tank and zones. The fast subsystem has very fast response, e.g., cooling coil, air flow and water flow subsystems. When the system involved in an optimal control problem consists of such multiple time-scales, it is possible to reduce the computational effort by using the perturbation method.

5.2.2 The perturbation method for multiple time-scale systems

The basic idea of the perturbation method is that the order of a model can be reduced by neglecting some small time-constant subsystems whose presence causes the model order to be higher than acceptable for practical design of optimal systems (Kokotovic and Sannuti 1968).

Constructing the model

The first step in the perturbation procedure is to examine the structure of the model. For simplification, let us consider the single stage optimal control problem. Let the VAV system can be described as $(n+m)$ th-order model such as

$$\dot{\mathbf{y}} = \mathbf{F}(\mathbf{y}, \mathbf{u}, \mu, t) \quad (5.37)$$

where \mathbf{y} is the $(n+m)$ -dimensional “plant state”, \mathbf{u} is r -dimensional “plant control”, and μ is a scalar parameter. The optimal control problem is to find an optimal control \mathbf{u}^* which minimizes the performance index,

$$J = \theta(\mathbf{y}(t_f), t_f) + \int_{t_0}^{t_f} \phi(\mathbf{y}(t), \mathbf{u}(t), t) dt \quad (5.38)$$

when the initial state $\mathbf{y}(t_0) = \mathbf{y}_0$ is fixed. It is assumed that the order $n+m$ of the plant (5.37) is too high for the optimization problem to be practically solvable by existing numerical methods. Therefore, an n th-order model is introduced,

$$\dot{\mathbf{x}} = \mathbf{f}(\mathbf{x}, \mathbf{u}, \mu, t) \quad (5.39)$$

where \mathbf{x} is the n -dimensional “model-state”, \mathbf{u} is the r -dimensional “model control”, and μ is the same scalar parameter as in (5.37). Then the plant equation (5.37) can be given a more specific form.

$$\dot{\mathbf{x}} = \mathbf{g}(\mathbf{x}, \mathbf{z}, \mathbf{u}, \mu, t) \quad (5.40a)$$

$$\mu \dot{\mathbf{z}} = \mathbf{G}(\mathbf{x}, \mathbf{z}, \mathbf{u}, \mu, t) \quad (5.40b)$$

where \mathbf{x} and \mathbf{z} are, respectively, the n -dimensional and the m -dimensional parts of the plant state \mathbf{y} ,

$$\mathbf{y} = \begin{bmatrix} \mathbf{x} \\ \mathbf{z} \end{bmatrix} \quad (5.41)$$

The performance index (5.38) can be rewritten as

$$J = \Theta(\mathbf{x}(t_f), \mathbf{z}(t_f), t_f) + \int_{t_0}^{t_f} \Phi(\mathbf{x}(t), \mathbf{z}(t), \mathbf{u}(t), t) dt \quad (5.42)$$

The perturbation method for single stage problems (Kokotovic and Sannuti 1968)

Let L be the Lagrangian function for the functional (5.42) and the plant (5.40)

$$L = \Phi(\mathbf{x}, \mathbf{z}, \mathbf{u}, t) + \lambda^T [\mathbf{g}(\mathbf{x}, \mathbf{z}, \mathbf{u}, \mu, t) - \dot{\mathbf{x}}] + \xi^T [\mathbf{G}(\mathbf{x}, \mathbf{z}, \mathbf{u}, \mu, t) - \mu \dot{\mathbf{z}}] \quad (5.43)$$

where λ and ξ are n - and m -dimensional costates associated with \mathbf{x} and \mathbf{z} , respectively.

By applying the maximum principle of Pontryagin, the plant optimal functions $\mathbf{u}^*(t, \mu)$, $\mathbf{x}^*(t, \mu)$, $\lambda^*(t, \mu)$, $\xi^*(t, \mu)$ are the solution of the cononic equations

$$\frac{\partial L}{\partial \mathbf{u}} = 0 \quad \frac{\partial L}{\partial \lambda} = 0 \quad \frac{\partial L}{\partial \xi} = 0 \quad (5.44a)$$

$$\frac{\partial L}{\partial \mathbf{x}} - \frac{d}{dt} \frac{\partial L}{\partial \dot{\mathbf{x}}} = 0 \quad \frac{\partial L}{\partial \mathbf{z}} - \frac{d}{dt} \frac{\partial L}{\partial \dot{\mathbf{z}}} = 0 \quad (5.44b)$$

with the boundary values

$$\mathbf{x}(t_0) = \mathbf{x}_0; \quad \mathbf{z}(t_0) = \mathbf{z}_0; \quad \lambda(t_f) = \frac{\partial \Theta}{\partial \mathbf{x}} \Big|_{t=t_f}; \quad \xi(t_f) = \frac{\partial \Theta}{\partial \mathbf{z}} \Big|_{t=t_f} \quad (5.44c)$$

Substituting Eq. (5.43) into Equations (5.44a) and (5.44b), Equations (5.44a) and (5.44b) can be rewritten as follows:

$$\nabla_{\mathbf{u}} \Phi + \lambda^T \mathbf{g}_{\mathbf{u}} + \xi^T \mathbf{G}_{\mathbf{u}} = 0 \quad (5.45)$$

$$\dot{\mathbf{x}} = \mathbf{g}(\mathbf{x}, \mathbf{z}, \mathbf{u}, \mu, t) \quad (5.46a)$$

$$\mu \dot{\mathbf{z}} = \mathbf{G}(\mathbf{x}, \mathbf{z}, \mathbf{u}, \mu, t) \quad (5.46b)$$

$$\dot{\lambda} = \nabla_{\mathbf{x}} \Phi + \mathbf{g}_{\mathbf{x}}^T \lambda + \mathbf{G}_{\mathbf{x}}^T \xi \quad (5.47a)$$

$$\mu \dot{\xi} = \nabla_z \Phi + \mathbf{g}_z^T \lambda + \mathbf{G}_z^T \xi \quad (5.47b)$$

The above problem is the one with $2(n+m)$ -dimensional boundary value problem, i.e., full optimal problem. By applying the perturbation principle, the problem will be reduced to one with $2n$ -dimensional boundary value problem which can be obtained by letting $\mu=0$ in Equations (5.45), (5.46) and (5.47):

$$\nabla_u \Phi + \lambda^T \mathbf{g}_u + \xi^T \mathbf{G}_u = 0 \quad (5.48)$$

$$\dot{\mathbf{x}} = \mathbf{g}(\mathbf{x}, \mathbf{z}, \mathbf{u}, 0, t) \quad (5.49a)$$

$$0 = \mathbf{G}(\mathbf{x}, \mathbf{z}, \mathbf{u}, 0, t) \quad (5.49b)$$

$$\dot{\lambda} = \nabla_x \Phi + \mathbf{g}_x^T \lambda + \mathbf{G}_x^T \xi \quad (5.50a)$$

$$0 = \nabla_z \Phi + \mathbf{g}_z^T \lambda + \mathbf{G}_z^T \xi \quad (5.50b)$$

where the boundary conditions are

$$\mathbf{x}(t_0) = \mathbf{x}_0; \quad \lambda(t_f) = \frac{\partial \Theta}{\partial \mathbf{x}} \Big|_{t=t_f} \quad (5.51)$$

The model-optimal function $\mathbf{u}^*(t)$, $\mathbf{x}^*(t)$, $\mathbf{z}^*(t)$, $\lambda^*(t)$, $\xi^*(t)$ are the solution of Equations (5.48) through (5.51).

Note that above stated method is valid for the single stage optimal control problems. However, the principle of the perturbation method can be extended to the multiple stage optimal control problems as described in the following section.

5.2.3 The multiple stage optimal operation problems with the perturbation method

The model structure

Let us still take the three stage optimal operation problem stated in Section 5.2.1 as an example, although the methodology developed here can be applied for the problems with as many stages as required.

The VAV system model can be written in a vector differential equation form over time interval $[t_0, t_f]$ with three stages:

$$\dot{\mathbf{x}} = \begin{cases} \mathbf{f}^1(\mathbf{x}, \mathbf{z}^1, \mathbf{u}^1, \mu^1, t) & \text{on } [t_0, t_1] \\ \mathbf{f}^2(\mathbf{x}, \mathbf{z}^2, \mathbf{u}^2, \mu^2, t) & \text{on } [t_1, t_2] \\ \mathbf{f}^3(\mathbf{x}, \mathbf{z}^3, \mathbf{u}^3, \mu^3, t) & \text{on } [t_2, t_f] \end{cases} \quad (5.52a)$$

$$\begin{aligned} \mu^1 \dot{\mathbf{z}}^1 &= \mathbf{F}^1(\mathbf{x}, \mathbf{z}^1, \mathbf{u}^1, \mu^1, t) & \text{on } [t_0, t_1] \\ \mu^2 \dot{\mathbf{z}}^2 &= \mathbf{F}^2(\mathbf{x}, \mathbf{z}^2, \mathbf{u}^2, \mu^2, t) & \text{on } [t_1, t_2] \\ \mu^3 \dot{\mathbf{z}}^3 &= \mathbf{F}^3(\mathbf{x}, \mathbf{z}^3, \mathbf{u}^3, \mu^3, t) & \text{on } [t_2, t_f] \end{aligned} \quad (5.52b)$$

where $\mathbf{x}(t)$ the n -dimensional “model-state” vector of slow system, and $\mathbf{u}^1(t)$, $\mathbf{u}^2(t)$, $\mathbf{u}^3(t)$ are the r^1 -, r^2 -, r^3 -dimensional control vectors corresponding to three stages. $\mathbf{z}^1(t)$, $\mathbf{z}^2(t)$, $\mathbf{z}^3(t)$ are the m^1 -, m^2 -, m^3 -dimensional fast state vectors corresponding to three stages.

The initial conditions of the model-states are given by

$$\mathbf{x}(t_0) = \mathbf{x}_0 \quad (5.53)$$

The three-stage performance index (5.19) can be redefined as

$$\begin{aligned} J(\mathbf{u}^1, \mathbf{u}^2, \mathbf{u}^3) &= \Theta(\mathbf{x}(t_f), \mathbf{z}^3(t_f), t_f) + \int_{t_0}^{t_1} \Phi^1(\mathbf{x}, \mathbf{z}^1, \mathbf{u}^1, t) dt + \int_{t_1}^{t_2} \Phi^2(\mathbf{x}, \mathbf{z}^2, \mathbf{u}^2, t) dt \\ &\quad + \int_{t_2}^{t_f} \Phi^3(\mathbf{x}, \mathbf{z}^3, \mathbf{u}^3, t) dt \end{aligned} \quad (5.54)$$

The problem has constraints on the state and control variables:

in the first stage t_0 to t_1

$$\mathbf{h}^1(\mathbf{u}^1, \mathbf{z}^1, t) \geq 0 \quad \mathbf{g}^1(\mathbf{x}, \mathbf{z}^1, t) \geq 0 \quad (5.55a)$$

$$u_{i,\min}^1 \leq u_i^1 \leq u_{i,\max}^1 \quad (5.55b)$$

in the second stage t_1 to t_2

$$\mathbf{h}^2(\mathbf{u}^2, \mathbf{z}^2, t) \geq 0 \quad \mathbf{g}^2(\mathbf{x}, \mathbf{z}^2, t) \geq 0 \quad (5.55c)$$

$$u_{i,\min}^2 \leq u_i^2 \leq u_{i,\max}^2 \quad (5.55d)$$

in the third stage t_2 to t_f

$$\mathbf{h}^3(\mathbf{u}^3, \mathbf{z}^3, t) \geq 0 \quad \mathbf{g}^3(\mathbf{x}, \mathbf{z}^3, t) \geq 0 \quad (5.55e)$$

$$u_{i,\min}^3 \leq u_i^3 \leq u_{i,\max}^3 \quad (5.55f)$$

the terminal condition at time t_f

$$\mathbf{N}[\mathbf{x}(t_f), \mathbf{z}^3(t_f), t_f] \geq 0 \quad (5.55g)$$

The perturbation method for multiple stage problems

The unconstrained multistage performance index is written as

$$\begin{aligned} J(\mathbf{u}^1, \mathbf{u}^2, \mathbf{u}^3) = & \int_{t_0}^{t_1} \{ \Phi^1(\mathbf{x}, \mathbf{z}^1, \mathbf{u}^1, t) + \lambda^{1T} [\mathbf{f}^1(\mathbf{x}, \mathbf{z}^1, \mathbf{u}^1, t) - \dot{\mathbf{x}}] + \xi^{1T} [\mathbf{F}^1(\mathbf{x}, \mathbf{z}^1, \mathbf{u}^1, t) - \dot{\mathbf{z}}^1] \\ & + \omega^{1T} \mathbf{h}^1(\mathbf{u}^1, \mathbf{z}^1, t) + \eta^{1T} \mathbf{g}^1(\mathbf{x}, \mathbf{z}^1, t) \} dt \\ & + \int_{t_1}^{t_2} \{ \Phi^2(\mathbf{x}, \mathbf{z}^2, \mathbf{u}^2, t) + \lambda^{2T} [\mathbf{f}^2(\mathbf{x}, \mathbf{z}^2, \mathbf{u}^2, t) - \dot{\mathbf{x}}] + \xi^{2T} [\mathbf{F}^2(\mathbf{x}, \mathbf{z}^2, \mathbf{u}^2, t) - \dot{\mathbf{z}}^2] \\ & + \omega^{2T} \mathbf{h}^2(\mathbf{u}^2, \mathbf{z}^2, t) + \eta^{2T} \mathbf{g}^2(\mathbf{x}, \mathbf{z}^2, t) \} dt \\ & + \int_{t_2}^{t_f} \{ \Phi^3(\mathbf{x}, \mathbf{z}^3, \mathbf{u}^3, t) + \lambda^{3T} [\mathbf{f}^3(\mathbf{x}, \mathbf{z}^3, \mathbf{u}^3, t) - \dot{\mathbf{x}}] + \xi^{3T} [\mathbf{F}^3(\mathbf{x}, \mathbf{z}^3, \mathbf{u}^3, t) - \dot{\mathbf{z}}^3] \\ & + \omega^{3T} \mathbf{h}^3(\mathbf{u}^3, \mathbf{z}^3, t) + \eta^{3T} \mathbf{g}^3(\mathbf{x}, \mathbf{z}^3, t) \} dt \\ & + \mathbf{v}^T \mathbf{N}[\mathbf{x}(t_f), \mathbf{z}^3(t_f), t_f] + \Theta[\mathbf{x}(t_f), \mathbf{z}^3(t_f), t_f] \end{aligned} \quad (5.56)$$

By defining the Hamiltonian functions

$$\begin{aligned}
H^1 &= \Phi^1 + \lambda^{1\top} \mathbf{f}^1 + \xi^{1\top} \mathbf{F}^1 + \omega^{1\top} \mathbf{h}^1 + \eta^{1\top} \mathbf{g}^1 \\
H^2 &= \Phi^2 + \lambda^{2\top} \mathbf{f}^2 + \xi^{2\top} \mathbf{F}^2 + \omega^{2\top} \mathbf{h}^2 + \eta^{2\top} \mathbf{g}^2 \\
H^3 &= \Phi^3 + \lambda^{3\top} \mathbf{f}^3 + \xi^{3\top} \mathbf{F}^3 + \omega^{3\top} \mathbf{h}^3 + \eta^{3\top} \mathbf{g}^3
\end{aligned} \tag{5.57}$$

Eq. (5.56) becomes

$$\begin{aligned}
J(\mathbf{u}^1, \mathbf{u}^2, \mathbf{u}^3) &= \Theta[\mathbf{x}(t_f), t_f] + \mathbf{v}^\top \mathbf{N}[\mathbf{x}(t_f), t_f] + \int_{t_0}^{t_1} (H^1 - \lambda^{1\top} \dot{\mathbf{x}} - \mu^1 \xi^{1\top} \dot{\mathbf{z}}^1) dt \\
&\quad + \int_{t_1}^{t_2} (H^2 - \lambda^{2\top} \dot{\mathbf{x}} - \mu^2 \xi^{2\top} \dot{\mathbf{z}}^2) dt + \int_{t_2}^{t_3} (H^3 - \lambda^{3\top} \dot{\mathbf{x}} - \mu^3 \xi^{3\top} \dot{\mathbf{z}}^3) dt
\end{aligned} \tag{5.58}$$

Letting the variation of cost function to be zero, the optimal conditions can be written as

$$\left(\frac{\partial H^1}{\partial \mathbf{x}} - \dot{\lambda}^1 \right) = 0 \qquad \left(\frac{\partial H^1}{\partial \mathbf{z}^1} - \mu^1 \dot{\xi}^1 \right) = 0 \tag{5.59}$$

$$\left(\frac{\partial H^2}{\partial \mathbf{x}} - \dot{\lambda}^2 \right) = 0 \qquad \left(\frac{\partial H^2}{\partial \mathbf{z}^2} - \mu^2 \dot{\xi}^2 \right) = 0 \tag{5.60}$$

$$\left(\frac{\partial H^3}{\partial \mathbf{x}} - \dot{\lambda}^3 \right) = 0 \qquad \left(\frac{\partial H^3}{\partial \mathbf{z}^3} - \mu^3 \dot{\xi}^3 \right) = 0 \tag{5.61}$$

$$\frac{\partial H^1}{\partial \mathbf{u}^1} = 0, \quad \frac{\partial H^2}{\partial \mathbf{u}^2} = 0, \quad \frac{\partial H^3}{\partial \mathbf{u}^3} = 0 \tag{5.62}$$

Now applying the perturbation principle, the problem is reduced to one with $2n$ -dimensional boundary value problem which can be obtained by letting $\mu=0$ in Equations (5.59)-(5.62), (5.52a), (5.52b):

$$\frac{\partial H^1}{\partial \mathbf{u}^1} = 0, \quad \frac{\partial H^2}{\partial \mathbf{u}^2} = 0, \quad \frac{\partial H^3}{\partial \mathbf{u}^3} = 0 \tag{5.63}$$

$$\begin{aligned}
\dot{\mathbf{x}} &= \mathbf{f}^1(\mathbf{x}, \mathbf{z}^1, \mathbf{u}^1, t) \\
0 &= \mathbf{F}^1(\mathbf{x}, \mathbf{z}^1, \mathbf{u}^1, t)
\end{aligned} \quad \text{on } [t_0, t_1] \tag{5.64a}$$

$$\begin{aligned}
\dot{\mathbf{x}} &= \mathbf{f}^2(\mathbf{x}, \mathbf{z}^2, \mathbf{u}^2, t) \\
0 &= \mathbf{F}^2(\mathbf{x}, \mathbf{z}^2, \mathbf{u}^2, t)
\end{aligned} \quad \text{on } [t_1, t_2] \tag{5.64b}$$

$$\begin{aligned}\dot{\mathbf{x}} &= \mathbf{f}^3(\mathbf{x}, \mathbf{z}^3, \mathbf{u}^3, t) \\ 0 &= \mathbf{F}^3(\mathbf{x}, \mathbf{z}^3, \mathbf{u}^3, t)\end{aligned}\quad \text{on } [t_2, t_f] \quad (5.64c)$$

$$\left(\frac{\partial H^1}{\partial \mathbf{x}} - \dot{\lambda}^1\right) = 0 \quad \frac{\partial H^1}{\partial \mathbf{z}^1} = 0 \quad (5.65a)$$

$$\left(\frac{\partial H^2}{\partial \mathbf{x}} - \dot{\lambda}^2\right) = 0 \quad \frac{\partial H^2}{\partial \mathbf{z}^2} = 0 \quad (5.65b)$$

$$\left(\frac{\partial H^3}{\partial \mathbf{x}} - \dot{\lambda}^3\right) = 0 \quad \frac{\partial H^3}{\partial \mathbf{z}^3} = 0 \quad (5.65c)$$

$$\lambda^1|_{t_1} = \lambda^2|_{t_1} \quad \lambda^2|_{t_2} = \lambda^3|_{t_2} \quad (5.66)$$

where the boundary conditions are

$$\mathbf{x}(t_0) = \mathbf{x}_0; \quad \lambda^3(t_f) = \left[\frac{\partial \mathbf{N}^T}{\partial \mathbf{x}} \mathbf{v} + \frac{\partial \Theta}{\partial \mathbf{x}} \right] \Big|_{t=t_f} \quad (5.67)$$

The model-optimal function $\mathbf{u}^{1*}(t)$, $\mathbf{u}^{2*}(t)$, $\mathbf{u}^{3*}(t)$, $\mathbf{x}^*(t)$, $\mathbf{z}^{1*}(t)$, $\mathbf{z}^{2*}(t)$, $\mathbf{z}^{3*}(t)$, $\lambda^{1*}(t)$, $\lambda^{2*}(t)$, $\lambda^{3*}(t)$, $\xi^{1*}(t)$, $\xi^{2*}(t)$, $\xi^{3*}(t)$ is the solution of Equations (5.63) through (5.67).

The computer algorithm for multiple stage optimal operation problems with the perturbation method

The computer algorithm for solving the multiple stage optimal operation problem involving fast and slow subsystem dynamics can be summarized as:

- (I). Divide the time domain $[t_0, t_f]$ into several nodes. Pick an initial control profile $\hat{\mathbf{u}}^1(t)$, $\hat{\mathbf{u}}^2(t)$, $\hat{\mathbf{u}}^3(t)$ and integrate the model-state equations (first equation at Eq. 5.64a, 5.64b, 5.64c) with given initial conditions to get $\hat{\mathbf{x}}(t)$. Note that during the

- integration, at each time node, solve the nonlinear equations (second equation of Eq. 5.64a, 5.64b, 5.64c) to get $\mathbf{z}^1, \mathbf{z}^2, \mathbf{z}^3$. Store $\hat{\mathbf{x}}(t)$ and $\mathbf{z}^1, \mathbf{z}^2, \mathbf{z}^3$, $t_0 \leq t \leq t_f$,
- (II). Determine $\lambda^3(t_f)$ by Eq. (5-67) and integrate the costate equations (first equation of Eq. 5.65a, 5.65b, 5.65c) backwards from t_f to t_0 with the continuous conditions of Eq. (5.66) to get $\lambda^3, \lambda^2, \lambda^1$. Note that during the backward integration, at each time step, solve the nonlinear equations (second equation of Eq. 5.65a, 5.65b, 5.65c) to get ξ^1, ξ^2, ξ^3 and during the backward integration calculate $(\frac{\partial H^1}{\partial \mathbf{u}^1})$, $(\frac{\partial H^2}{\partial \mathbf{u}^2})$, $(\frac{\partial H^3}{\partial \mathbf{u}^3})$,
- (III). Solve Eq. (5.54) forward with $\mathbf{u}^1 = \hat{\mathbf{u}}^1 - k^1(\frac{\partial H^1}{\partial \mathbf{u}^1})$, $\mathbf{u}^2 = \hat{\mathbf{u}}^2 - k^2(\frac{\partial H^2}{\partial \mathbf{u}^2})$, $\mathbf{u}^3 = \hat{\mathbf{u}}^3 - k^3(\frac{\partial H^3}{\partial \mathbf{u}^3})$ for several values of a pair (k^1, k^2, k^3) and determine the corresponding values of J , The continuity of the state vector \mathbf{x} must be satisfied at the switching times t_1, t_2 ,
- (IV). Find the best value of pair (k^1, k^2, k^3) (the value that yields the least value of J) and use this value to determine the next estimate for $\mathbf{u}^1, \mathbf{u}^2, \mathbf{u}^3$. Note that the corrected controls $\mathbf{u}^1, \mathbf{u}^2, \mathbf{u}^3$ should be clipped off if they violate the control constraints (5.55b), (5.55d), (5.55f),
- (V). Return to step (I) and repeat. The process ends when the change in the performance meets the stopping criterion.

In next chapter, the developed optimal control methodology is applied to find optimal solutions to typical VAV system operation problems.

Chapter 6

Applications of the Optimization Methodology

Based on the methodology developed in Chapter 5, a computer program for solving multiple stage optimal operation problems has been developed. In this chapter, we will present three examples showing the applications of the developed methodology to determine the optimal operation strategies for the VAV system.

6.1 Introduction

As pointed in Chapter 1, a supervisory control system such as the energy management and control system (EMCS) should have the capabilities to compute the global optimal control trajectories for the local controllers. Each local controller will track the appropriate optimal trajectory that acts as a reference signal. The local controller will regulate the process outputs against any mismatches in the predicted and actual loads. These two-tier control schemes will improve the performance of VAV system in terms of providing good temperature and humidity control and as well as in reducing the energy costs significantly.

For example, let us consider a multizone VAV system illustrated in Fig. 3.1. In practice, the system can be decentralized into several local loops, (i) zone loop, the output zone temperature of which can be controlled by modulating the zone damper position; (ii) discharge air loop, the output (discharge air temperature) can be controlled by changing the mass flow rate of chilled water by modulating the valve position and/or the pump

voltage input; (iii) chiller and storage tank loop, the chilled water temperature can be controlled by modulating the energy input to the chiller; (iv) fan and airflow loop, the static pressure in ductwork can be controlled by modulating the fan voltage.

In most HVAC control applications, the final control objective is to control the zone temperatures and humidity ratios within the desired range based on human comfort. Among these outputs, except the zone temperature, which is the final control objective, other outputs are only the intermediaries and their optimal setpoints are not known. Thus the question is how to choose the setpoints for these outputs.

Usually the setpoints for these outputs are chosen based on experience. For example, in many HVAC systems the setpoint of the discharge air temperature is selected as 13°C in normal operation mode. The static pressure setpoint in the ductwork is held at some constant value. This will lead to energy waste and even discomfort. In reality, the setpoints should be changed as a function of load acting on the zones. Therefore, there is potential to save energy and improve comfort of the occupants by determining the optimal setpoint profiles. Because of the large capacity of the building and the storage tank, one must consider the dynamic characteristics of the overall system. In other words, the determination of the optimal setpoint profiles should be based on the dynamic optimal search method rather than static programming techniques. In this chapter, several applications of the dynamic optimal control methodology developed in Chapter 5 will be presented. In this regard, three typical examples are chosen. In the first example, the energy efficiency of two basic operating modes namely constant volume and variable air volume are compared. Example two and three deal with multizone VAV system operation.

In particular a multizone heating problem is examined in Section 6.3. In section 6.4 a detailed five zone cooling problem (temperature and humidity control) is addressed.

6.2 Comparison of Operational Efficiency of Constant- and Variable-Air-Volume HVAC Systems

As mentioned in Chapter 1, HVAC systems are broadly classified in two categories: Constant Volume (CV) and Variable-Air-Volume (VAV) systems. In CV mode of operation, air-supply temperature is varied in response to building loads while holding air-flow rate constant. On the other hand in VAV mode, air-supply temperature is held at some constant setpoint while varying air-flow rate according to building loads.

In addition to CV or VAV mode of operation, the energy efficiency of HVAC systems depends on several design and operating factors, viz., building operation schedules, time-of-day rates offered by the utilities and energy storage techniques. Buildings are operated in time scheduled modes (Payne and McGowan 1988) such as off-normal operation, start-up phase and occupied period. Consequently, it is necessary to synchronize the response of HVAC system not only with different needs of the building's operation schedules but also with variable heating/cooling loads and occupancy patterns. Therefore, in evaluating the energy efficiency potential of HVAC systems, all the above cited factors must be considered. With this as the motivation, we consider here, the application of multi-stage optimization techniques to evaluate and compare the energy efficiency potential of HVAC systems operated in CV and VAV modes.

To illustrate the methodology a single zone spacing heating system is considered and an analytical model is derived (Section 6.2.1). The statement of the optimization

problem, its formulation are described in Section 6.2.2. Simulation results obtained are discussed in Section 6.2.3 followed by discussions in Section 6.2.4.

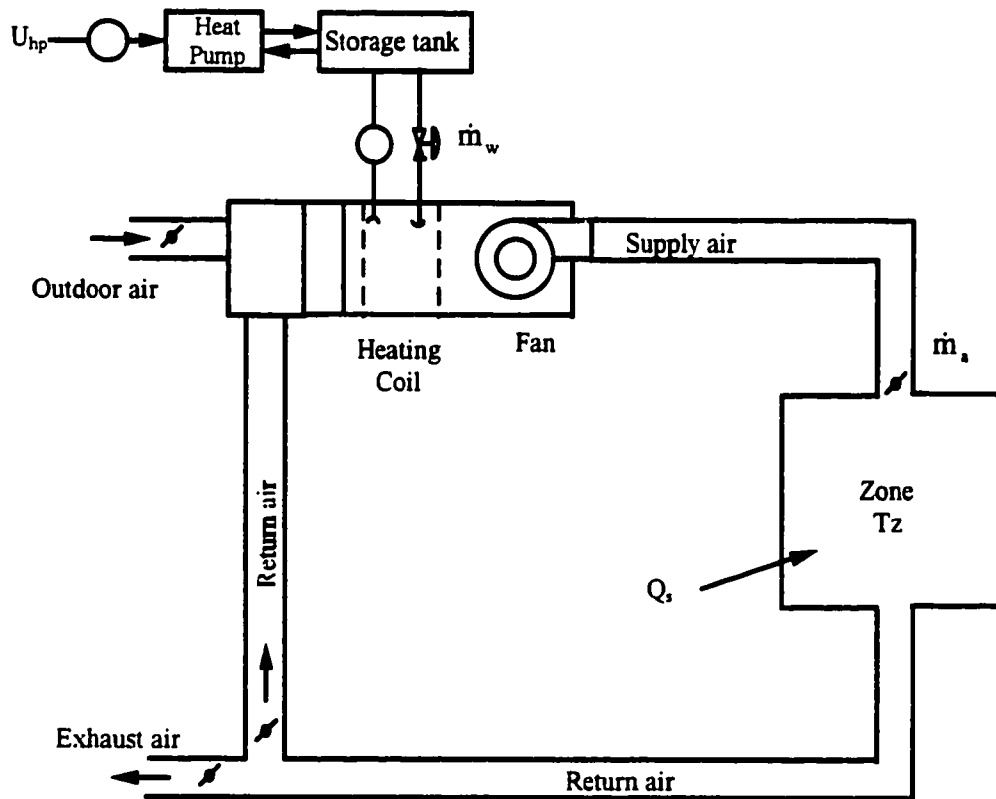


Figure 6.1 The schematic diagram of a single-zone VAVH system

6.2.1 Dynamic model of a single zone space Heating (SZSH) system

Figure 6.1 shows a schematic diagram of single zone Heating (SZSH) system. A water-source heat pump with a storage tank is used as a primary system. Hot water from storage tank is circulated in a heating coil in which air is sensibly heated. The discharge air so heated is circulated in the zone via fan and ductwork. In response to heating loads acting on the zone, either air-supply temperature or air-flow rate or both temperature and

air-flow rate can be varied. Thus there are three different modes of operation. In CV mode, zone temperature is taken as a feedback signal to modulate the mass flow rate of hot water (\dot{m}_w) via the valve. As a result, air-supply temperature continuously changes as a function of heating load. In VAV mode, air flow rate to Zone (\dot{m}_a) is modulated by varying the fan-speed. The discharge air temperature remains constant at some chosen setpoint. In a more general case both air-supply temperature and flow rate are continuously modulated as a function of load. We identify this mode as the general variable air volume (GVAV) mode.

6.2.2 Formulation of optimal operation of a Single Zone Space Heating (SZSH) system

By making use of the mass and energy balance principle, model equations for each subsystem of the SZSH system were derived. These are

Zone Model

$$\frac{dT_z}{dt} = \frac{1}{\rho_a c_{p,a} V_z} \{ \dot{m}_a c_{p,a} (T_{a,s} - T_z) + q_s + \alpha_z (T_{out} - T_z) \} \quad (6.1)$$

Storage Tank Model

$$\frac{dT_{ws}}{dt} = \frac{1}{\rho_w c_w V_{tank}} \{ -\dot{m}_a c_w (T_{ws} - T_{wr}) + U_{hp} U_{hp,max} COP + \alpha_h (T_{\infty,t} - T_{ws}) \} \quad (6.2)$$

Heating Coil Model

Air Temperature

$$\frac{dT_a}{dt} = -\frac{h_i \eta_{s,ov} A_o}{\rho c_v A} (\bar{T}_a - \bar{T}_i) - \frac{\gamma \dot{m}_a}{\rho A L_c} (T_a - T_{a,in}) \quad (6.3)$$

Water Temperature

$$\frac{dT_{wr}}{dt} = \frac{\dot{m}_w}{m_w L_c} (T_{ws} - T_{wr}) + \frac{h_{it} A_{it}}{m_w c_w} (\bar{T}_t - \bar{T}_w) \quad (6.4)$$

Tube Temperature

$$\begin{aligned} \frac{d\bar{T}_t}{dt} = \frac{1 - \eta_s}{\eta_s + \frac{m_t c_t}{m_{fin} c_{fin}}} & \left\{ \frac{\gamma \dot{m}_a}{\rho A L_c} (T_a - T_{a,in}) - \frac{h_{it} A_{it}}{m_{fin} c_{fin} (1 - \eta_s)} (\bar{T}_t - \bar{T}_w) \right. \\ & \left. + \left(\frac{\eta_{s,ov} h_c A_o}{\rho c_v A} + \frac{\eta_{s,ov} h_c A_o}{m_{fin} c_{fin} (1 - \eta_s)} \right) (\bar{T}_a - \bar{T}_t) \right\} \end{aligned} \quad (6.5)$$

$$\text{where } \bar{T}_a = \frac{\dot{m}_a c_{pa} T_{a,in} + \dot{m}_w c_w T_a}{\dot{m}_a c_{pa} + \dot{m}_w c_w}, \quad \bar{T}_w = \frac{\dot{m}_a c_{pa} T_{wr} + \dot{m}_w c_w T_{ws}}{\dot{m}_a c_{pa} + \dot{m}_w c_w},$$

$$T_{a,in} = 0.15 T_{a,out} + 0.85 T_z.$$

Heat Pump Model

The coefficient of performance of heat pump is simulated using the following empirical equation

$$COP = 1 + (COP_{\max} - 1) \left(1 - \frac{T_{ws} - T_o}{\Delta T_{\max}} \right) \quad (6.6)$$

Building Operation

A typical three stage building operation schedule is assumed. Stage 1 (1700h - 0700h) is off-normal operation in which building temperature is allowed to setback between 15-18°C and outdoor air flow is shut-off. In stage 2 (0700-0800h), start-up mode, the water valve is full open and the zone temperature is allowed to rise to the setpoint as quickly as possible. In stage 3, occupied period (0800h - 1700h), zone temperature is held within 21±0.5°C and minimum outdoor airflow rate is maintained. The

three stage building operation requirements must be met irrespective of CV, VAV or GVAV mode of operation.

Multi-stage optimal control

The SZSH system shown in Figure 6.1 has three control inputs: (i) energy input to the heat pump (U_{hp}), (ii) mass flow rate of hot water (\dot{m}_w), and (iii) mass flow rate of air to the zone (\dot{m}_a). One or more of these control inputs are modulated according to CV, VAV or GVAV mode of operation. Control input U_{hp} is used to improve energy efficiency of the SZSH system. On the other hand, \dot{m}_w and \dot{m}_a are used to improve zone temperature regulation and minimize fan/pump energy requirements. The control problem is defined as follows: find an optimal strategy for 24-hour operation of the SZSH system in the presence of time-of-day energy price incentives such that energy efficiency is improved and good zone temperature control is achieved for a given building operated in three stages (off-normal, start-up and occupied period) under each of the three (CV, VAV and GVAV) modes of air distribution strategies. Thus, the problem is one of tradeoffs between energy storage, versus price incentives synchronized with building schedules and operating costs of SZSH system.

Formulation of multi-stage optimization problem

The model equations (6.1-6.6) of the SZSH consists of two time-scale processes: a fast fan-coil heating process and a slow thermal process in the zone/storage tank. By using the singular perturbation method developed in Chapter 5, the multistage optimization problem for the SZSH system was formulated and solved. The model states of the SZSH

system were decomposed into a slow sub-system with $\mathbf{x}=[T_z, T_{ws}]^T$ and a fast sub-system with $\mathbf{z}=[T_a, T_{w,r}, T_i]^T$. The control inputs were defined by $\mathbf{u}=[U_{hp}, \dot{m}_w, \dot{m}_a]^T$.

The continuity of \mathbf{x} is assumed over the entire 24-hour period including at the switch over points between three stages 1, 2 and 3. During each of the prescribed stages the following operating conditions were assumed.

Constraints at different stages:

Stage 1 (1700h - 0700h) night setback stage

In this unoccupied stage, night setback is used to save energy. The building temperature is allowed to float between 15-18°C, and outdoor air is completely shut off.

Stage 2 (0700-0800h) start-up phase

In this stage, the pump is full-on and the building temperature is allowed to rise to the occupied setpoints as quickly as possible, minimum outdoor air (15% of total) is supplied to meet the ventilation requirement of the building.

Stage 3 (0800h- 1700h) occupied period

In stage 3, zone temperature is maintained within $21 \pm 0.5^\circ\text{C}$ while providing minimum outdoor air for ventilation.

These requirements are common to the CV, VAV and GVAV modes of operation. However, what is different is the manner in which the control inputs $\mathbf{u}=[U_{hp}, \dot{m}_w, \dot{m}_a]^T$ are operated.

In CV mode

$$\mathbf{u}=[U_{hp}, \dot{m}_w]^T, \quad \dot{m}_a = \dot{m}_{a,\max}, \text{ and } T_a \text{ is variable.}$$

In VAV mode

$$\mathbf{u}=[U_{hp}, \dot{m}_w, \dot{m}_a]^T, \quad T_a = T_{a,set}$$

In GVAV mode

$$\mathbf{u}=[U_{hp}, \dot{m}_w, \dot{m}_a]^T, \quad T_a \text{ is variable.}$$

Here T_a is the discharge air temperature also known as the air-supply temperature. The optimization problem to be solved was defined as the minimization of a three stage performance measure

$$\begin{aligned} J = & \int_{t_0}^{t_1} EP(t) \{U_{fan} V_{fan,max} I_{fan} + U_{hp} E_{hp,max} + U_p V_{p,max} I_p\} dt \\ & + \int_{t_1}^{t_2} EP(t) \{U_{fan} V_{fan,max} I_{fan} + U_{hp} E_{hp,max} + U_p V_{p,max} I_p\} dt \\ & + \int_{t_2}^{t_f} EP(t) \{U_{fan} V_{fan,max} I_{fan} + U_{hp} E_{hp,max} + U_p V_{p,max} I_p\} dt \end{aligned} \quad (6.7)$$

subject to model equations and constraints as described above. The terminal condition at t_f was defined by

$$N[\mathbf{x}(t_f), \mathbf{z}^3(t_f), t_f] \geq 0 \quad (6.8)$$

A time-of-day price structure for electrical energy (Winn and Winn 1985) as shown in Figure 6.2 was assumed to be in effect.

6.2.3 Simulation Results

A zone with 167 m² floor area undergoing typical winter day heating load in Montreal was simulated. The zone heat loss rate varied throughout the day ranging between a high and low of about 9 and 3 kW, respectively. A 4-ton heat pump with 3 m³ storage tank was connected to a heating coil via a 1/3 hp variable speed pump with a rated flow of 10 gallons per minute. Air flow to the zone was supplied by a variable speed fan

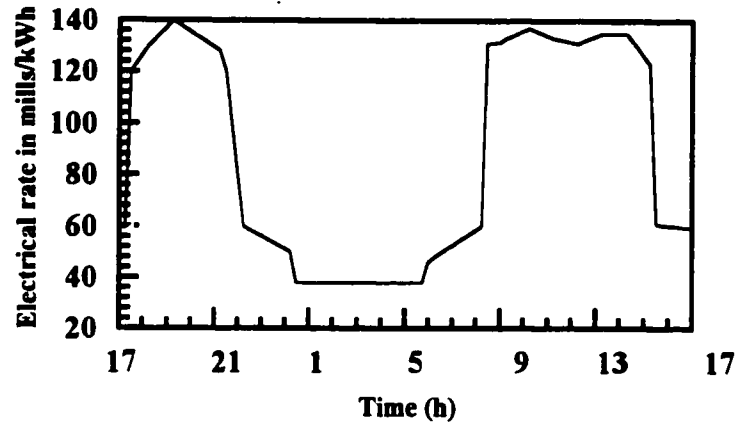


Figure 6.2 Time-of-day energy price structure

with a rated power of 1 kW at 1 kg/s flow rate. The heating coil used was a four row, 10 tube high finned-tube configuration with a total heat transfer area of 80.5 m^2 . Three sets of simulation runs were made under identical initial conditions, zone loads and price incentives one for each of the CV, VAV and GVAV modes of operation. The intent was not only to evaluate the energy efficiency potential of these modes of operation but as well to compare them.

Figures 6.3a-h constitute an optimal set for the constant volume mode of operation. Air flow rate to the zone is constant throughout the day as shown in Fig. 6.3a while the air-supply temperature (Fig. 6.3f) and consequently the hot water temperature (Fig. 6.3e) were continuously modulated throughout the day. In Figures 6.3a-h two sets of curves are shown: one with the assumption that the price incentives are in effect and the other without. We note that irrespective of the time-of-day rate, the zone temperature must be maintained within the chosen limits: $15 - 18^\circ\text{C}$ between 1700h - 0700h and $21 \pm 0.5^\circ\text{C}$ during occupied period, i.e., 0800h -1700h. The optimal solution obtained in

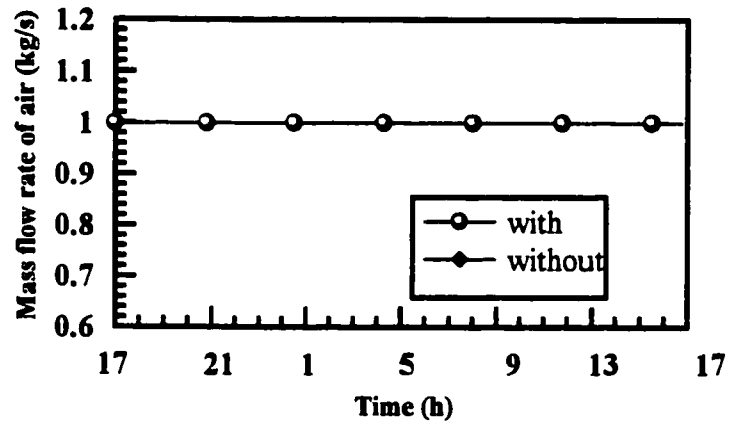
respecting these limits is shown in Fig. 6.3d. However, as one might expect to see the advantage of storing energy during low price time (see Fig. 6.2) for use later in the day resulting in significant savings are not quite apparent from Figs. 6.3a-h. Particularly, if we compare the with and without cases in Figs. 6.3g-h. We note that the total power required and the corresponding operating costs show marginal savings. The reason for this less than expected savings is due to the fact that the storage had sufficient energy stored from the previous day and therefore there was no need to store more energy between 2100h - 0700h than the minimum required. For this reason there appears to be no significant difference in the heat pump energy input (Fig. 6.3b) between with and without cases during low price time (2100h -0800h). Therefore charging the storage during low price time, even though intuitively appears to be the right choice, may turn out to be not optimal under all conditions. Thus it is necessary to seek a tradeoff between storage, time-of-day rate, demand for heating and the residual storage energy already available in the system. Results show that a careful balance between these variables can only be achieved through optimization of the system operation.

Shown in Figures 6.4a-h are the results for the optimal VAV mode of operation of the SZSH system. In this mode, the air-supply temperature is held constant at chosen setpoint and airflow rate is modulated in response to zone loads. In fact, one of the difficulty in VAV mode of operation comes from the fact that the magnitude of air-supply temperature is difficult to estimate. In practice, various techniques are used which range from those based on operating experience to more sophisticated ones involving outdoor air reset control and discriminator control (Haines 1988). The following results illustrate the nature of this difficulty. Consider the following values for the air-supply temperature:

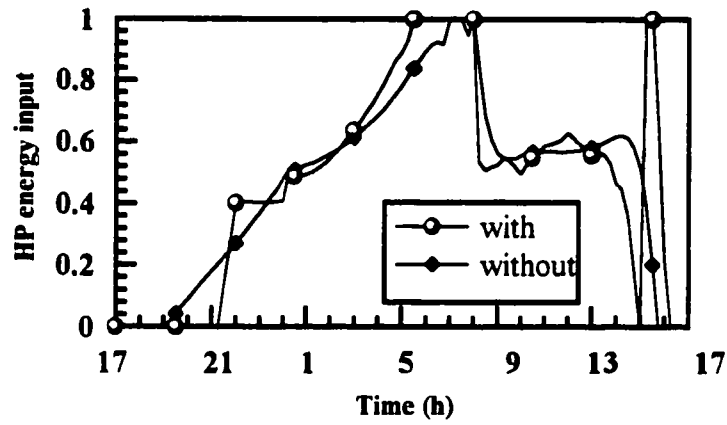
$T_{a,set} = 40 \pm 0.5^\circ\text{C}$ between 0700h - 1700h and $T_{a,set} = 35 \pm 0.5^\circ\text{C}$ during off-normal hours i.e., between 1700h - 0700h. These limits correspond to those generally practiced in buildings.

Figure 6.4f depicts air-supply temperature which satisfies the chosen limits. The corresponding hot water temperature response is shown in Fig. 6.4e. Zone temperature (Fig. 6.4d) is maintained at the high end (18°C) during off-normal hours. This would result in higher energy consumption. One reason for higher zone temperature in off-normal hours is due to the imposition of air-supply temperature setpoint.

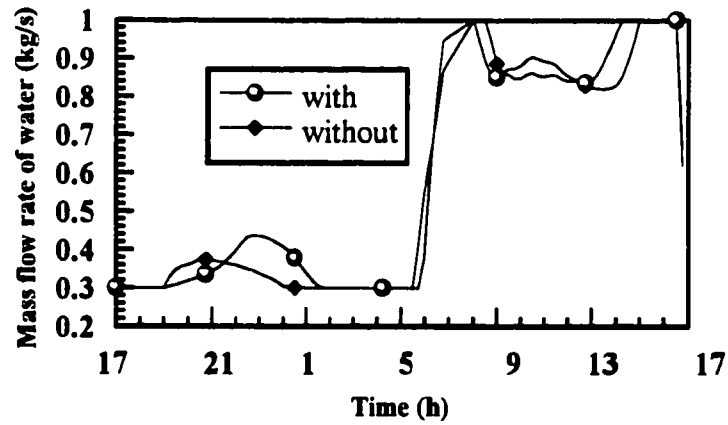
A different air-supply temperature setpoint would produce a different optimal strategy. It is worth noting the variable air flow rate (Fig. 6.4a) to the zone which is less than 50% of the maximum for most of the day. Thus significant fan energy saving can be achieved by using VAV mode of operation. On the other hand, the heat pump energy input (Fig. 6.4b) and operating costs (Fig. 6.4h) do not vary significantly as a function of time-of-day rates. The reasons for this marginal savings between with and without cases is not only due to residual energy stored in the tank but also due to the additional constraints imposed on the system in the form of discharge air temperature setpoints in VAV systems.



(a) Mass flow rate of supply air

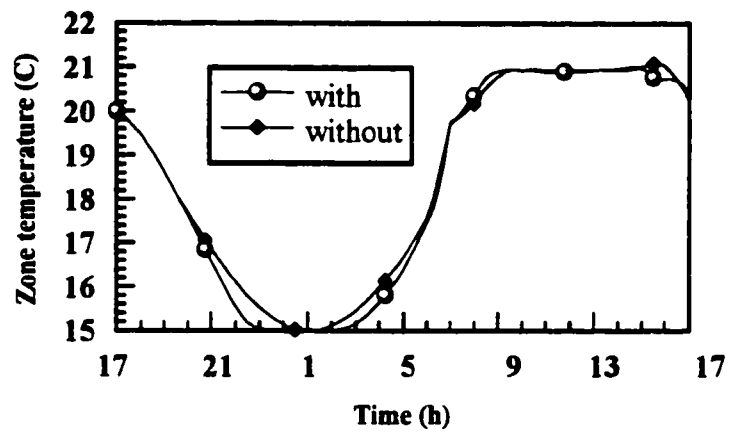


(b) Normalized heat pump energy input

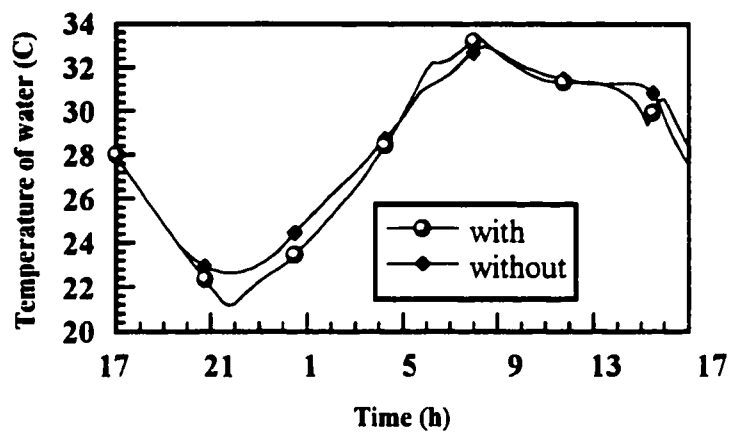


(c) Mass flow rate of water

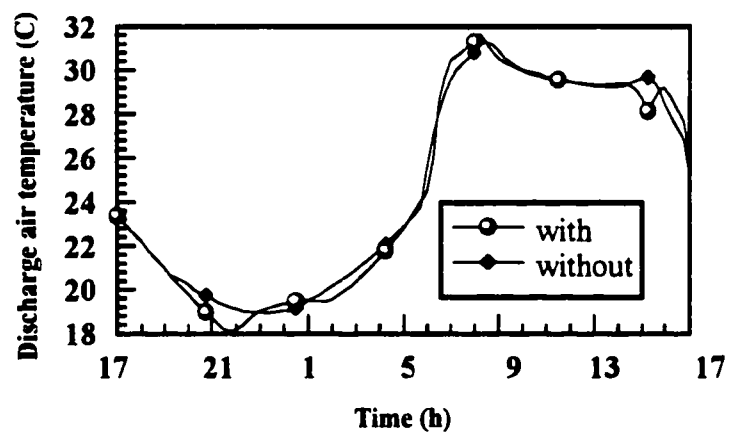
Figure 6.3 Optimal operation of a SZSH system(CV mode)



(d) Response of zone temperature

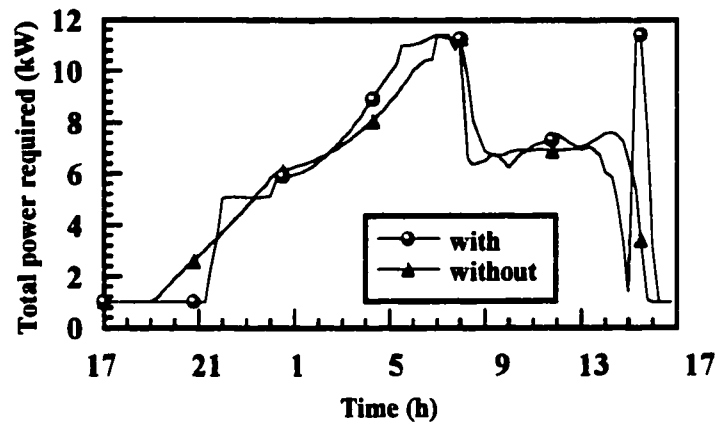


(e) Response of supply water temperature

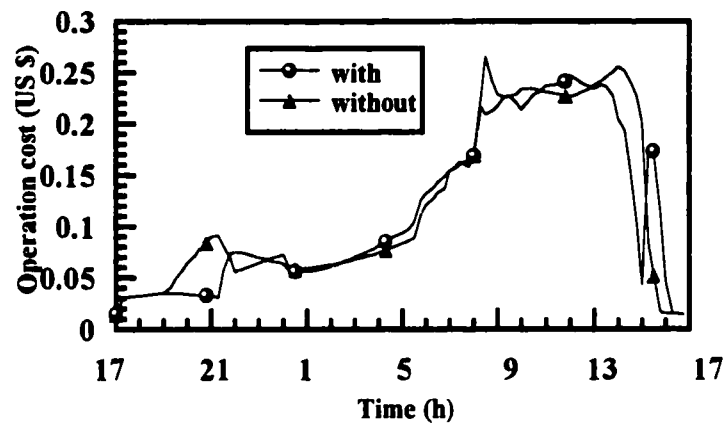


(f) Response of discharge air temperature

Figure 6.3 Optimal operation of a SZSH system (CV mode)

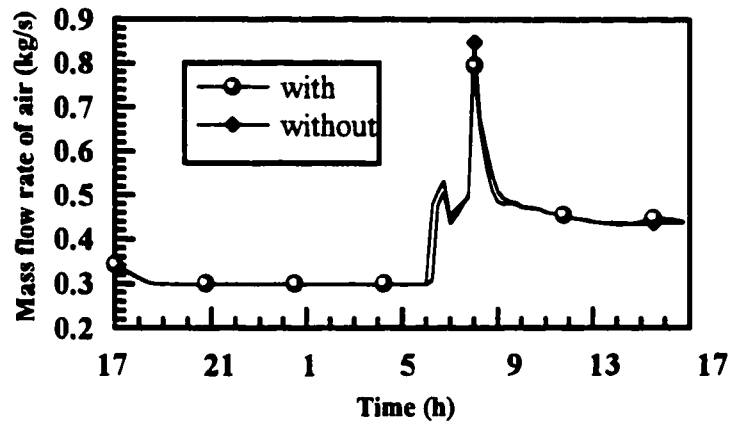


(g) Total power required

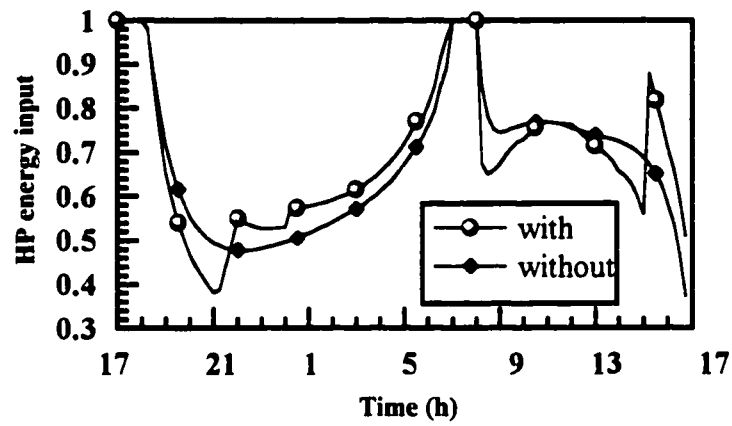


(h) Operation cost in US \$

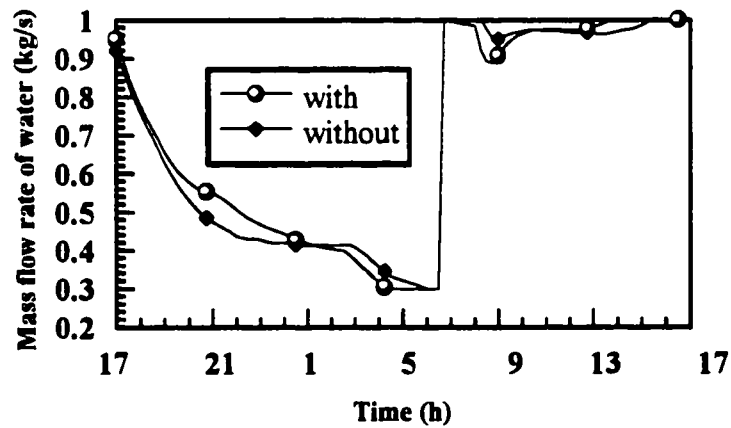
Figure 6.3 Optimal operation of a SZSH system (CV mode)



(a) Mass flow rate of supply air

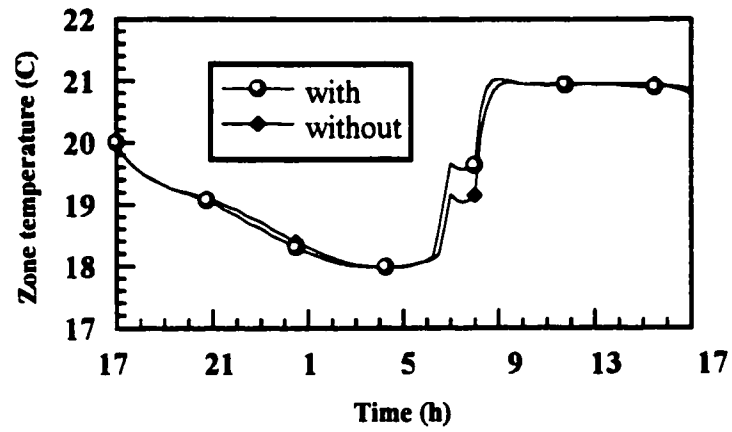


(b) Normalized heat pump energy input

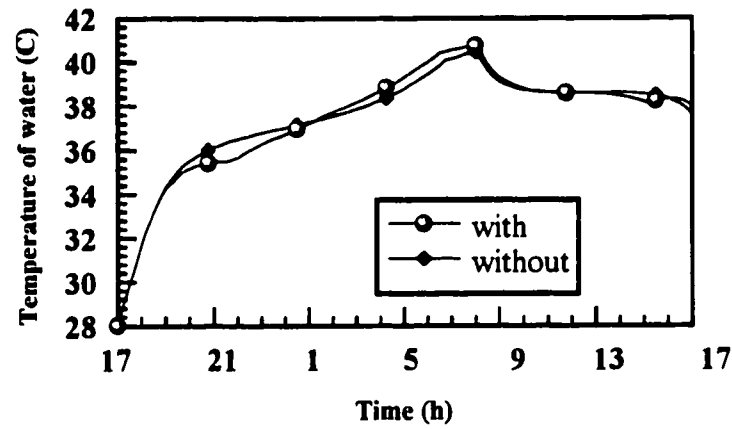


(c) Mass flow rate of water

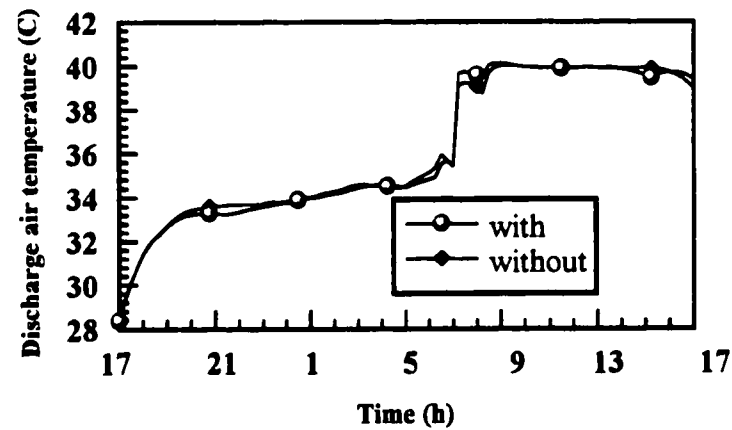
Figure 6.4 Optimal operation of a SZSH system (VAV mode)



(d) Response of zone temperature

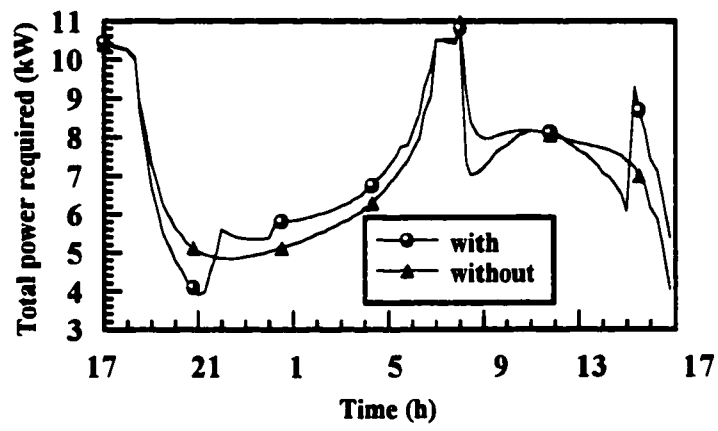


(e) Response of supply water temperature

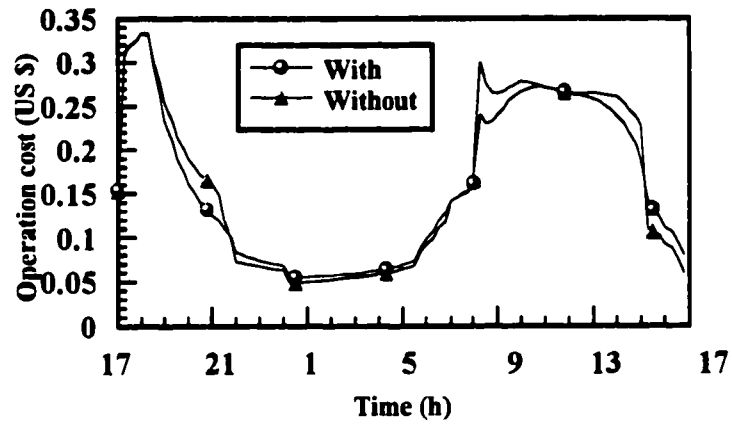


(f) Response of discharge air temperature

Figure 6.4 Optimal operation of a SZSH system (VAV mode)

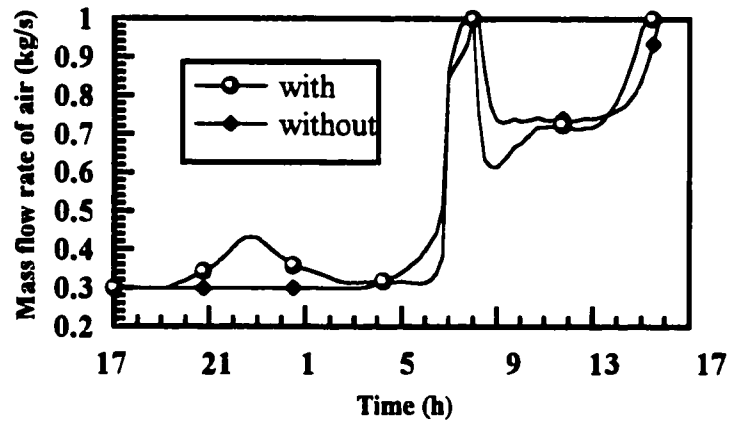


(g) Total power required

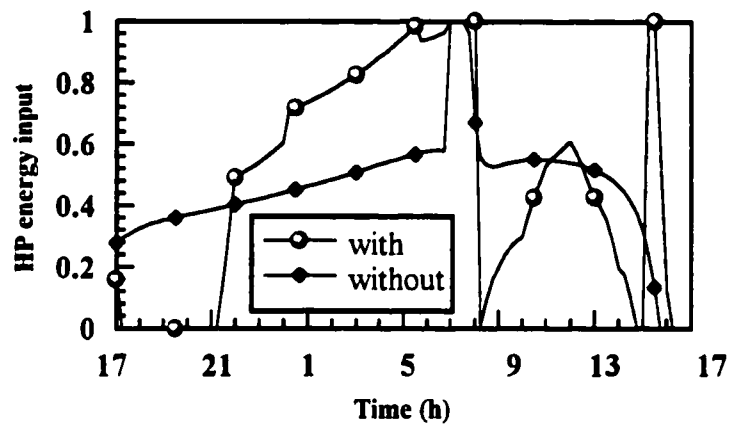


(h) Operation cost in US \$

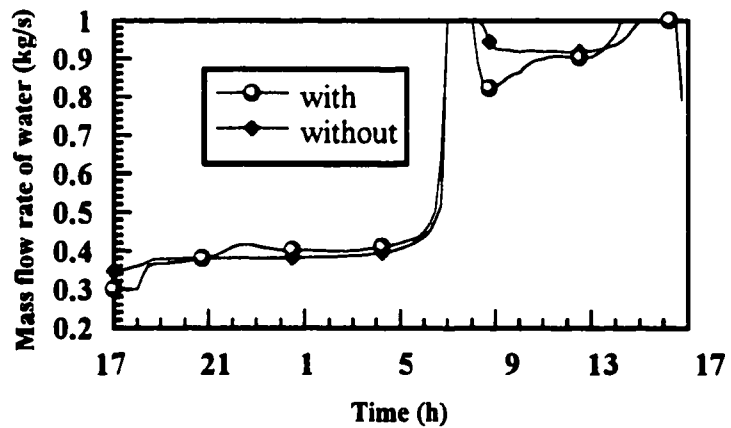
Figure 6.4 Optimal operation of a SZSH system (VAV mode)



(a) Mass flow rate of supply air

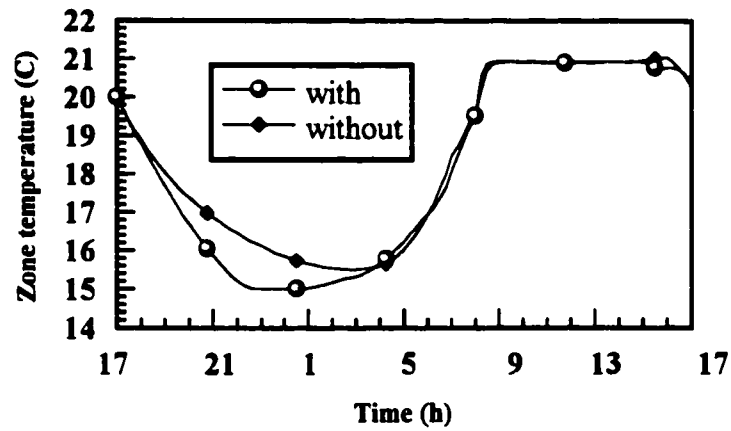


(b) Normalized heat pump energy input

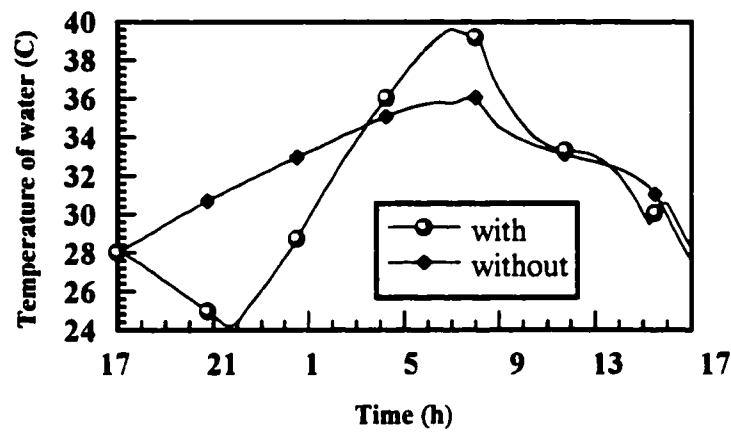


(c) Mass flow rate of water

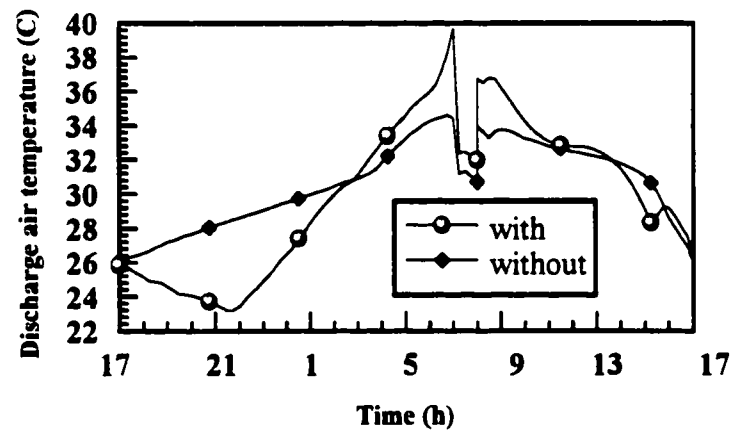
Figure 6.5 Optimal operation of a SZSH system (GVAV mode)



(d) Response of zone temperature

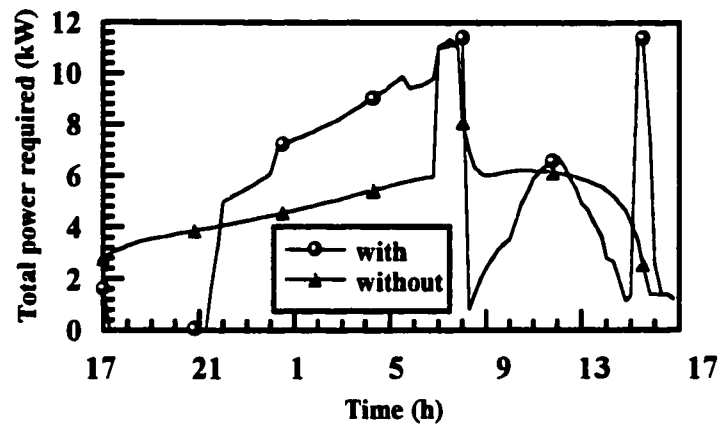


(e) Response of supply water temperature

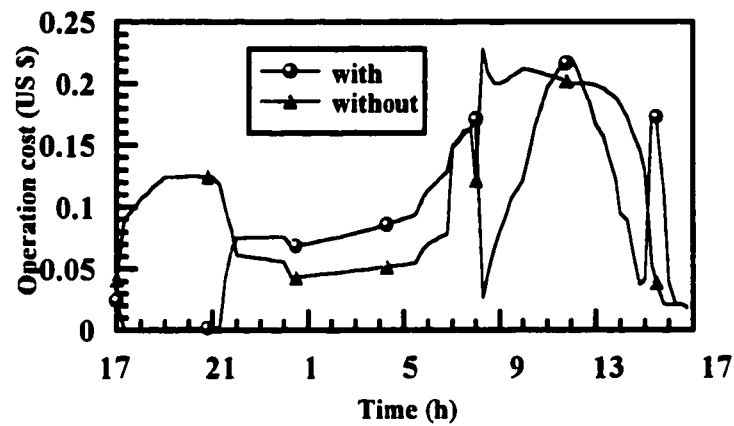


(f) Response of discharge air temperature

Figure 6.5 Optimal operation of a SZSH system (GVAV mode)



(g) Total power required



(h) Operation cost in US \$

Figure 6.5 Optimal operation of a SZSH system (GVAV mode)

The optimal control profiles corresponding to the GVAV mode of operation are depicted in Figs 6.5a-h. In this mode both air-supply temperature and air flow rate are continuously modulated throughout the day. From the viewpoint of optimization it is desirable to let the optimization problem seek optimal air-supply temperature and the corresponding air flow rates. For the SZSH system these are depicted in Figs 6.5e-f. Note that air-supply temperature (Fig. 6.5f) is decreased to as low as 22°C during the off-normal hours. Consequently hot water temperature (Fig. 6.5e) is also at its minimum

during the night time. Note also that there are significant differences in air supply and hot water temperatures when time-of-day price discounts are considered. In other words, the optimal strategy is taking advantage of low rates and charging the storage. This is also evident by examining Figs. 6.5g-h. The operating costs when price discounts are in effect are significantly lower than those without.

6.2.4 Discussion

A comparison of the performance of the SZSH system operated in three different modes offers the energy efficiency potential resulting from these strategies. A summary of the energy consumptions and operating costs for these three modes of operation is given in Table 6.1. It is apparent that GVAV strategy enjoys a 22% cost advantage with time-of-day rate in effect than without. The corresponding saving for CV and VAV are 4.4% and 2.4% respectively. Given that time-of-day rate is in effect, the potential energy savings that could be achieved by operating the system in GVAV mode compared to CV and VAV modes are respectively 25% and 46%. The 25% saving in operating costs between GVAV and CV mode of operation is due to saving in fan energy consumption.

Clearly the variable air volume mode of operation in which air flow rate and air-supply temperature are modulated is superior to CV mode of operation. Even though HVAC systems in buildings are operated in VAV mode, the discharge air temperature setpoint is rarely reset to match the load. In this regard, the methodology presented in this study is useful for computing such optimal setpoint profiles examples of which are shown in Figs. 6.3f, 6.4f and 6.5f.

The multistage optimal control technique has been shown to be effective in achieving an optimal balance between building schedules, time-of-day rates, energy storage, building loads and mode of operation in which both air-supply temperature and flow rate are modulated offers significant savings (25%) in operating costs compared to constant volume mode. The variable air volume mode of operation in which discharge air temperature is held constant is shown to be not an energy efficient strategy.

Table 6.1: Summary of energy consumptions and operating costs

System mode	Energy consumption (kW-h)		Cost/day (\$)	
	with	without	with	without
GVAV	123.20	121.50	8.25	10.59
CV	142.00	140.40	10.99	11.49
VAV	171.20	169.60	15.26	15.63

6.3. Example 2: Optimal operation of a two-zone VAV heating system

In this section, the developed methodology for the multiple stage optimal operation problems will be applied to determine the optimal operation strategies for a two-zone VAV heating system.

Temperature setback, or night setback is used during unoccupied hours. Also in colder climates, temperature setback prevents a building from overcooling during the evening hours by continuing to heat the building at a lower setpoint. The HVAC system can easily bring the zone air temperature up in the morning when occupancy begins.

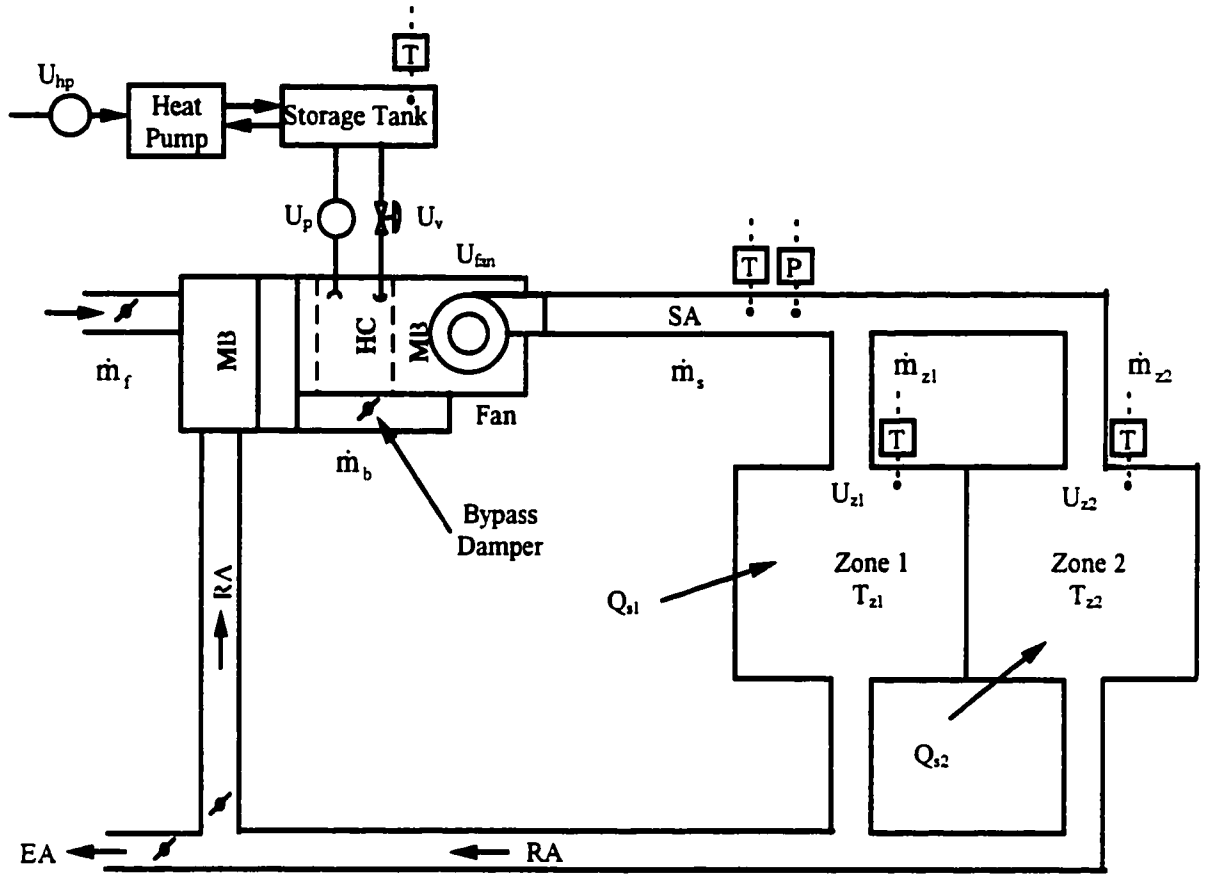


Figure 6.6 The schematic diagram of a two-zone VAV heating system

6.3.1. Two-zone VAVH system

Figure 6.6 shows a schematic diagram of the two-zone VAVH system considered in this study. It consists of two zones, a fan and duct work, a heating coil, a pump and piping system, a heat pump and a storage tank. In response to demand for heating from the zone temperatures, warm air is supplied to the zones. The air system is modeled by four state variables: \dot{m}_s total mass flow rate of air, \dot{m}_f outdoor air mass flow rate; \dot{m}_b air bypassed in the coil and \dot{m}_{z1} mass flow rate of air entering zone1. Since only the sensible

heating problem is addressed here, the environmental zone dynamics are modeled by two state variables T_{z1} and T_{z2} which are respectively zone 1 and 2 temperatures. The heat transfer between hot water from the storage tank (T_{ws}) and air supply takes place in the heating coil which is modeled by three state equations: T_{wr} temperature of water returning to the tank, T_t tube temperature and T_{as} air supply temperature.

The overall VAVH system consists of a fast subsystem (airflow system and heating coil system) and a slow subsystem (environmental zones and the storage tank). There are several control loops in the system. In order to maintain zone air temperatures at chosen setpoints the mass flow rate of air is modulated by the zone dampers (U_{z1} and U_{z2}); to maintain optimal temperature of air supply temperature T_{as} , the mass flow rate of hot water in the heating coil is varied via the valve control (U_v) and/or pump speed control (U_p). The static pressure in the system is varied via fan speed control. Hot water temperature in the storage tank is controlled by heat pump capacity control (U_{hp}). Outdoor air for ventilation is modulated by the outdoor air damper control. Thus there are six different control loops in the VAVH system (Figure 6.6). For simplicity the exhaust and return air dampers are held at fixed position and the bypass damper is fully closed.

6.3.2. Building operation schedule

Given the above VAVH system with six local control loops, we consider the following building operation problem. The 24-hour operation of building is divided into three stages: off-normal setback mode (stage 1) between 1700 - 0700h, start-up mode (stage 2) between 0700 - 0800h and normal mode operation during occupied period between 0800 - 1700h (stage 3). In stage 3, both thermal comfort and energy efficiency

are of prime concern, whereas in stage 1 energy efficiency is the main issue, in stage 2 fast response and energy efficiency are important considerations. During a typical day operation, the VAVH system undergoes such a multistage sequence, consequently during each stage some of local control loops could be turned off or allowed to operate at fixed open-loop position. For example, outdoor air dampers are closed in off-normal hours (stage1), and the variable speed pump is operated at a fixed low speed. After defining the performance requirements for all three stages and appropriately choosing the local control loop tasks (off, open-loop or closed-loop) the optimization problem to be solved is to determine an optimal operating strategy for the VAVH system which meets all of the above requirements. In the sequel we formulate and solve the optimal supervisory control problem and discuss the results obtained.

6.3.3. Formulation of the problem

From the knowledge of the VAVH system dynamics it is well known that the airflow system is faster than the dynamics of environmental zones (the slow subsystem). In other words, in the time scale of the slow subsystem, the fast subsystem responds much faster and as such it can be assumed to be under steady state. The storage tank is also a slow subsystem. The water flow subsystem and heating coil are fast subsystems. Therefore, the state variables of the system consist of the zone temperatures T_{z1} , T_{z2} and the supply hot water temperature $T_{w,s}$, i.e., the vector $\mathbf{x}=[T_{z1}, T_{z2}, T_{w,s}]^T$. The mass flow rates of air and hot water, fan speed and current, temperature of supply air, return water, tube temperature of heating coil, pump speed and current are considered as the fast state vector \mathbf{z} , i.e., $\mathbf{z}=[\dot{m}_f, \dot{m}_s, \dot{m}_b, \dot{m}_{z1}, N_{fan}, I_{fan}, T_{a,s}, T_{w,r}, T_t, \dot{m}_w, N_p, I_p]^T$.

The input vector $\mathbf{u}=[U_{z1}, U_{z2}, U_{fan}, U_p, U_{hp}, U_f]^T$ represents control inputs to the six local loops. By defining superscripts 1, 2 and 3 to represent respectively the three building operating stages the overall system model in vector notation is

$$\dot{\mathbf{x}} = \begin{cases} \mathbf{f}^1(\mathbf{x}, \mathbf{z}^1, \mathbf{u}^1, \mu^1, t) & \text{on } [t_0, t_1] \\ \mathbf{f}^2(\mathbf{x}, \mathbf{z}^2, \mathbf{u}^2, \mu^2, t) & \text{on } [t_1, t_2] \\ \mathbf{f}^3(\mathbf{x}, \mathbf{z}^3, \mathbf{u}^3, \mu^3, t) & \text{on } [t_2, t_f] \end{cases} \quad (6.9)$$

$$\begin{aligned} \mu^1 \dot{\mathbf{z}}^1 &= \mathbf{F}^1(\mathbf{x}, \mathbf{z}^1, \mathbf{u}^1, \mu^1, t) & \text{on } [t_0, t_1] \\ \mu^2 \dot{\mathbf{z}}^2 &= \mathbf{F}^2(\mathbf{x}, \mathbf{z}^2, \mathbf{u}^2, \mu^2, t) & \text{on } [t_1, t_2] \\ \mu^3 \dot{\mathbf{z}}^3 &= \mathbf{F}^3(\mathbf{x}, \mathbf{z}^3, \mathbf{u}^3, \mu^3, t) & \text{on } [t_2, t_f] \end{aligned} \quad (6.10)$$

The continuity of \mathbf{x} is assumed over the entire 24-hour period including the switch-over points between stage 1, 2 and 3.

Notice that the dynamics of the system and as well as the local control loop structure changes as the VAVH system goes through the three prescribed stages. In the example considered here the following options will be exercised. In the unoccupied stage (stage 1), night setback will be used to save energy and prevent the building from overcooling. Zone air temperature will be restricted within chosen high-low limits that are lower than the normal setpoint in occupied stage. The local controls $\mathbf{u}^1=[U_{z1}, U_{z2}, U_{fan}, U_p, U_{hp}]^T$ will be effected to maintain the zone temperatures within the chosen high-low limits. In start-up stage (stage 2), while the pump is fully on, the local inputs $\mathbf{u}^2=[U_{z1}, U_{z2}, U_{fan}, U_{hp}]^T$ will be activated so that the zone temperatures will be brought to their normal setpoints just before occupancy begins. In the occupied stage (stage 3), the local control inputs $\mathbf{u}^3=[U_{z1}, U_{z2}, U_{fan}, U_p, U_{hp}]^T$ will be used to maintain the zone temperatures close to their normal setpoints.

For the specific optimization problem considered here the performance measure corresponding to three stages is

$$\begin{aligned}
 J = & \int_{t_0}^{t_1} EP(t) \{U_{fan} V_{fan,max} I_{fan} + U_{hp} E_{hp,max} + U_p V_{p,max} I_p\} dt \\
 & + \int_{t_1}^{t_2} EP(t) \{U_{fan} V_{fan,max} I_{fan} + U_{hp} E_{hp,max} + 1.0 V_{p,max} I_p\} dt \\
 & + \int_{t_2}^{t_f} EP(t) \{U_{fan} V_{fan,max} I_{fan} + U_{hp} E_{hp,max} + U_p V_{p,max} I_p\} dt
 \end{aligned} \tag{6.11}$$

where $V_{fan,max}$ is maximum fan voltage, E_{hp} is maximum heat pump input energy, $V_{p,max}$ is maximum pump voltage, and $EP(t)$ is the price of energy. The terms $U_{fan} V_{fan,max} I_{fan}$, $U_{hp} E_{hp,max}$, $U_p V_{p,max} I_p$ indicate the power required by fan, heat pump, and pump. The sum represents the total power requirement of the whole system.. In this example, $V_{fan,max}=220V$, $V_{p,max}=110V$, $E_{hp,max}=15kW$.

The constraints corresponding to the three stages are

stage 1 — night setback $[t_0, t_1)$ (1700 - 0700h)

$$\begin{array}{lll}
 T_{z1,low} \leq T_{z1} \leq T_{z1,high} & T_{z2,low} \leq T_{z2} \leq T_{z2,high} & \\
 (15^\circ C) & (18^\circ C) & (15^\circ C) \quad (18^\circ C) \\
 \\
 U_{z1,min} \leq U_{z1} \leq U_{z1,max} & U_{z2,min} \leq U_{z2} \leq U_{z2,max} & U_{fan,min} \leq U_{fan} \leq U_{fan,max} \\
 (0.1) & (1.0) & (0.1) \quad (1.0) \quad (0.4) \quad (1.0) \\
 \\
 U_{hp,min} \leq U_{hp} \leq U_{hp,max} & U_{p,min} \leq U_p \leq U_{p,max} & \dot{m}_f = 0.15 \dot{m}_s \\
 (0.0) & (1.0) & (0.4) \quad (1.0)
 \end{array}$$

stage 2 — the start-up stage $[t_1, t_2)$ (0700 - 0800h)

$$\begin{array}{lll}
 U_{z1,min} \leq U_{z1} \leq U_{z1,max} & U_{z2,min} \leq U_{z2} \leq U_{z2,max} & \\
 (0.1) & (1.0) & (0.1) \quad (1.0) \\
 \\
 U_{fan,min} \leq U_{fan} \leq U_{fan,max} & U_{hp,min} \leq U_{hp} \leq U_{hp,max} & \dot{m}_f = 0.15 \dot{m}_s \\
 (0.4) & (1.0) & (0.0) \quad (1.0)
 \end{array}$$

stage 3 — the occupied stage [t_2, t_f]

$$T_{z1,set} - \Delta T_{z1,set} \leq T_{z1} \leq T_{z1,set} + \Delta T_{z1,set}$$

$$(21^{\circ}\text{C}-0.5^{\circ}\text{C}) \quad (21^{\circ}\text{C}+0.5^{\circ}\text{C})$$

$$T_{z2,set} - \Delta T_{z2,set} \leq T_{z2} \leq T_{z2,set} + \Delta T_{z2,set}$$

$$(23^{\circ}\text{C}-0.5^{\circ}\text{C}) \quad (23^{\circ}\text{C}+0.5^{\circ}\text{C})$$

$$U_{z1,min} \leq U_{z1} \leq U_{z1,max} \quad U_{z2,min} \leq U_{z2} \leq U_{z2,max} \quad U_{fan,min} \leq U_{fan} \leq U_{fan,max}$$

$$(0.1) \quad (1.0) \quad (0.1) \quad (1.0) \quad (0.4) \quad (1.0)$$

$$U_{hp,min} \leq U_{hp} \leq U_{hp,max} \quad U_{p,min} \leq U_p \leq U_{p,max} \quad \dot{m}_f = 0.15 \dot{m}_s$$

$$(0.0) \quad (1.0) \quad (0.4) \quad (1.0)$$

the terminal condition was defined as

$$T_{ws}(t_0) = T_{ws}(t_f)$$

6.3.4. Simulation Results

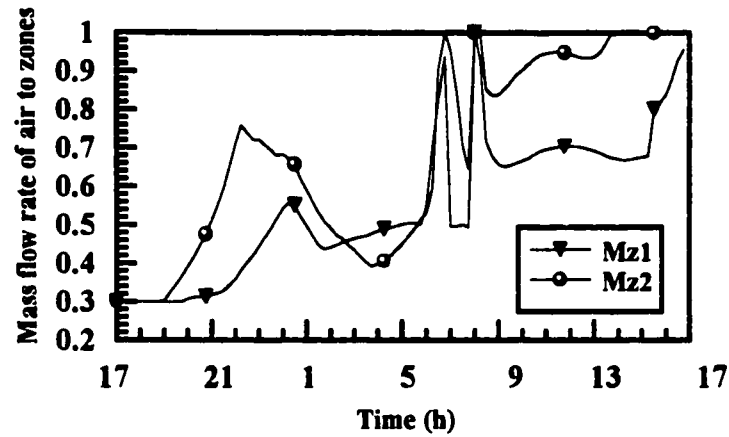
The results correspond to a typical winter day operation with outdoor temperature ranging between -2 to -10°C . The building operation schedule consists of three stages with setpoints and controls as defined in Section 6.3.3. Furthermore, it was assumed that the utility offers an energy price incentive, with the rate structure depicted in Figure 6.2 (Winn and Winn 1985). Using these specifications, an optimal operation strategy for the VAVH system was computed. The results are depicted in Figures 6.7a-e.

The results will be examined in the light of building operating stages, performance needs and price discount opportunities. During the off-normal (night setback - stage 1) mode from 1700 - 0700h, zone temperatures (Figure 6.7e) are decreasing from their respective setpoints to as low as 15°C . Note that T_{z2} is decreasing at a faster rate than T_{z1} due to differences in thermal capacity of the zones. Furthermore the temperature in zone 2

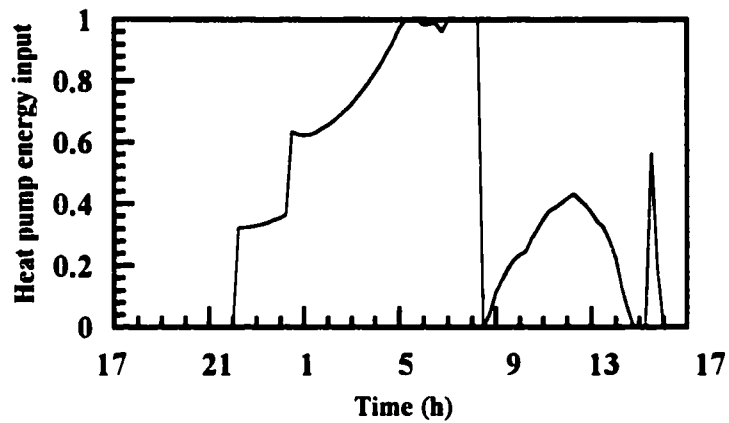
is held at the low limit (15°C) for over 8 hours in the night compared to only about 4 hour in zone 1. The reasons for the nature of T_{z1} and T_{z2} responses can be further understood by examining, simultaneously, the energy price profile (Figure 6.2), heat pump energy input (Figure 6.7b) and hot water temperature in the storage tank (T_{ws} in Figure 6.7d). In view of higher price of energy between 1700-2100h, the heat pump is turned off (Figure 6.7b) and energy stored in the storage tank together with the stored energy in the zones is utilized to let zone temperatures reach the lowest allowable limit of 15°C. From 2100-0700h the lower energy price is in effect, as such the heat pump capacity is modulated to store energy. Consequently, the hot water temperature rises to 40°C at about 0700h. Furthermore, the zone thermal capacity is also utilized, which is evident by noting that T_{z1} and T_{z2} are allowed to rise to the high limit of 18°C during last hour of stage 1 (0600 - 0700h).

In the start-up mode (stage 2) from 0700 - 0800h the energy price is low (Figure 6.2) so the heat pump is operated at full capacity (Figure 6.7b). During this time, zone temperatures, T_{z1} and T_{z2} , which were at 18°C at 0700h, rise to 21°C and 23°C respectively at 0800h, again satisfying the start-up mode specifications.

In the last stage (occupied period between 0800-1700h) the energy price is high, consequently the heat pump is operated at reduced capacity. Both zone 1 and 2 temperatures are maintained within occupied setpoint range. Note that the hot water (T_{ws} in Figure 6.7d) and air supply temperatures (T_{as} in Figure 6.7d) decrease during this stage because more energy is withdrawn from the storage tank than charged by the heat pump. A decrease in hot water and air supply temperatures is compensated by increasing the air flow rates to zone 1 and 2 (Figure 6.7a). Note also that the heat pump is turned off about



(a) Mass flow rate of air to zone 1 and 2

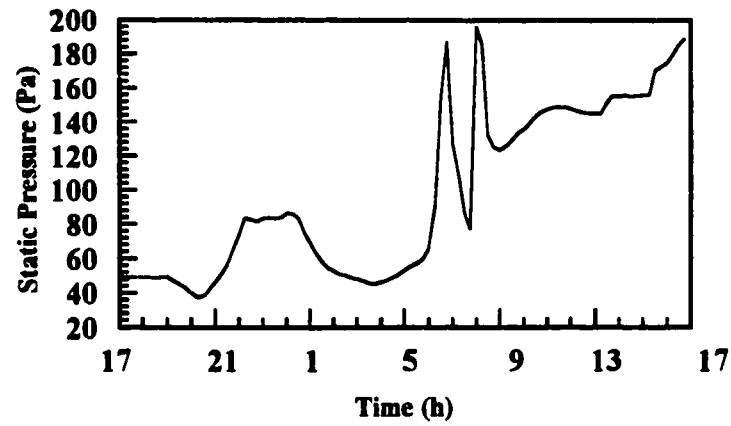


(b) Normalized heat pump energy input

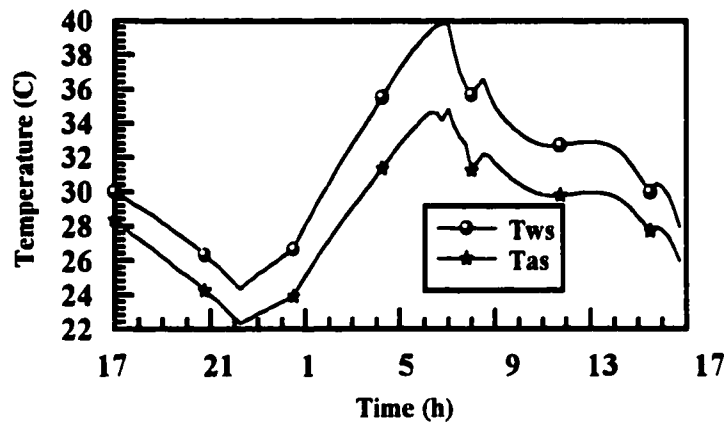
Figure 6.7 Global optimal operation of a two-zone VAV heating system

15 minutes before 1700h thereby causing the water temperature and air supply temperature to decrease before the occupancy period ends. In order to compensate for this decrease in air supply temperature, mass flow rates to zones are increased to their maximum allowable value as shown in Figure 6.7a.

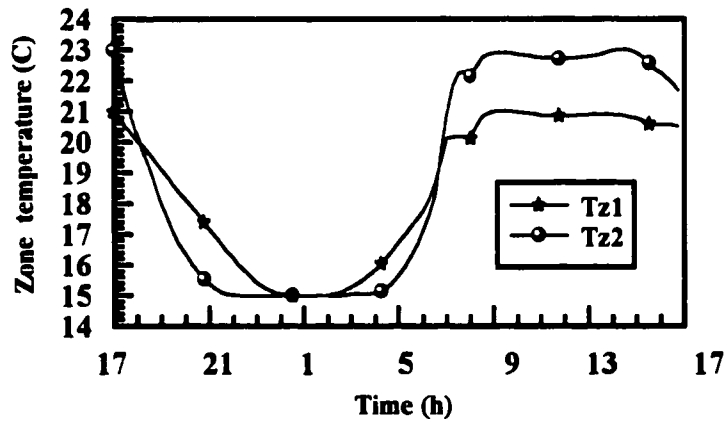
Taken together the results show that the optimization methodology is responsive to the zone performance needs and the price discount opportunities and storage capacities as the building and the VAVH system goes through three stages of operation. From the



(c) Static pressure of air flow



(d) Temperatures of supply air and water



(e) Zone temperatures

Figure 6.7 Global optimal operation of a two-zone VAV heating system (continued)

example, it can be seen the global optimal operation of HVAC system can be achieved without violating the thermal comfort requirements in the occupied stage.

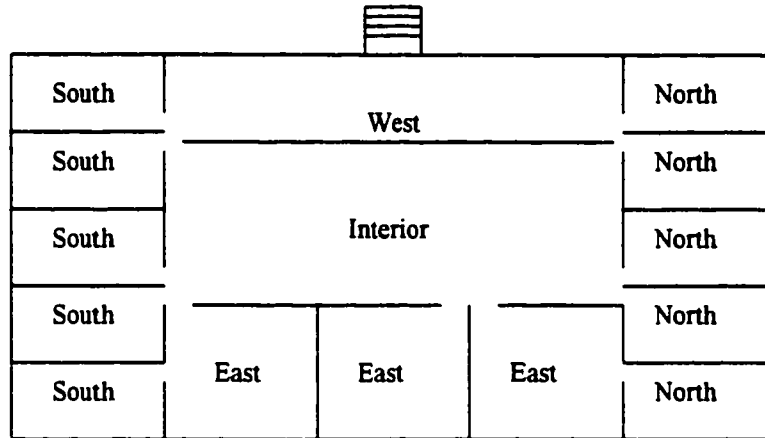
6.4. Example 3: Optimal operation of a five-zone VAV cooling system

To further show the applications of the optimal operation strategy we consider a five zone office building served with a multizone VAV system. As opposed to only sensible heating cases considered in the previous two examples, we examine both temperature and humidity control in VAV mode while respecting minimum airflow requirements in the zones.

6.4.1. Five-zone VAVC system

The floor plan of the single-story building considered in this study is shown in Figure 6.8. The floor has been divided into five zones. The first zone consists of interior room of size 24 ft x 90 ft. The second zone consists of a 27 ft x 90 ft room on the west side. The third zone includes 3 rooms (24 ft x 30 ft each) on the east side. The fourth zone includes 5 rooms (15 ft x 30 ft each) in the south side. The fifth zone consists of 5 rooms (15 ft x 30 ft each) in the north side.

The schematic diagram of five-zone VAVC system is shown in Figure 6.9. It consists of five zones, a fan and duct work, a cooling and dehumidifying coil, a pump and piping system, a chiller and a storage tank. In response to demand for cooling from the zone thermostats, cool air is supplied to the zones. The air system is modeled by six state variables: \dot{m} , total mass flow rate of air, \dot{m}_f outdoor air mass flow rate; \dot{m}_b air bypassed in the coil, and $\dot{m}_{z,1}$, $\dot{m}_{z,2}$, $\dot{m}_{z,3}$, $\dot{m}_{z,4}$, $\dot{m}_{z,5}$ are mass flow rates of air to zones 1 through 5 respectively. Since the sensible and latent heat transfers occurring in the environmental zones are considered, the environmental zone dynamics are modeled by ten state variables



Zone 1 – interior (2160 ft²) Zone 4 – north (2250 ft²)
 Zone 2 - west (2430 ft²) Zone 5 – south (2250 ft²)
 Zone 3 - east (2160 ft²)

Figure 6.8 The floor plan of a five-zone building

T_{z1} , W_{z1} , T_{z2} , W_{z2} , T_{z3} , W_{z3} , T_{z4} , W_{z4} , and T_{z5} and W_{z5} which are respectively zone 1, 2, 3, 4 and 5 temperatures and humidity ratios. The heat transfer between chilled water from the storage tank (T_{ws}) and air supply takes place in the cooling and dehumidifying coil which is modeled by four state equations: T_{wr} is the temperature of water returning to the tank, T_t is the tube temperature, T_{as} and W_{as} are the air supply temperature and humidity ratio respectively.

In the system, there are several local control loops. In order to maintain zone air temperatures at chosen setpoints the mass flow rates of air are modulated by the zone VAV dampers; the valve control (U_v) and/or pump speed control (U_p) is used to vary the mass flow rate of chilled water in the cooling and dehumidifying coil to maintain optimal temperature of air supply T_{as} . The static pressure in the system is varied via fan speed (U_f) control. Chilled water temperature in the storage tank is controlled by chiller capacity

control (U_c). Outdoor air for ventilation is modulated by the outdoor air damper control (U_o). Thus there are nine different control loops in the VAVC system (Figure 6.9). For simplicity the exhaust and return air dampers are held at fixed position and the bypass damper is fully closed.

Given outdoor conditions such as temperature, humidity ratio, solar radiation as time varying inputs together with occupancy patterns, and other internal loads in the zones, time varying cooling loads acting on the zone were computed using the method described in Appendix A. Thus together with reduced order state space model of the VAV system developed in Chapter 4, the overall building and VAV system model represents a significant modeling effort. Such a detailed representation of the building and the VAV system was used in this example for capturing the dynamics of the overall system.

In the next step the optimal operation problem was formulated by combining the building operation schedules and system constraints.

6.4.2. Building operation schedule

In a manner similar to the previous examples, the 24-hour operation of building was divided into three stages: off-normal mode (stage 1) between 1700 - 0700h, start-up mode (stage 2) between 0700 - 0800h and normal mode operation during occupied period between 0800 - 1700h (stage 3).

6.4.3. Formulation of the problem

The slow subsystem state variables of the system consist of the zone temperatures T_{z1} , T_{z2} , T_{z3} , T_{z4} , and T_{z5} and supply chilled water temperature $T_{w,s}$, i.e., the vector $\mathbf{x} = [T_{z1},$

$T_{z2}, T_{z3}, T_{z4}, T_{z5}, T_{w,s}]^T$. The humidity ratios of zone air, The mass flow rates of air and chilled water, fan speed and current, temperature and humidity ratios of supply air, returned water, tube temperature of cooling and dehumidifying coil, pump speed and current were considered as the fast subsystem states \mathbf{z} , i.e., $\mathbf{z}=[W_{z1}, W_{z2}, W_{z3}, W_{z4}, W_{z5}, \dot{m}_f, \dot{m}_s, \dot{m}_b, \dot{m}_{z1}, \dot{m}_{z2}, \dot{m}_{z3}, \dot{m}_{z4}, N_{fan}, I_{fan}, T_{a,s}, W_{a,s}, T_{w,r}, T_t, \dot{m}_w, N_p, I_p]^T$.

The control inputs corresponding to the nine local loops were represented by the input vector $\mathbf{u}=[U_{z1}, U_{z2}, U_{z3}, U_{z4}, U_{z5}, U_{fan}, U_p, U_c, U_f]^T$.

In the unoccupied stage (stage 1), the cooling coil and pump will be shutoff to save energy. Zone air temperatures will be allowed to float. The fan will be operated at minimum speed to allow the cooler fresh air in the building to achieve free-cooling. The local controls $\mathbf{u}^1=[U_c]$ will be activated to store energy in the storage tank during the low price period. In start-up stage (stage 2), while the pump and chiller are full on, the local inputs $\mathbf{u}^2=[U_{z1}, U_{z2}, U_{z3}, U_{z4}, U_{z5}, U_{fan}]^T$ will be activated so that the zone temperatures will be brought to their normal setpoints just before occupancy begins. In the occupied stage (stage 3), the local control inputs $\mathbf{u}^3=[U_{z1}, U_{z2}, U_{z3}, U_{z4}, U_{z5}, U_{fan}, U_p, U_c]^T$ will be used to maintain the zone temperatures close to their setpoints.

The performance measure used for this optimization problem is

$$\begin{aligned} J = & \int_{t_0}^{t_1} EP(t) \{0.4V_{fan,max} I_{fan} + U_c E_{chiller,max}\} dt \\ & + \int_{t_1}^{t_2} EP(t) \{U_{fan} V_{fan,max} I_{fan} + 1.0 E_{chiller,max} + 1.0 V_{p,max} I_p\} dt \\ & + \int_{t_2}^{t_f} EP(t) \{U_{fan} V_{fan,max} I_{fan} + U_c E_{chiller,max} + U_p V_{p,max} I_p\} dt \end{aligned} \quad (6.12)$$

where $V_{fan,max}$ is maximum fan voltage, $E_{chiller}$ is maximum chiller input energy, $V_{p,max}$ is maximum pump voltage. The terms $U_{fan} V_{fan,max} I_{fan}$, $U_c E_{chiller,max}$, $U_p V_{p,max} I_p$ indicate the

power required by fan, chiller, and pump. The sum represents the total power requirement of the whole system. In this example, $V_{fan,max}=220V$, $V_{p,max}=110V$, $E_{chiller,max}=30$ kW. The performance measure (6.12) was minimized subject to state equations of the system, energy price structure (Fig. 6.2) and the following constraints.

stage 1 — off-normal [t_0 , t_1) (1700 - 0700h)

operating strategy:

pump, cooling coil:	off;
fresh air (for free cooling):	100%
fan operation:	minimum speed
chiller:	variable
zone temperatures:	no constrains
$U_{c,min} \leq U_c \leq U_{c,max}$	$\dot{m}_f = \dot{m}_s$
(0.0) (1.0)	

stage 2 — the start-up stage [t_1 , t_2) (0700 - 0800h)

operating strategy:

chiller, pump:	full capacity
fresh air (for free cooling):	minimum (15%)
fan operation:	variable
damper control:	variable
zone temperatures:	no constrains
$U_{z1,min} \leq U_{z1} \leq U_{z1,max}$	$U_{z2,min} \leq U_{z2} \leq U_{z2,max}$
(0.1) (1.0)	(0.1) (1.0)
$U_{z3,min} \leq U_{z3} \leq U_{z3,max}$	$U_{z4,min} \leq U_{z4} \leq U_{z4,max}$
(0.1) (1.0)	(0.1) (1.0)
$U_{z5,min} \leq U_{z5} \leq U_{z5,max}$	$U_{fan,min} \leq U_{fan} \leq U_{fan,max}$
(0.1) (1.0)	(0.4) (1.0)
$\dot{m}_f = 0.15 \dot{m}_s$	$U_p = 1.0$ $U_c = 1.0$

stage 3 — the occupied stage [t_2 , t_f]

operating strategy:

all control inputs in modulating mode
 minimum fresh air
 zone temperatures closing to their setpoints
 upper limit humidity control

$$T_{z1,set} - \Delta T_{z1,set} \leq T_{z1} \leq T_{z1,set} + \Delta T_{z1,set}$$

(24°C-0.5°C) (24°C+0.5°C)

$$T_{z2,set} - \Delta T_{z2,set} \leq T_{z2} \leq T_{z2,set} + \Delta T_{z2,set}$$

(23°C-0.5°C) (23°C+0.5°C)

$$T_{z3,set} - \Delta T_{z3,set} \leq T_{z3} \leq T_{z3,set} + \Delta T_{z3,set}$$

(22°C-0.5°C) (22°C+0.5°C)

$$T_{z4,set} - \Delta T_{z4,set} \leq T_{z4} \leq T_{z4,set} + \Delta T_{z4,set}$$

(21°C-0.5°C) (21°C+0.5°C)

$$T_{z5,set} - \Delta T_{z5,set} \leq T_{z5} \leq T_{z5,set} + \Delta T_{z5,set}$$

(20°C-0.5°C) (20°C+0.5°C)

$$U_{z1,min} \leq U_{z1} \leq U_{z1,max} \quad U_{z2,min} \leq U_{z2} \leq U_{z2,max}$$

(0.1) (1.0) (0.1) (1.0)

$$U_{z3,min} \leq U_{z3} \leq U_{z3,max} \quad U_{z4,min} \leq U_{z4} \leq U_{z4,max}$$

(0.1) (1.0) (0.1) (1.0)

$$U_{z5,min} \leq U_{z5} \leq U_{z5,max} \quad U_{p,min} \leq U_p \leq U_{p,max}$$

(0.1) (1.0) (0.4) (1.0)

$$U_{fan,min} \leq U_{fan} \leq U_{fan,max} \quad U_{c,min} \leq U_c \leq U_{c,max}$$

(0.4) (1.0) (0.0) (1.0)

$$W_{zi} \leq 0.012 \text{ kg/kg} \quad \dot{m}_f = 0.15 \dot{m}_s$$

the terminal condition was defined as

$$T_{ws}(t_0) = T_{ws}(t_f)$$

6.4.4. Simulation Results

Results showing the optimal operation of the multizone VAV system corresponding to a typical summer day with building operation schedule, and constraints as noted before are given in Figures 6.10a-s.

The modulation of zone dampers (Figs. 6.10a-e) and the corresponding airflow rate to the zones (Figs. 6.10f-j) show that

- (i). during off normal operation (stage 1) airflow rates to the zones are kept constant at the minimum values
- (i). During start-up stage (stage 2) air flow rates to the zones rise to their maximum values in most zones.
- (ii). In normal occupied mode (stage 3) air flow rates are continuously modulated to maintain zone setpoint temperatures. (Fig. 6.10k) and humidity ratios (Fig. 6.10l).

The modulation of zone damper positions in response to changes in zone loads, causes corresponding changes in the static pressure in the system (Fig. 6.10q). Such an optimal static pressure profile in the system is useful in controlling the fan speed (Fig. 6.10n). This result has significant benefits in terms of achieving saving in fan energy consumption via variable speed fan control. It is worth noting here that without detailed modelling of air flow rates in the system it could not be feasible to determine optimal static pressure profiles in a VAV system.

Fig. 6.10m shows how the energy input to the chiller must be varied to minimize energy consumption. It should be noted that during stage 1 when price of energy is low, the chiller does store energy but only to the extent that minimizes the overall daily cost.

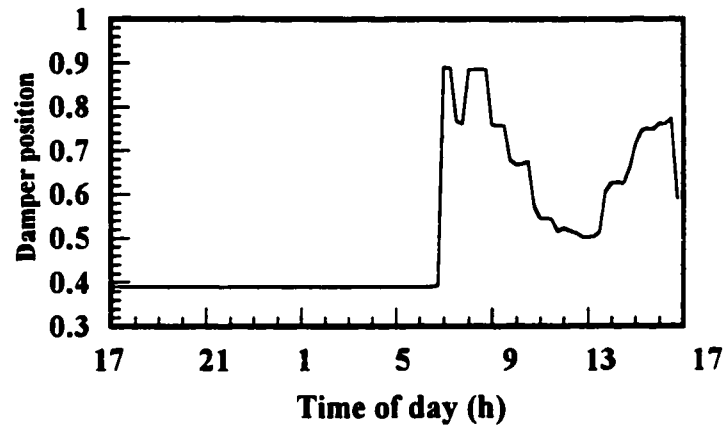
Contrary to the common notion that the storage should be charged fully in the low price time is not always true. This depends on the next day cooling load and the standby losses from the tank. Therefore global optimization is necessary to determine optimal operating strategies. The chiller is full-on (Fig. 6.10m) during start-up and is modulated the rest of the occupied period. The corresponding optimal profiles of chilled water temperature (Fig. 6.10p) and the discharge air temperature (Fig. 6.10r) serve as variable setpoint profiles for the local controllers. For example, the chilled water temperature profile is used as a feedback signal for chiller input energy controller and the discharge air temperature profile is used for the valve control.

The multizone nature of the optimization problem is evident if we examine the zone loads (Figs. 6.10s) together with discharge air temperature profile (Fig. 6.10r). From Fig. 6.10s, note that in the start-up and occupied mode between 7 to 10 a.m. zone 1 experiences the highest load. However during afternoon hours (12 to 17 hours) zone 2 experiences highest load. Under these circumstances the discharge air temperature should be such that it meets the needs of the zone with highest cooling load. The discharge air temperature profile shown in Fig. 6.10r achieves this objective in an optimal way. The magnitude of the discharge air temperature varies between 14.7 to 16.5°C which is greater than the usual air supply temperature (13°C) used in buildings. The results show that it is optimal to increase the air supply temperature while matching the cooling load by increasing the airflow rates within acceptable range since the chiller consumption is the dominant part of the total energy consumption.

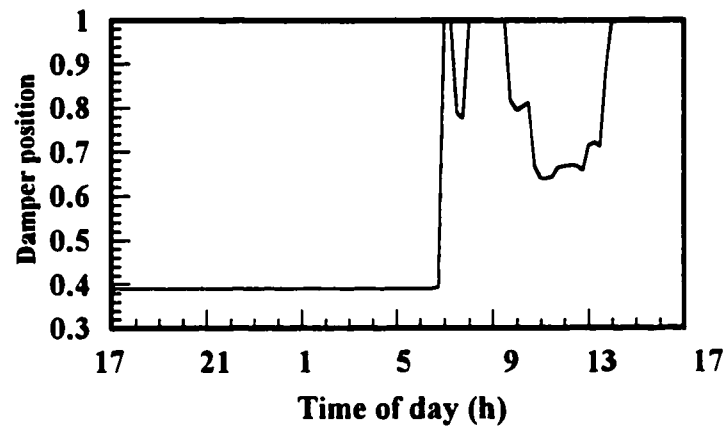
The zone temperatures and humidity ratios are depicted in Figs. 6.10k. and 6.10l respectively. Following the shut down of the chiller, cooling coil and initiation of outdoor

air for free cooling, the zone temperatures rise between 30 to 32°C and gradually decrease close to 28°C. At this time (0700h), the chiller and cooling system is turned full on (start-up mode) which causes the zone temperatures to decrease rapidly and hence they reach close to the setpoint temperatures at 8 a.m. when the occupants arrive. Thereupon zone temperatures are held within $\pm 0.5^{\circ}\text{C}$ of their respective setpoints.

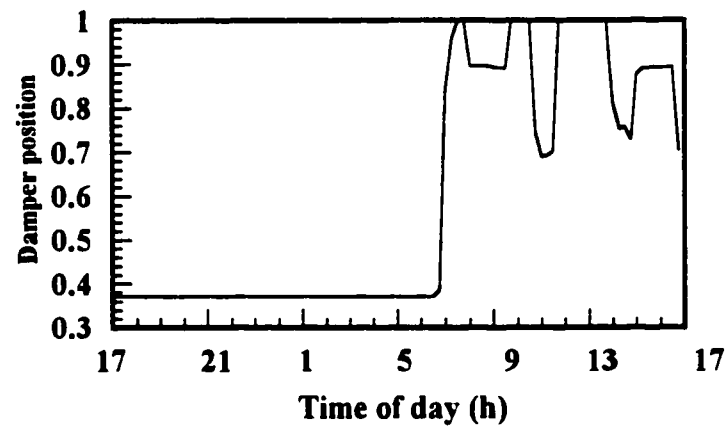
We note that the zone humidity ratios do not change significantly. This is due to the fact that the sensible loads are dominant in the example considered here. Nevertheless the humidity ratios are maintained within the chosen limits. Taken together Figures 6.10a-s constitute the an optimal set and demonstrate the application of the multistage optimization methodology developed in this study.



(a) Damper position (zone 1)

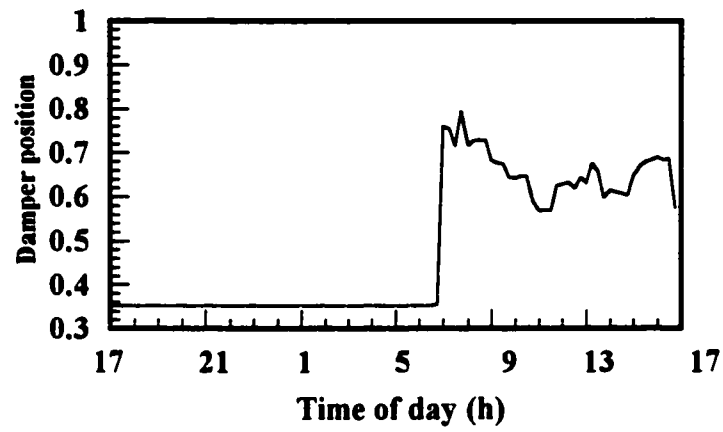


(b) Damper position (zone 2)

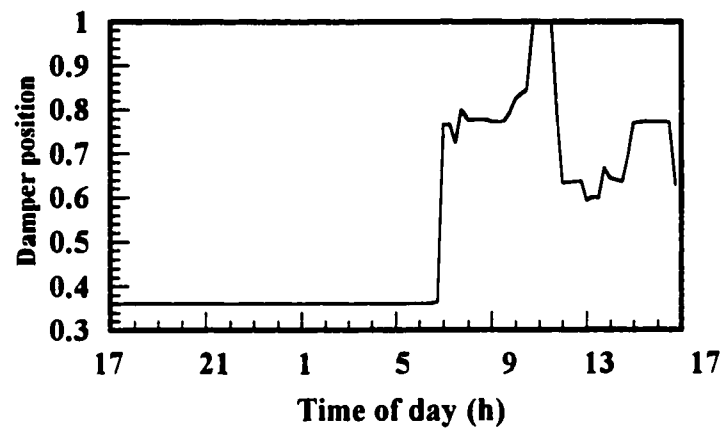


(c) Damper position (zone 3)

Figure 6.10 Global optimal operation of a five-zone VAV cooling system (continued)

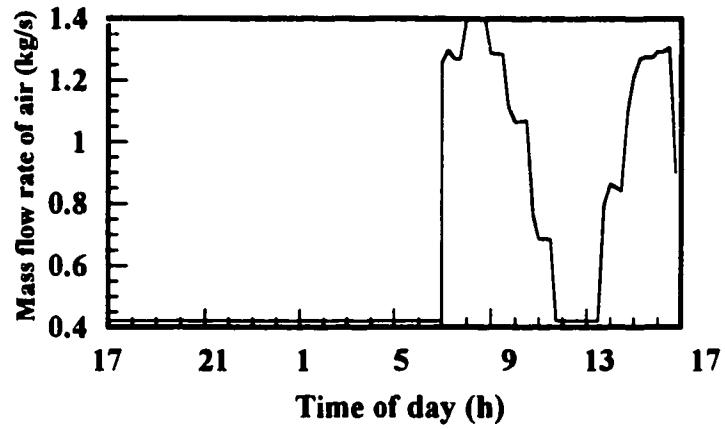


(d) Damper position (zone 4)

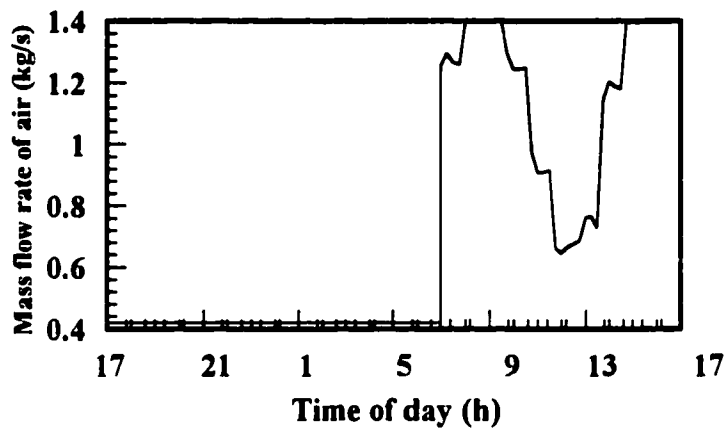


(e) Damper position (zone 5)

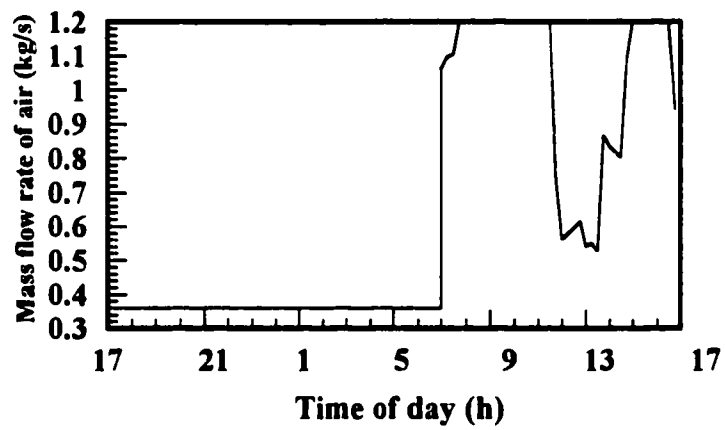
Figure 6.10 Global optimal operation of a five-zone VAV cooling system (continued)



(f) Mass flow rate of air entering to zone 1

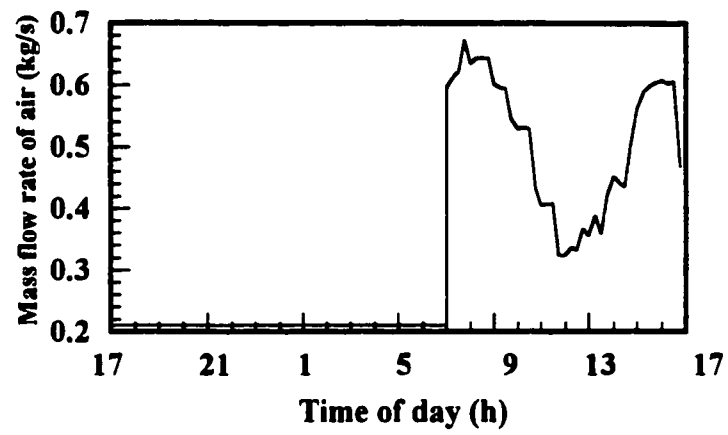


(g) Mass flow rate of air entering to zone 2

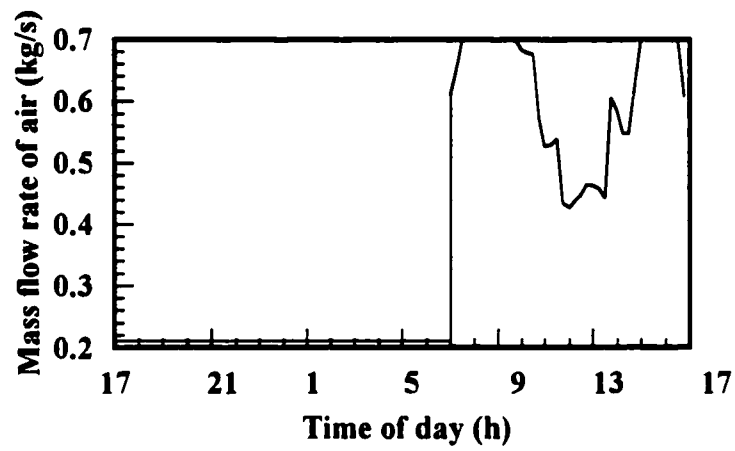


(h) Mass flow rate of air entering to zone 3

Figure 6.10 Global optimal operation of a five-zone VAV cooling system (continued)

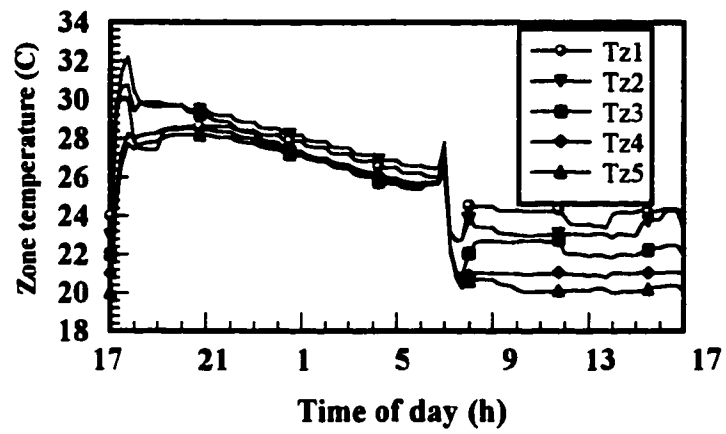


(i) Mass flow rate of air entering to zone 4

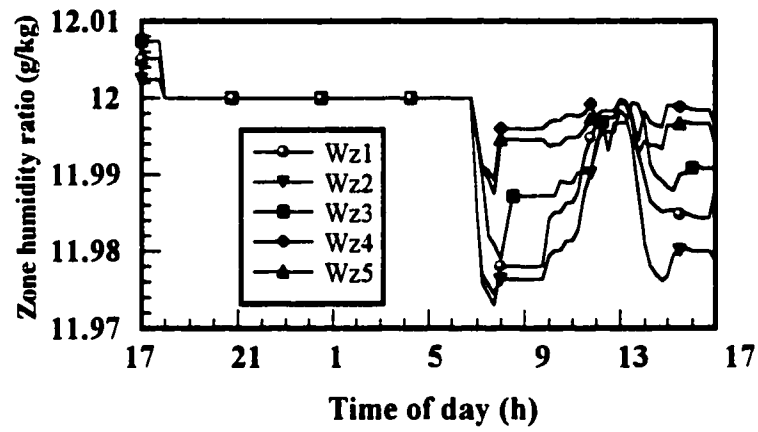


(j) Mass flow rate of air entering to zone 5

Figure 6.10 Global optimal operation of a five-zone VAV cooling system (continued)

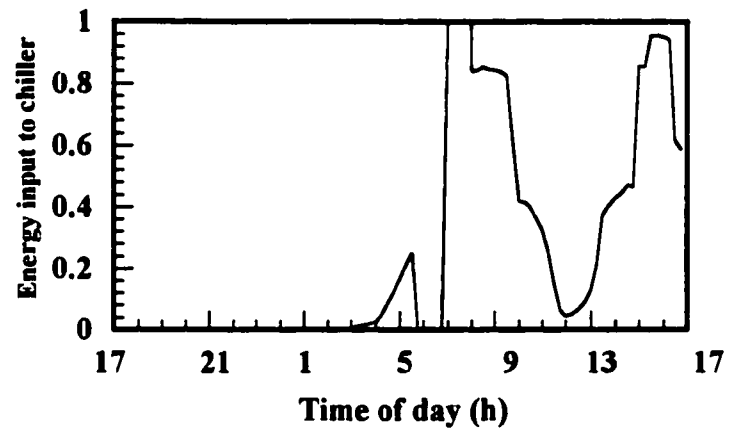


(k) Zone temperature responses

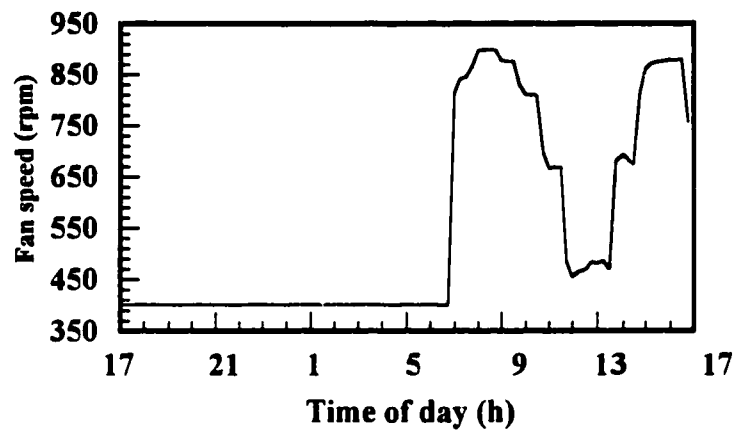


(l) Zone humidity ratio response

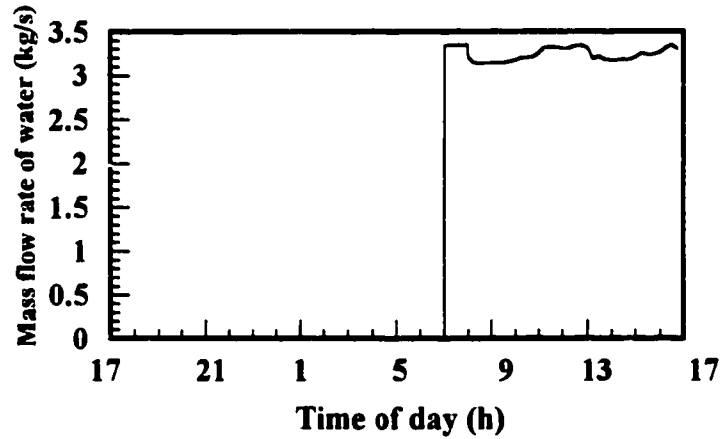
Figure 6.10 Global optimal operation of a five-zone VAV cooling system (continued)



(m) Normalized chiller energy input

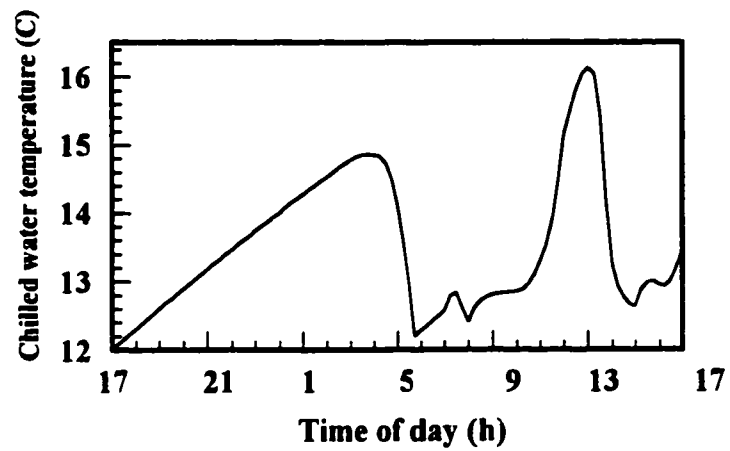


(n) Fan speed

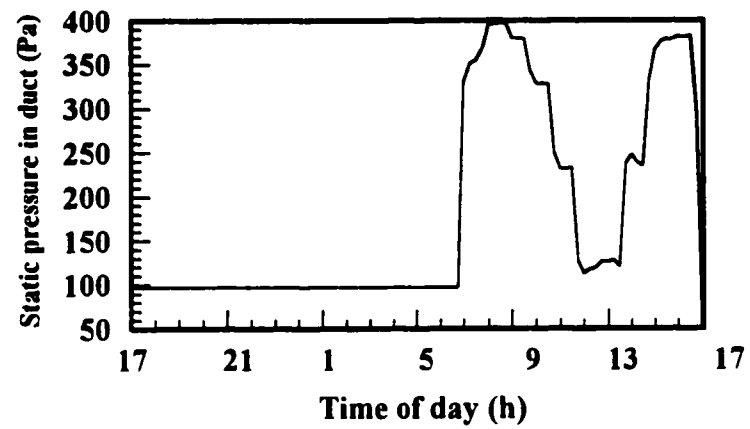


(o) Mass flow rate of water

Figure 6.10 Global optimal operation of a five-zone VAV cooling system (continued)

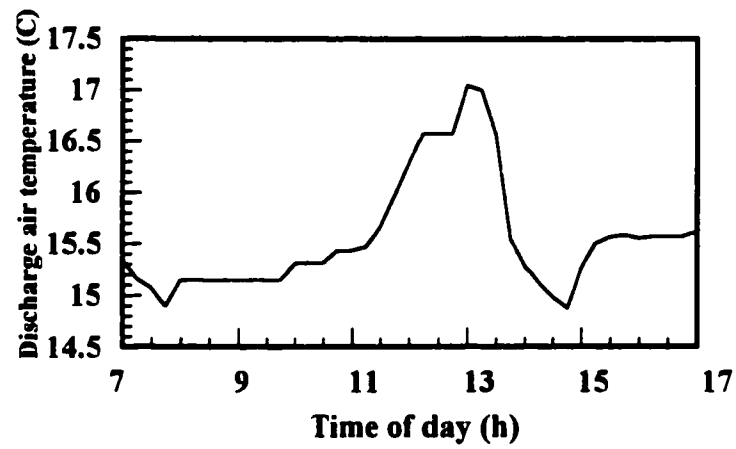


(p) Chilled water temperature

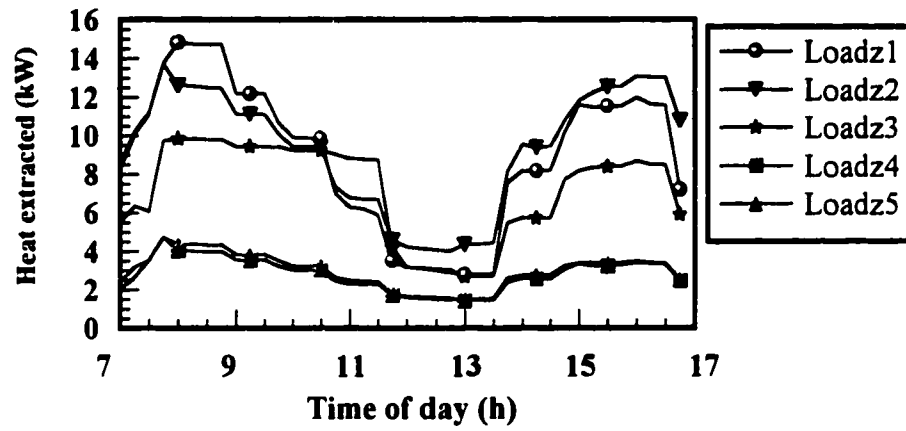


(q) Static pressure

Figure 6.10 Global optimal operation of a five-zone VAV cooling system (continued)



(r) Discharge air temperature



(s) Heat extracted from zones

Figure 6.10 Global optimal operation of a five-zone VAV cooling system (continued)

Chapter 7

Conclusions and Recommendations for Future Research

The development of a comprehensive modeling and optimization methodology for global multiple-stage optimal operation of HVAC and building systems has been presented in this thesis.

To achieve global optimal operation of HVAC and building systems, the system-level model is required. Two approaches for modeling of HVAC and building systems have been applied, namely, bottom-up and top-down approaches. In the bottom-up approach, first component models are developed and then they are interconnected to develop an overall model according to the chosen VAV system configuration. This approach results in the large-scale dynamic model. In the top-down approach, the VAV is subdivided into several subsystems and their relationships are identified. The state space models for each subsystem are developed. This approach together with simplifications resulted in the reduced-order model.

The bottom-up approach is easy to understand but is not flexible enough to accommodate changes in system configuration. On other hand, the top-down approach is flexible enough to accommodate changes in system configuration and is useful for developing software application to let users build their custom models of overall VAV and building systems.

The main contributions of the research in terms of model development can be summarized as follows:

- 1) Dynamics of variable speed fan motors and the corresponding variable flow of air and chilled water are considered.
- 2) Dynamics of heat and mass transfer processes taking place in the coil, duct and elsewhere in the system corresponding to variable flow of air and chilled water are modeled.
- 3) Dynamics of static pressure in the duct is modeled which is useful for balancing the system under variable load conditions.
- 4) Nonlinear damper characteristics (pressure drop vs valve lift or damper position) are considered.
- 5) Air-side and water-air heat transfer coefficients are computed as a function of temperature and flow field characteristics. The efficiency of the coil is variable thus accounting for the part-load performance of the system.
- 6) Both sensible and latent loads acting on the zones and due to outdoor air intake are considered.

The conclusions on modeling methodology can be summarized as follows:

- i). Large scale distributed capacity VAV system models can capture the dynamic interactions between thermal and flow fields accurately. Even though the large scale model requires extensive computations, it serves as a benchmark for developing and validating simple models.
- ii). A methodology for state space modeling of VAV systems has been developed.
- iii). By assuming constant density of air, and developing weighted average lumped model for cooling coil, significant reduction in the order of the model has been achieved.
- iv). The weighted average lumped capacity cooling coil model developed in this thesis is found to be more accurate than the existing simple average coil models.

Specific conclusions drawn from the open-loop simulation results are:

- a) Variable air volume HVAC processes can be grouped into fast and slow time scale processes.
- b) For the chosen system configuration the air flow subsystem has fast dynamics with steady state time ranging up to 30s.
- c) The steady state time for the slow thermal subsystem is of the order of 3 hours.

The application of the developed model is illustrated with an example in which several EMC functions viz., off normal operation and duty cycling are simulated. Results show that reduced capacity night time fan operation keeps zone temperatures lower and is a useful strategy prior to the morning start-up. Typical daily simulation results show that suitably tuned zone damper controllers can maintain zone temperatures close to their respective setpoints in the presence of variable cooling loads and duty cycling of the VAV system.

Once the system-level model of HVAC and building systems is obtained, the next key issue is the global optimal operation of VAV systems. The following specific conclusions are drawn from the global optimal operation analysis presented in the thesis:

- 1) HVAC systems in buildings are operated in time scheduled (multiple stage) mode. Furthermore the HVAC processes consists of multiple time scales. The existing single stage optimal control techniques are not suitable for solving such building operation problems. A global optimal control methodology to deal with multiple stage operation and multiple time scale processes has been developed.
- 2) Results demonstrate that improper choice of setpoints based on experience alone leads to less than optimal energy savings. The best solution is obtained by letting the global methodology to optimize between zone load, operating schedules, energy storage, time-of-day price of electrical energy and the comfort requirements together with the equipment capacity constraints.
- 3) Results shows that up to 25% energy saving can be achieved by optimal operation of HVAC system in VAV mode compared to CV mode.
- 4) Energy efficiency of HVAC systems depends on three most important time-of-day setpoints, namely, chilled water temperature, discharge air temperature and static pressure in the system. Examples showing the use of global optimization methodology for computing such time-of-day setpoints have been demonstrated in the thesis.

Recommendations for Future Research

Research conducted in this thesis provides opportunities for further developments in global optimal operation of HVAC and building systems.

- 1) The methodology for weather and load prediction may be combined with the multi-stage optimization methodology to build a real-time energy management and control system.
- 2) More efficient algorithms may be required to improve the computational efficiency.
- 3) Fuzzy rule-based system and artificial neural networks may be incorporated with the modeling methodologies to identify the components of HVAC systems so as to extend this work to deal with a number of uncertainties.
- 4) The component and system models developed in this thesis could be extended to on-line adaptive control applications.

REFERENCES

- Ahmed, O. 1991. "DDC applications in variable-water-volume systems." *ASHRAE Transactions*, Vol.97, Part 1, pp. 751-758.
- Albert, T.P.S. 1995. "A Neural-Network-based identifier/controller for modern HVAC control." *ASHRAE Transactions*, Vol. 101, Part 2, pp. 14-31.
- Athans, M. 1966. "The status of optimal control theory and applications for deterministic systems." *IEEE Transactions, Automatic Control*, Vol. AC-11, No.3, July, pp. 580-596.
- ASHRAE, 1986. *Fundamentals Handbook*. Atlanta: American Society of Heating, Refrigerating and Air-Conditioning Engineers.
- Balarkrishnan, A.V. and Neustadt, L.W. (Eds.) 1964. *Computing Methods in Optimization Problem*. Academic Press.
- Bekker, J.E. et al. 1991. "A tuning method for first-order processes with PI controller." *ASHRAE Transactions*, Vol.97, Part 2, pp. 19-23.
- Belghith, S., Benard, C. Bourdache-Siguerdidjane, H., Fliess, M., Guerrier, B., Lamnabhi-Lagarrigue, F., and Rosset, M.-M. 1985. "Some solutions for nonlinear optimal heat transfer problems", *Proc. 24th IEEE Conf. Decision and Control*, Fort Lauderdale, FL.
- Benard, C., Boileau, E., Guerrier, B. and Rosset-Louerat, M.-M. 1987. "Optimal control of a building as a function of meteorological conditions." *Proc. 3rd Int. Cong. Building Energy Management*, Vol. 4, A. Faist et al. eds., pp. 439-446.
- Benard, C., Guerrier, B. and Rosset-Louerat, M.-M. 1992a. "Optimal building energy management: Part I ---modeling." *J. Solar Energy Eng.*, Vol. 114, No.2, pp. 2-12.
- Benard, C., Guerrier, B. and Rosset-Louerat, M.-M. 1992b. "Optimal building energy management: Part II ---control." *J. Solar Energy Eng.*, Vol. 114, No.2, pp. 13-22.
- Benton, R. MacArthur, J.W., Mahesh, J.K. and Cockroft, J.P. 1982. "Generalized modelling and simulation software tools for building systems." *ASHRAE Transactions*, Vol.88, pp. 839-855
- Berkovitz, L.D. 1961. "Variational methods in problems of control and programming." *Journal Math. Anal. Appl.*, Vol. 3, pp. 145-169

- BESA, 1987. *BESA: Building Energy System Analysis Technical Reference*. CandaPlan Group Inc., Ontario, Canada.
- Bhargava, S.C., McQuiston, F.C. and Zirkle, L.D. 1975. "Transfer function for crossflow multirow heat exchangers." *ASHRAE Transactions*, Vol.81, Part 2, pp. 294-314
- BLAST, 1979. *Blast 3.0: Building Loads Analysis and System Thermodynamics Program, User Manual*, Support Office, Dept. of Mechanical and Industrial Engineering, University of Illinois, Urbana- Champaign.
- Bloomfield, D.P. and Fisk, D.J. 1977. "The optimization of intermittent heating." *Building and Environment*, Vol. 12, pp. 43-55.
- Borresen, B.A. 1981. "Thermal room models for control analysis." *ASHRAE Transactions*, Vol. 87, Part 2, pp. 251-260.
- Boyens, A. and Mitchell, J.W. 1991. "Experimental validation of a methodology for determining heating system control strategies." *ASHRAE Transactions*, Vol.97, Part 2, pp. 24-30.
- Brandt, S.G. 1986. "Adaptive control implementation issues." *ASHRAE Transactions*, Vol. 92, Part 2B, pp. 211-219.
- Braun, J.E., Mitchell, J.W., Klein, S.A. and Beckman, W.A. 1987. "Performance and control characteristics of a large cooling system." *ASHRAE Transactions*, Vol. 93, Part 2, pp. 1830-1852.
- Braun, J.E., Klein, S.A. and Mitchell, J.W. 1989a. "Effectiveness models for cooling towers and cooling coils." *ASHRAE Transactions*, Vol. 95, Part 2, pp. 164-174.
- Braun, J.E., Klein, S.A., Beckman, W.A., and Mitchell, J.W. 1989b. "Methodologies for optimal control of chilled water systems without storage." *ASHRAE Transactions*, Vol. 95, Part 1, pp. 652-662.
- Braun, J.E., Klein, S.A., Mitchell, J.W., and Beckman, W.A. 1989c. "Applications of optimal control to chilled water systems without storage." *ASHRAE Transactions*, Vol. 95, Part 1, pp. 663-675.
- Braun, J.E. and Diderrich, G. T. 1990. "Near-optimal control of cooling towers for chilled-water systems." *ASHRAE Transactions*, Vol. 96, Part 2, pp. 806-813.
- Brothers, P.W. and Warren, W.L. 1986. "The energy use in variable volume systems." *ASHRAE Transactions*, Vol. 92, Part 2B, pp. 19-29.

- Chen, Y.H. and Lee, K.M. 1990. "Adaptive robust control scheme applied to a single-zone HVAC system." *ASHRAE Transactions*, Vol.96, Part 2, pp. 896-903.
- Cherches, D.B., Abdelmessih, A. and Townsend, M.A. 1985. "A direct digital control algorithm for control of a single environmental space.", *Journal Dynamic Systems, Measurement and Control*, Vol.107, No.4, pp. 324-331.
- Clark D.R., Hurley, C.W. and Hill, C.R. 1985. "Dynamic models for HVAC system components.", *ASHRAE Transactions*, Vol.91, Part 1B, pp. 737-751.
- Coley, D.A. and Penman, J.M. 1992. "Second order system identification in the thermal response of real buildings. Paper II: Recursive formulation for on-line building energy management and control.", *Building and Environment*, Vol. 27, pp. 93-103.
- Crawford, R.R. et al. 1991. "A segmented linear least-squares modeling procedure for nonlinear HVAC components." *ASHRAE Transactions*, Vol.97, Part 2, pp. 11-18.
- Croome, J.D. and Roberts, B.M. 1981. *Airconditioning and Ventilation of Building*, Pergamon Press Inc., p. 310.
- DOE-2, 1981. "DOE-2: Building energy user analysis program, engineering manual, Version 2.1A", Laurence Berkeley Laboratory.
- Dorato, P. 1983. "Optimal temperature control of solar energy.", *Solar Energy*. Vol. 30, pp.147-153.
- Elmahdy, A.H. 1975. "Analytical and experimental multi-row, finned-tube heat exchanger performance during cooling and dehumidification process", Ph.D thesis, Dept. of Mechanical and Aeronautical Eng., Carleton University, Ottawa, Canada.
- Englander, S. L. and Norford, L. K. 1992a. "Saving fan energy in VAV systems --- Part 1, Analysis of a variable speed-drive retrofit." *ASHRAE Transactions*, Vol.98, Part 1, pp. 3-18.
- Englander, S. L. and Norford, L. K. 1992b. "Saving fan energy in VAV systems --- Part 2, Supply fan control for static pressure minimization using DDC zone feedback." *ASHRAE Transactions*, Vol.98, Part 1, pp. 19-32.
- Fan, L.T., Hwang, Y.S. and Hwang, C.L. 1970a. "Application of modern optimal control theory to environmental control of confined spaces and life support systems. Part 1 --- Modeling and simulation." *Building Science*, Vol. 5, pp. 57-71.
- Fan, L.T., Hwang, Y.S. and Hwang, C.L. 1970b. "Application of modern optimal control theory to environmental control of confined spaces and life support systems. Part 2

- Basic computational algorithm of Pontryagin's maximum principle and its applications." *Building Science*, Vol. 5, pp. 81-94.
- Fan, L.T., Hwang, Y.S. and Hwang, C.L. 1970c. "Application of modern optimal control theory to environmental control of confined spaces and life support systems. Part 3 --- Optimal control of systems in which state variables have equality constraints at the final process time." *Building Science*, Vol. 5, pp. 125-136.
- Fan, L.T., Hwang, Y.S. and Hwang, C.L. 1970d. "Application of modern optimal control theory to environmental control of confined spaces and life support systems. Part 4 --- Control of systems with inequality constraints imposed on state variables." *Building Science*, Vol. 5
- Fan, L.T., Hwang, Y.S. and Hwang, C.L. 1970e. "Application of modern optimal control theory to environmental control of confined spaces and life support systems. Part 5 --- Optimality and sensitivity analysis." *Building Science*, Vol. 5
- Farris, D.R., Melsa, J.L. Murray, H.S. McDonald, T.E. and Springer, T.E. 1977. "Energy conservation by adaptive control for a solar heated building." International Conference on Cybernetics and Society, Washington, pp.329-335.
- Fenstel, H.E. and Raynor-Hoosen, A. 1990, *Fundamentals of the Multizone Air Flow Model COMIS*, Air Infiltration and Ventilation Centre, Technical Note AIVC 29, Document AIC-TN-29-90.
- Forrester, J.R. and Wepfer, W.J. 1984. "Formulation of a load prediction algorithm for a large commercial building." *ASHRAE Transactions*, Vol. 90. Part 2B, pp. 536-551.
- Franklin, G.F., Powell, G.D. and Workman, H.L. 1990. *Digital Control of Dynamic Systems*. Addison-wesley Publishing Co., New York.
- Gartner, J.R., 1972. "Simplified dynamic response relations for finned-coil heat exchangers." *ASHRAE Transactions*, Vol. 78 Part 2, pp. 163-169.
- Gartner, J.R. and Daane, L.E., 1969. "Dynamic response relations for a serpentine crossflow heat exchanger with water velocity disturbance." *ASHRAE Transactions*, Vol. 75 Part.1, pp. 53-68.
- Gartner, J.R. and Harrison, H.L. 1963. "Frequency response transfer functions for a tube in crossflow." *ASHRAE Transactions*, Vol. 69, pp. 320-330.
- Gartner, J.R. and Harrison, H.L. 1965. "Dynamic characteristics of water-to-air cross-flow heat exchangers." *ASHRAE Transactions*, Vol. 71, pp. 212-224.

- Gear, C.W., 1971. *Numerical Initial Value Problems in Ordinary Differential Equations*, Prentice-Hall
- Gerald, C.F. and Wheatley, P.O. 1984. *Applied Numerical Analysis*, Addison-Wesley Publishing Company, California
- Goh, P.A., 1990. "Modeling and control of a variable air volume (VAV) system.", Master Thesis, The Centre for Building Studies, Concordia University, Montreal, Canada.
- Grot, R.A. and Harje, D.T. 1981. "The transient performance of a forced warm air duct system." *ASHRAE Transactions*, Vol. 87, Part 1, pp. 795-804.
- Gupta, V.K. 1987. "Despite popularity problems do exist." *ASHRAE Journal*, August, pp. 22-24.
- Haines, R.W. 1988. *HVAC System Design Handbook*, TAB Book Inc., 1988,. Blue Ridge Summit, PA, pp. 229-248.
- Hamilton D.C., Leonard, R.G. and Pearson, J.T. 1974. "Dynamic response characteristics of discharge air temperature control system at near full and part heating load." *ASHRAE Transactions*, Vol. 83, Part 1, pp. 251-268.
- Hamilton D.C., Leonard, R.G. and Pearson, J.T. 1977. "A system model for a discharge air temperature control system", *ASHRAE Transactions*, Vol. 83, Part 1, pp. 251-268.
- Harriott, P. 1964. *Process Control*, McGraw-Hill, Chapter II.
- Harrison, H.L., Hansen, W.S. and Zelenski, R.E. 1968. "Development of a room transfer function model for use in the study of short term transient response." *ASHRAE Transactions*, Vol. 74, Part 2, pp. 198-210.
- Hartman, T.B. 1988. "Dynamic control: fundamentals and considerations." *ASHRAE Transactions*, Vol. 94, Part 1, pp. 599-609.
- Hestenes, M.R. 1966. *Calculus of Variations and Optimal Control Theory*, John Wiley and Sons, Inc.
- Hill, J.M. and Jeter, S.M. 1991. "A linear subgrid cooling and dehumidification coil model with emphasis on mass transfer" *ASHRAE Transactions*, Vol. 97, Part 2, pp. 118-128.
- House, J.M., Smith, T.F. and Arora, J.S. 1991. "Optimal control of a thermal system" *ASHRAE Transactions*, Vol. 97, Part 2.

- House, J.M. and Smith, T.F. 1995. "A system approach to optimal control for HVAC and building systems." *ASHRAE Transactions*, Vol. 101, Part 2, pp. 647-660.
- Huang, S. and Nelson, R.M. 1991. "A PID-law-combining fuzzy controller for HVAC applications." *ASHRAE Transactions*, Vol. 97, Part 2, pp. 768-774.
- HVACSIM⁺, 1986. *Building Systems and Equipment Simulation Program Reference Manual*, U.S. Department of Commerce, National Technical Information Service.
- Johnson, G.A. 1985. "Optimization techniques for a centrifugal chiller plant using a programmable controller." *ASHRAE Transactions*, Vol.91, Part 2B, pp. 835-847.
- Kamimura, K. et. al. 1994. "CAT (Computer-aided tuning) software for PID controllers" *ASHRAE Transactions*, Vol. 100, Part 1, pp. 180-190.
- Kawashima, M., Dorgan, C.E., and Mitchell, J.W.. 1995. "Hourly thermal load prediction for the next 24 hours by ARIMA, EWMA, LR and AN Artificial Neural Network." *ASHRAE Transactions*, Vol. 101, Part 1, pp. 186-200.
- Kaya, A. 1976. "Analytical techniques for controller design." *ASHRAE Journal*, Vol. 18, April, pp. 35-39.
- Kaya, A. 1979. "Modeling of an environmental space for optimum control of energy use." *Proceedings of 7th IFAC World Congress*, Helsinki, Finland, pp. 327-334.
- Kaya, A. 1981. "Optimum control of HVAC system to save energy." *Proceedings of 8th IFAC Triennial World Congress*, Kyoto, Japan, pp. 3231-3240.
- Kaya, A., Chen, C.S. Raina, S. and Alexander, S.J. 1982. "Optimum control policies to minimize energy use in HVAC systems." *ASHRAE Transactions*, Vol.88, Part 2, pp. 235-248.
- Keeney, K., and Braun, J. 1996. "A simplified method for determining optimal cooling control strategies for thermal storage in building mass." *Journal of HVAC&R Research*, Vol. 2, No.1.
- Kelly, G.E. 1988. "Control system simulation in North America.", *Energy and Buildings* Vol.10, pp.193-202.
- Kirshenbaum, M. 1987. "Variable flow chilled water." *ASHRAE Journal*, August, pp. 32-36.
- Kimbara, A. et. al. 1995. "On-line prediction for load profile of an air conditioning system." *ASHRAE Transactions*, Vol. 101, Part 2, pp. 198-207.

- Kintner-Meyer, M. and Emery A.F. 1995a. "Optimal control of an HVAC system using cold storage and building thermal capacitance." *Energy and Buildings*, Vol. 23, pp. 19-31.
- Kintner-Meyer, M. and Emery A.F. 1995b. "Cost optimal analysis and load shifting potentials of cold storage equipment." *ASHRAE Transactions*, Vol. 101, Part. 2, pp. 539-548.
- Khan, A.Y. 1994. "Heat and mass transfer performance analysis of cooling coils at part-load operating conditions." *ASHRAE Transactions*, Vol.93, Part 1, pp. 52-62.
- Klein, S.A. *et al.* 1983. *TRANSYS, A Transient Simulation Program, Report 38-12, Version 12.1*, Engineering Experimentation Station, University of Wisconsin-Madison.
- Kokotovic, P.V. and Sannuti, P. 1968. "Singular perturbation method for reducing the model order in optimal control design." *IEEE Trans. Automat. Contr.*, Vol. AC-13, pp. 377-384, Aug.
- Kopp, R.E. and Moyer, H.G. 1966. "Trajectory optimization techniques." *Advances in Control Systems*, Vol.4, (Ed. Leondes, C.T.) Academic Press, pp. 103-155.
- Kovacs, P.K. 1984. *Transient Phenomena in Electrical Machines*. Akademiai Kiado, Budapest, pp. 319-326.
- Krakow, K.I. and Lin, S. 1995. "PI control of fan speed to maintain constant discharge pressure." *ASHRAE Transactions*, Vol. 101, Part 2, pp. 398-407.
- Kreider, J.F. and Wang, X.A. 1991. "Artificial neural networks demonstration for automated generation of energy use predictions for commercial buildings." *ASHRAE Transactions*, Vol.98, Part 2, pp. 775-779.
- Kuo, B.C. 1991. *Automatic Control Systems. 6th Edition*, Englewood Cliffs, N.J.
- Li, X.M. and Wepfer, W.J. 1985. "Implementation of adaptive control of building HVAC systems." Proceeding of the 8th World Energy Engineering Congress. Chapter 21. pp. 143-152
- Li, X.M. and Wepfer, W.J. 1987. "Recursive estimation methods applied to a single-zone HVAC system." *ASHRAE Transactions*, Vol.93, Part 1, pp. 1814-1829.
- Lyons, J.L., 1982. *Lyon's Valve Designer's Handbook*, Van Nostrand Reinhold Co.
- MacArther, J.W. and Foslien, W.K. 1993. "A novel predictive strategy for cost-optimal control in buildings." *ASHRAE Transactions*, Vol. 99, Part 1, pp. 1025-1036.

- MacArther, J.W. and Woessner, M.A. 1993. "Receding horizon control: a model-based policy for HVAC applications." *ASHRAE Transactions*, Vol. 99, Part 1, pp. 139-148.
- Maxwell, G.M., Shapiro, H.N. and Westra, D.G. 1989. "Dynamics and control of a chilled water coil." *ASHRAE Transactions*, Vol.95, Part 1, pp. 1243-1255.
- McCullagh, K.R., Green, G.H. and Chandrasekar, S. 1969. "An analysis of chilled water cooling dehumidifying coil using dynamic relationships." *ASHRAE Transactions*, Vol. 75, Part 2, pp. 200-209.
- McGill, R., 1965. "Optimal control, inequality state constraints, and the generalized Newton-Raphson algorithm." *SIAM J. Control*, Vol. 3, pp. 291-298.
- McNamara, R.T. and Harrison, H.L. 1967. "A lumped parameter approach to crossflow heat exchanger dynamics." *ASHRAE Transactions*, Vol. 73, Part 2, pp. IV.1.1-IV.1.9.
- McQuiston, F.C. 1978. "Correlation of heat, mass and momentum transport coefficients for plate-fin-tube heat transfer surfaces with staggered." *ASHRAE Transactions*, Vol. 84, Part 1, pp. 294-309.
- McQuiston, F.C. and Parker, J.D. 1988. *Heating Ventilating and Air-Conditioning*. John Wiley & Sons Inc. 3ed.
- Mehta, D.P. 1980. "Dynamic thermal responses of buildings and systems." Dissertation, Iowa State University.
- Mehta, D.P. and Woods, J.E. 1980. "An experimental validation of a rational model for dynamic responses of buildings." *ASHRAE Transactions*, Vol. 86.
- Mehta, D.P. 1984. "Modeling of environmental control components." *Workshop on HVAC Control: Modeling, and Simulation*, Georgia Institute of Technology, Atlanta.
- Mehta, D.P. 1987. "Dynamic performance of PI controller: experimental validation." *ASHRAE Transactions*, Vol. 93. Part 1, pp. 1775-1793.
- Miller, D.E. 1982. "A simulation to study HVAC processes." *ASHRAE Transactions*, Vol. 88, Part 2, pp. 809-825.
- Mitchell, J. 1988. "Analysis of energy use and control characteristics of a large variable speed drive chiller system." *ASHRAE Journal*, January, pp. 33-34.

- Mufti, I.H. 1972. *Computational Methods in Optimal Control Problems*. Springer-Verlag, Berlin
- Myers, G.E., Mitchell, J.W., and Nagaoka, R. 1965. "A method of estimating cross-flow heat exchanger transients." *ASHRAE Transactions*, Vol. 71, Part.1, pp. 225-230.
- Myers, G.E., Mitchell, J.W., and Norman, R.F. 1967. "The transient response of crossflow heat exchangers, evaporators, and condensers." *ASME J. of Heat Transfer*, Vol. 89, No.1, pp. 75-80.
- Myers G.E., Mitchell, J.W., and Lindeman JR., C.F. 1970. "The transient response of crossflow heat exchangers having an infinite capacitance rate fluid." *ASME J. of Heat Transfer*, Vol. 92, No.2, pp. 269-275.
- Nakanishi, E., Pereira, N.C., Fan, L.T. and Hwang, C. L. 1973a. "Simultaneous control of temperature and humidity in confined space: Part 1 --- Mathematical modeling of the dynamic behavior of temperature and humidity in a confined space." *Building Science*, Vol. 8, Part 2. pp. 39-49.
- Nakanishi, E., Pereira, N.C., Fan, L.T. and Hwang, C. L. 1973b. "Simultaneous control of temperature and humidity in confined space: Part 2 --- Feedback control synthesis via classical control theory." *Building Science*, Vol. 8, Part 2. pp. 51-64.
- Nesler C. G. 1986. "Automated controller tuning in HVAC applications." *ASHRAE Transactions*, Vol. 92, Part 2. pp. 189-200.
- Nesler C. G. and Stoecker, W.F. 1984. "Selecting the proportional and integral constants in the direct digital control of discharge air temperature." *ASHRAE Transactions*, Vol. 90, Part 2B. pp. 834-845.
- Nizet, J.L., Lecomte, J. and Litt, F.X. 1984. "Optimal control applied to air conditioning in buildings." *ASHRAE Transactions*, Vol. 90, Part 1B, pp. 587-600.
- O'Neill, P.J. 1988. "Thermal performance analysis of finned tube heat exchangers at low temperature and airflow rates." *ASHRAE Transactions*, Vol. 94, Part 2, pp. 244-260.
- Oskarsson, S.P., Krakow, K.I. and Lin, S. (1990a) "Evaporator models for operation with dry, wet and frosted finned surfaces Part I: heat transfer and fluid flow theory." *ASHRAE Transactions*, Vol. 96, Part 1, pp. 373-380.
- Oskarsson, S.P., Krakow, K.I. and Lin, S. (1990b) "Evaporator models for operation with dry, wet and frosted finned surfaces Part II: evaporator models and verification." *ASHRAE Transactions*, Vol. 96, Part 1, pp. 381-392.

- Park, C. Clark, D.R. and Kelly, G.E. 1985. "An overview of HVACSIM": a dynamic building/HVAC/Control systems simulation program." Building Energy Simulation Conference, Seattle, August, pp. 175-185.
- Patel, R.V. and Munro, N. 1982. *Multivariable System Theory and Design*, Pergamon Press, Oxford.
- Payne, F.W. and McGowan, J.J. 1988. *Energy Management & Control System Handbook*, The Faimont Press Inc., Lilburn, GA.
- Pearson T.J. and Leonard, R.G. 1974. "Gain and time constant for finned serpentine crossflow heat exchangers." *ASHRAE Transactions*, Vol. 80, Part 2, pp. 255-267.
- Pinnella, M.J. 1986. "Modeling, tuning and experimental verification of a fan static pressure control system." M.S. Thesis, Department of Illinois, Urbana-Champaign.
- Pinnella, M.J., Wechselberger, E., Hittle, D.C. and Pedersen, C.O. 1986. "Self-tuning digital integral control." *ASHRAE Transactions*, Vol. 92, Part 2B, pp. 202-209.
- Roberts, A.S. and Oak, M. P. 1991. "Nonlinear dynamics and control for thermal room models." *ASHRAE Transactions*, Vol.97, Part 1, pp. 722-726.
- Roberts, M.M. 1987. "Opportunities exist to improve design." *ASHRAE Journal*, August, pp. 25-29.
- Schumann. R. 1980. "Digital parameter adaptive control of an air conditioning plant." Fifth IFAC/IFIP Conference on Digital Computer Applications, Dusseldorf. FRG.
- Shavit, G. 1977. "Energy conservation and fan systems: computer control with floating space temperature." *ASHRAE Journal*, October, pp. 29-34.
- Shavit, G. and Brandt, S.G. 1982. "The dynamic performance of a discharge air temperature system with a PI controller." *ASHRAE Transactions*, Vol.88, Part 2, pp. 826-838.
- Shoureshi, R. and Rahmani, K. 1989. "Intelligent control of building systems." ASME Winter Meeting, San Francisco, CA, DSC-Vol. 16, pp. 7-15
- Spethmann, D.H. 1985. "Optimized control of multiple chillers." *ASHRAE Transactions*, Vol.91, Part 2B, pp. 848-856.
- Spitler, J.D. et al. 1986. "Fan electricity consumption for variable air volume." *ASHRAE Transactions*, Vol. 92, Part 2B, pp. 5-18.

- Stoecker, W.F. 1976. *Procedures for Simulating the Performance of Components and Systems for Energy Calculations*. Third Edition.
- Stoecker, W.F., Rosario, L.A., Heidenreich, M.E., and Phelan, T.R. 1978. "Stability of an air-temperature control loop." *ASHRAE Transactions*, Vol.84, Part 1, pp. 35-53.
- Sud, I. 1984. "Development of a simulation technique for evaluating control strategies for minimum energy usage." *Workshop on HVAC Control: Modeling, and Simulation*, Georgia Institute of Technology, Atlanta.
- Tamm, H. 1969. "Dynamic response relations for multi-row cross flow heat exchangers." *ASHRAE Transactions*, Vol.75, Part 1, pp. 69-80.
- Tamm, H. and Green, G.H. 1973. "Experimental multi-row cross flow heat exchanger dynamic." ASHRAE Paper. No. 2276.
- Thompson, J.G. 1981. "The effect of room and control systems dynamics on energy consumption." *ASHRAE Transactions*, Vol.87 Part 2. pp.883-896.
- Thompson, J.G. and Chen, P.M.T. 1979. "Digital simulation of the effect of room and control system dynamics on energy." *ASHRAE Transactions*, Vol.85 Part 1.
- Tobias, J.R. 1973. "Simplified transfer function for temperature response of fluids flowing through coils, pipes or ducts." *ASHRAE Transactions*, Vol.79, Part 2, pp. 19-22
- Townsend, M.A., Cherchas, D.B., and Abdelmessih, A. 1986. "Optimal control of a general environmental space." *Journal Dynamic Systems, Measurement and Control*, Vol.108, No.4, pp. 203-212.
- Underwood, D.M. and Crawford, R.R. 1991. "Dynamic nonlinear modeling of a hot-water-to-air heat exchange for control applications." *ASHRAE Transactions*, Vol.97, Part 1, pp. 149-155.
- Virk, G.S., and Loveday, D.L. 1991. "A comparison of predictive, PID, and On/Off techniques for energy management and control." *ASHRAE Transactions*, Vol.97, Part 2, pp. 3-10.
- Wallenborg, A.O. 1991. "A new self-tuning controller for HVAC systems." *ASHRAE Transactions*, Vol. 97, pp. 19-25.
- Waller, B. 1988. "Various flow rates in condenser water." *ASHRAE Journal*, January, pp. 30-32

- Walton, G.N. 1983. *Thermal Analysis Research Program (TARP) Reference Manual*. U.S. Dept. of Commerce, National Bureau of Standards, National Eng. Lab., Washington, D.C.
- Wessel, D.J. 1987. "Electric controls revolutionize VAV." *ASHRAE Journal*, August, pp. 27-28
- Williams, V.A. 1985. "Optimization of chiller plant's energy consumption utilizing a central EMCS and DDC." *ASHRAE Transactions*, Vol.91, Part 2B, pp. 857-861.
- Winn, R.C. and Winn, C.B. 1985. "Optimal control of auxiliary heating of passive solar heated building.", *Solar Energy*. Vol. 35, No.5, pp. 419-427.
- Wong S.P.W. and Wang, S.K. 1989. "System simulation of the performance of a centrifugal chiller using a shell-and-tube-type water-cooled condenser and R-11 as Refrigerant." *ASHRAE Transactions*, Vol. 95, Part 1, pp. 445-454.
- Woods, J. 1990. *IAQU "Indoor air quality update."* Cuttle Information Corp., Vol. 3, No.6, pp. 1-7.
- Yuill, G.K., and Wray, C.P. 1990. "Overview of the ASHRAE TC 4.7 annotated guide to models and algorithms for energy calculation relating to HVAC equipment." *ASHRAE Transactions*, Vol.96 Part 2.
- Zaheer-uddin, M. 1986. "A two-component thermal model for a direct gain passive house with a heated basement." *Building and Environment*, Vol. 21.
- Zaheer-uddin, M. 1989. "Sub-optimal controller for a space heating system." *ASHRAE Transactions* , Part 2, Vol. 92.
- Zaheer-uddin, M. 1990. "Combined energy balance and recursive least squares method for the identification of system parameters." *ASHRAE Transactions* , Part 2, Vol. 96.
- Zaheer-uddin, M. 1992a. "Optimal control of a single zone environmental space." *Building and Environment*, Vol. 27, pp. 93-103.
- Zaheer-uddin, M. 1992b. "Decentralized control systems for HVAC", *ASHRAE Transactions* , Part 2, Vol. 98, pp. 114-126.
- Zaheer-uddin, M. and Goh, P.A. 1991. "Transient Response of a closed-loop VAV system." *ASHRAE Transactions*, Vol. 97, Part 2.
- Zaheer-uddin, M. and Patel, R.V. 1993. "The design and simulation of a sub-optimal controller for space heating." *ASHRAE Transactions*, Vol. 99, pp. 554-564.

- Zaheer-uddin, M. and Wang, J.C.Y., 1992. "Start-stop control strategies for heat recovery in multi-zone water loop heat pump systems." *J. of Heat Recovery System & CHP*, Vol. 12, No.4, pp.335-346
- Zaheer-uddin, M. and Zheng, G. R. 1992. "Static Pressure Control for Balancing VAV Systems and Minimizing Energy Consumption: A Computer Simulation Study", *Indoor Air Quality, Ventilation and Energy Conservation*, Proceeding of 5th International Jacques Cartier Conference, Montreal, October.
- Zaheer-uddin, M. and Zheng, G. R. 1993. "Part-load Performance Characteristics of A Multizone HVAC System", *the 14th Canadian Congress of Applied Mechanics, CANCAM'93*, Kingston, Canada, May
- Zaheer-uddin, M. and Zheng, G. R. 1994. "A VAV System Model to Simulate Energy Management Control Functions: Off-normal Operation and Duty-cycling", *Energy Conversion & Management*, Vol.35, No.11, pp.917-932
- Zermuehlen, R.O. and Harrison, H.L. 1965. "Room temperature response to a sudden heat disturbance input." *ASHRAE Transactions*, Vol. 71, Part 1, pp. 206-211.
- Zhang, X. and Warren, M.L. 1988. "Use of a general control simulation program." *ASHRAE Transactions*, Vol. 94, Part 1, pp. 1776-1791.
- Zhang, Z. and Nelson, R.M. 1992. "Parametric analysis of a building space conditioned by a VAV system." *ASHRAE Transactions*, Vol. 98, Part 2, pp. 43-48.
- Zheng, G. R. and Zaheeruddin, M. 1996. " Optimization of Thermal Processes in a Variable Air Volume HVAC System", *Energy*, Vol. 21, (5), pp. 407- 420.

Appendix A The modeling of building shell

The calculation of cooling load for a zone involves calculating a surface-by-surface conductive, convective, and radiative heat balance for each room surface and a convective heat balance for the room air.

1. Heat balance of air in the zone

The sensible heat balance equation for the air in the zone can be written:

$$\begin{aligned} \frac{dT_{z,j}(n)}{dt} = & \frac{\dot{m}_j}{\rho V_j} [T_j(n) - T_{z,j}(n)] + \frac{\sum_{r=1}^{N_r} \left\{ \sum_{i=1}^{N_s} h_i^c [T_i(n) - T_{z,j}(n)] A_i \right\}}{\rho V_j} \\ & + \frac{\dot{m}_{in}}{\rho V_j} [T_o(n) - T_{z,j}(n)] + RS_a(n) + RL_a(n) + RE_a(n) \end{aligned} \quad (A.1)$$

$$j = 1, 2, \dots, N_z$$

where

- N_z = number of zones
- N_r = number of rooms at the zone
- N_s = number of surfaces in room
- $T_i(n)$ = average temperature of interior surface i at time n
- $\dot{m}_{z,j}$ = mass flow rate of outdoor air infiltrating into zone at time n
- \dot{m}_{in} = mass flow rate of supply air into zone j at time n
- $T_{z,j}(n)$ = air temperature of zone j at time n
- $T_o(n)$ = outdoor air temperature at time n
- $T_{s,j}(n)$ = supply air temperature into zone j at time n
- $RS_a(n)$ = rate of solar heat coming through windows and convected into room air at time n
- $RL_a(n)$ = rate of heat from lights convected into zone air at time n
- $RE_a(n)$ = rate of heat from equipment and occupants and convected into room air at time n

If we find the relationship between surface temperature T_i and zone air temperature T_z , Eq. (A.1) can be used to calculate the zone air temperature T_z .

2. Heat balance in the room

To calculate zone cooling load directly by heat balance procedures, it requires solution of energy balance equations involving the zone air, surrounding walls and windows of each room, infiltration and ventilation air, and internal energy sources at each room.

1.1 Heat balance on the internal surface of the room

For each internal surface in the room, the heat balance equation can be established.

In words, the equation should be:

the heat transfer through conduction + heat transfer through convection + heat transfer through radiation with other surfaces + heat transfer through direct radiation = 0

The calculations that govern energy exchange at each inside surface at a given time n are

$$q_i(n)A_i + \left\{ h_i^c [T_{z,i}(n) - T_i(n)] + \sum_{k=1 \neq i}^{N_s} g_{ik} [T_k(n) - T_i(n)] \right\} A_i + RS_i(n) + RL_i(n) + RE_i(n) = 0$$

for $i=1,2,\dots,m$

(A.2)

where

$q_i(n)$ = rate of heat conducted into surface i at unit area of inside surface at time n

A_i = area of surface i

h_i^c = convective heat transfer coefficient at interior surface i

g_{ij} = radiation heat transfer factor between interior surface i and interior surface j

$T_{z,i}(n)$ = inside air temperature of zone j at time n

$RS_i(n)$ = rate of solar energy coming through windows and absorbed by surface i at time n

$RL_i(n)$ = rate of heat radiated from light and absorbed by surface i at time n

$Re_i(n)$ = rate of heat radiated from equipment and occupants and absorbed by surface i at time n

Since each structure has heat capacity and the disturbances vary with time, equation (A.2) is not a set of linear equations rather than a set of differential equations. To simplify the problem, we use z-transfer function to calculate the rate of heat conducted into surface i (at inside surface) at time n

$$q_i(n) = \sum_{l=0}^N b_i(l)T_{oi}(n-l) - \sum_{l=0}^N c_i(l)T_i(n-l) - \sum_{l=1}^N d_i(l)q_i(n-l) \quad (\text{A.3})$$

where

N = numbers of z-transfer factors
 b_i, c_i, d_i = z-transfer factor
 $T_{oi}(n-l)$ = temperature of air at other side of surface i at a time $n-l$
 $q_i(n-l)$ = rate of heat conducted into surface i at inside surface at time $n-l$

substituting Eqs. (A.3) into Eq. (A.2), we have

$$\left[\sum_{l=0}^N b_i(l)T_{oi}(n-l) - \sum_{l=0}^N c_i(l)T_i(n-l) - \sum_{l=1}^N d_i(l)q_i(n-l) \right] + \left\{ h_i^c [T_{z,i}(n) - T_i(n)] + \sum_{k=1}^{N_z} g_{ik} [T_k(n) - T_i(n)] \right\} + \frac{RS_i(n) + RL_i(n) + RE_i(n)}{A_i} = 0 \quad (\text{A.4})$$

Note that the surface i may be exposed to the outdoor environment or another room. If the surface i is an external surface, the temperature of air on other side of surface T_{oi} should be the sol-air temperature at that surface $T_{sol-air,i}$. This temperature is an external disturbance that is known. If the surface i is an internal surface, the temperature of air at other side of surface T_{oi} should be the air temperature of the adjacent room $T_{z,m,i}$, where m refers to the zone subscript. Therefore we have two kinds of equations, one for the external structure and another for the internal structure:

for external structure

$$\begin{aligned} & \sum_{l=0}^N b_i(l) T_{sol-ar,i}(n-l) - \sum_{l=0}^N c_i(l) T_i(n-l) - \sum_{l=1}^N d_i(l) q_i(n-l) + h_i^c [T_{z,j}(n) - T_i(n)] \\ & + \sum_{k=1}^{N_i} g_{ik} [T_k(n) - T_i(n)] + \frac{RS_i(n) + RL_i(n) + RE_i(n)}{A_i} = 0 \end{aligned} \quad (A.5)$$

for internal structure

$$\begin{aligned} & \sum_{l=0}^N b_i(l) T_{z,m,i}(n-l) - \sum_{l=0}^N c_i(l) T_i(n-l) - \sum_{l=1}^N d_i(l) q_i(n-l) + h_i^c [T_{z,j}(n) - T_i(n)] \\ & + \sum_{k=1}^{N_i} g_{ik} [T_k(n) - T_i(n)] + \frac{RS_i(n) + RL_i(n) + RE_i(n)}{A_i} = 0 \end{aligned} \quad (A.6)$$

Because the z-transfer factors, internal and external disturbances, all the surface temperatures, zone air temperatures and heat transfer q_i before time n are known, we rearrange the equations:

for external structure

$$\begin{aligned} & \left(c_i(0) + h_i^c + \sum_{k=1}^{N_i} g_{ik} \right) T_i(n) - \sum_{k=1}^{N_i} g_{ik} T_k(n) = h_i^c T_{z,j}(n) + \sum_{l=0}^N b_i(l) T_{sol-ar,i}(n-l) \\ & - \sum_{l=1}^N c_i(l) T_i(n-l) - \sum_{l=1}^N d_i(l) q_i(n-l) + \frac{RS_i(n) + RL_i(n) + RE_i(n)}{A_i} \end{aligned} \quad (A.7)$$

for internal structure

$$\begin{aligned} & \left(c_i(0) + h_i^c + \sum_{k=1}^{N_i} g_{ik} \right) T_i(n) - \sum_{k=1}^{N_i} g_{ik} T_k(n) = b_i(0) T_{z,m,i}(n) + h_i^c T_{z,j}(n) \\ & + \sum_{l=1}^N b_i(l) T_{z,m,i}(n-l) - \sum_{l=1}^N c_i(l) T_i(n-l) - \sum_{l=1}^N d_i(l) q_i(n-l) + \frac{RS_i(n) + RL_i(n) + RE_i(n)}{A_i} \end{aligned} \quad (A.8)$$

Therefore, for the room, we have

$$\mathbf{A} \mathbf{T}_{surf}(n) = \mathbf{B} + \mathbf{C} \mathbf{T}_z(n) \quad (A.9)$$

where \mathbf{A} is a $N_1 \times N_1$ matrix whose elements are known and do not vary with time, \mathbf{C} is a $N_1 \times N_2$ matrix whose elements are also constant. \mathbf{B} is a vector with dimension N_1 whose element at i can be written:

for external structure

$$B_i = \sum_{l=0}^N b_i(l) T_{sol-air,i}(n-l) - \sum_{l=1}^N c_i(l) T_i(n-l) - \sum_{l=1}^N d_i(l) q_i(n-l) + \frac{RS_i(n) + RL_i(n) + RE_i(n)}{A_i}$$

for internal structure

$$B_i = \sum_{l=1}^N b_i(l) T_{z,m,i}(n-l) - \sum_{l=1}^N c_i(l) T_i(n-l) - \sum_{l=1}^N d_i(l) q_i(n-l) + \frac{RS_i(n) + RL_i(n) + RE_i(n)}{A_i} \quad (\text{A.10})$$

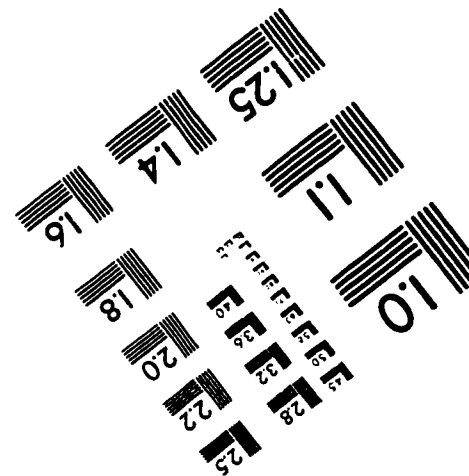
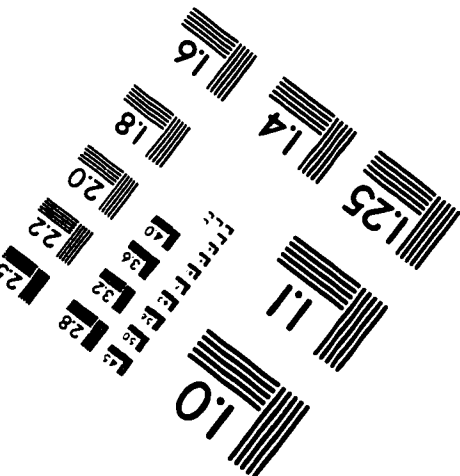
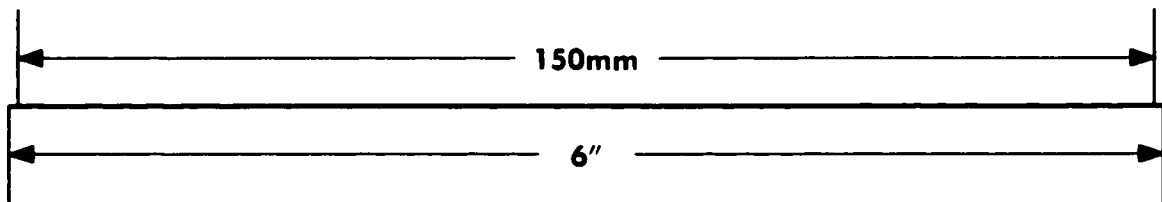
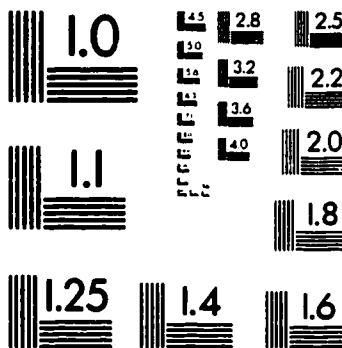
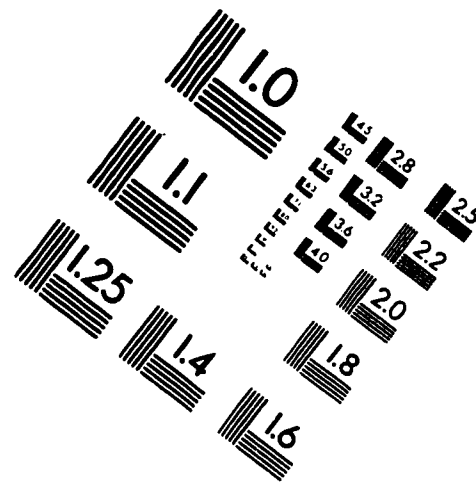
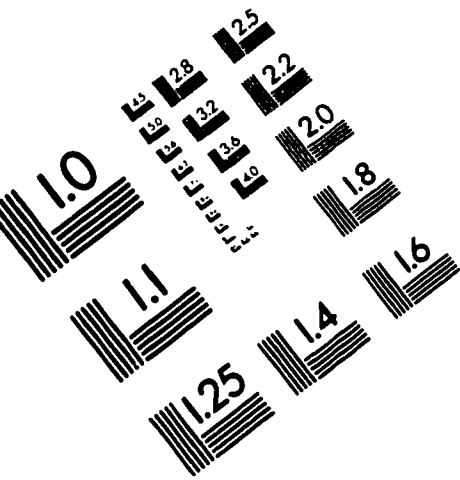
Note that the elements of vector \mathbf{B} vary with time.

We can rewritten Eq. (A-8) in the form

$$\mathbf{T}_{surf}(n) = \mathbf{A}^{-1} \mathbf{B} + \mathbf{A}^{-1} \mathbf{C} \mathbf{T}_z(n) \quad (\text{A.11})$$

Eq. (A.11) states the relationship between surface temperatures and zone air temperatures that is what we want. Once we have this relationship, air temperature equation (A.1) at zone model can be solved without any difficulty.

IMAGE EVALUATION TEST TARGET (QA-3)



APPLIED IMAGE, Inc
1653 East Main Street
Rochester, NY 14609 USA
Phone: 716/482-0300
Fax: 716/288-5989

© 1993, Applied Image, Inc., All Rights Reserved